THE UNIVERSITY OF HULL

"ANALYTICAL CHEMISTRY OF LANTHANIDES"

A THESIS SUBMITTED

BY

KAMAIL HUSSAIN AL-SOWDANI

B.Sc (BASRAH)

A CANDIDATE FOR THE DEGREE

OF

DOCTOR OF PHILOSOPHY

DECEMBER 1986

T O

M Y F A M I L Y

ACKNOWLEDGEMENTS

The work presented in this thesis was carried out in the Department of Chemistry, University of Hull from January 1983 to December 1986.

I am deeply indebted to my supervisor, Professor Alan Townshend, for his advice, interest and encouragement throughout the research period. I would also like to thank Dr. P. J. Worsfold for many helpful discussions.

My thanks go to all fellow members of the Analytical Research Group for many valuable discussions and comments; to the technical staff, especially Mr. G. E. Palin, Mr. N. Parkin, Mr. A. Rendell and Mrs. M. Staples for their valuable help and to Miss J. E. Anson for typing this thesis.

I am also grateful to the Ministry of Higher Education and Scientific Research of the Republic of Iraq and the University of Basrah for providing a scholarship, and the University of Hull for providing research facilities.

Finally I am very grateful to my family for their help in many ways.

SUMMARY

The work described in this thesis consists of nine chapters.

The first chapter is a general introduction, where lanthanide elements and their application are presented. Candoluminescence is defined as a type of solid state luminescence excited by hydrogen-based flame, and its relation to similar phenomena are clarified. A detailed historical review of candoluminescence of the lanthanides and its theoretical aspects are reported. Also a general introduction on vidicon detectors is given.

In chapter two instrumental developments for monitoring candoluminescence spectra and intensities and methods of improving the reproducibility of candoluminescence measurements are reported. Automated matrix introducing and matrix making devices are described, and methods for wavelength calibration of the Optical Spectrum Analyzer are reported.

Chapters three and four describe the candoluminescence of terbium and europium respectively. Terbium gives a characteristic green emission in MgO and rare earth oxides (Y_2O_3 , La_2O_3 , Gd_2O_3 and Lu_2O_3) coated on CaO matrices. It was possible to determine 0.1 - 50 ng of terbium in Gd_2O_3 coated matrices with a 0.01 ng detection limit and 2.5% relative standard deviation (r.s.d.).

Europium was a new activator for the above rare earth oxides coated on CaO matrices in which it gives a red

emission. It was possible to determine 0.1 - 15 ng of europium in such a matrix with a detection limit of 0.05 ng and 2.6% r.s.d.

In chapter five a general introduction for fluorescence analysis and flow injection analysis (FIA), their principles, instrumentation and applications for lanthanides determination are given. Chapter six describes a flow injection spectrofluorimetric method for determination of cerium(III) (1-100 ng ml^{-1}) based on its native fluorescence in an acidic carrier stream. Cerium(IV) can similarly be determined by incorporating a zinc reductor minicolumn into the system. Splitting the injection sample so that only part passes through the reductor, and the remainder by-passes it, allows total cerium and cerium(III) to be detected from the two sequential fluorescence peaks obtained.

Chapter seven describes a very selective flow injection method for determination of 0.5 - 4 μg ml^{-1} europium. A zinc reductor minicolumn is used for reduction of europium(III) to europium(II), which is indirectly detected either spectrofluorimetrically by reaction with cerium(IV), and measurement of the cerium(III) produced, or spectrophotometrically by reaction with iron(III), and determination, with 1,10-phenanthroline, of the iron(II) formed.

Chapter eight describes a sensitive and selective flow injection spectrofluorimetric method for samarium, terbium and europium determinations. The method utilizes the formation of energy-transfer complexes between the lanthanide ions and hexafluoracetylacetone.

Finally in chapter nine, some general conclusions are drawn, and possible areas of future research are suggested.

CONTENTS

PART 1

CANDOLUMINESCENCE OF LANTHANIDES

CHAPTER ONE

INTRODUCTION

1.1 The Lanthanides

The lanthanide elements are the series of 15 elements appearing between lanthanum (atomic number = 57) and lutetium (atomic number = 71), in the extended sixth row of the periodic table. It is customary to add scandium and yttrium to the lanthanide series and then refer to the whole group as the rare earth elements, as shown in Fig. 1.1. The rare earths are the largest naturally occurring group in the periodic table. The term rare is a misnomer in the sense that all the elements of the group are not rare in nature. If we except prometheum (having only radioactive isotopes) the two rarest lanthanides (thulium and lutetium) are more abundant than familiar elements such as mercury, bismuth and silver.

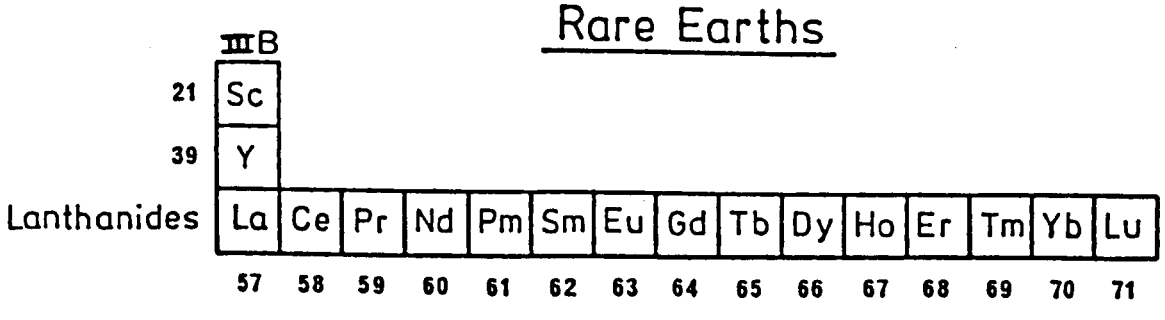

Fig. 1.1 The rare earth metals, their atomic numbers and chemical symbols (1).

But because of their strikingly similar characteristic properties and their occurrence as a group in nature, it is necessary to include all these elements as a single group. Thus there is considerable difficulty in isolating, detecting and determining a desired individual chemical species in the group.

Table 1.1 shows some physical data of the lanthanides. The lanthanides themselves are often also referred to as the 4f metals because each new electron, added as one proceeds from lanthanum to lutetium, enters the 4f-shell. Furthermore, since the 4f-shell is located inside the shell of the 5d6s - conduction states the nature of the latter changes little as a function of atomic number. Thus there is a significant and steady decrease in the size of the atoms and ions of the lanthanide elements with increasing atomic number, that is lanthanum has the greatest and lutetium the smallest radius. The imperfect shielding of one electron by another in the same subshell causes this contraction which is termed the lanthanide contraction.

The properties of the lanthanide group show a certain degree of gradual change in character with a sharp break between europium and gadolinium, permitting a division of the group into subgroups. The first is the cerium or light group that contains cerium as a major component along with lanthanum, praseodymium, neodymium, promethium, samarium and europium. The second is the yttrium or heavy group containing yttrium as a major component. The rest

Element	Symbol	Atomic Number	Electronic Configuration	Atomic Radius/nm	Ionic Radius/nm M^{+3}
Lanthanum	La	57	$4f^{0}5s^{2}5p^{6}5d^{1}6s^{2}$	0.187	0.115
Cerium	Ce	58	$4f^{2}5s^{2}5p^{6}5d^{0}6s^{2}$	0.183	0.111
Praseodymium	Pr	59	$4f^{3}5s^{2}5p^{6}5d^{0}6s^{2}$	0.182	0.109
Neodymium	Nd	60	$4f^{4}5s^{2}5p^{6}5d^{0}6s^{2}$	0.181	0.108
Prometheum	Pm	61	$4f^{5}5s^{2}5p^{6}5d^{0}6s^{2}$		0.106
Samarium	Sm	62	$4f^{6}5s^{2}5p^{6}5d^{0}6s^{2}$	0.179	0.104
Europium	Eu	63	$4f^{7}5s^{2}5p^{6}5d^{0}6s^{2}$	0.204	0.112
Gadolinium	Gd	64	$4f^{7}5s^{2}5p^{6}5d^{1}6s^{2}$	0.180	0.102
Terbium	Tb	65	$4f^{9}5s^{2}5p^{6}5d^{0}6s^{2}$	0.178	0.100
Dysprosium	Dy	66	$4f^{10}5s^{2}5p\ 5d^{0}6s^{2}$	0.177	0.099
Holmium	Ho	67	$4f^{11}5s^{2}5p^{6}5d^{0}6s^{2}$	0.176	0.097
Erbium	Er	68	$4f^{12}5s^{2}5p^{6}5d^{0}6s^{2}$	0.175	0.096
Thulium	Tm	69	$4f^{13}5s^{2}5p^{6}5d^{0}6s^{2}$	0.174	0.095
Ytterbium	Yb	70	$4f^{14}5s^{2}5p^{6}5d^{0}6s^{2}$	0.194	0.094
Lutetium	Lu	71	$4f^{14}5s^{2}5p^{6}5d^{1}6s^{2}$	0.174	0.093

Table 1.1 The Lanthanide Elements (2)

of the associated elements are gadolinium, terbium, dysprosium, holmium, erbium, thulium, ytterbium, scandium and lutetium. The classification of rare earths into the cerium and yttrium groups was first based on the occurrence of the elements of these groups in different minerals. According to the later classification of Goldschmidt, it was supported by certain differences in chemical and physical properties, solubility of salts, complex formation, paramagnetism and today by the electronic structure of their atoms.

During the past 25 years the lanthanides have been one of the most studied group of elements. This study was brought about primarily by the observation of lanthanide elements as radioactive byproducts of nuclear reaction, and their industrial uses, as shown in Table 1.2. These applications have necessitated the development of sensitive, selective and rapid analytical methods for lanthanides.

1.2 Definition of Candoluminescence

Luminescence is a term given to the emission of electromagnetic radiation stimulated when a particular material is exposed to an excitation source. The term was first defined by Wiedman[7] in 1889. There is no generally accepted classification of luminescence methods. As a rule, luminescence is classified according to the method or source of excitation, and by the mechanism or kinetics of the luminescence process. Depending on the excitation source used, luminescence techniques are divided as shown in

Glass,	as abrasives, decolourization, manufacture of speciality glass.
Ceramics,	as glaze.
Movie Projection,	in cored carbon arc for lighting which resembles sunlight.
Lasers,	as active constituent (4).
Colour Television,	for improved colour. Rare earth phosphor, usually europium-activated yttrium (5).
Solid State Microwave Devices,	Transmit shortwave energy with low energy loss.
Metals,	as a getter, desulphurization, alloying additive, and as a major constituent with cobalt in permanent magnets (6).
Petroleum,	as catalyst to produce higher yield of a desired petroleum fraction.

Table 1.2 Industrial uses of lanthanides (3)

Phenomenon	Excitation Sources
Photoluminescence (8)	Low energy photons (visible light, U.V. or I R.)
Cathodoluminescence (9)	Cathode rays
Electroluminescence	Electrical current
Radioluminescence	Alpha particles
Ionoluminescence	Ions
Triboluminescence	Mechanical disruption of crystals
Sonoluminescence	Sound waves
Crystoluminescence	Crystallisation of dissociation energy
Galvanoluminescence	Electrolytic energy
Chemiluminescence	Chemical reactions
Candoluminescence	Flame radicals (hydrogen flame)
Bioluminescence	Biochemical reactions
Thermoluminescence (10)	Chemical reaction between reactive species trapped in a rigid matrix and released by raising the temperature

Table 1.3 Types of luminescence and their sources

Table 1.3. In another classification based on the luminescence process, the following types can be distinguished:-

1.2.1 Resonance Luminescence

This is exhibited by atoms and certain simple molecules in the gas phase. If sodium atoms excited by light of wavelength 588 nm are promoted to an excited state, when they return to their ground state, they emit luminescence quanta equal in energy to the absorbed quanta. This emission of radiation, called resonance luminescence, is rarely observed.

1.2.2 Molecular Luminescence

This type of luminescence called molecular luminescence because it is characteristic of molecular systems (complex organic molecules, their complexes with metal ions and certain inorganic molecular crystalline lattices). It consists of a short-time emission of radiation which occurs spontaneously at room temperature; and a persistent fluorescence generally observed at low temperature or in rigid media (polymer films, glassy media and solid adsorbents).

1.2.3 Recombination Luminescence

This type of luminescence is observed when radicals or ions recombine to yield excited molecules e.g., the emission of radiation from the radical recombination in a

hydrogen flame. It may also occur in different gases and especially in phosphors in solid crystals. In all cases of these types of luminescence the system is raised to an unstable excited state by absorption of the energy from the excitation source, and emission occurs during the process of relaxation to the ground state.

Candoluminescence is a particular type of luminescence that occurs when certain inorganic solids (matrices) containing trace amounts of activating ions (activators) are placed at the outer edge of a flame of hydrogen burning in air. Second activators can be added to enhance the intensity of emission, which are called co-activators. The intensity of emission depends on the activator concentration, and also on the matrix material. Consequently it is possible to apply candoluminescence for analytical purposes, the activator being the analyte. Thus candoluminescence provides a very sensitive means of quantitative inorganic analysis, especially for lanthanide elements. There are two similar phenomena which should be differentiated from candoluminescence.

(a) Black Body Radiation

Every substance gives a thermal incandescence when it is heated, and the intensity of candoluminescence should be greater than the thermal radiation of a black body at the same temperature. Candoluminescence is usually defined as emission of non-black body radiation[11-13]. Candoluminescence produced above the temperature of red

heat has been a controversial phenomenon because of the difficulty of accurate measurement of temperature of an emitting surface.

(b) Radical Recombination Luminescence

This is a type of chemiluminescence and occurs when free radicals recombine, and it should also be differentiated from candoluminescence. In a hydrogen flame there are two free radical recombination reactions which cause the radical recombination luminescence. These are:-

$$H^{\bullet} + H^{\bullet} \longrightarrow H_2 + h\nu \qquad (1)$$

$$H^{\bullet} + {}^{\bullet}OH \longrightarrow H_2O + h\nu \qquad (2)$$

However these two reactions have more chance to occur on the surface of the matrix and this is a major source of candoluminescence.

1.3 Candoluminescence of Lanthanides. Historical Review.

Candoluminescence has been known and studied for many years. It was first reported by Balmain[14] in 1842. He observed different emission colours from his synthesized boron nitride due to different metals, added as their cyanides to boric acid during the synthesis of the matrix. The candoluminescence of materials containing lanthanide elements was studied quite early; the mineral gadolinite, which usually contains cerium as an impurity, was observed to emit brightly in flames[12,15,16]. Other

lanthanide elements such as pradeodymium, neodymium and erbium were studied by various workers including Bunsen[17] and Bahr[18]. At the end of the last century candoluminescence achieved technological importance for gas lighting, and Welsback invented the gas mantle[19]. A Welsback mantle of pure thorium (IV) oxide emits a weak pink light, and more than a few percent of added cerium provides a dull yellow.

Donau[20,21] in 1913 first applied analytically the phenomenon of candoluminescence. He showed that ng of bismuth and manganese could be detected by adding the test solution to a calcium carbonate bead on a platinum wire and inserting the bead into the lower edge of a hydrogen diffusion flame.

In the period 1918-1932 Nichols and his colleagues [22-26] did a large amount of work on candoluminescence. They studied various activators in various matrices at fairly high temperatures in the flame[22]. They compared the emission of unactivated matrices to those of activated matrices under the same conditions. The results of their work are shown in Table 1.4. Nichols and Wick[23] reported that Al_2O_3 : Tb, La_2O_3 : Eu, ThO_2 : Pr and CaO : Pr responded to ultraviolet radiation from a spark only after exposure to a hydrogen flame; the emission of ThO_2 : Dy excited by a spark or by cathode rays was also enhanced by prior exposure to a flame. Nichols and Howes[24] reported that Gd_2O_3 emits a "Nile green" emission in a flame. This emission peaked at about 120°

and disappeared above 400°C, followed by a new red emission with a peak at 530°C which disappeared above 600°C. The red emission presumably arose from traces of samarium or europium and the green emission from some other impurity. Nichols and Ewer[25] heated ThO_2 : Tb in a crucible to dull red heat, and then applied a Bunsen flame to the surface of the heated powder with the following result:

> "The material, hitherto inert, immediately assumed a ruddy candoluminescence due to flame excitation. Later, as the temperature rose, this was supplanted by a brilliant pale yellow-green glow. When the latter had become well established, the flame was quickly removed or was quenched by cutting off the gas. The luminescence vanished at once to be followed a fraction of a second later by a sudden red (flash up)".

Similar results were obtained with ThO_2 : Pr and La_2O_3 : Eu. No "flash up" was observed with unactivated oxides of ThO_2, TiO_2, Al_2O_3 or MgO nor with any materials (activated or not) heated from below the crucible only, ie. not in contact with the flame.

Wick and Troop[27] studied ThO_2 activated by Pr, Tb or Sm and excited by ultraviolet radiation, cathode rays or a hydrogen flame. For flame excitation the optimium concentration was 4.1% for Sm, 0.63% for Tb and 0.38% for Pr.

In 1940 Smith[28] reviewed the experiments of Nichols and his colleagues[22-26], he carefully repeated some and corrected several of their misconceptions. He studied the candoluminescence from CaO activated with 1% of praseodymium which gave a pink colour with a characteristic band

(540-650 nm). Emission occured only at the edge of the flame and disappeared as the surface approached red heat, and the emission in a coal-gas flame was always less than in a hydrogen flame. This was because the energy originating from recombination of hydrogen atoms was the principal cause of luminescence and the activity of the combination of radicals to produce energy was dependent on the nature of the solid used.

	Matrices								
Activator	Al_2O_3	BeO	CaO	CeO_2	MgO	SiO_2	ThO_2	TiO_2	ZrO_2
Dy	N		D	N	S		D		
Er	N		M		M		D		
Eu	S		S	N	Dh		N		
Gd	S		M		D		S		
La	N		S	N	M		D		
Nd	M	S	N	M	S	D	S	M	Dh
Pr	S	S	M	N	N	N	S	N	M
Sm	N	N	D	N	N	N	N	N	N
Tb	S		S	N	M		D		

S - strong, N - no effect, M - medium,
D - diminished, Dh - dehanced

Table 1.4 Candoluminescence of some lanthanides in various matrices (22-26)

In 1951 Neunhoeffer[29] extended Donau's[19,20] analytical work to provide a qualitative test for a number of lanthanide elements in a calcium carbonate matrix, as shown in Table 1.5. Neunhoeffer prepared the matrix by adding calcium nitrate to the test solution and co-precipitating the carbonate with the activator. He was able to detect as little as 1 ng of yttrium in 0.1g of calcium oxide by its visible luminescence.

Sokolov et al.[30,31] studied the radical recombination luminescence of various phosphors, including ZnS activated with Sm, Eu or Tm. Excitation was usually by atomic hydrogen from a microwave discharge, but oxygen and nitrogen were also used. The luminescence efficiency was measured with the following results for hydrogen excitations:

ZnS : Eu, 0.6×10^{-7}; ZnS : Sm, 1.4×10^{-5};

ZnS : Tm, 1.1×10^{-4}.

The efficiency depended upon activator concentration.

Activator	Colour
La	brick red
Ce	yellowish-green
Pr	red
Nd	orange-red
Sm	yellowish-green
Dy	pale green
Tm	yellow-green

Table 1.5 Various activators in calcium carbonate (29)

In 1967 Mason[32] studied the emission of lanthanide elements on a copper strip, fire brick as pure oxide or mixed with CaO. His results are summarized in Table 1.6. In 1970, White et al.[33-35] studied the candoluminescence of some rare earth oxides (La_2O_3 , Y_2C_3 , Gd_2O_3 , Lu_2O_3) and silicate glass activated with Tb or Eu by a hydrogen flame. They identified the spectra and reported a concentration dependence of the intensity between 27 and 11200 ng terbium.

Jorgensen et al.[36-38] studied the candoluminescence emission spectra emitted by sesquioxides and mixed oxides of thorium (IV) or yttrium (III) activated by various lanthanides. These oxides were studied in the form of Aure mantles in the blue flame of natural gas or hydrogen. They found that the obtained spectra were the same in these gases. Also they reported that Aure mantles with Ce (IV), Pr and Tb even as traces produce broad continuous spectra, whereas trivalent Nd, Ho, Er and Tm provide a narrow band.

Belcher et al.[39-48] established the possibility of using candoluminescence emission for the quantitative determination of elements at the trace level using different matrices. Table 1.7 summarizes their work on the lanthanide elements in different matrices investigated at Birmingham University, 1970-8.

Kassir et al.[49,50] and Al-Muaibed[51] in Basrah University studied the candoluminescence of terbium in

Element	Metal Conc. in CaO wt%	Light Emission with H_2 on Cu strip	Light Emission with H_2 on Fire Brick	Light Emission with CH_4 on Cu strip	Light Emission with CH_4 on Fire Brick	Colour
Y	0.0	W	T	T	N	Green and Orange
	0.2	T	W	N	N	Violet
	1.0	T	T	N	N	Violet
Ce	0.0	N	T	N	N	Pink
La	0.0	W	T	N	N	Green and Orange
	0.2	T	W	N	N	Lavender
	1.0	T	W	N	N	Lavender
Pr	0.0	N	T	N	N	Red
	0.2	T	S	T	S	Red
	1.0	N	T	N	N	Red
Nd	0.0	N	T	N	N	Red
	0.2	T	T	N	N	Violet
	1.0	T	W	N	N	Lavender
Sm	0.0	N	N	N	N	-
	0.2	T	T	T	T	Orange
	1.0	T	T	N	T	Orange

/Continued

Element	Conc. in CaO wt%	Light Emission with H_2 on Cu strip	Light Emission with H_2 on Fire Brick	Light Emission with CH_4 on Cu strip	Light Emission with CH_4 on Fire Brick	Colour
Gd	0.0	S	S	T	W	Red
	0.2	T	T	N	N	Violet
	1.0	T	W	N	N	Violet
Dy	0.0	N	N	N	N	-
	0.2	T	T	N	N	Lavender
	1.0	T	W	N	N	Blue
Ho	0.0	N	T	N	T	Red
	0.2	T	T	N	N	Blue
	1.0	N	T	N	T	Red
Er	0.0	T	T	N	N	Red
	0.2	T	T	N	N	Blue
	1.0	W	W	N	N	White
Yb	0.0	N	N	N	N	-
	0.2	T	T	N	N	Lavender
	1.0	T	T	N	N	Red

T = Trace W = Weak N = Nil S = Strong

Table 1.6 Light emission of yttrium oxide and lanthanides (pure and in CaO) in hydrogen and methane-air flames (32)

Activator	Matrix	Colour	Wavelength of main peak (ng)	Calibration range (ng)	Detection limit	Reproducibility (%)	Ref.
Ce (III)	$CaO - CaSO_4$	Green	560	0.01 - 6.0	0.001	4.0	44, 47
	$CaO - SiO_2$	Blue	440	0.05 - 10	0.05	6.0	46
Pr (III)	CaF_2	Orange-Red	600	0.01 - 5.0	0.01	4.2	46
	$CaO - CaSO_4$	Red	600	0.05 - 1.0	0.05	3.0	41, 44
Eu (III)	$CaWO_4$	Red	610	0.6 - 60	0.2	8.0	45, 48
	$CaO - CaSO_4$	Orange	600	0.01 - 15	0.005	5.0	44, 42, 47
	$SrO - CaSO_4$	Orange	570	0.2 - 10	0.2	13	48
Tb (III)	$CaO - CaSO_4$	Green	550	0.1 - 25	0.1	6.5	41, 44
	$Mg(OH)_2$	Green	550	1.0 - 20	0.05	5.0	47
	$Sr(OH)_2$	Green	550	1.0 - 20	2.0	8.0	47
	CaF_2	Green	545	1.0 - 60	1.0	7.0	47
Sm (III)	$CaHPO_4$	Yellow	590	1.0 - 60	0.5	12	45
	$Sr_3(PO_4)_2$	Yellow	590	1.0 - 60	0.5	5.0	45
Er (III)	$CaWO_4$	Green	525	1.0 - 60	0.2	5.0	45

Table 1.7 Candoluminescence of various activators in different matrices investigated at Birmingham University

different matrices (Y_2O_3 , Gd_2O_3 , ThO_2 , La_2O_3 and $CaSiO_3$) coated on CaO - $CaSO_4$ rods. Candoluminescence spectra of terbium in these matrices were recorded, which are the same in all matrices, and only two peaks were noticed (490 and 550 nm). The peak at 550 nm was used for the analytical measurement. The calibration graphs were found to be linear in different ranges up to 90 ng in the La_2O_3 matrix, with a 0.2 - 0.3 ng detection limit and 2.8 - 3.2% relative standard deviation.

1.4 A Concise Review of the Theoretical Approach in Candoluminescence.

Several theoretical approaches have been suggested to explain the luminescence emitted by an activated matrix at the edge of a hydrogen diffusion flame. In 1918 Paneth and Winternitz[52] reported that the U.V. radiation from the flame was the main excitation source for candoluminescence. However the luminescence could not be stimulated unless the activator matrix contacted the flame. Tiede and Buescher[53] found that the luminescence from zinc sulphide or zinc silicate matrices could be stimulated even when quartz glass separated it from the flame. This means that U.V. radiation is not involved as the excitation source for the luminescence. Nichols et al.[23,26,54] reported that since the luminescence occurred in a hydrogen environment next to the oxygen, rapid reduction and oxidation should be responsible for the luminescence. They suggested the "redox theory" which can be explained as follows[46].

"... The production of an easily oxidizable substance (ie. by reduction) and the presence of free or easily available oxygen or its equivalent are essential. These are commonly the direct result of a simple oxidation-reduction process and the luminescence glow may follow immediately from the recombination of the separated components. ... The glow may be due to subsequent reunion with oxygen thus set free in active form or with oxygen derived from another source".

Minchin[55] in 1939, in his general review on candoluminescence, was probably the first to mention that the energy produced by radical recombination is responsible for stimulating the blue-green luminescence from the boron nitride excited by town gas. He stated:

"... in the flame gases there are atoms and atomic aggregates which possess an exceptional amount of energy that they are unable immediately to liberate. The conjunction of a flame with a crystal lattice of suitable structure would then enable this energy to be released in the flame as light radiation and the process of combustion would be accelerated".

In 1925 Bonhoeffer[56] suggested the luminescence was caused by the recombination of hydrogen atoms at the solid surface. In 1940 Smith[28] explored the work done by Nichols[22-26] and Donan[20,21] suggested many corrections to their ideas. He reported that the energy produced by recombination of hydrogen atoms,

$$H^{\cdot} + H^{\cdot} \longrightarrow H_2 + 100 \text{ Kcal.}$$

was the principal cause of luminescence. Also he studied the effect of the solid matrices' nature on the activity of the recombination of the radicals. He used two thermometer

bulbs for comparison past which flowed hydrogen atoms produced by electrical discharge at low pressure. One of the two bulbs had an adsorbed film of water to discourage the recombination of atoms, and the other was coated with platinum foil to allow atoms to recombine freely. The rise in temperature at the latter thermometer because of the exothermic reaction was direct evidence of the energy released by the recombination of hydrogen atoms.

Townend[57] was impressed with Smith's view on radical recombination for candoluminescence. In his paper entitled "The mechanism of flame propagation", he stated:

> "... A good illustration is provided by the work of Smith, on the luminescence of promoted calcium oxide surface in contact with flames of hydrogen-containing combustibles. This luminescence gives rise to an emission identical with the fluorescence spectrum and has been shown to depend upon recombination on such surface of hydrogen present in the flame gases".

Arthur[58] supported the fact that the hydrogen atom recombination is the cause of the luminescence. He commented that:

> "... A very convenient demonstration of the presence of hydrogen atoms in a flame is the luminescence observed when the flame is brought into contact with certain activated oxides; the luminescence has its origin in the reaction $H^{\cdot} + H^{\cdot} \rightarrow H_2$ which occurs on the oxide surface and is most marked with hydrogen flames".

He investigated the suppression effect of gases and vapours other than carbon monoxide which was studied previously by Smith, and the "critical %" of the total gas needed completely to extinguish the luminescence. The results

are given in Table 1.8. He concluded that the consumption of hydrogen atoms in the flame by the additive caused this depressive effect.

Additive	$C_6H_5C_2H_5$	SO_2	$C_6H_5CH_3$	C_6H_{14}	C_6H_6
%	1.8	2.3	2.4	2.7	2.9
Additive	CH_4	CO	NH_3	N_2	
%	6.6	15	19	37	

Table 1.8

Critical % of various flame additives required to suppress the candoluminescence of calcium oxide activated by manganese.

In 1951 Neunhoeffer[29] put forward a different theory to explain the mechanism of candoluminescence. He pointed out that the positive and negative charge carriers ie. protons and electrons in the hydrogen flame were responsible for the excitation of the activated matrix rather than the U.V. radiation from the flame. He suggested that the recombination of the charged particles on the surface of the solid matrix stimulated the emission. The addition of hydrocarbon gases to the hydrogen flame would increase the charged particle concentration, so that the luminescence intensity should increase as well. However Arthur's experiment[58] shows that such addition of hydrocarbons depresses the emission seriously. Consequently

Neunhoeffer's theory involving electrons and protons seems to be unacceptable.

Sancier and his co-workers[59] studied the luminescence produced by U.V. radiation and heterogeneous recombination of nitrogen atoms on bismuth-activated calcium oxide and stated that although a considerable amount of recombinations occur at the surface of the activated oxide, it does not contribute to the luminescence. They found that the luminescence intensity produced by the nitrogen atoms' excitation was equal to the oxygen atoms' excitation and both of these atoms' excitation were much greater than by photoexcitation, but the characteristic spectrum of the activator obtained by all these excitation processes was the same. They concluded that the increased intensity in the case of atom excitation arose from the variation of the active surface sites on the luminescent solid or change of solid structure or energy transfer between the recombination sites and luminescence centres as the temperature increased. Also they found that the longer the matrices were exposed to the recombination of atoms, the more the luminescence intensity decreased because of a decrease in the catalytic effect of calcium oxide or decrease in efficiency of transferring the energy gained to the luminescence centre.

Sancier et al.[59] were the first to point out that crystal defects are responsible for a luminescence centre when excited by atom recombination on matrix surface.

Sokolov's radical recombination semiconductor theory [60-64] introduced the band model of semiconductors

combined with recombination of radicals on the matrix. The proposed model is illustrated in Fig. 1.2. The solid matrix is considered to have valence and conduction bands. The stages that occur for the emission of light can be summarized as follows:-

1. Chemisorption of a radical (C) from the flame onto the lattice surface. This chemisorbed particle is thermally ionized, raising a free electron into the conduction band (transition 7) and leaving a hole at the level of the adsorbed species.

2. A second radical arrives from the gas phase and combines with the positively-charged adsorbed species. This results in the movement of an electron from the valence band (transition 6), thus leaving a hole here.

3. The activator atom (A) is ionized and an electron drops into the valence band in one of two possible ways:

   i) an electron at level A recombines with the hole in the valence band. (transitions 4 and 5).

   ii) an electron at level A is directly raised to the conduction band (transition 1).

   Both cases result in a hole at level A.

4. The free electron in the conduction band drops down to the activator species (transition 3), and neutralizes it. This transition is accompanied by the emission of a quantum of light, as candoluminescence. Another possibility of neutralizing the activator species is transition 2, but it requires absorption of energy,

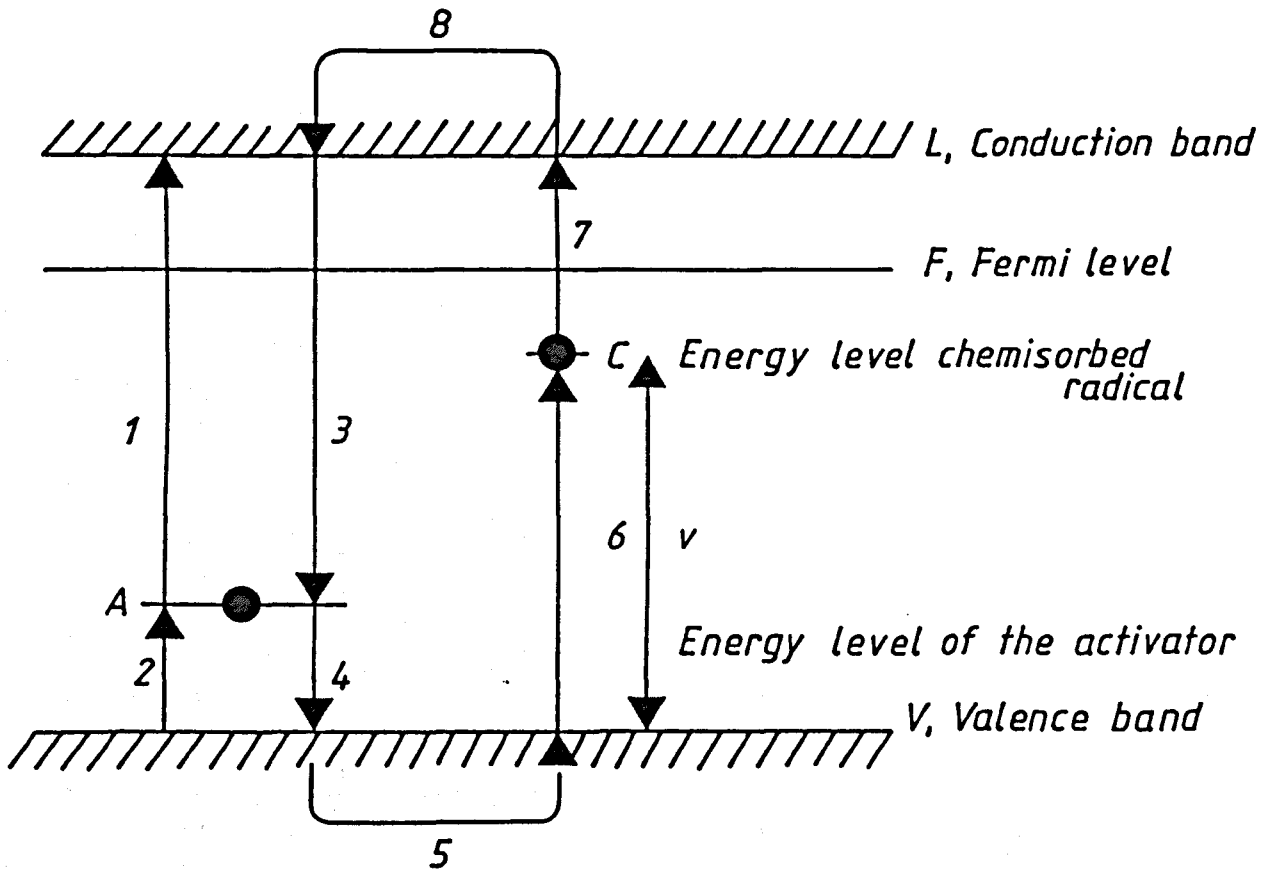

Fig. 1.2 Energy levels on the semiconductor surface, and a possible mechanism for candoluminescence [56].

not emission. The closed cycle process (transitions 3-8), can be repeated when another radical is adsorbed from the gas phase onto the lattice surface.

Sokolov deduced an equation for the intensity obtained in the above system by treating the problem thermodynamically. He found that the Fermi level at the lattice surface affected the luminescence intensity. Most importantly, Sokolov et al. recognised two types of luminescence below red heat, one involving an activator and matrix system, excited by the energy of the atoms' recombination, which is quenched at higher temperatures, and the other involving free radical recombination luminescence.

Finally White et al.[35] concluded that

> "... It may be said that candoluminescence and radical recombination luminescence are processes like photo - and cathode - luminescence. The rare earth ion activators behave in the same way and produce the same spectra. The flame and radical excitation process are also very similar to each other, differing mainly in the details of the recombining species with corresponding differences in excitation energies".

They suggested a possible mechanism for candoluminescence which is illustrated in Fig. 1.3. They supposed that some active species, H, is adsorbed on the matrix surface and remains there until a second active species, H, collides with it. The adsorbed atoms combine forming a H_2 molecule which may remain adsorbed on the surface for a time and is then desorbed to the gas phase. The recombination energy is transferred to an activator atom, A, near the surface. Atom, A, then transfers the energy to other activators within the bulk of the matrix or emits a luminescence

photon. The energy is either lost through non-radioactive decay or is emitted as luminescence.

It is of interest that the candoluminescence spectra are very similar to the spectra obtained in photoluminescence including many details of the crystal field fine structure in the rare earth activated system, which indicates that the activator atoms emitting the luminescence are on sites with a well defined crystal field. The crystal field of the surface atoms is distorted and varies from site to site so that, A, in Fig. 1.3 cannot be a surface atom. The recombination energy must be transferred first to an activator centre which lies at a depth less than the critical interaction depth below the surface. It must be deep enough, a few atomic layers, to have a uniform crystal field but still be close enough to the surface to permit direct coupling with recombining atoms. It is suggested that Dexter-Forster dipole-dipole or resonance exchange is the required mechanism of energy transfer from the recombination site to activator sites in the bulk. This suggestion was supported by the fact that the lifetimes of the rare earth-activated oxide luminescences are more than the dipole-dipole or resonance exchange time, which means that the energy can be exchanged among many activators before it is radiated or lost.

The effect of the temperature on the luminescence intensity was explained as follows. At low temperature, the surface of the matrix will be covered with an adsorbed layer of cold gas which effectively blocks the surface

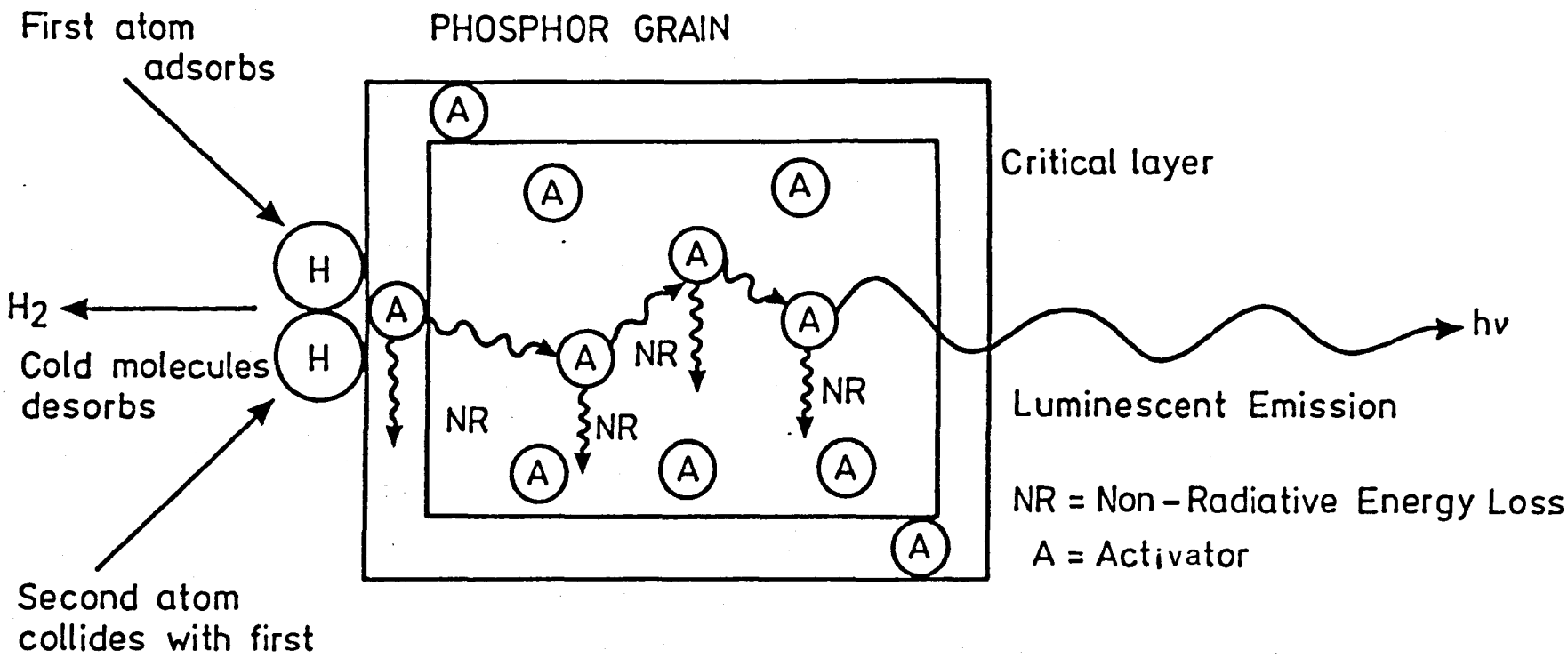

Fig. 1.3 Schematic diagram illustrating the energy transfer processes (35)

from the active species in the flame. As the temperature rises, the cold gas layer is removed exposing more and more surface to active species and the intensity of luminescence is increased. But at high temperatures the adsorbed species will also be removed from the surface before a second atom can collide to produce a recombination.

Sokolov's radical recombination semiconductor theory to explain the mechanism of candoluminescence thus far has been accepted. However, it is not absolutely certain whether it can be applied to every matrix-activator system. In particular, it is suspected that with many lanthanide activators the actual luminescence transition may differ from that proposed by Sokolov, even if the initial energisation of the lattice follows the same mechanism. Transitions within the inner 4f electron shell are responsible for many types of luminescence encountered with the lanthanide metals and candoluminescence is not an exception. This is described in more detail in the following section.

1.5 Luminescence of the Lanthanides

The chemical properties of the lanthanide elements are strikingly similar. Mixtures of these elements have often defied analysis by classical methods. These characteristics of each of the individual lanthanides depend on their optical properties. Spectroscopic methods are the most important for lanthanide determinations. Atomic emission spectroscopy is difficult to apply, since the spectra of most of lanthanide elements are very complex,

containing thousands of lines[65]. Even under high dispersion the probability of line interferences is very high. Additionally such a method suffers from low sensitivity. However under more sensitive recording conditions these lines are readily detectable at concentrations as low as 2 ppm[66].

Considerable attention has been paid to the luminescence properties of the lanthanides, which are produced by electronic transitions within the 4f shell. Table 1.9 shows the wavelengths of the principal peaks obtained from various activators obtained by using different excitation sources. It seems that the peaks for lanthanide-activated candoluminescence emissions are very similar to those obtained by other excitation processes. The similarity of wavelengths indicate that the emissions for given ions are due to the same specific electronic transitions. This is not in agreement with Sokolov's mechanism of candoluminescence, which suggests that the luminescence transition takes place between the conduction band of the solid and the activator.

1.5.1 Some Types of Luminescence

The luminescence of lanthanide elements can be classified as following:

1.5.1.1 Pure Salts and Solutions

Pure crystalline salts of lanthanide elements are capable of emitting radiation when subjected to U.V.,

X-rays, cathode rays or some other form of excitation. The electronic transitions take place within the inner 4f shell and the position of the narrow luminescence band is independent of the means of excitation used.

Element	Excitation Sources			
	Cathode ray	X-ray	U.V.	Candoluminescence
Pr	641	490,645	499	610
Sm	606	595	606	598
Tb	554	542	543	550
Eu	612	590	614	600
Er	554	550	544	525

Table 1.9 Wavelengths (nm) obtained for various activators by using different excitation sources (44)

Some lanthanide ions (Ce, Pr, Sm, Eu, Tb and Dy) together with those of uranium and thorium are the only inorganic elements that can be detected in solution by the luminescence of their simple ions. This type of lanthanide luminescence will be discussed in detail later.

1.5.1.2 Organic Complexes

Most luminescence in inorganic analysis is achieved by complexing the metal ion with a fluorescent or non-fluorescent ligand, which then forms the basis of highly

sensitive and selective methods of lanthanide determinations. The electron transition in the lanthanide metal bound to a chelating agent occurs by intermolecular energy transfer[67]. This is discussed in more detail later.

1.5.1.3 Crystalline Phosphors

The optical luminescence exhibited by some of the lanthanide ions incorporated in inorganic solids has been utilized for the detection and determination of the lanthanide elements at trace and ultratrace level for many years[68]. The luminescences and lifetimes of these phosphors are determined by the concentration of these ions activated in the matrix.

The crystallophosphors are most often photoexcited by U.V. light from a mercury or xenon lamp, a spark, or, recently a laser, and also by cathode and x-rays[68-70]. The activator ion luminescences by absorbing energy either directly from the source or from the energy trapped by the crystal lattice of the main component of the phosphor.

The value of the detection limit in photoexcitation is usually, 10^{-4}- 10^{-6}% and in cathode or x-ray excitation, 10^{-7}- 10^{-8}%[69]. It is well known that the luminescence of these crystallophosphors is influenced by many factors; the ionic radius of the activator, the way the activator is inserted into the crystal structure of the host matrix; the ratio of the activator ionic radius to that of the ions in the crystal lattice; and finally by the nature of the host matrix.

The dependence of lanthanide ions' absorption spectra on the immediate environment of the ion has led to methods for the determination of non-fluorescent ions such as La, Gd and Lu by coprecipitating them with Er^{3+} and calcium fluoride. This association of Er^{3+} with the non-fluorescent ion is excited with a dye laser. Detection limits of around 4 pg have been observed[70].

A technique known as selective excitation of probe ion luminescence has been used to determine various lanthanides[71,72]. The method requires the formation of a crystalline host lattice containing a lanthanide ion whose transitions are sharp and modified by the lattice. A tunable dye laser is used to excite a specific ion at a specific site. Much work has been done on the interference effects of lanthanide ions which are together in the same host matrix. The enhancing and quenching effects which occur have been attributed by most investigators to a non-radiative energy exchange between impurity ions.

1.6 Vidicon Detectors

1.6.1 Introduction

To identify spectral lines, their wavelengths and intensities are needed. The technique for the spatial dispersion of spectra is based on the diffraction grating. For this, grating spectrographs, grating polychromators and grating monochromators are used, whereby the wavelength depends on the positional angle of the grating.

The two main detection systems used to measure such spectral intensities have been the photographic emulsion (plate) and the photomultiplier (PM) tube. The photographic plate, although capable of integrating and recording thousands of lines in a single exposure as a permanent record, has a non-linear response, limited dynamic range and tedious readout. Thus, even though the PM-tube is limited to the measurement of one spectral resolution element at a time, its wide linear dynamic range, sensitivity, and the fact that it can transduce light intensity directly into an electronic signal lead to its wide used in spectrochemical measurements.

However, a very large number of spectrochemical measurements would be greatly facilitated if an effective detection system were available that combined the desirable characteristics of the PM-tube with the one major advantage of the photographic plate, that of simultaneous multichannel detection.

One multichannel approach has been accomplished by placing an array of mini-PM-tubes in predetermined positions (corresponding to spectral regions of interest) across the focal plane of a spectrograph, each with its associated readout electronics[73]. Although excellent sensitivity, wide dynamic range and rapid response are achieved, this detector in practice provides a limited number of channels aligned for a predetermined specific application and thus lacks the capability and flexibility required of a real multichannel detector.

Gloersen[74] in 1958 described a new type of multichannel detector, the vidicon tube; its potential in analysis has been predicted by Margoshes[75] in 1970. This device, used as spectrometric parallel detector, has been demonstrated and gradually gained acceptance among spectroscopists.

The vidicon tube detector comprises three basic components:

(a) A device for converting photon images into their electrical analogs.

(b) A device for storing these electrical images.

(c) A readout (video) mechanism to reconstruct the stored images and transmit them (in real-time) to a display monitor, converting image intensity to vertical displacement and spatial distribution to horizontal displacement (Fig. 1.4).

Vidicon imagers and particularly the silicon vidicon with its various image-intensified derivatives are more readily available and their behaviour and performance better controlled, than other television camera detectors[76].

A brief description of silicon vidicon (SV) and silicon intensified target (SIT) and intensified silicon intensified target vidicon (ISIT) are presented in the succeeding sections.

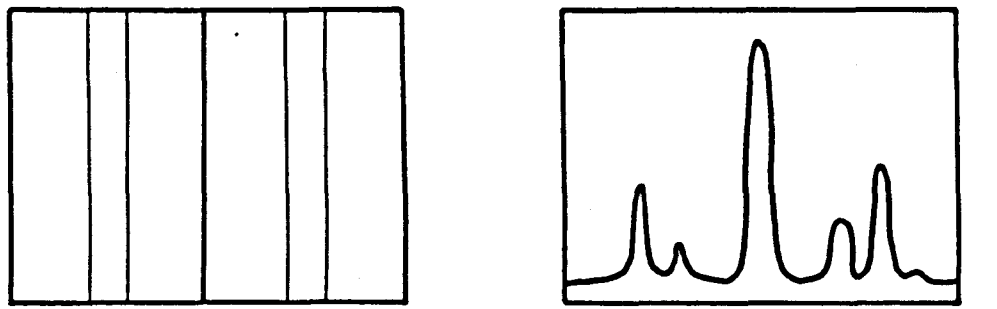

Photograph of spectrum

Vidicon display of same spectrum

Fig. 1.4 The vidicon display associated with the spectrum 'photograph' on the left.

1.6.2 Silicon Vidicon (SV)

This is the most promising vidicon tube presently available for spectroscopic work, first conceived at Bell Laboratories[77]. The heart of the SV is a single monolithic silicon crystal wafer with a microscopic array of a few million diode junctions grown on it. It functions as the target of the vidicon detector.

The active area of the target measures 12.5 x 10.0 mm and each diode has an active area 8 μm in diameter, separated by only 25 μm (centre to centre) as shown in Fig. 1.5. All diodes have a common cathode and isolated anodes selectively addressed by a scanning (readout) electron beam. The diodes function as photodiodes, generating the production and storage of electron-hole pairs upon incidence of UV to near-IR photons.

The diodes are scanned continuously by a focused electron beam which recharges all photodiodes to an equal and preset reversed-bias potential. Exposure of the target to photons or electrons causes production of electron-hole pairs that combine to deplete the surface charge. When the beam scans a partially depleted region, a recharging current flows. This current is proportional to the depleted charge and likewise to the density of the electron-hole pairs. Therefore, it is proportional to the radiation intensity incident on the diodes which are registered by online computer or microcomputer. Thus, an instantaneous record of spectral intensity VS. wavelength is generated

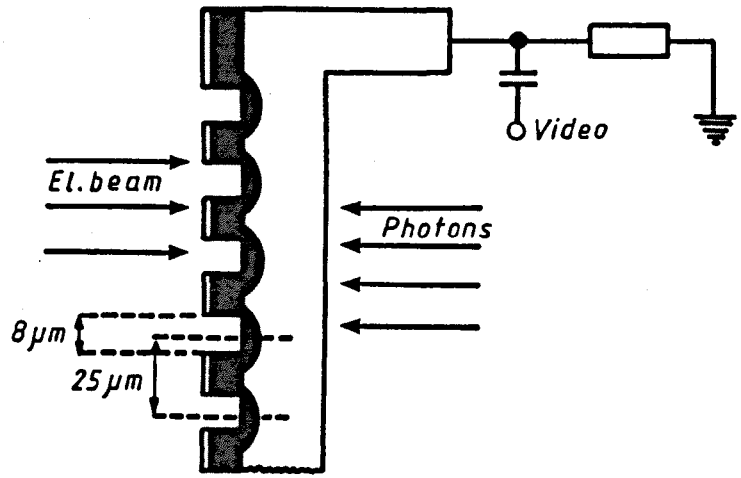

Fig.1.5 Silicon multi-diode target.

in the computer memory.

The imaging and spectral resolution of the SV is limited by the diameter of the scanning electron beam, typically 25 μm. The spectral sensitivity of the SV depends on the thickness of the target and the material used for the entry window. A standard SV has a spectral sensitivity in the range 300-1200 nm. A SV which is also sensitive below 200 nm has a quartz entry and a silicon target only 4 μm thick. Maximum sensitivity lies at 450 nm with 2400 photons per channel.

1.6.3 Silicon Intensified Target Vidicon (SIT)

The SIT vidicon, or Silicon Intensified Target Camera, shown in Fig. 1.6 is essentially the same as the SV with the addition of an intensifier stage.

The intensifier stage consists of a fibre-optic faceplate which is optically coupled to a photocathode. This photocathode converts the photon image into a corresponding photoelectron image. The generated electron image is accelerated (7-9KV) and focused onto the silicon target. Since the number of electron-hole charge pairs produced on the target is proportional to the number of incident electrons (approximately one charge pair per 3.6 eV) an internal gain of approximately 1500 is typically achieved, ie., this is the number of electrons produced from each photoelectron emitted from the photocathode (the electron energy is partially absorbed by the silicon oxide overcoat). With this gain, the signal is sufficiently

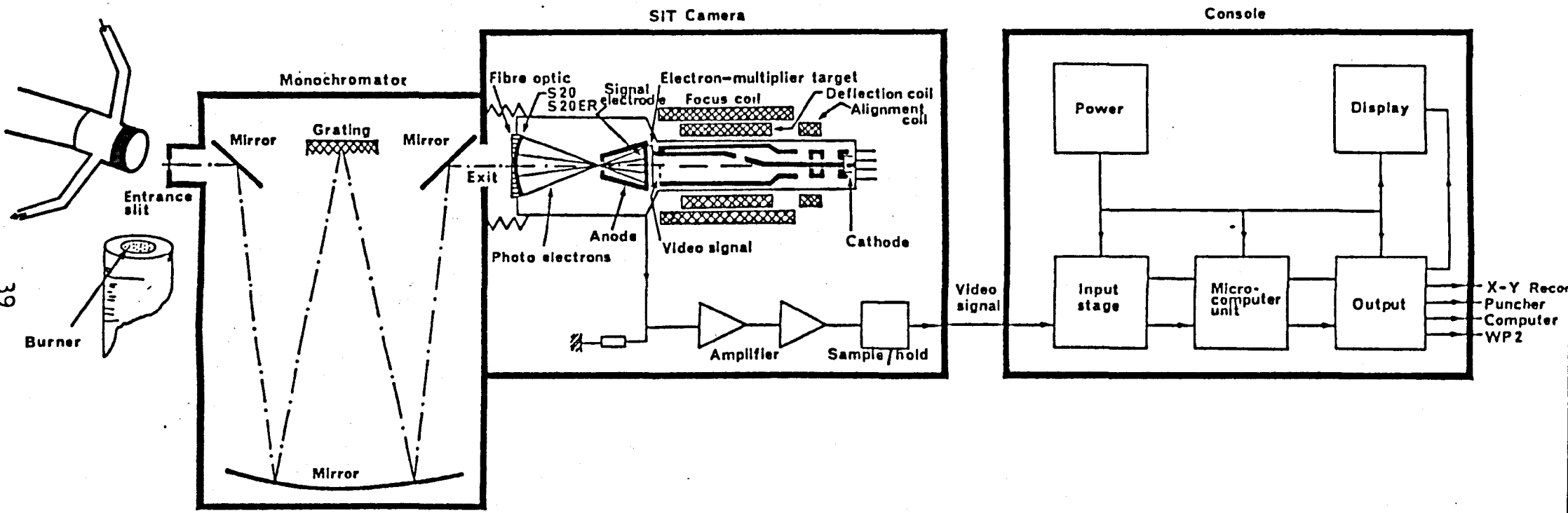

Fig. 1.6 Silicon Intensified Target Camera

enhanced, compared to readout noise, to allow the detection of very weak signals. Unfortunately, electrostatically focused intensifiers use a fibre-optics faceplate window which limits the short wavelength response to 340 nm. At the same time, the response photocathode, which has 5-20 characteristics similar to those used in many photomultipliers, limits the long wavelength response to 850 nm.

1.6.4 Intensified Silicon Intensified Target Vidicon (ISIT)

The sensitivity can be improved further by adding another stage of intensification, resulting in an ISIT vidicon. Another photocathode of either extended red response or ERMA (Extended Red Multi-Alkali Photocathode) can be coupled to the front of an SIT vidicon and a more sensitive detector is obtained. The sensitivity is such that it is possible to detect single photo-electrons or about 6 incident photons.

The vidicon tubes are highly reliable detectors for qualitative and quantative applications. They have been used for several different types of spectral measurements[78] but greater emphasis has been placed on developing atomic absorption and emission[79,80] systems capable of performing simultaneous multielement analysis.

They have also been used as multi-wavelength detectors in liquid chromatography and HPLC[81,82] and other applications include the simultaneous measurement of excitation and emission spectra in fluorescence studies[83-85].

1.7 Research Objectives

This research is aimed at the use of various techniques to achieve determination of lanthanide elements. Candoluminescence provides the basis of a simple, low cost, selective and highly sensitive technique. It is known to give emission from several lanthanides, with high sensitivity. Recently an automated device for molecular emission cavity analysis (MECA) was introduced based on earlier candoluminescence devices. This device was rebuilt and modified and is used in the first part of this work of studying for candoluminescence of the lanthanides. It was anticipated that it would improve the precision of the measurement.

In this work a silicon-intensified target (SIT) vidicon camera is used as a detector in combination with an optical spectrum analyser to control and steer all the functional processes of the vidicon camera. This detector is expected to provide a very sensitive and versatile detector for rapid measurement of candoluminescence emission and spectra of lanthanides.

It is difficult to predict new matrix-activator combinations, but the use of matrices coated with rare earth oxides should allow a range of matrices to be studied rapidly and inexpensively.

Flow injection analysis (FIA) is that type of continuous flow analysis that utilizes an analytical stream, unsegmented by air bubbles, into which highly reproducible

volumes of sample are injected. Application of this principle to chemical analysis yields a fast, precise, accurate and extremely versatile system that is simple to operate.

Spectrofluorimetry has long been known as a very sensitive technique, but its application as a means of detection for FIA is relatively new. The combination of FIA with spectrofluorimetry has been applied for many types of analysis. However very little investigation has been done with respect to application to inorganic analysis and specially to lanthanide elements.

The main aim of the second part of this project therefore is to apply this combination of FIA with spectrofluorimetry to provide rapid, reproducible, sensitive and selective analytical methods for lanthanides.

CHAPTER TWO

CANDOLUMINESCENCE MEASUREMENTS

EXPERIMENTAL PARAMETERS

CANDOLUMINESCENCE MEASUREMENTS EXPERIMENTAL PARAMETERS

2.1 Apparatus

The spectrometer used for monitoring candoluminescence spectra, shown in Fig. 2.1 incorporated a modified matrix-introducing device and water-cooled matrix holder, a burner and gas control unit, a monochromator, a silicon intensified target (SIT) vidicon detector and associated electronic and microprocesser equipment. The apparatus was placed in a dark room in order to get rid of any external sources of illumination.

2.1.1 Matrix Introducing Device

For any quantitative purpose, the analyte responses must be repeatable. To get reproducible results, there are different parameters that have to be controlled. In candoluminescence since the activated matrix should be introduced reproducibly into a critical zone of the flame, a special type of sample introducing device was needed.

In early work platinum wires were used to support the matrix material. Sokolov's rotating brass cylinder is quite unique[62]. Bogdanski[86] introduced the activated matrix to the hydrogen flame by different methods. For quantitative measurements, he found that the sample holder shown in Fig. 2.2 was satisfactory. He found that hexagonal cavity head of an Allen screw was suitable for holding the matrix. Difficulty in screwing in the Allen screw reproducibly into the holder each time was the main

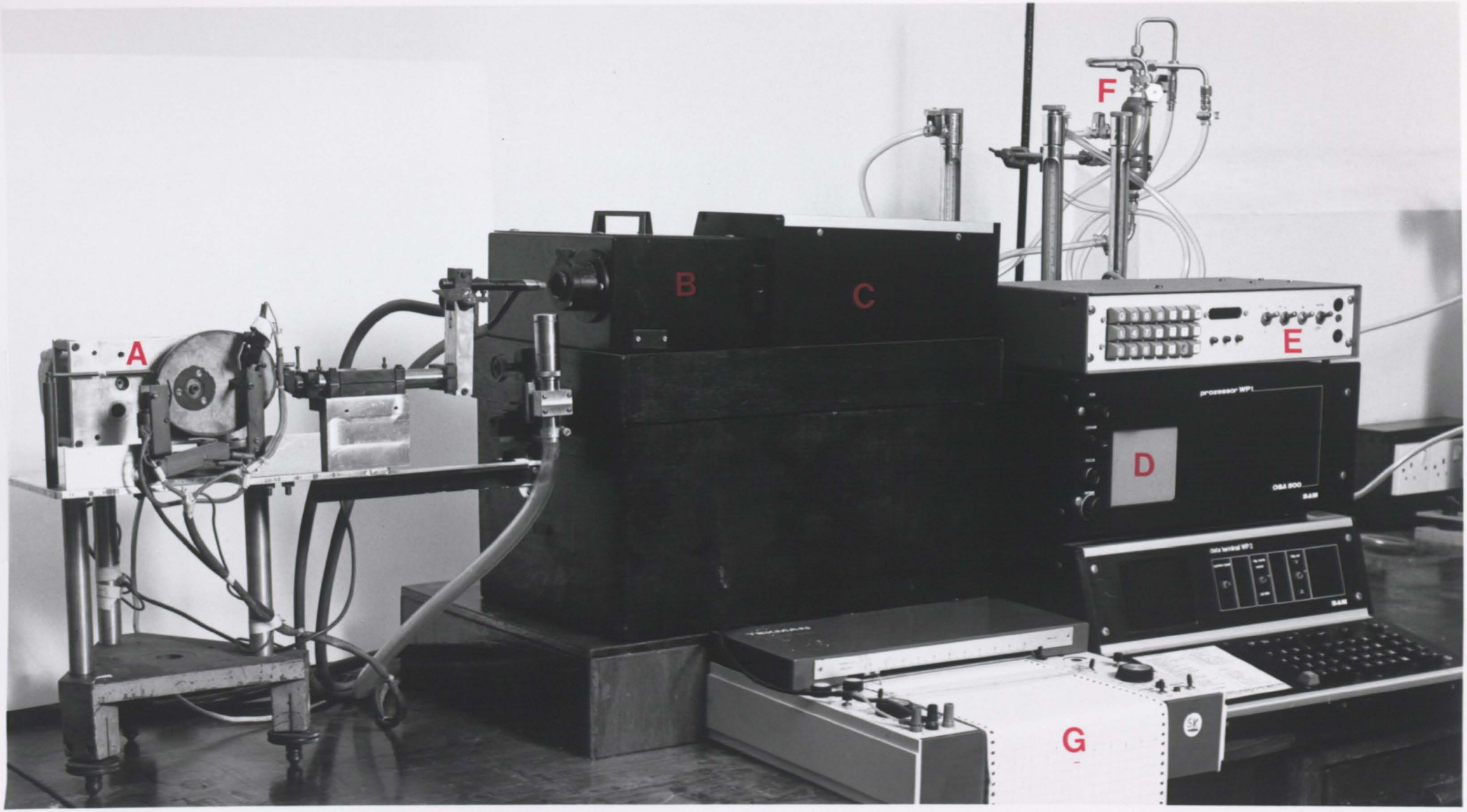
A
B
C
D
E
F
G
prozessor WP1
OSA 800
Data terminal WP1

(A) Matrix introducing device.

(B) BM25 Monochromator.

(C) SIT Vidicon Camera.

(D) Optical Spectrum Analyser OSA 500.

(E) Microprocessor Controlled Timer.

(F) Gas Control Unit.

(G) Recorder.

Fig. 2.1 Candoluminescence apparatus assembly

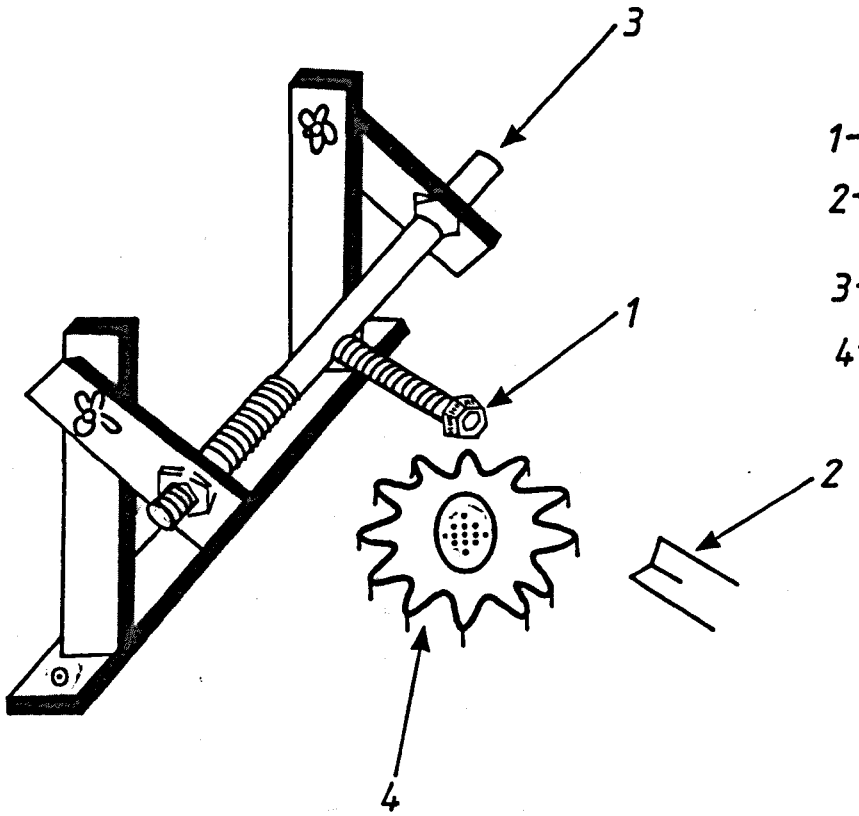

1- Matrix holder.
2- Collimator, leading to detection system.
3- Sample holder adjustment.
4- Burner head.

Fig. 2.2 Earlier sample holder.

disadvantage of using this sample.

Ranjitkar[44] developed a different type of sample holder shown in Fig. 2.3. By this device the activated matrix can be introduced quickly into the flame. Also it can be possible to adjust the matrix horizontally or vertically with respect to the flame. Matsuoka[48] used Ranjitkar's device with a shorter Allen screw to let the screw head rest on the bar of the socket, in order to eliminate the effect of slight fluctuations in the length of the Allen screw which could cause a variation of the candoluminescence intensity.

Matsuoka also built a new device which mechanically moved the cavity to place the matrix reproducibly at the wanted position in the flame. It was the first semi-automated device that lets the matrix enter the critical zone with the same velocity at each introduction. Fig. 2.4 shows this device. It consists of a motor (a) with a normal speed of 10 rpm which can be increased by the gear box (b) to 35 rpm. A cam (c) is fixed at the middle of the gear box. A rod of stainless steel (d), pushed by the cam as it rotates, is allowed to slide within the hole in the brass block (e). A piece of stainless steel guide rod (f) is connected in parallel to the main rod (d) by brass collars (g) in order to let rod (d) slide smoothly without shaking or rotation. The guide rod (f) is allowed to slide through a rectangular slot cut out of the brass block (e). A cam follower (h) is attached to one end of the rod (d) to ensure a steady and smooth contact with cam. A spring

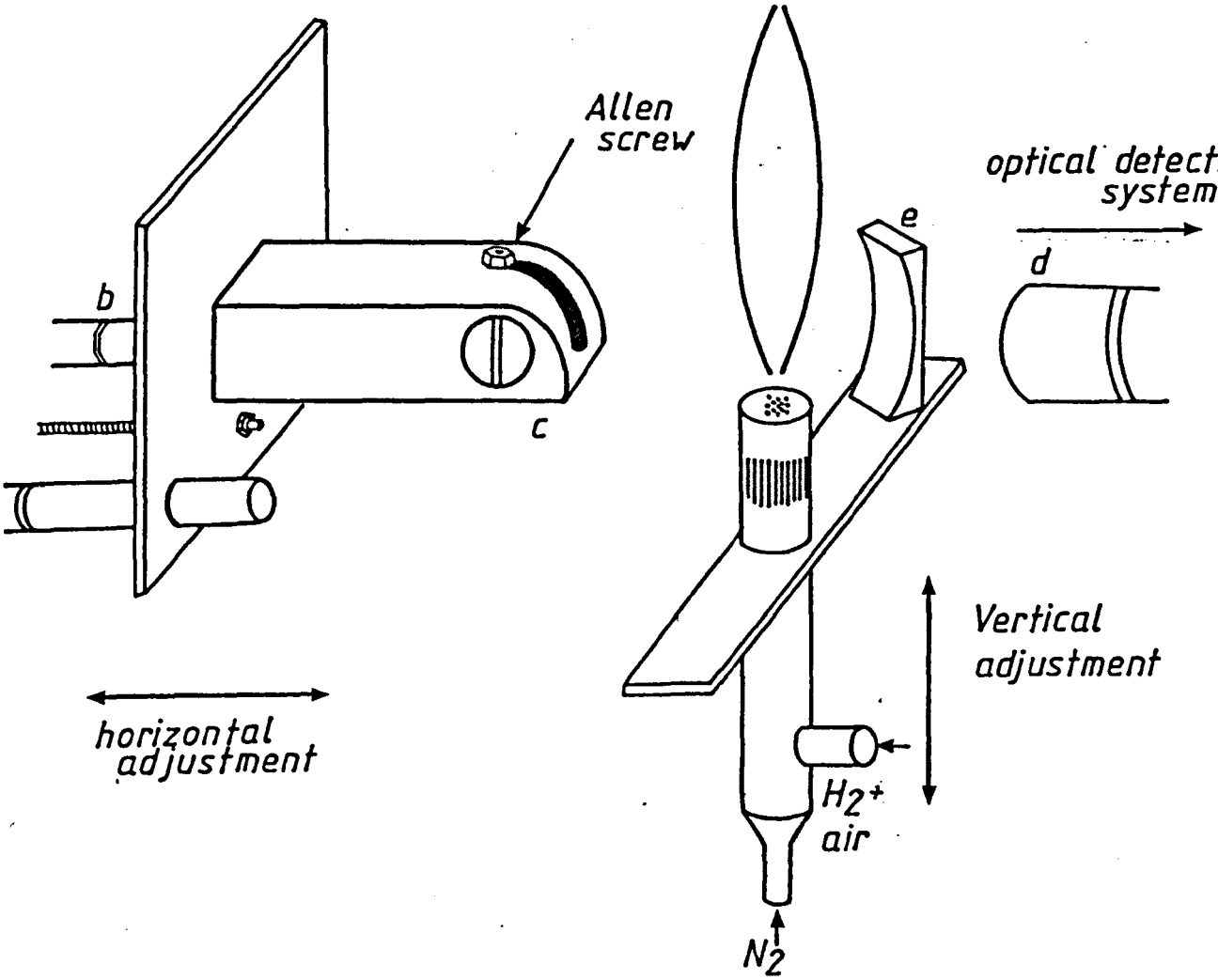

Fig. 2.3 Sample holder assembly used.

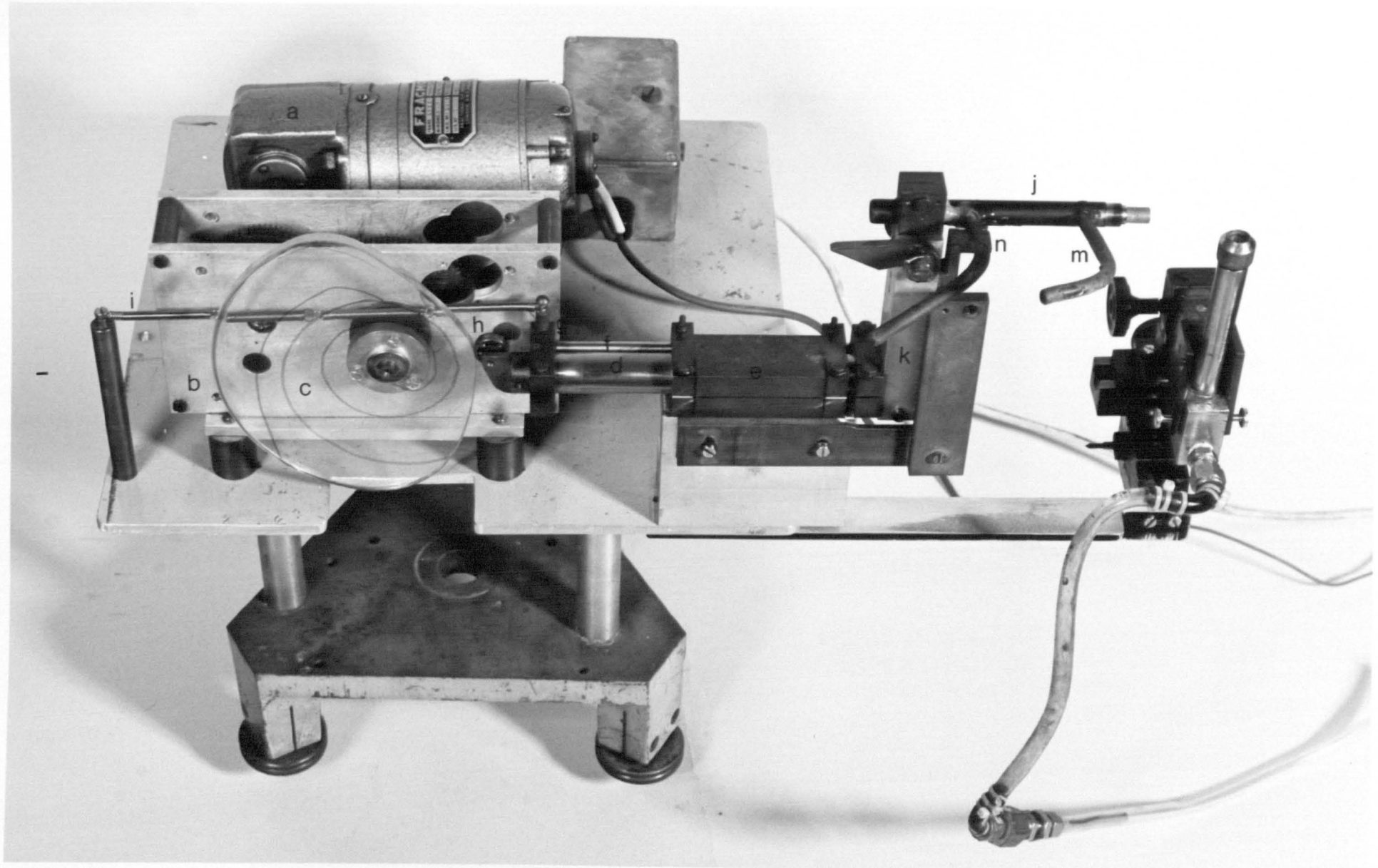

Fig. 2.4 Matrix Introducing Device.

mechanism (j) is used to pull back the cam, so that the cam follower can follow the rotating edge of the cam.

The cavity assembly consists of a stainless steel rod (j) which is connected to brass block (k) by a piece of pyrophyllite support (l) as shown in Fig. 2.5, (pyrophyllite is a soft natural stone which can be readily machined to any required shape). This piece of pyrophyllite was used to cut off heat transfer from the cavity assembly to the other parts of this device. The other end of rod (j) is slit to form a socket to accommodate a special cavity (i in Fig. 2.9). The rod (j) is drilled inside for a water cooling system; (m) and (n) are the water entrance and exit, respectively. Without this water cooling system, the cavity holder gets hotter during repeated introduction into the flame. This means that the initial temperature for the cavities will not be the same and this will lead to poor reproducibility of the candoluminescence emission. Plate (o) is used as a base for all the components of the device, which stands on adjustable legs (p). The matrix cavity can be lined up with the slit of the monochromator by adjusting these legs.

The cam which is used in this device is kidney-shaped. This shape gives a uniform acceleration, but with one side cut away to allow a quick withdrawal from the flame. The difference between the longest and the shortest radii of the cam is 4cm, which gives enough room to change the cavity when outside the flame (see Fig. 2.5 and Fig. 2.6).

The main disadvantage of Matsuoka's device is that the kidney-shaped cam offered only particular times inside and

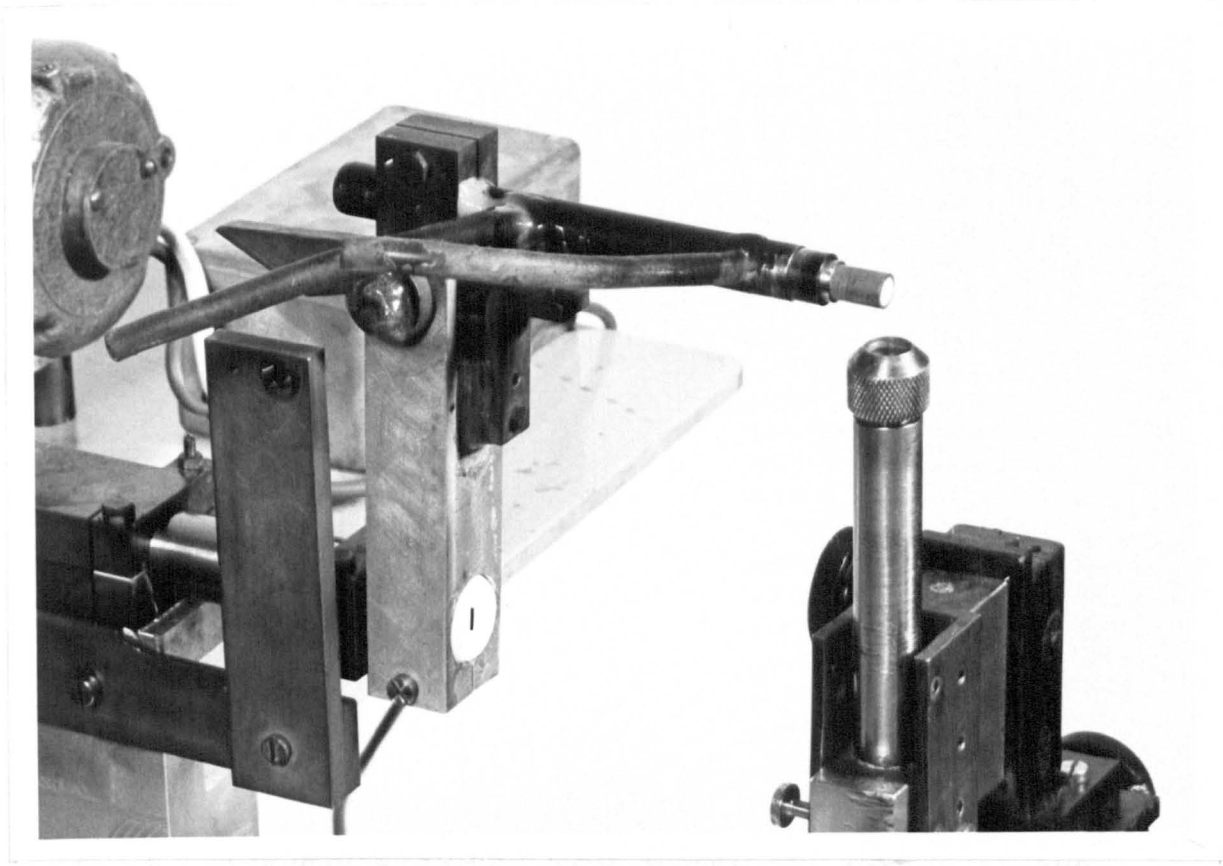

Fig. 2.5 The matrix inside the flame

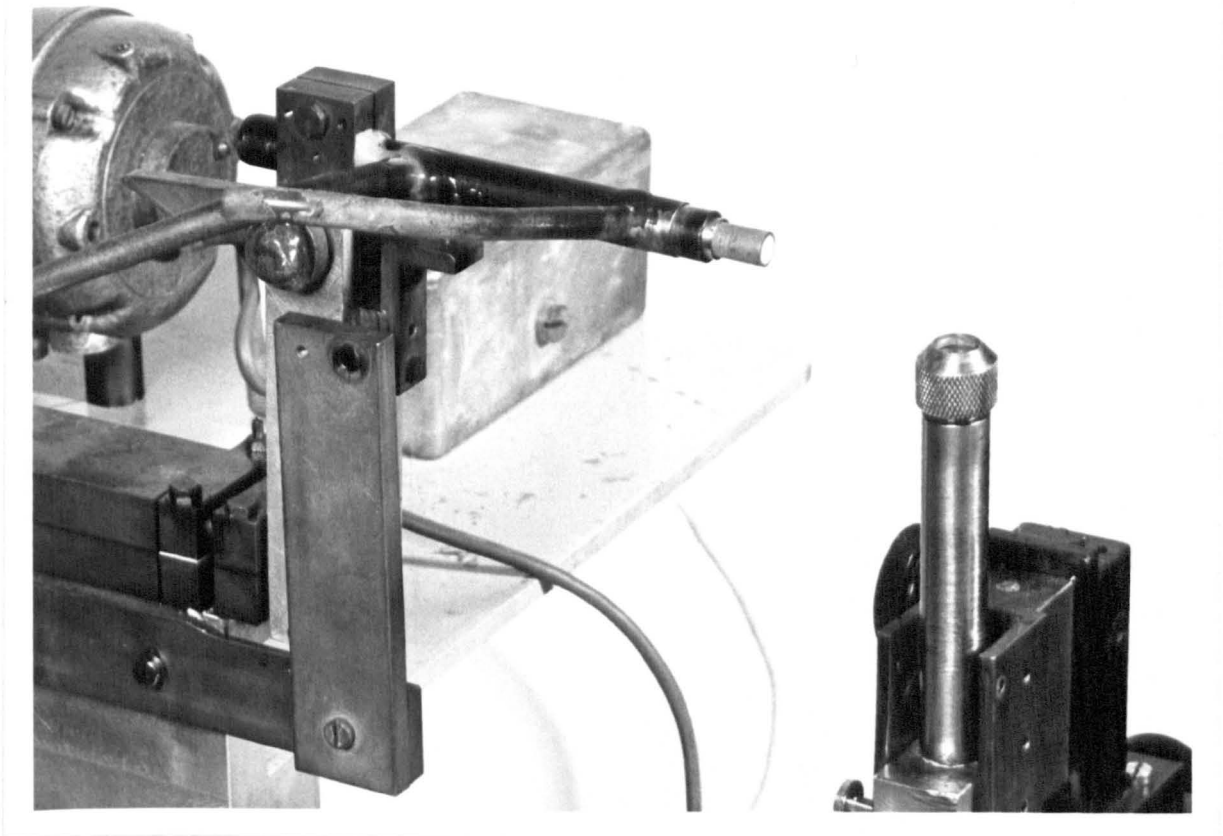

Fig. 2.6 The matrix outside the flame

outside the flame. When the matrix is introduced to the flame and left in the flame for 5 sec (for example) and removed from the flame to cool for 10 sec (for example), and then reintroduced to the flame these 5 sec and 10 sec periods are defined as preheating and cooling times, respectively. These two parameters should be optimized to give intense and reproducible candoluminescence emission. In order to change the preheating and cooling times it is necessary to use a differently shaped cam.

El-Hag[87] developed this device further in order to automate molecular emission cavity analysis (MECA). In order to overcome the disadvantages of Matsuoka's device, he used a new egg-shaped cam with a mounted peg on it and four microswitches connected to a microprocessor controlled timer to provide precise and variable preheating and cooling times. Fig. 2.7 shows the layout of the microswitches around the cam.

In this developed device the MECA cavity tilts from the vertical position to the horizontal position in four stages, where the vertical stage was used for the injection of solution into the cavity by an automatic sample dispenser. The other two stages were controlled by the two microswitches (M_2 and M_3 in Fig. 2.7) which were added to control the cooling time. The last stage is the horizontal one which is the optimum position of the cavity inside the flame. The backwards movement of the cavity is done in a similar reverse fashion.

This device was modified to suit candoluminescence

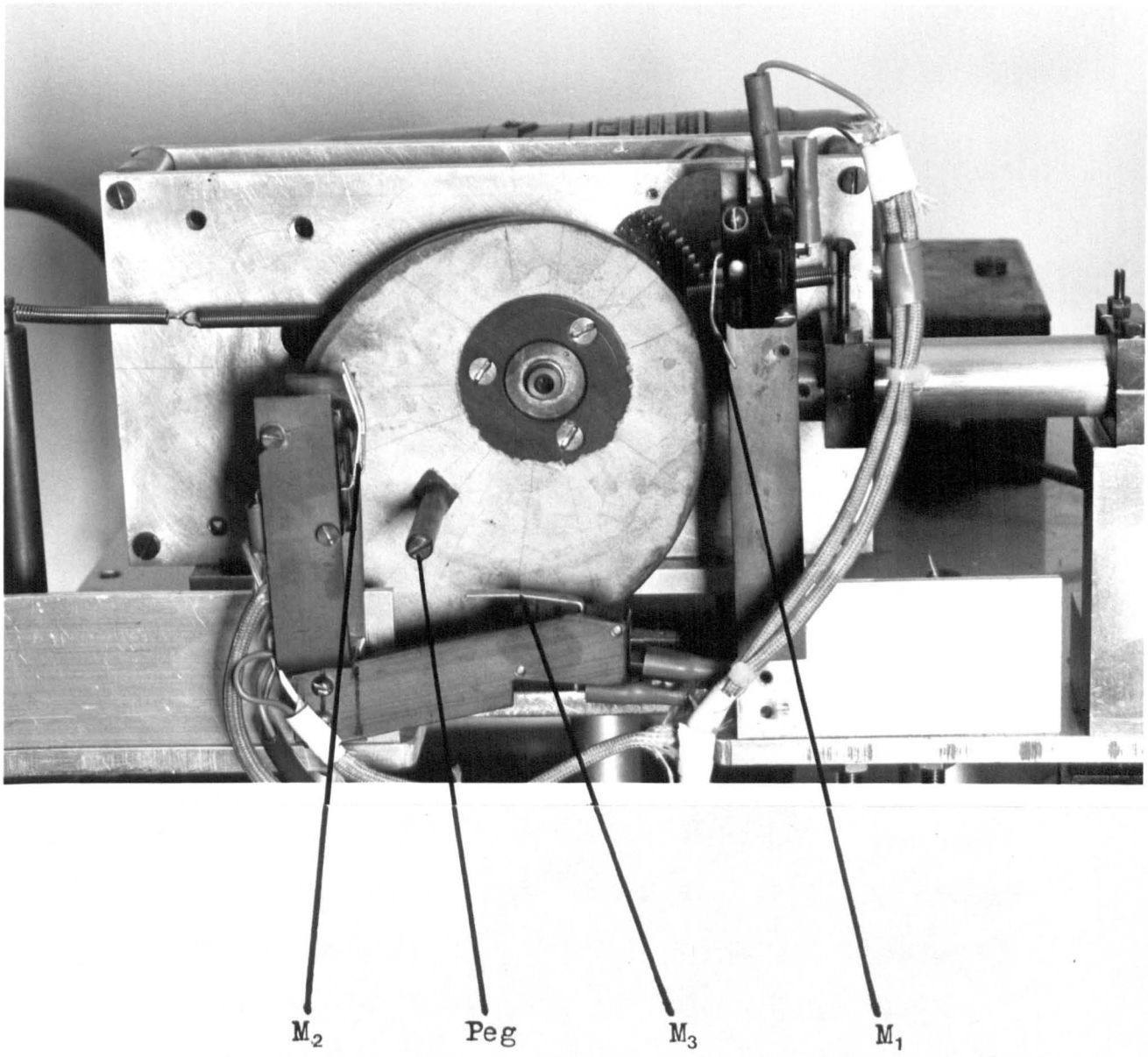

Fig. 2.7 The layout of the microswitches around the cam.

M = microswitch

measurements where the matrix holder is required to move only horizontally into two positions, inside and outside the flame, as shown in Fig. 2.5 and Fig. 2.6. Two micro-switches only are fixed around the cam and are closed by the action of the peg during cam rotation. The cavity assembly was changed, and Matsuoka's cavity assembly was used which is shown in Fig. 2.3. The cam is egg-shaped. The longest radius is 7.5cm and the shortest radii of the cam is 4.5cm. This provides enough room to change the matrix when it is out of the flame.

2.1.2 The Microprocessor Controlled Timer

2.1.2.1 Description

The Microprocessor controlled timer (E in Fig. 2.1) was used to automate the matrix introduction device. The unit is housed in a steel instrument case (43 x 20 x 9cm) with an aluminium front panel. All the controls are front panel mounted. As Fig. 2.8 shows, the circuit diagram of the basic components in the control unit include an INS 8060N monolithic, 8-bit, N-channel microprocessor with address capability of 64k. It has direct memory access (IMA), two sense inputs, multiprocessor, bus logic and a serial input/output port. Instructions are capable of operating multi-addressing modes of the immediate program counter. The INS 8060N clock drive is driven from a quartz crystal oscillator.

The system operating program is stored in an N825131N

A = INS8060N

B = INS8154N

C — F = ROM

G, H = RAM

I = Keyboard

J = Power supply unit

K = Quartz crystal

I/P = Interface board

O/P = Output interface board

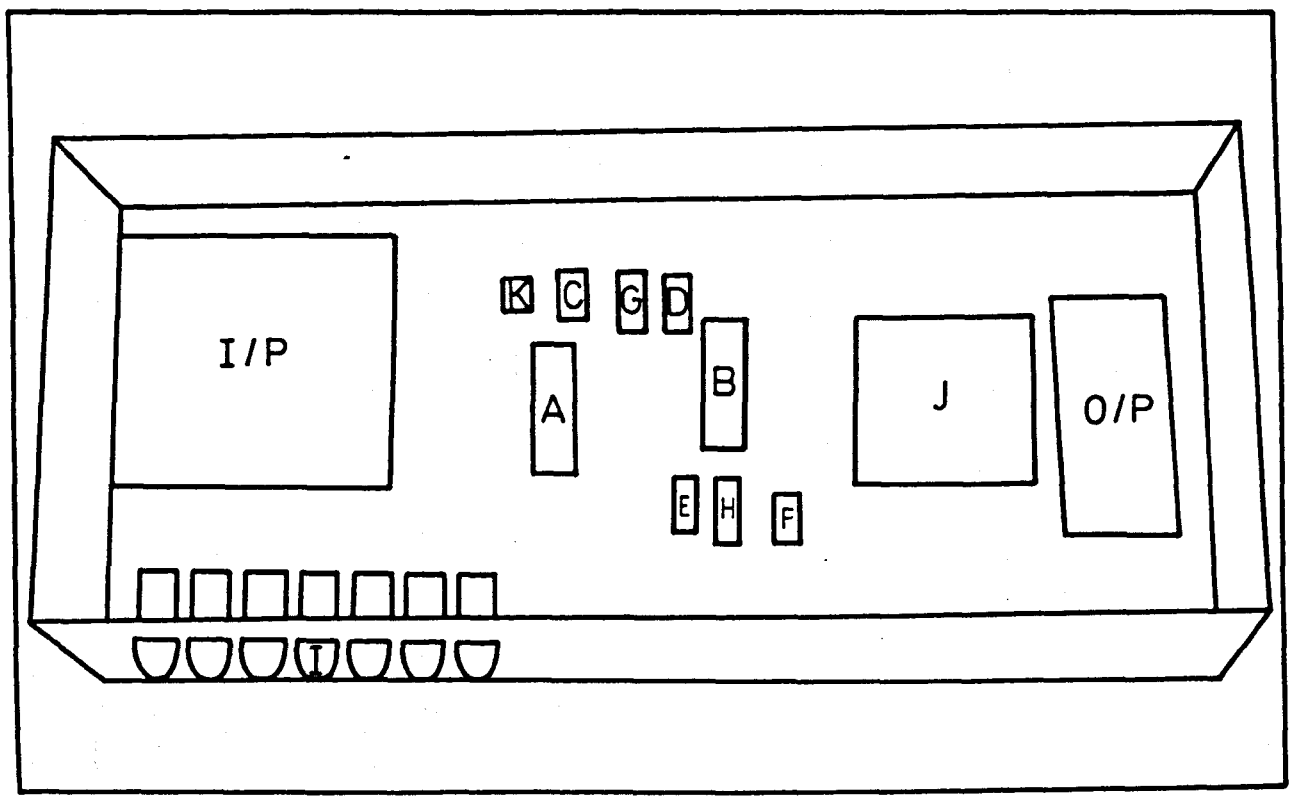

Fig. 2.8 The circuit diagram of the microprocessor controlled timer.

non-volatile read-only memory (ROM). The times T_1 , T_2 which control the residence time of the cavity in the flame (T_1) and the cooling time (T_2) are stored in a SYP211N volatile random access memory (RAM). Hence these times require setting after a mains power interruption. The timer has also an INS 8154N programmable input/output on-board ROM. The output of the microprocessor unit is interfaced to the motor using a triac-based TTL/240v optocouple unit.

2.1.2.2 Principles of Operation

The principles of operation can be summarized as below:-

(a) The a.c. power to the motor is supplied under the control of the microprocessor.

(b) The motor rotates the cam, until it closes the microswitch (e.g. M_1) in Fig. 2.7 by the action of the peg.

(c) The motor stops and simultaneously the clock starts and runs in the microprocessor unit for the required times (put into the microprocessor by a special program). The motor starts to run when the clock has reached the required time.

The programming of the unit is achieved by entering the selected times. In this way the residence times of the matrix in the flame and outside the flame can be adjusted and controlled. Verification of the set times is achieved

by a front-panel mounted LED display which also indicates the elapsed real time during unit operation.

The programming process is started by "start address OBD8". The location address is shown in Table 2.1. To change or set any period of time the following program must be carried out:

(1) Press R (Rest);

(2) Enter location address (e.g. CEDA, from Table 2.1);

(3) Press T (term);

(4) Enter digit required;

(5) Press M to move to next address;

(6) Press R, CBD8-G (go)

The complete program can be summarized as:

R - EDA - T - Periods - R - CBD8 - G

For correct operation none of the two time starts should contain 8 zeros.

Time (s)	T_1	T_2
0.1	OEDA	OEEE
1	OEDB	OEEF
10	OEDC	OEF0
10^2	OEDD	OEF1
10^3	OEDE	OEF2
10^4	OEDF	OEF3
10^5	OEE0	OEF4
10^6	OEE1	OEF5

Table 2.1 Location addresses of the three periods of time in the microprocessor controlled timer.

The system operation can be explained by the following hypothetical example. If Tc = real clock time, Ty = T_1 or T_2 . The cam of the moveable matrix introducing device operates the two microswitches (M_1 and M_2) , the outputs of which are encoded and fed to the two sense inputs of the INS 8060N microprocessor thus enabling self synchronization. If:

(a) the times, T_1 and T_2 , are set and ;

(b) the motor is running, the following sequence of events will take place.

(1) After a time Tx a microswitch (M_1 or M_2) operates.

(2) The motor stops and simultaneously the clock starts and runs until Tc = Ty.

(3) The motor starts and the clock resets to zero.

(4) After time (time travelled by the peg on the cam between one microswitch and the other) the next microswitch operates etc.

2.1.3 The Flame

A hydrogen-air flame is usually used for candoluminescence. Nitrogen is sometimes added to make the flame more rigid, cooler and to make the flame almost colourless (very slightly blue) by removing any yellow colour possibly produced by sodium from dust impurities. Helium or argon can be used instead of nitrogen but Ranjitkar[44] reported that there was only a little difference in the emission intensity produced when helium or nitrogen was used. Nitrogen is preferred because it is

more easily available and cheaper so that was used in the present work.

The flow rates of hydrogen, nitrogen and air were metered by CPE series flow tubes from Glass Precision Engineering Ltd., Mark Road, Hemel Hempstead, Herts. with maximum flow rates 7 l min^{-1}, 12 l min^{-1} and 15 l min^{-1} for air, hydrogen and nitrogen, respectively.

Hydrogen and nitrogen gases are supplied from cylinders and the air is supplied from the air line in the laboratory. These gases were premixed in a steel cross union connected to a mixing chamber (340cm), which is connected to the burner.

The burner was a hollow steel tube 15.5cm long, 1.8cm head diameter and containing thirteen small holes of about 1mm diameter arranged symmetrically. This burner was fixed by two screws to a piece of steel which attached to a horizontal adjustment and a vertical adjustment. This allowed the vertical distance between the head of the burner and the centre of the matrix, the vertical distance, to be changed. The distance which the matrix surface is inserted into the flame is called the horizontal distance. These parameters as well as the angle which the matrix inserted in the flame should be optimized to obtain the most intensifier and reproducible candoluminescence emission.

2.1.4 The BM25 Monochromator

An Ebert-mounting monochromator (EDT Research,

14 Trading Estate Road, London) was used. The emission produced from the activated matrix in the hydrogen based flame was focussed, by the adjustment of the adjustable legs (p in Fig. 2.4), on the 0.1mm slit of this monochromator.

The monochromator was bolted onto the silicon intensified target (SIT) vidicon camera at the exit slit.

2.1.5 The SIT Vidicon Camera

The SIT Vidicon Camera (B&M Spectronik GmbH Co. KG, Boschstr. 8,8031 Puchheim, Federal Republic of Germany) was used as a detector. The main characteristics of the SIT are:

Spectral range	340 - 850 nm
Sensitivity	15 photons per count per channel and per scan
Dark current	2nA
Dynamic Range	1-65535
Target diameter	16mm

2.1.6 The Ortical Spectrum Analyser (OSA 500)

The CSA 500 (B&M Spectronik GmbH Co. KG, Boschstr. 8,8031 Puchheim, Federal Republic of Germany) forms the central control and data processing units of the B&M measuring device and is referred to as the console.

The console controls and steers all functional processes of the vidicon camera, processes the measurement signals provided by the detector and generates the digital

or analog signals required by external equipment (xy recorder, printer, computer etc.). The console has 45 fixed programs, which can be called from the keyboard. The accumulation and subtraction programs are the most useful. Accumulation is always used in this study, over a preselected number of scans; the spectrum is automatically displayed on the screen during and after accumulation. The subtraction program is another useful program, which allows subtraction of one spectrum from the another, e.g. subtraction of a blank spectrum.

2.2 The Matrix

The candoluminescence emission depends on the matrix quality and quantity. Since the candoluminescence technique is highly sensitive, great importance must be attached to the purity of the matrix material. Pure oxides (CaO, SrO), a pure hydroxide $Mg(OH)_2$, or mixed materials such as SrO with $CaSO_4$ and CaO with $CaSO_4$, were used as matrix materials, the mixed materials making the matrix more rigid in the flame[47,48]. Also coated matrices were used[50], which the pure rare earth oxides (Y_2O_3 , Gd_2O_3 , La_2O_3 , Lu_2O_3) were coated on a $CaO/CaSO_4$ rod.

Matricesprepared by the former way was done by filling the matrix material into the head of the Allen screw. The material was first mixed with double distilled water, until it was sufficiently moist to make a suitable paste[47]. The matrix material was transferred by clean spatula into the cavity (the head of an Allen screw, hexagonal-shaped; the

hexagon had a side of about 2mm, and 5.2mm area, which represents the matrix area). A fitting Allen screw was used to press the matrix material into the cavity. Excess of material was added, and later shaved off flat by a razor blade, when the matrix had dried.

This manual method of matrix making can be criticized because:

(1) Cavities do not contain the same amount of matrix material.
(2) The pressure which has been used is not the same for all matrices.
(3) It is not easy to get a smooth and flat matrix surface.
(4) Some of the matrices have a gap between the matrix material and the holder.

In order to overcome these difficulties, Matsuoka[48] made a device based on a press for preparation of infra red pellets. Fig. 2.9 shows this device which was used in this work. Special cavities (a in Fig. 2.9) were used. They are hollow stainless steel tubes (12mm in length, 7mm o.d and 5mm i.d). Steel disc (b) is a support for the cavities, which has six holes to accommodate cavities. Plate (c) is of hardened stainless steel, which is placed at the bottom and on to which the matrix material is pressed down. Plate (d) is placed at the top, which has six holes to guide the plungers (e). The plungers press the matrix material, which is contained in the cavities, down to the surface of the plate (c). All the plates are lined up and fixed by the screws (f).

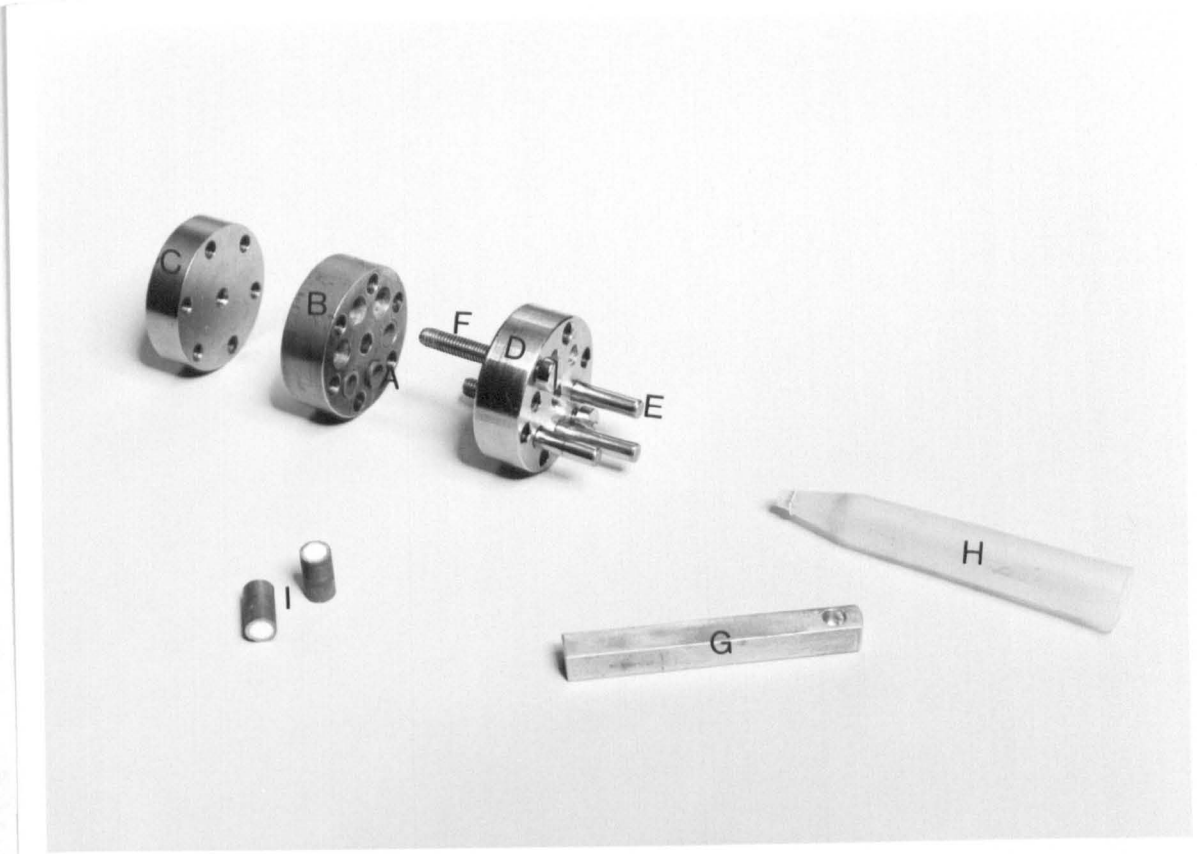

Fig. 2.9 Matrix making device

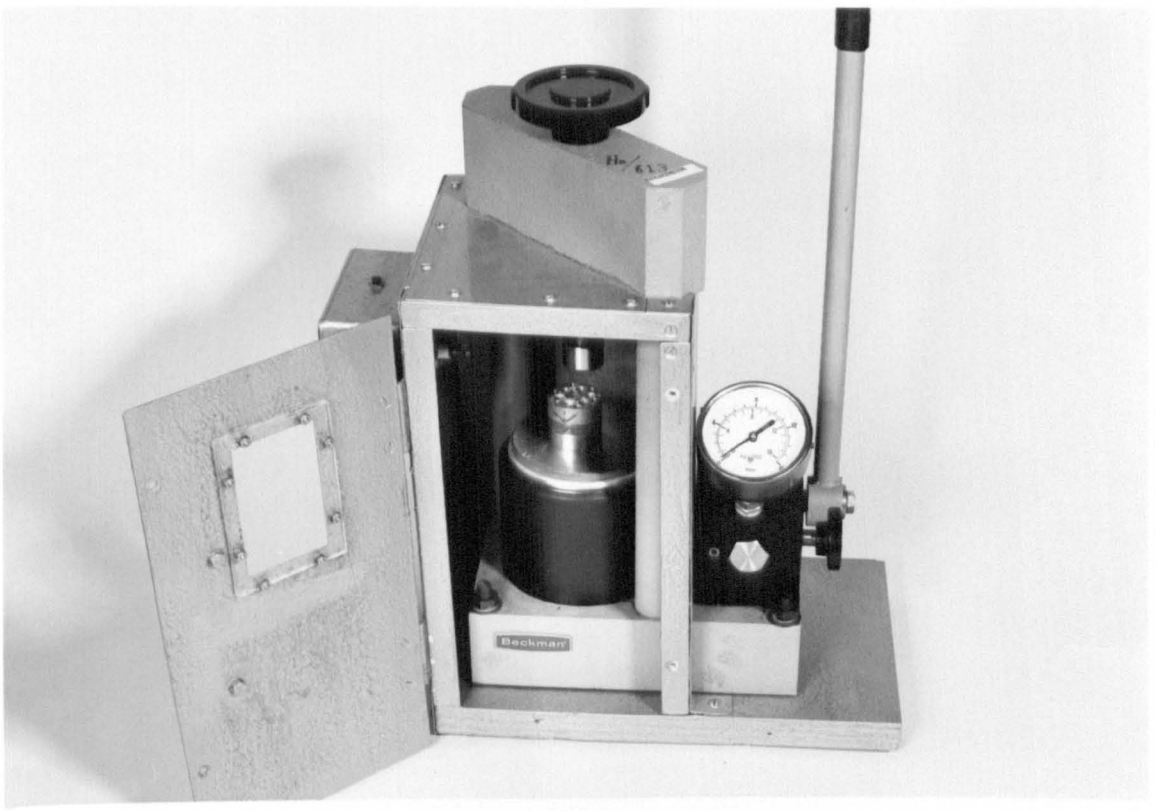

Fig. 2.10 Backman Type P16 pressing machine

A constant amount of the matrix material is taken by the concave dent which was made on the surface of the sampler (g), and is added to the cavity through a plastic tube (h). The same amount must be added to each of the six cavities. The matrix material is now on the surface of the bottom plate (c) and inside the cavities.

Finally, six plungers are inserted through the guide holes of plate (d) and pressed by the pressing machine for a certain time (usually 5 min.). In this manner, six matrices are made at the same time (the finish is shown by i), which are rigid enough and have extremely uniform, flat and smooth surfaces.

The pressing machine used is a Beckman Type-P16 (hand operated) press whose rated maximum pressure is 16 tons (Fig. 2.10).

2.3 Wavelength Calibration of the OSA Screen

The OSA screen shows a spectral range which is a function of the grating. This range is not easy to predict so three methods were used to measure the spectral range and to calibrate the wavelength of the OSA screen.

2.3.1 Neon and Mercury Discharge Tubes

2.3.1A Neon Discharge Tube

The neon discharge tube has a complex spectrum, which is well defined[88]. It contains many lines in the visible region of interest to this project. The neon discharge

tube was placed at the entrance of the monochromator slit. Fig. 2.11 shows the neon spectrum obtained in the range 578-646 nm.

2.3.1B Mercury Discharge Tube

The spectrum of mercury has well-spaced lines in the visible region, at 579.1, 577.0, 546.1, 435.8 and 404 nm. The spectrum in the range 526-594 nm, was displayed on the OAS screen as for the neon. Fig. 2.12 shows this spectrum.

2.3.2 Helium-Neon Laser

A helium-neon laser (Scientifica-Cook Ltd.,) was used to calibrate the OSA screen. This laser gives a resonance line at 633 nm. This laser was also used to calibrate the monochromator because it is easy to operate and gives only the 633 nm line.

2.3.3 The Atomic Emission of The Alkali Metals (Na and K)

The atomic emission generated from sodium or potassium solutions when injected onto a calcium oxide matrix surface and introduced to the hydrogen flame can be used to calibrate the wavelength of the OSA screen. Sodium gives a doublet at 589.0 nm and potassium gives lines at 766.5 nm and 769.9 nm. Fig. 2.13 shows a sodium spectrum in the range 555-623 nm and Fig. 2.14 shows a potassium spectrum in the range 732-800 nm.

The spectral range, displayed on the OSA screen was

found to be 67.6 nm, held in 499 channels so that each nm corresponded to 7.4 channels.

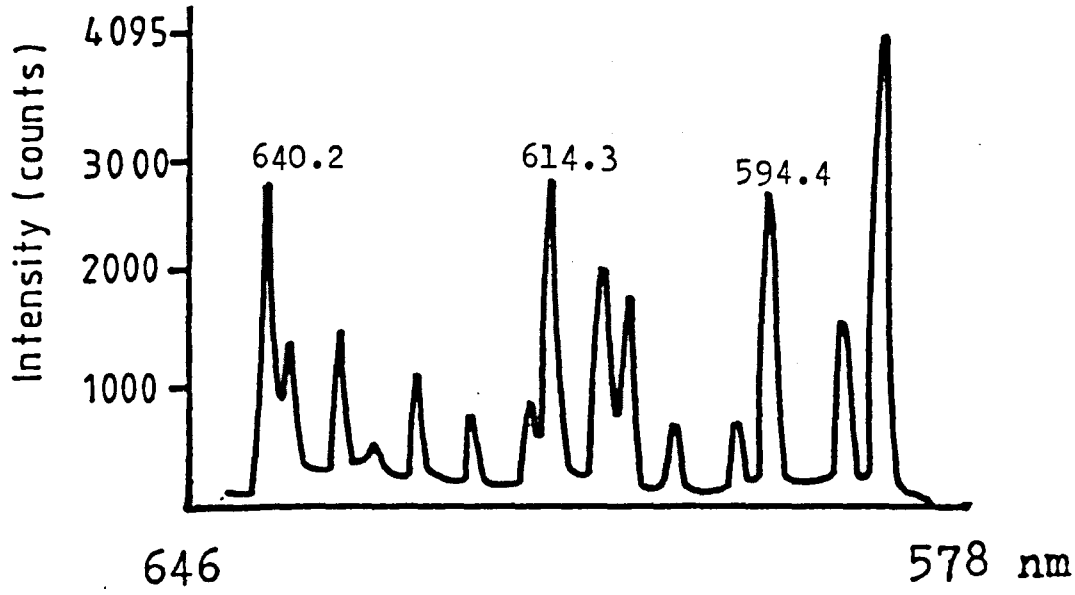

Fig. 2.11 Neon spectrum in the range 578 - 646 nm.

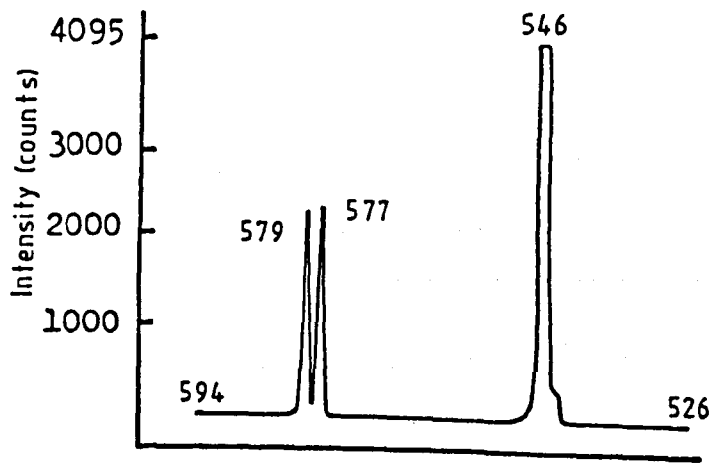

Fig. 2.12 Mercury spectrum in the range 526 - 594 nm.

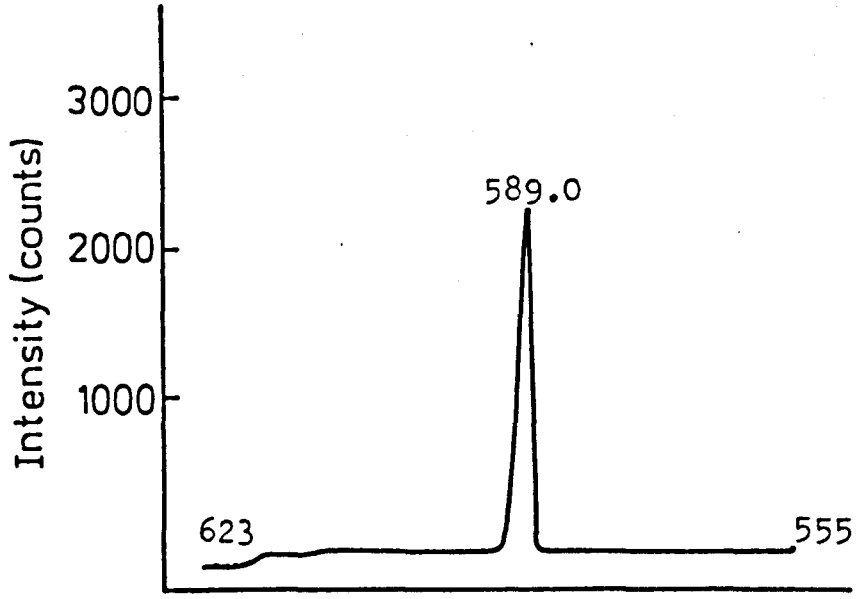

Fig. 2.13 Sodium spectrum in the range 555 - 623 nm.

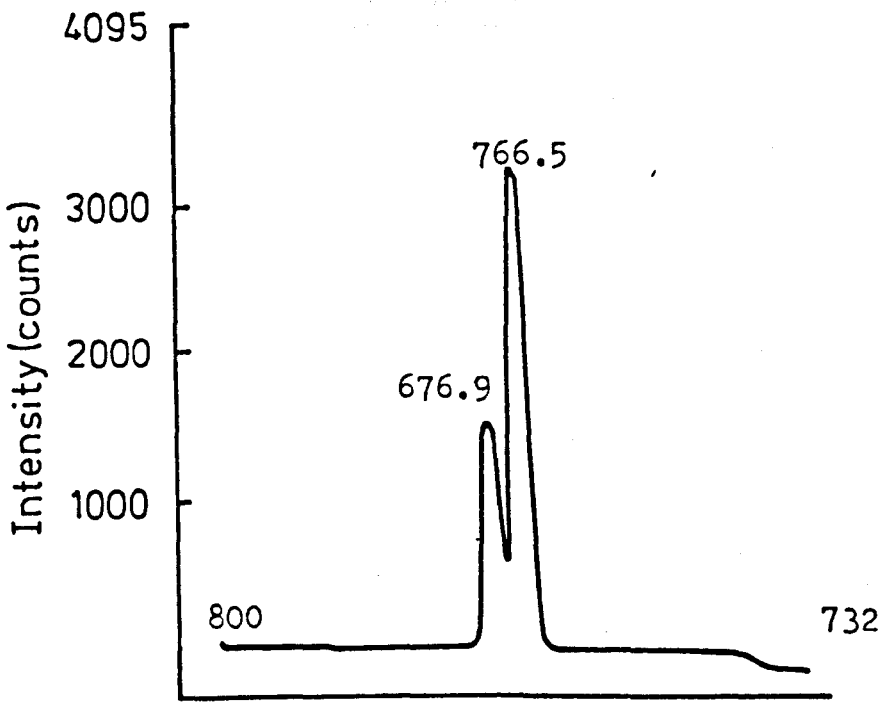

Fig. 2.14 Potassium spectrum in the range 732 - 800 nm.

CHAPTER THREE

CANDOLUMINESCENCE OF TERBIUM

IN

DIFFERENT MATRICES

Candoluminescence of Terbium in Different Matrices

3.1 Preliminary Study

Terbium was known for many years to emit a yellow-green emission in a calcium oxide matrix. The candoluminescence of terbium was first used for analytical purposes as such in 1970 by Sweet et al.[33], who identified the spectra and reported a concentration dependence of the intensity between 27 and 11 200 ng l^{-1} terbium in doped yttrium oxide and lutetium oxide.

In 1974 Ranjitkar[44] used the deposition technique to develop a method for the determination of 1-25 ng of terbium at 550 nm in a CaO matrix, using the edge of a hydrogen flame. Karpel[45] briefly examined the stimulation of terbium candoluminescence in calcium tungstate and found that terbium gives a weak green emission in pre-heated calcium tungstate. Nasser[47] studied the candoluminescence emission of terbium in $Ca(OH)_2$, $Mg(OH)_2$, $Sr(OH)_2$ and CaF_2 matrices. The calibration graphs were found to be linear over different ranges, up to 60 ng in some cases, with 0.05-2 ng detection limits and 5.0-8.0% relative standard deviations. He used 545 nm as the wavelength for analytical purposes.

Matsuoka[48], in his survey for activators for the SrO : $CaSO_4$ matrix, found that terbium gives a weak green emission at 540 nm.

In Basrah University, Kassir et al.[50] and Al-Muaibed[51], using a rod technique, studied the candoluminescence of terbium in five different coated matrices, Y_2O_3 , Gd_2O_3 ,

ThO_2 , La_2O_3 and $CaSiO_3$ coated on CaC-CaSO rods. Candoluminescence spectra of terbium in these matrices were recorded which were the same in all matrices. There were only two peaks, at 490 nm and 550 nm. The former was used for analytical measurements. The calibration graphs were linear over different ranges up to 90 ng in the La_2O_3 matrix, with 0.2-0.3 ng detection limits and 2.8-3.2% relative standard deviation.

In the present work, stimulation of candoluminescence of terbium in a new matrix (MgO) will be described. In addition, the determination of terbium by its candoluminescence in Y_2O_3 , Gd_2O_3 , La_2O_3 and Lu_2O_3 coated on CaO matrices, will also be described. The work is also aimed at extending the range of terbium determination and to improve the reproducibility, by using the new matrix making device and the automatic matrix introducing device.

3.2 Experimental

3.2.1 Reagents and Chemicals

A 1000 $\mu g\ ml^{-1}$ terbium solution was prepared by dissolving 0.1176 g of 99.9% terbium oxide (Tb_2O_3 , Koch-Light Laboratories) in the minimum (3.5 ml) of AnalaR concentrated nitric acid by gentle warming and diluting to exactly 100 ml with water.

AnalaR MgO (BDH) was used as the matrix material. All other reagents were of analytical reagent grade, except for:

(a) La_2O_3 , Gd_2O_3 , Lu_2O_3 and Y_2O_3 , 99.9% , 99.999% and 99.9999% were obtained from different companies (Koch-Light, BDH, Sigma and Ventron Corporation);

(b) The 1000 $\mu g\ ml^{-1}$ lanthanide ion solutions used in the interference study were prepared by dissolving the required amount of the hydrated lanthanide nitrate (99.9%), obtained from different companies (Koch-Light, BDH, Sigma, Ventron Corporation) in 100 ml of the deionised water which was used throughout.

3.3 Apparatus

The complete candoluminescence instrument is shown in Fig. 2.1. It consists of the following main components :-

(a) matrix introducing device,
(b) the gas control unit,
(c) the BM25 monochromator,
(d) the SIT vidicon camera,
(e) the optical spectrum analyser OSA500,
(f) the Tekman Labwriter TE-200 recorder.

The apparatus was described in Chapter 2.

3.4 Experimental Parameters and Optimization

3.4.1 Matrix Preparation

A set of matrices of MgO and rare earths (Y_2O_3 , La_2O_3 , Gd_2O_3 and Lu_2O_3) coated on CaO was prepared. The procedure described in section 2.5 was used for MgO. For the coated matrices a constant amount of rare earth oxide was taken by

a small sampler (g in Fig. 2.7) and added to the cavity first in order that the final matrix surface is covered with rare earth oxides.

The amount of MgO and CaO and the pressure applied for each matrix were 2 portions by the sampler and 2 tons per sq. in. (for 5 min.) as recommended by Matsuoka[48] who found no significant effect of pressure or amount of matrix on the candoluminescence emission of manganese in CaO.

3.4.2 Injection Technique

There are three techniques of introducing the activator ion into the matrix, deposition, pre-mixing and coprecipitation. In the last two techniques the activator ion is added to the matrix material as a powder or solution during the matrix preparation. These two techniques gave very irreproducible results, e.g. pre-mixing gave 10-210% R.S.D.[47], for terbium intensity measurement. In the deposition method 1 µl of activator solution was injected onto the matrix surface. The sensitivity and reproducibility of this simple method depends on the porosity of the matrix[44,47].

A direct deposition method was applied throughout the present work, 1-µl of terbium solutions being deposited onto the centre of freshly prepared MgO or rare earth oxides coated on CaO matrices. This volume was used because it has been reported to give good reproducibility[48], for manganese intensity measurements in a CaO matrix.

3.4.3 Initial Survey of Activators for MgO and Coated Matrices

All lanthanide ions (except promethium) were tested in MgO to see whether or not they are useful activators in these matrices; 1 μl of a 50 μg ml^{-1} solution of each lanthanide nitrate (including Tb_2O_3 dissolved in nitric acid was used) was injected onto the MgO matrix and introduced into a hydrogen flame.

Only Tb gave a strong green emission. Ce, Pr, Sm, Eu and Er, which were already known as activators in other matrices (see Table 1.7) gave red emissions with various intensities, as did the matrix itself when introduced into the flame for more than 30 sec. This red matrix emission reaches a dull red glow after 60 sec. All other lanthanide ions showed no candoluminescence characteristics before the matrix itself gave a red emission.

The rare earth coated matrices, prepared from 99.9% pure material, themselves gave emissions when introduced into the hydrogen flame, owing to the presence of impurities of other lanthanide ions. La_2O_3 and Gd_2O_3 coatings gave an orange-red emission and Y_2O_3 and Lu_2O_3 gave a green emission. When 99.999% or 99.9999% pure oxides were used, a small background (1-8mV) was still obtained, which compared with the 40mV signal from 20 ng of Tb in a Gd_2O_3 - coated matrix. The background should be subtracted electronically.

As it had been reported that Tb and Eu give candoluminescence in rare earth oxide matrices[33,50,51], whereas no other lanthanide activators appeared to emit in

these matrices[34], these two elements were investigated in detail, as described in this and the next chapter. MgO also was studied as a matrix for candoluminescence emission of Tb, as described in this chapter.

3.4.4 Spectra

The SIT camera was used for instant detection of a 68 nm section of the spectrum of Tb luminescence, thus allowing spectra to be measured rapidly under normal candoluminescence conditions. The spectra are more accurate and realistic than those obtained by tracing the Tb spectra point by point, scanning using a photomultiplier detector[50,51] or recording on a photographic plate[33,34].

Terbium gives a strong green emission in MgO and rare earth oxide-coated matrices (Y_2O_3 , La_2O_3 , Gd_2O_3 and Lu_2O_3), with spectra comprising two peaks, at 541 nm and 532 nm, as shown in Fig. 3.1. The spectral range covered, 507- 575nm, was selected in order to exclude sodium atomic emission at 589 nm, which was always present when the flame was in operation.

The band at 541 nm, also noted by others[33], was the more intense and was used for analytical purposes.

The spectrum of the hydrogen flame should contain besides the sodium D-line at 589 nm an OH emission band around 300 nm[44-51]. The spectral range of the SIT camera, however, is 340-850 nm so that the OH band could not be recorded in the first order.

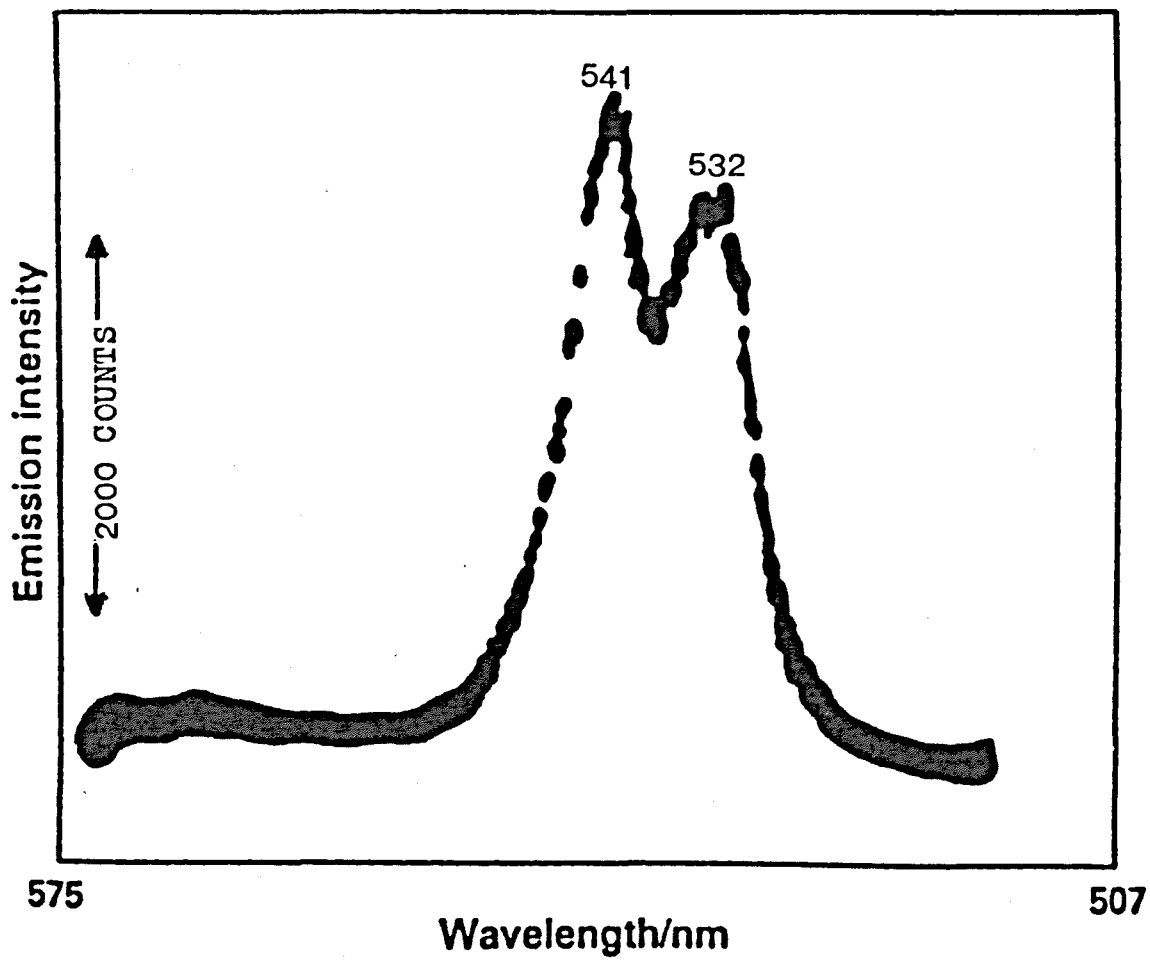

Fig. 3.1 Terbium spectrum in the range of 507 - 575 nm.

3.4.5 The Characteristics of Terbium Candoluminescence Emission

When 1 µl of 50 µg ml^{-1} terbium solution was injected onto the MgO matrix and inserted in the edge of a hydrogen flame, a very weak blue emission appeared. This was due to the MgO matrix itself and disappeared after 3 s . A strong green emission from the terbium then appeared and reached its maximum after 8 s . This emission largely disappeared within 30 s , as shown in Fig. 3.2.

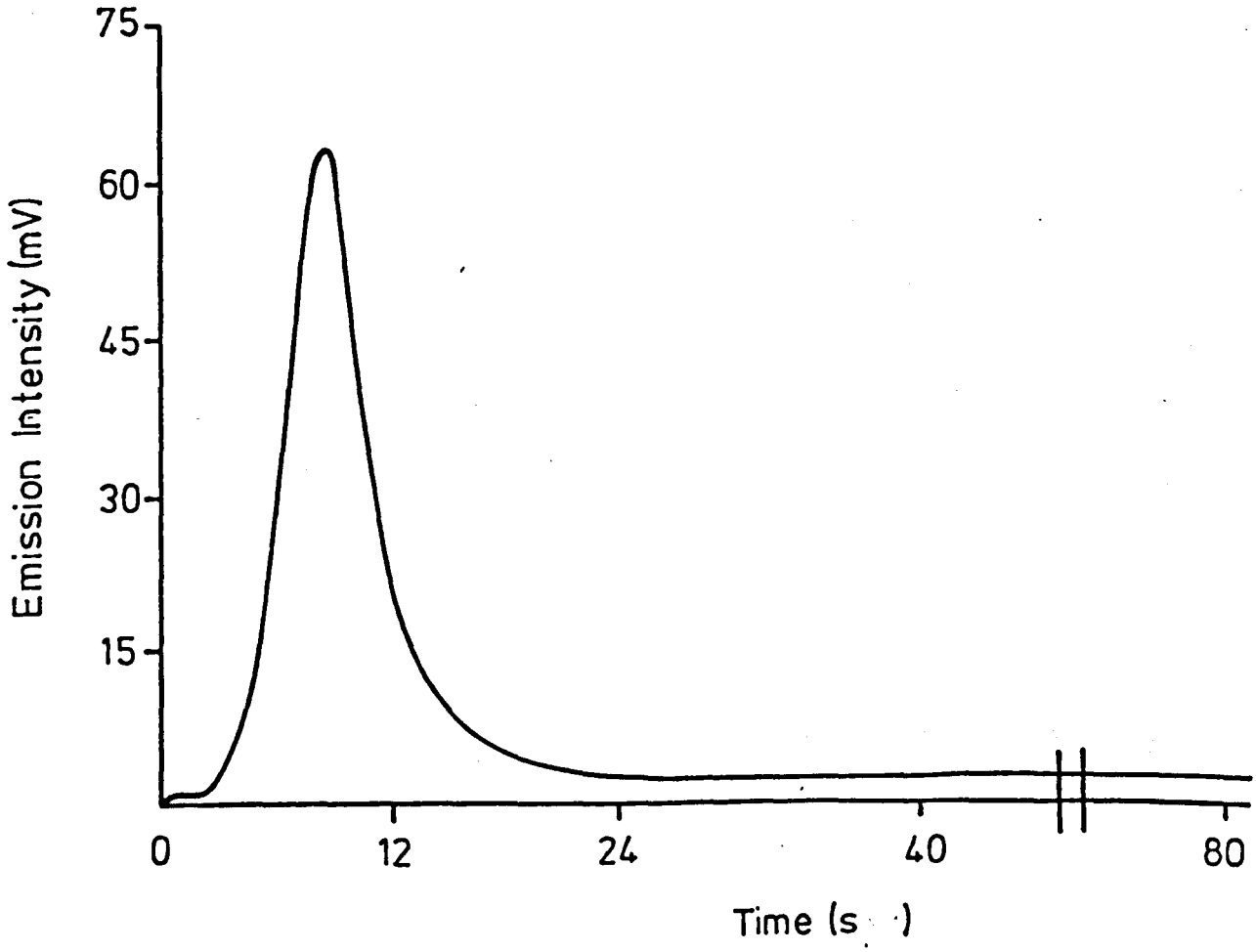

Fig. 3.2 Change in Tb (50 µg ml^{-1}) candoluminescence with time in a MgO matrix after introduction into a hydrogen flame.

The time characteristics of the emission from terbium-activated MgO and the rare earth oxides coated on CaO are shown in Table 3.1. It shows that the time to maximum emission for terbium-activated Y_2O_3 and Lu_2O_3 coated matrices and for MgO is achieved faster than the emission in La_2O_3 and Gd_2O_3 coated matrices.

The flame composition and the matrix position in the flame were fixed as follows:

flame composition : H_2 = 2.0 , air = 2.0 and N_2 = 8.0 l min^{-1}, matrix at the edge of the flame, 2.5cm above the burner head.

3.4.6 Pre-heating and Cooling Times

During the study of the pre-heating and cooling times, the other parameters were fixed as given above. If the emission intensity is enhanced by the pre-heating and cooling, the times of these processes must be optimized.

Figure 3.3 shows the results for all the combinations of pre-heating and cooling times investigated for 50 μg ml^{-1} Tb in MgO.

This figure shows that if the pre-heating time was less than the time required for a maximum intensity (8 s), the emission could not be enhanced by the cooling (see curve for p = 5).

The matrix gives an emission each time it is inserted into the flame and the emission intensity decreases with number of the matrix introductions to the flame as shown in

Matrix	Time to initiate emission (s)	Duration of emission (s)	Maximum emission (s)
MgO	3	90	8
Y_2O_3	2	140	6
La_2O_3	6	$<$100	14
Gd_2O_3	8	120	15
Lu_2O_3	2	150	7

Table 3.1 Some characteristics of candoluminescence of terbium in different matrices

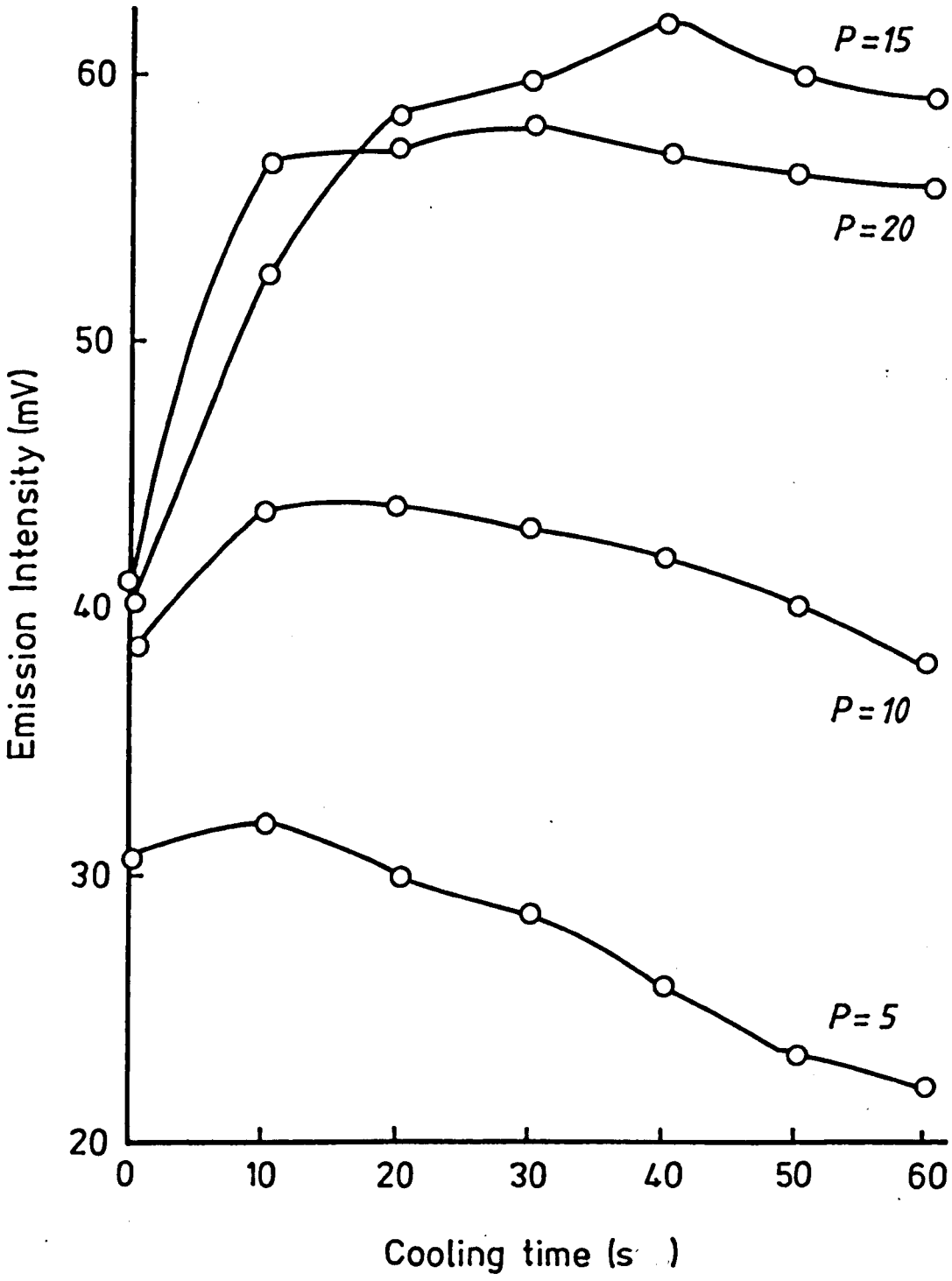

Fig. 3.3 Effect of pre-heating and cooling times on the terbium emission (50 $\mu g\ ml^{-1}$) in MgO.
*P = pre-heating time (s).

Fig. 3.4.

Prolonged heating (p = 20) caused a slight decrease in emission intensity possibly due to loss of some activator ions to the flame. The greatest intensity was obtained at 15 s pre-heating and after cooling for 40 s under these conditions. The emission intensity is almost constant as shown in Fig. 3.5 for several introductions into the flame. This would seem to be because the activator ions are optimally incorporated into the cation vacancies in the lattice of the matrix, created by the heat, on the first introduction into the flame.

Table 3.2 shows the optimum pre-heating and cooling times for terbium-activated MgO matrices and rare earth coated CaO matrices.

Matrix	Pre-heating time (s)	Cooling time (s)
MgO	15	40
Y_2O_3	8	30
La_2O_3	15	40
Gd_2O_3	20	50
Lu_2O_3	10	40

Table 3.2 The optimum pre-heating and cooling times for terbium in different matrices.

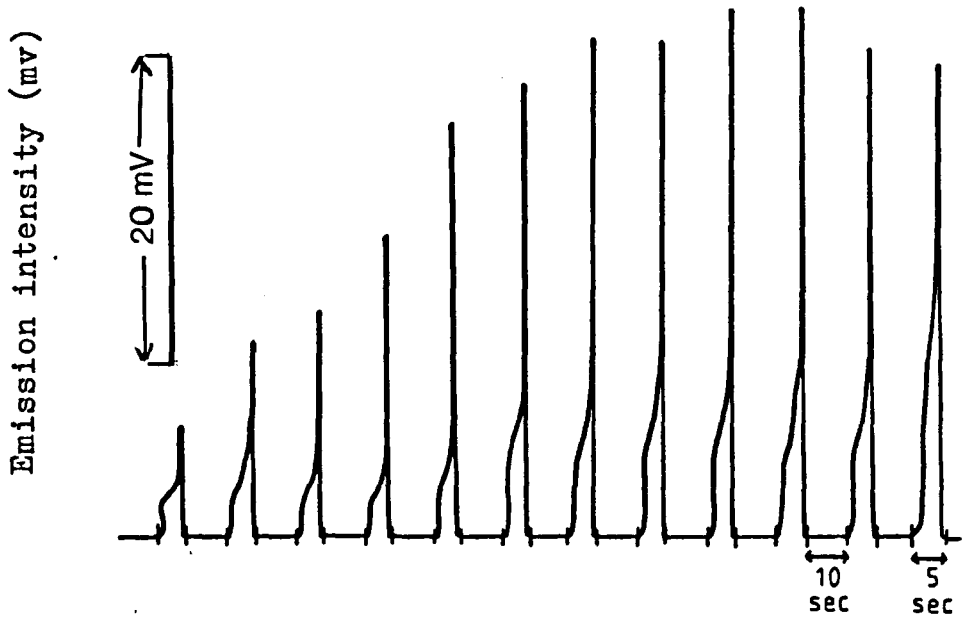

Fig. 3.4 Profiles of terbium emission by repeated insertions at 5 s pre-heating and 10 s cooling times.

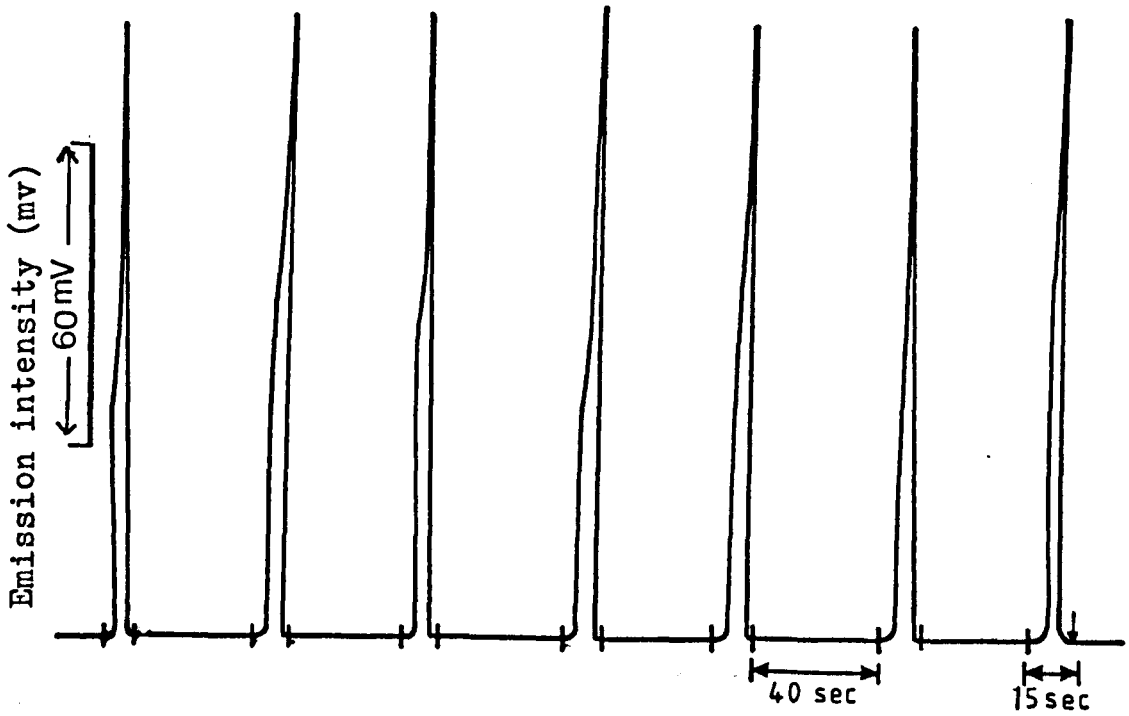

Fig. 3.5 Profiles of terbium emission by repeated insertions at 15 s pre-heating and 40 s cooling times.

3.4.7 Flame Composition and Matrix Position

The flame composition and the horizontal and vertical positions of the activated matrix in the flame are also very important parameters. They are mainly related to the variation of concentration of the radicals (H• and •OH) in the flame.

Initially, the flow rates of the three gases were set at 2.0, 2.0 and 8.0 l min^{-1} for hydrogen, air and nitrogen respectively, and the position of the matrix surface was fixed at the edge of the flame. The optimum flow rate for each of these gases was established by keeping two of the flow rates constant while the third was varied. This cycle was repeated until the optimum flow rates for all three gases were obtained.

Figure 3.6 shows the effect of flame composition on the emission intensity for 50 $\mu g\ ml^{-1}$ Tb in MgO. It shows that the optimum flow rates for both hydrogen and air were 2.0 l min^{-1} and these flow rates affected the emission intensity to a considerable extent whereas the nitrogen flow rate appeared not to be very critical. Lowering the flow rate of nitrogen below 5 l min^{-1} resulted in the flame becoming unstable, flabby and increasing in sodium emission. Conversely, when the flow rate was increased above the optimum rate (8.0 l min^{-1}) the flame would become narrow and the temperature would be lowered too much, thus depressing the emission.

The effect of the matrix position in the flame is shown

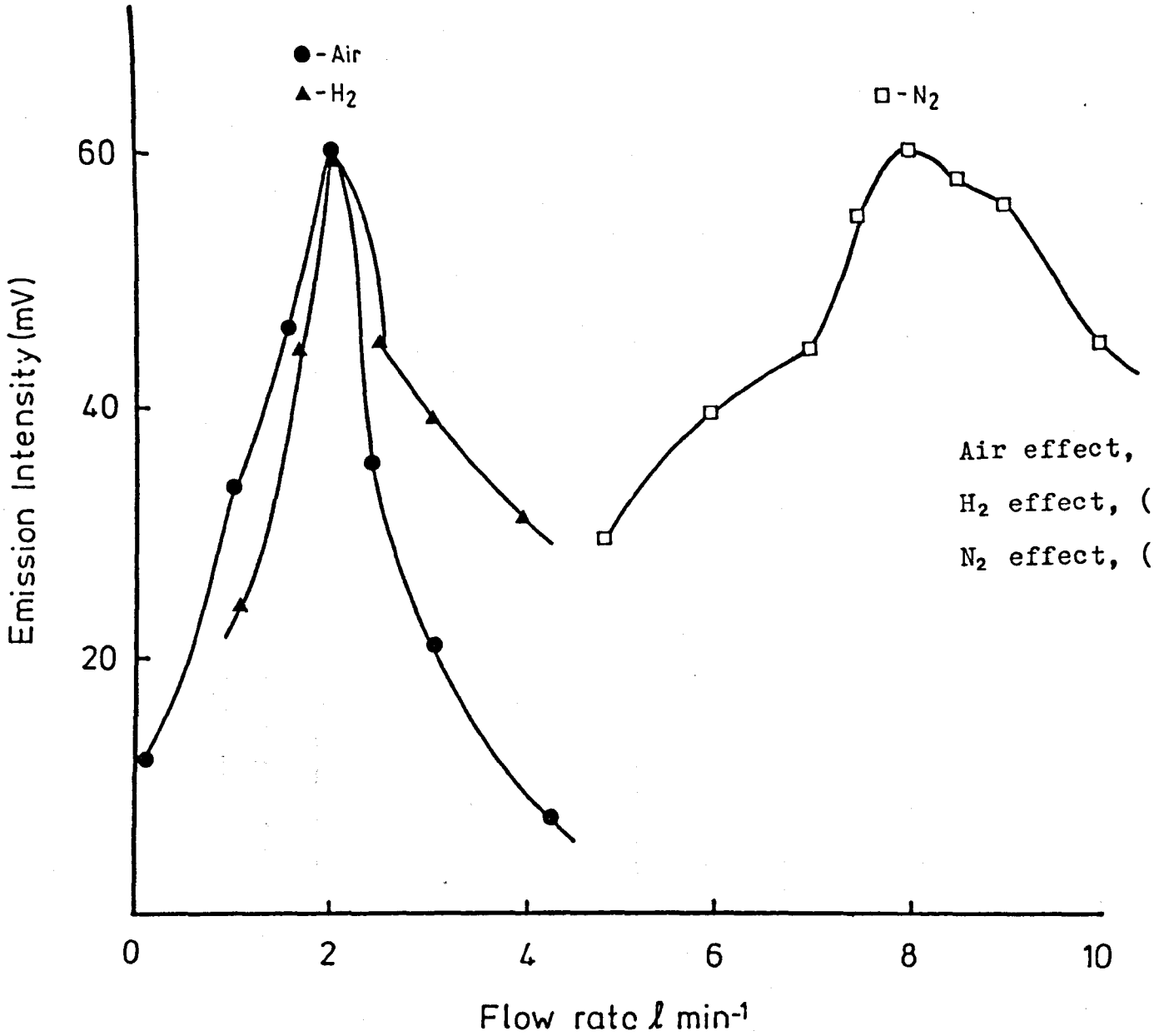

Air effect, (H_2 and N_2 fixed at 2.0 and 8.0 l min^{-1}

H_2 effect, (air and N_2 fixed at 2.0 and 8.0 l min^{-1}

N_2 effect, (H_2 and air fixed at 2.0 and 2.0 l min^{-1}

Operating conditions

λ = 541 nm

matrix used MgO

1 μl of 50 μg ml^{-1}

Fig. 3.6 Effect of flame composition on 50 μg ml^{-1} Tb emission.

in Fig. 3.7. The flame composition used was the optimum established above. The vertical distance between the burner head and the centre of the matrix surface was examined only at the edge of the flame. The vertical distance was found not to be very critical within a range of 1-3cm and the optimum position was found to be 2.5cm above the burner head.

The horizontal position was very critical. This was examined with the matrix placed 2.0cm above the burner head. Only three positions were examined, namely the edge, the centre of the flame and the middle position between the two. The results of these observations are shown in Fig. 3.7.

Table 3.3 summarizes the optimum flame conditions and matrix positions for activated MgO and rare earth coated matrices. There is little difference in the conditions for each matrix.

Matrix	Flow rate ($l\ min^{-1}$)			Matrix Position	
	H_2	Air	N_2	Vertical (cm)	Horizontal
MgO	2.0	2.0	8.0	2.5	edge of flame
Y_2O_3	2.0	1.5	7.5	2.0	"
La_2O_3	1.5	2.0	8.0	2.0	"
Gd_2O_3	2.0	1.5	7.5	2.5	"
Lu_2O_3	2.0	2.0	8.0	2.0	"

Table 3.3 The optimum flame conditions and matrix positions for Tb in different matrices.

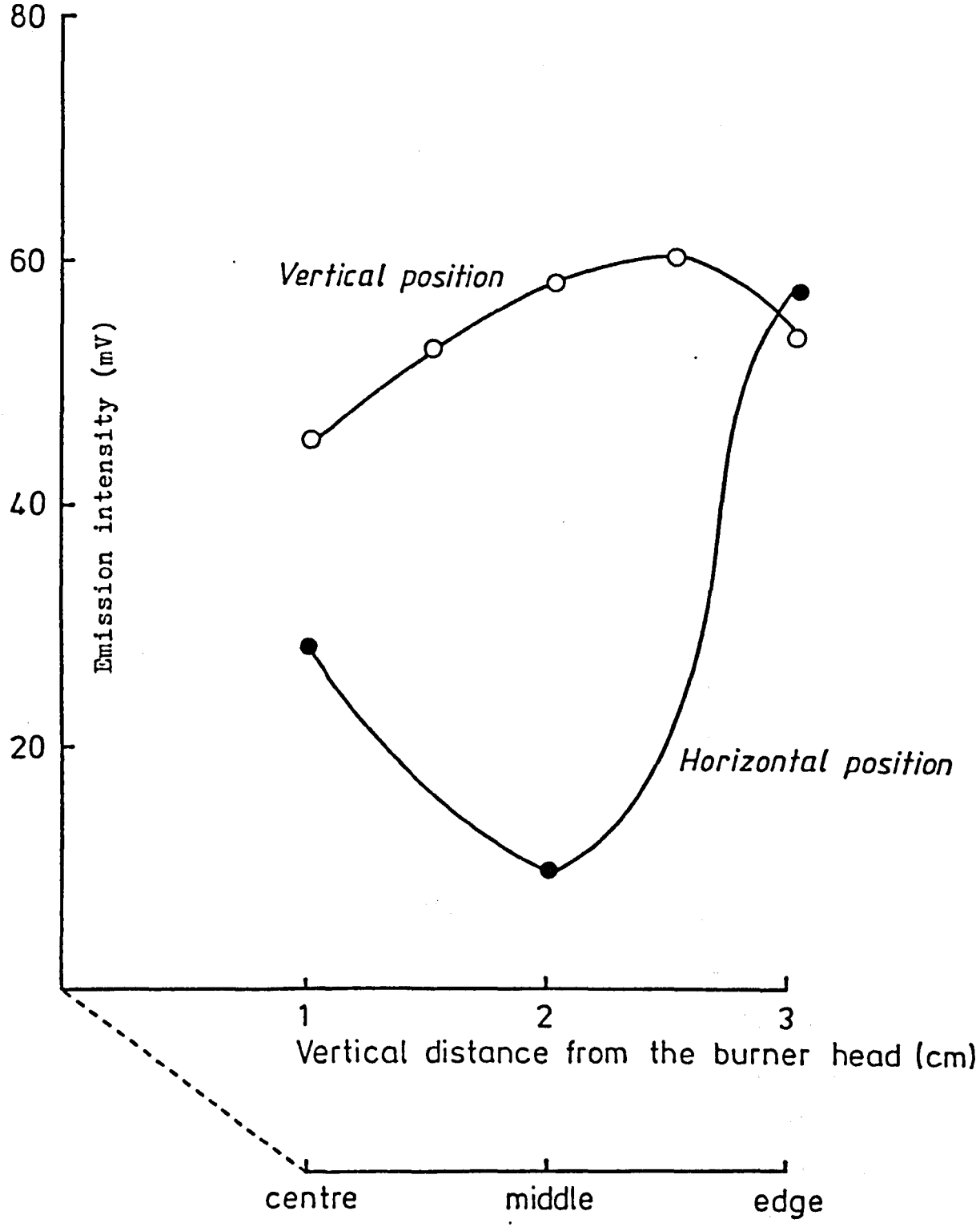

Flame Composition:

H_2 : 2.0 l min^{-1} , air : 2.0 l min^{-1} , N_2 : 8.0 l min^{-1}

Operating Conditions:

λ = 543 nm , matrix = MgO

Fig. 3.7 Effect of the matrix position in the flame on Tb emission (50 $\mu g\ ml^{-1}$).

3.5 Quantitative Measurements

3.5.1 Calibration

Candoluminescence was measured by injection (1 µl) of terbium solution onto a smooth, uniform and flat matrix surface. The change in candoluminescence intensity with time after insertion of the matrix into the flame was measured and the maximum intensity noted. These measurements were done under the optimum conditions noted above. The amount of terbium was plotted vs. peak emission intensity in different matrices as shown in Figs. 3.8, 3.9 and 3.10. Table 3.4 summarizes the analytical characteristics for Tb in all the matrices investigated, under these conditions.

3.5.2 Detectability and Reproducibility

Solutions containing various low concentrations of terbium were injected onto the surface of the different matrices in order to determine the detection limit, and the stimulated emission was compared to that obtained from a blank solution (containing no terbium), where the background emissions in the different matrices were in range of 1-8mV.

The detection limits (2 x noise) for terbium in different matrices are shown in Table 3.4. The reproducibility was calculated for 50 µg ml^{-1} , 10 ng and 25 ng of terbium in MgO, Y_2O_3 , La_2O_3 and Lu_2O_3 coated matrices and a Gd_2O_3 coated matrix, respectively, from 10 determinations each in a new matrix. The relative standard deviation was found to be 2.5-3.2%, as shown in Table 3.4.

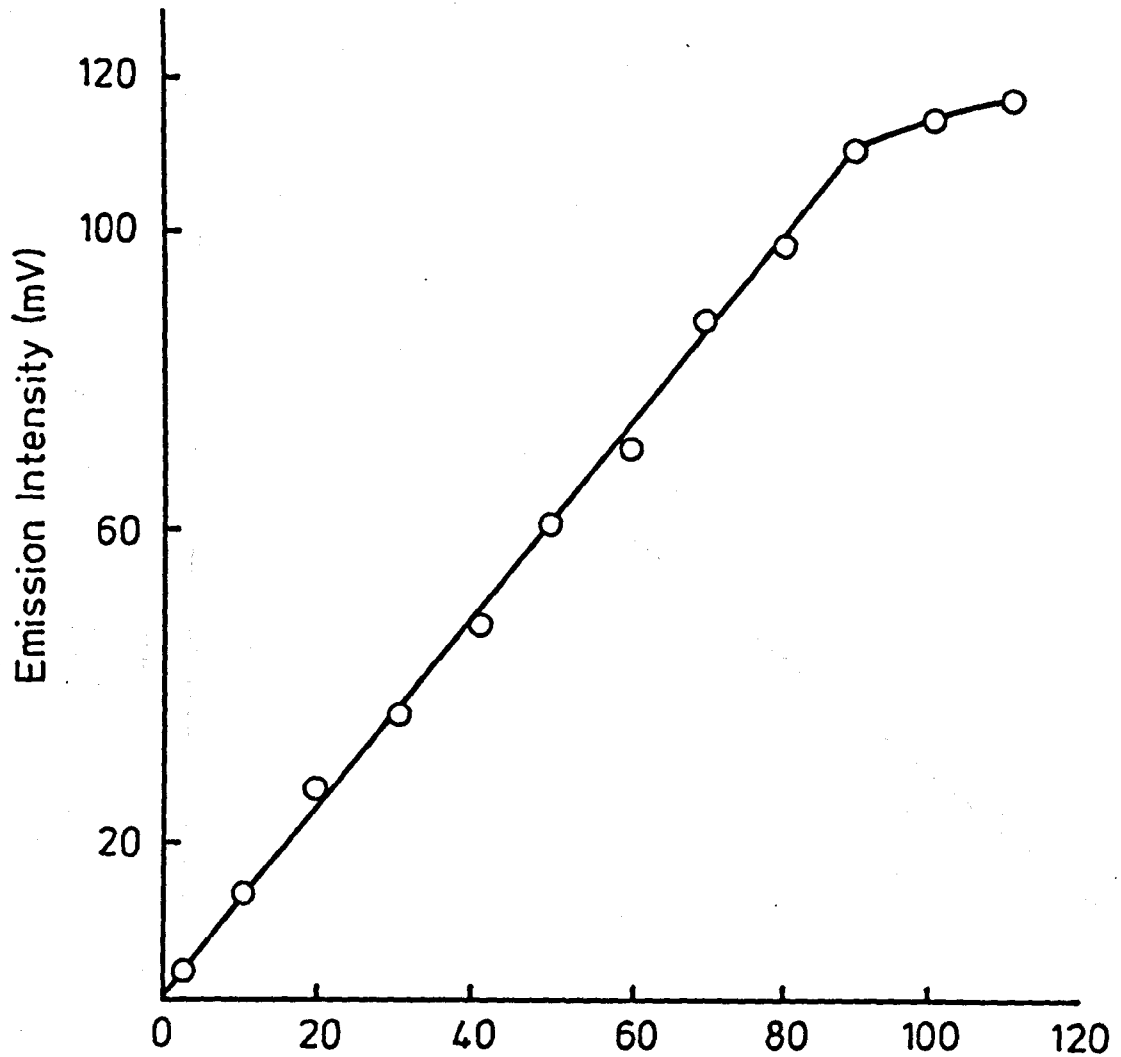

Fig. 3.8 Calibration graph of Tb in MgO matrix.

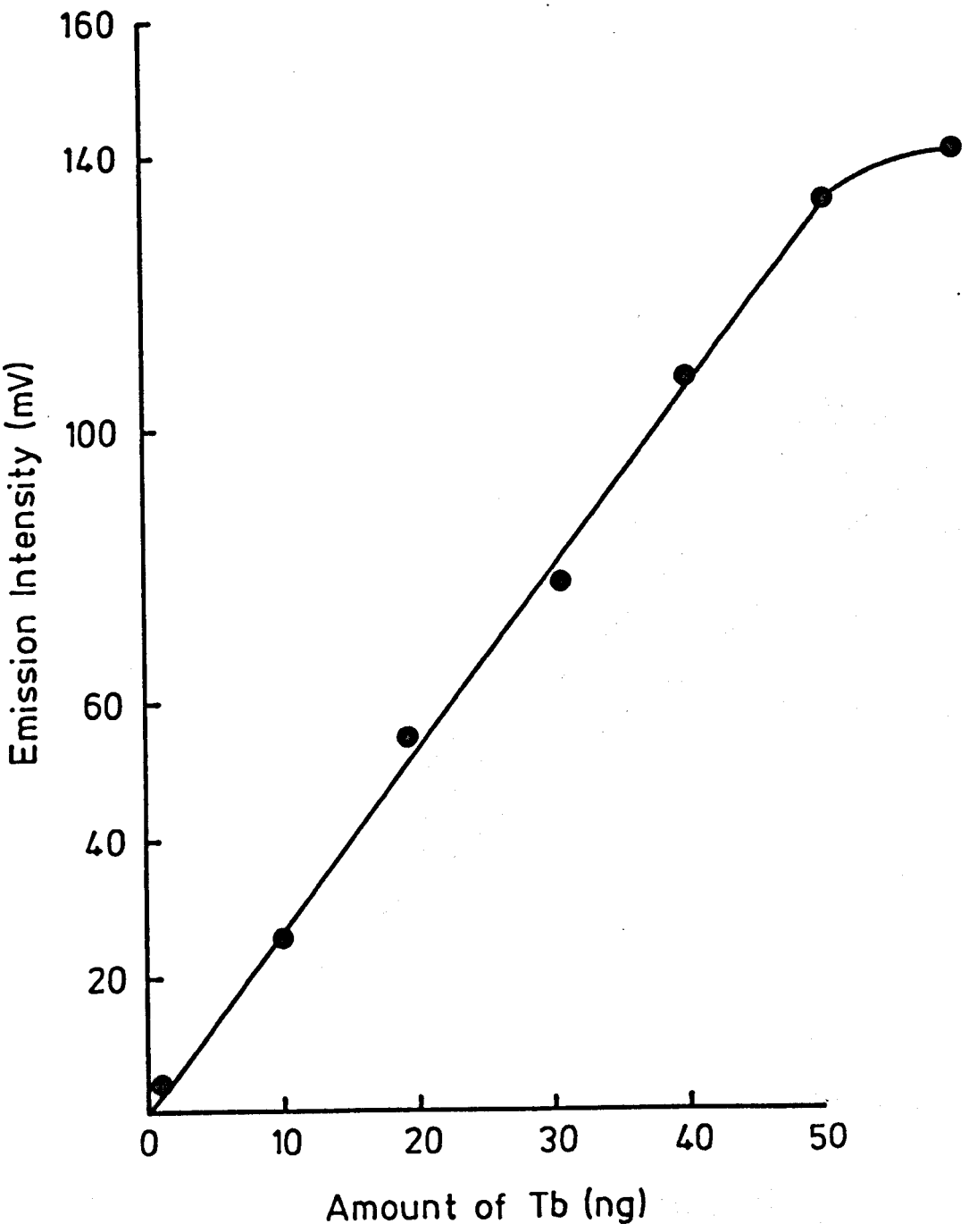

Fig. 3.9 Calibration graph of Tb in Gd_2O_3 coated matrix.

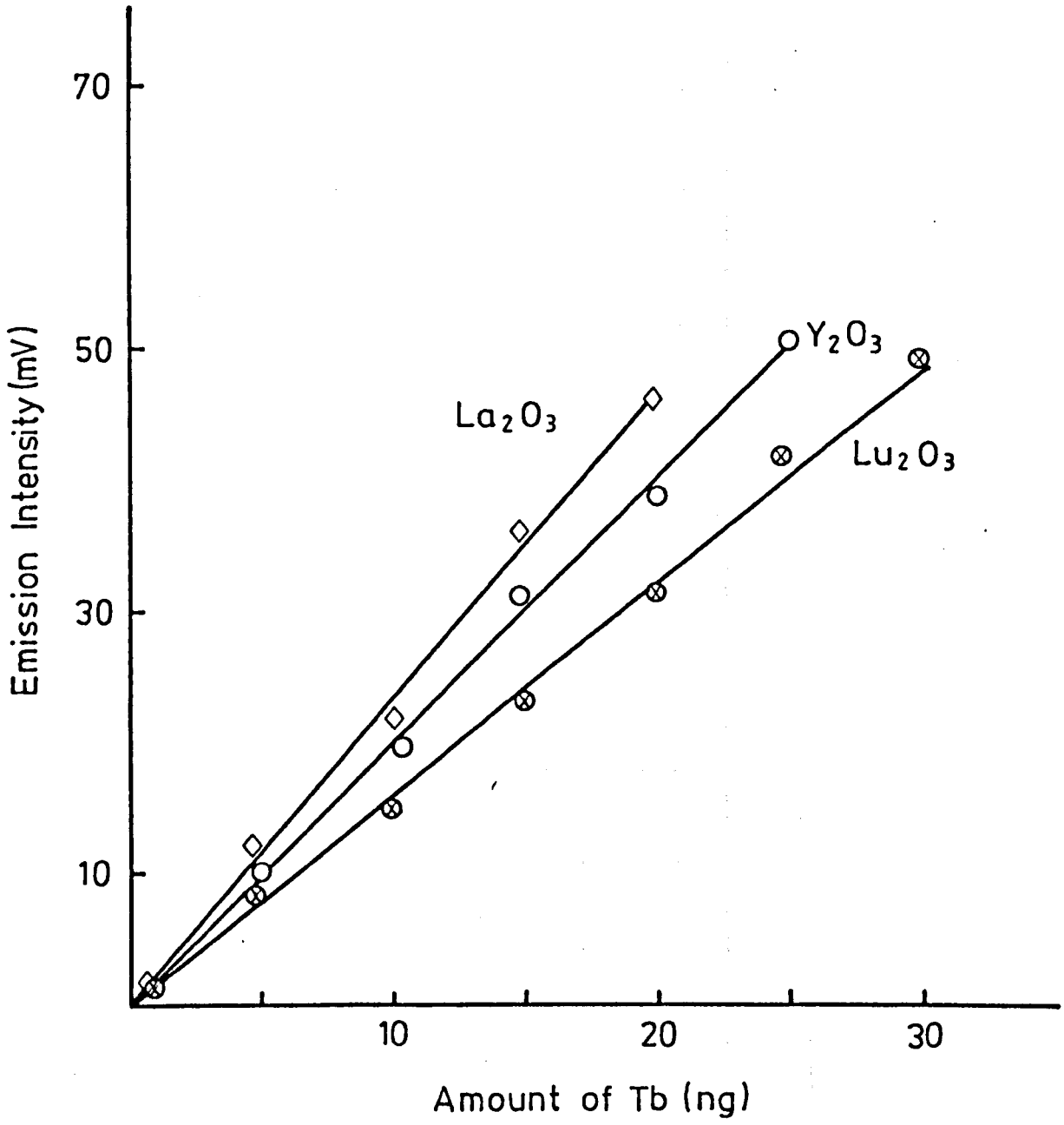

Fig. 3.10 Calibration graph of Tb in different coated matrices.

Matrix	Linear range (ng)	Sensitivity (mV ng^{-1})	Detection limit (ng)	R. S. D. % (n = 10)
MgO*	1 - 90	1.2	1	3.2
Y_2O_3	0.1 - 25	2.0	0.05	2.5
La_2O_3	1 - 20	2.2	0.1	2.9
Gd_2O_3	0.1 - 50	2.7	0.01	2.5
Lu_2O_3	0.1 - 30	1.6	0.05	3.0

Table 3.4 Analytical characteristics for Tb in different matrices
* The linear range and detection limit are in $\mu g\ ml^{-1}$ and the sensitivity in ($mV/\mu g\ ml^{-1}$)

The results show that the detection limits achieved are lower than 0.2-3 ng reported previously[50,51], and the reproducibility achieved by the automated device is better than the 3.1-7% r.s.d. obtained manually[47,50,51].

3.5.3 Interference Study

A study of interferences from other lanthanides was carried out on the response from 10 ng of Tb in a Gd_2O_3 coated matrix. A series of solutions containing a constant concentration of terbium with a different concentration of interfering ion up to 10 times by weight of the Tb concentration was prepared. A 1-µl portion of the mixture was injected onto the surface of the coated matrix in each instance and compared with the average emission of five determinations of 10 ng of Tb alone. This coated matrix was chosen because it gives most sensitivity for Tb.

Figures 3.11 and 3.12 show that cerium interfered seriously by depressing the Tb emission, and Nd, Eu and Sm depressed the emission at 5 : 1 metal : terbium weight ratios as did 100 ng of the other lanthanides, except for La, Lu and Yt which enhanced the luminescence.

3.6 Conclusions

Terbium was found to give a strong green emission in the MgO matrix. This emission was used for the first time for the analytical purpose of Tb determination. Also terbium was found to be a sensitive activator in rare earth coated matrices. Best sensitivity was achieved by using Gd_2O_3

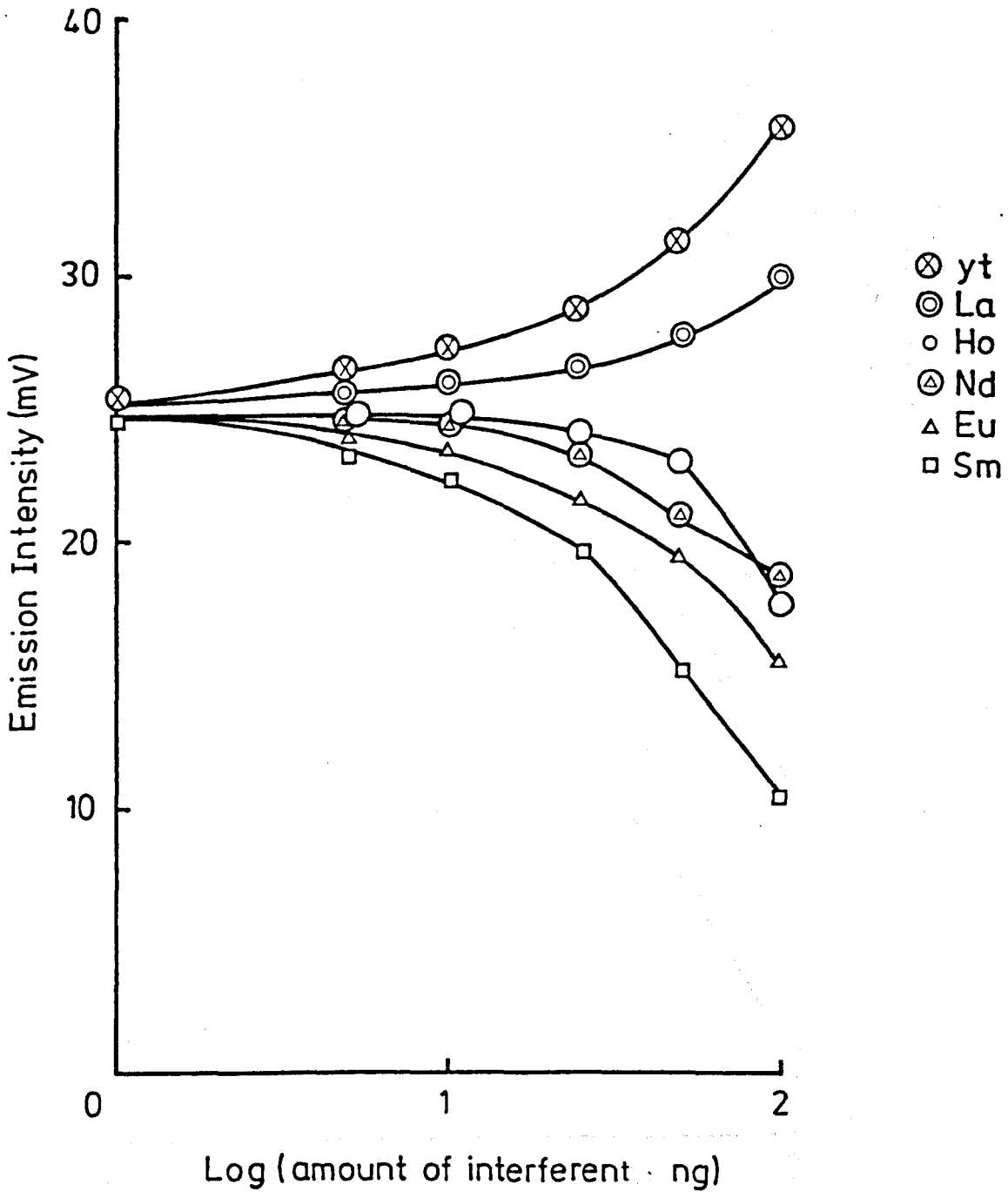

Fig. 3.11 Effect of other lanthanides on Tb emission (10 ng)

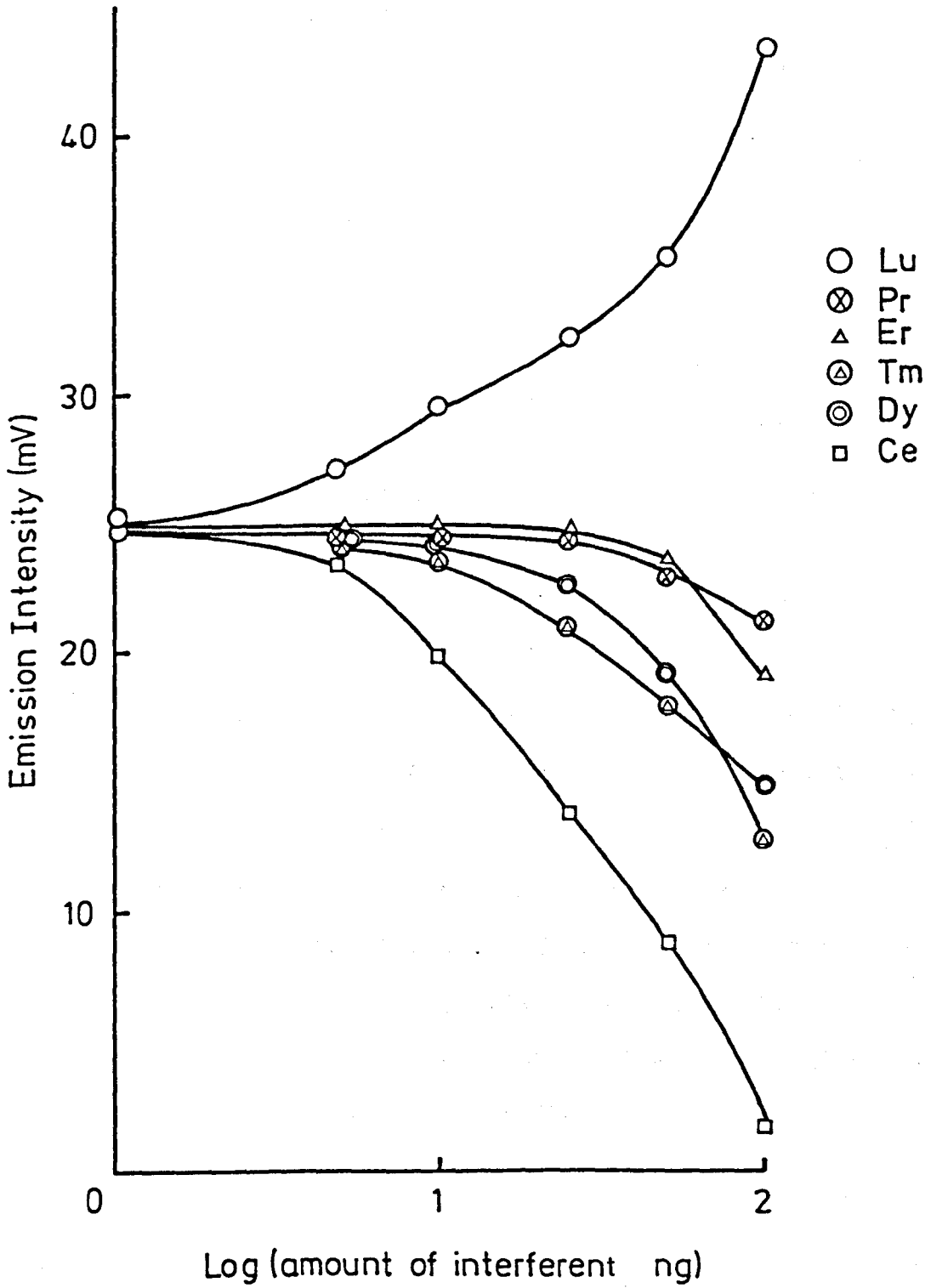

Fig. 3.12 Effect of other lanthanides on Tb emission (10 ng).

coated CaO matrices.

A comparison between the results obtained from this work with reported results[50,51] in the Gd_2O_3 coated matrix, are shown below:

Gd_2O_3* : Tb

	Old	New
reproducibility :	3.1%	2.5%
detection limit :	0.3 ng	0.01 ng
linear range :	up to 30 ng	up to 50 ng

* Gd_2O_3 coated on CaO in the new work and on a rod of CaO/CaSO in the old work.

It is clear from these results that the reproducibility and detection limit have been improved and the linear range of calibration is expanded.

These improvements in Tb measurements are attributed to the use of the matrix making and introduction devices and also to the SIT vidicon camera, which provided a very sensitive and versatile detector for rapid measurement of candoluminescence emission and spectra.

CHAPTER FOUR

CANDOLUMINESCENCE OF EUROPIUM

IN

DIFFERENT MATRICES

Candoluminescence of Europium in Different Matrices

4.1 Preliminary Study

The orange-red emission of europium-activated CaO, when placed at the edge of a hydrogen flame, has been known for a long time. The candoluminescence of europium was first used for analytical purposes in 1971 by Sweet and White[34], who identified the spectra and reported 0.1% europium in doped Y_2O_3 , Gd_2O_3 , La_2O_3 and Lu_2O_3 matrices.

Ranjitkar[44] found that europium produced a bright orange-yellow emission in a CaO matrix when placed at the edge of a hydrogen flame, the spectrum being a single peak at 585 nm. A 1 to 10 ng calibration graph was reported with a coefficient of variation of 9.5%. He subsequently found that the emission was coactivated by sulphuric acid which enhanced the luminescence as well as shifted the spectral peak from 585 nm to 600 nm.

Further investigation by Nasser[47] showed that the optimum emission from CaO activated with europium can be achieved when the matrix position is not right at the edge of the flame but about half of the way in towards the centre. The emission peaks were measured on the first entry into the flame and other acids (HCl, HBr or $HClO_4$) besides H_2SO_4 were found to coactivate the europium emission. The coactivated emission was found to be very sensitive at 600 nm, and a calibration graph between 0.01 ng and 15.0 ng using H_2SO_4 as coactivator and a 5 pg detection limit were reported.

Karpel[45] found that europium gave a deep red luminescence in a $CaWO_4$ matrix at the edge of a hydrogen flame. The spectrum consisted of a main peak at 616 nm and a shoulder at 535 nm. A calibration graph between 0.6-6.0 ng with a detection limit 0.2 ng and 8.0% coefficient of variation were reported.

Matsuoka[48] investigated the candoluminescence of europium in a new matrix SrO : $CaSO_4$ (4 : 1 by weight). He reported that europium gave an orange-red emission at the edge of a hydrogen flame, the spectrum being a single peak at 570 nm. The emission was measured after 20 s' and 35 s' preheating and cooling times respectively. A calibration graph between 0.2-10 ng with a detection limit of 0.2 ng and 13% coefficient of variation were reported.

In this work rare earth oxides (Y_2O_3 , La_2O_3 , Gd_2O_3 and Lu_2O_3) coated on a CaO matrix were used. The work was aimed to investigate the candoluminescence of europium in detail for the first time in these coated matrices and to improve the reproducibility and the sensitivity of europium determination.

4.2 Experimental

4.2.1 Reagents and Chemicals

A 1000 $\mu g\ ml^{-1}$ europium solution was prepared by dissolving 0.3095 g of $Eu(NO_3)_3 .5H_2O$ (Koch-Light Laboratories) in deionised water in a 100-ml volumetric flask and diluting to volume with deionised water, which was used

throughout.

The other reagents and chemicals were the same as described in Chapter 3.

4.2.2 Apparatus

The complete candoluminescence instrument is shown in Fig. 2.1.

4.3 Experimental Parameter and Optimization

4.3.1 Matrix Preparation

A set of matrices of rare earth oxides (Y_2O_3 , La_2O_3 , Gd_2O_3 and Lu_2O_3) coated on CaO was prepared according to the procedure described previously in Chapter 2 and Chapter 3.

4.3.2 Injection Technique

Like the terbium solution the europium solution was injected as 1 µl of solution onto the surface of rare earth coated on CaO matrices.

4.3.3 Spectra

Europium gives a strong orange-red emission, maximum at 610 nm, in all the rare earths coated on CaO matrices (Y_2O_3 , La_2O_3 , Gd_2O_3 and Lu_2O_3) as shown in Fig. 4.1. The spectral range covered (629-697 nm), was selected in order to exclude sodium atomic emission at 589 nm, which was always present when the flame was in operation.

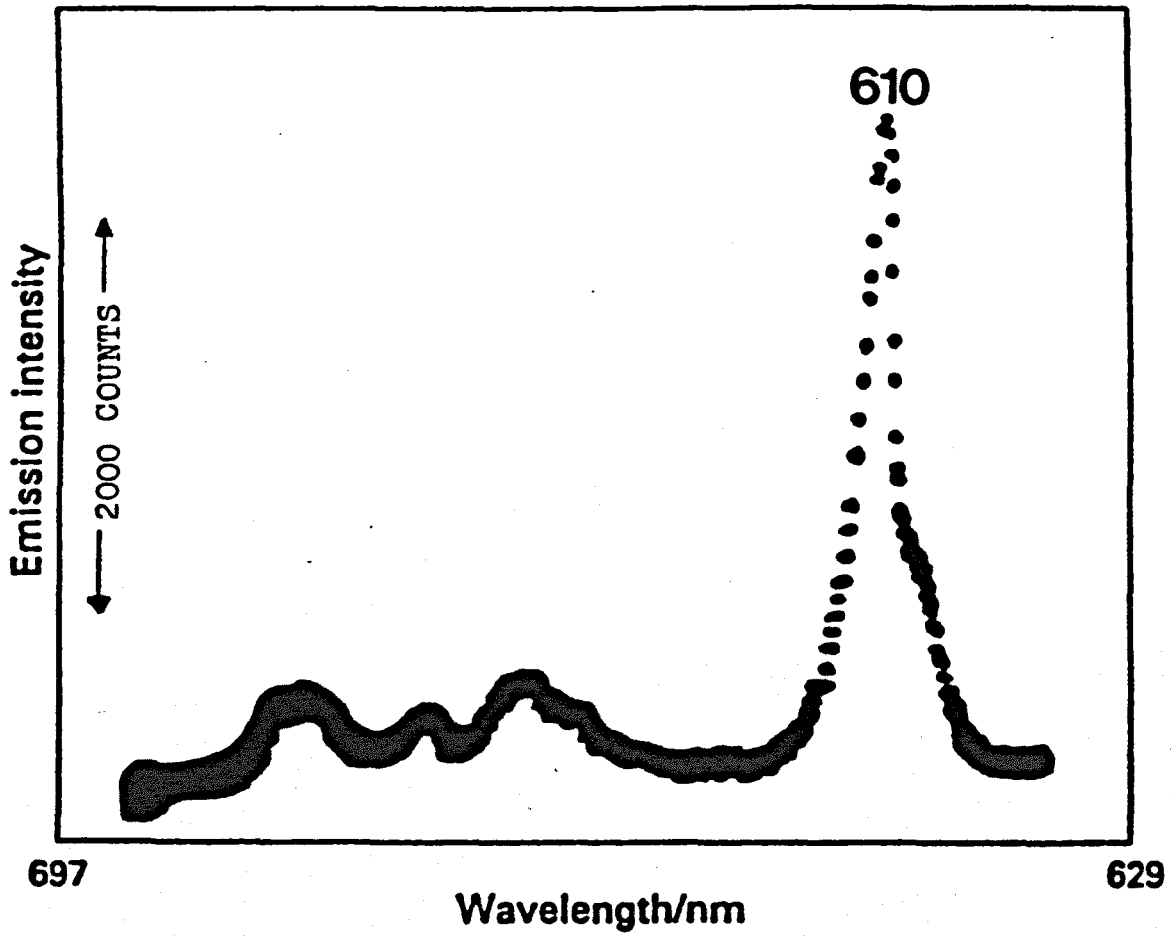

Fig. 4.1 Europium spectrum in the range of 629 - 697 nm.

This band at 610 nm, which was also noted by others[45,48], was used for analytical purposes.

4.3.4 The Characteristics of Europium Candoluminescence Emission

The emission was stimulated in rare earth oxides coated on CaC matrices by injection of 1 µl of europium solution (15 ng) onto the matrix surface. Each matrix was examined by heating at the edge of a hydrogen flame. The rare earth coated matrices although 99.9% pure themselves gave an emission when introduced into the flame owing to the presence of impurities of other lanthanide ions, as described in Chapter 3. When 99.999% or 99.9999% pure oxides were used, a small background (1-8mV) was still obtained, which compared with the 45 mV signal from 15 ng of Eu in a Y_2O_3 coated matrix. The background should be subtracted electronically.

Figure 4.2 shows the change in europium candoluminescence with time in any Y_2C_3 coated matrix after introduction into a hydrogen flame. A very weak green emission appeared initially when the matrix was introduced into the flame. This emission was due to the Y_2C_3 coated matrix itself. It disappeared within 5 sec., and a much stronger orange-red emission began to glow. The orange-red emission reached its maximum intensity after 25 s and disappeared within 160 s.

The time characteristics of the emission from europium activated rare earth oxides coated on CaO matrices are shown in Table 4.1. It shows that the maximum emission from europium-activated Gd_2O_3 and La_2C_3 coated matrices is

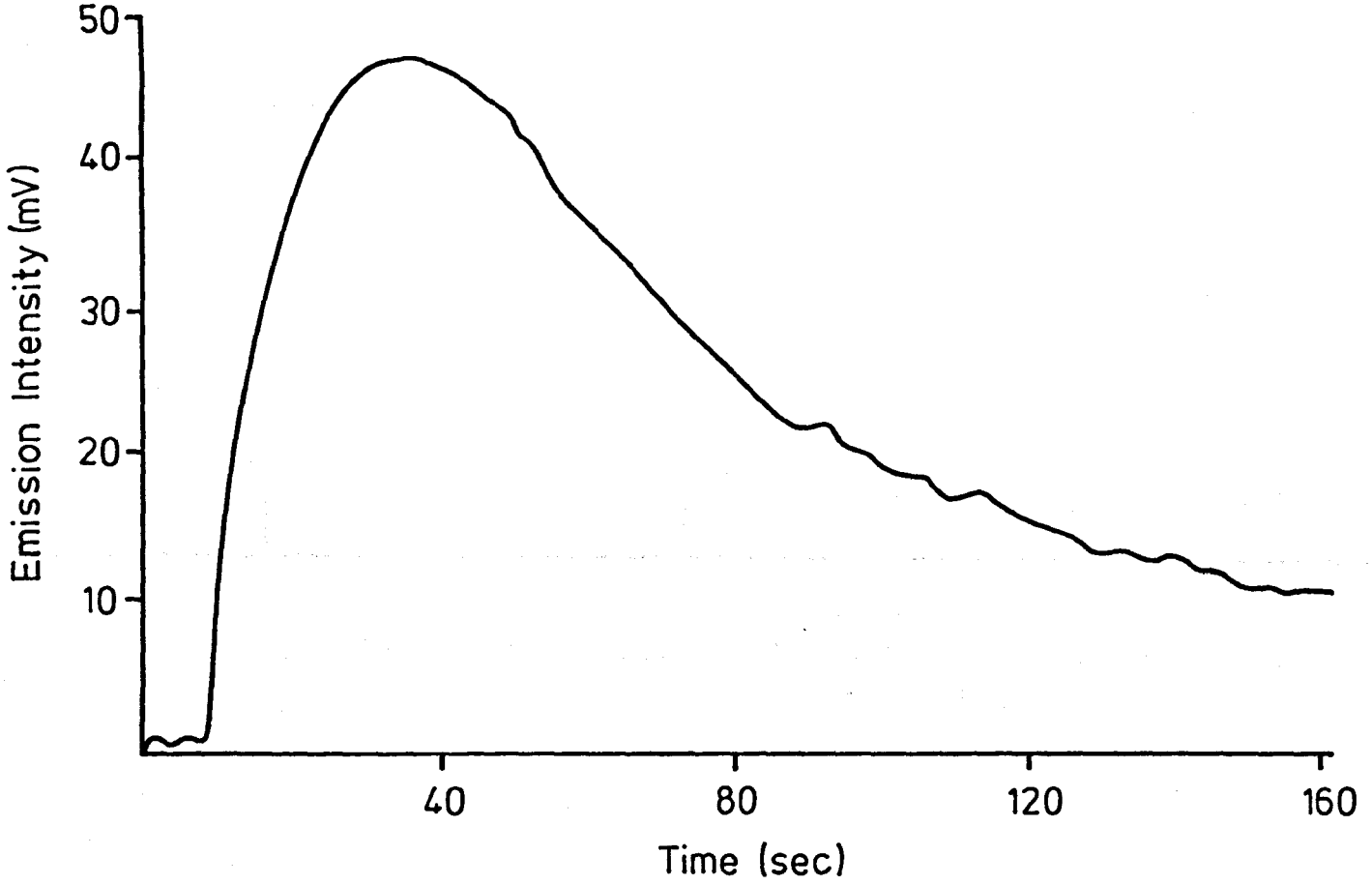

Fig. 4.2 Change in europium (10 ng) candoluminescence with time in Y_2O_3 coated matrix after introduction into a hydrogen flame.

Matrix	Time of initial emission (s)	Maximum emission (s)	Duration of emission (s)
Y_2O_3	5	25	>160
La_2O_3	3	15	>100
Gd_2O_3	3	15	110
Lu_2O_3	8	20	140

Table 4.1 Some characteristics of candoluminescence of europium in different matrices

achieved faster than the emission in Y_2C_3 and Lu_2C_3 coated matrices.

The flame composition and the matrix position in the flame were fixed as follows:

flame composition : H_2 = 2.0 , air = 2.0 and N_2 = 7.0 l min , matrix at the edge of the flame 2.5cm above the burner head.

4.3.5 Pre-heating and Cooling Times

During a study of pre-heating and cooling times the other parameters were fixed as given above. When a europium-activated Y_2C_3 coated matrix was removed from the flame after having reached the maximum intensity, and re-introduced to the flame, much enhanced emission was obtained. Consequently it was necessary to optimize pre-heating and cooling times to obtain the maximum intensity reproducibility. Fig. 4.3 shows the results for all combinations of pre-heating and cooling times investigated for 10 ng of europium in a Y_2C_3 coated matrix. This figure shows that if the pre-heating time was less than the time required for a maximum intensity (25 s), the emission could not be enhanced by cooling (see curves for p =15 to p = 20). Prolonged heating (p = 35) caused a slight decrease in the emission intensity possibly due to loss of some activator ions to flame. The greatest intensity was obtained at 30 s pre-heating and after 30 s cooling. Under these conditions the emission intensity was almost constant, as shown in Fig. 4.4 for several introductions into the flame. This would seem to be because the activator ions

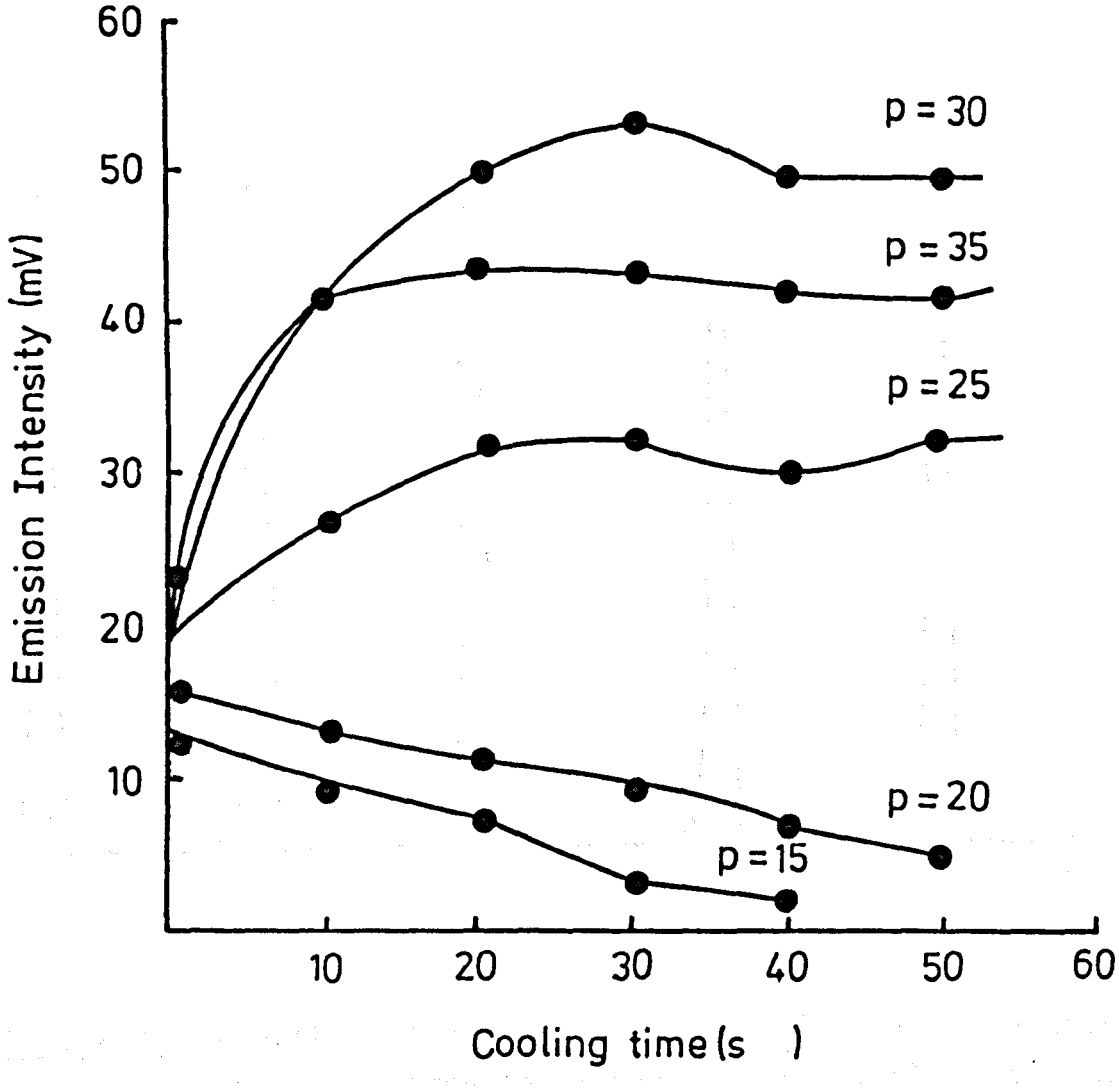

Fig. 4.3 Effect of pre-heating and cooling times on europium emission (10 ng) in Y_2O_3 coated on CaO matrix.
* p = pre-heating time (s)

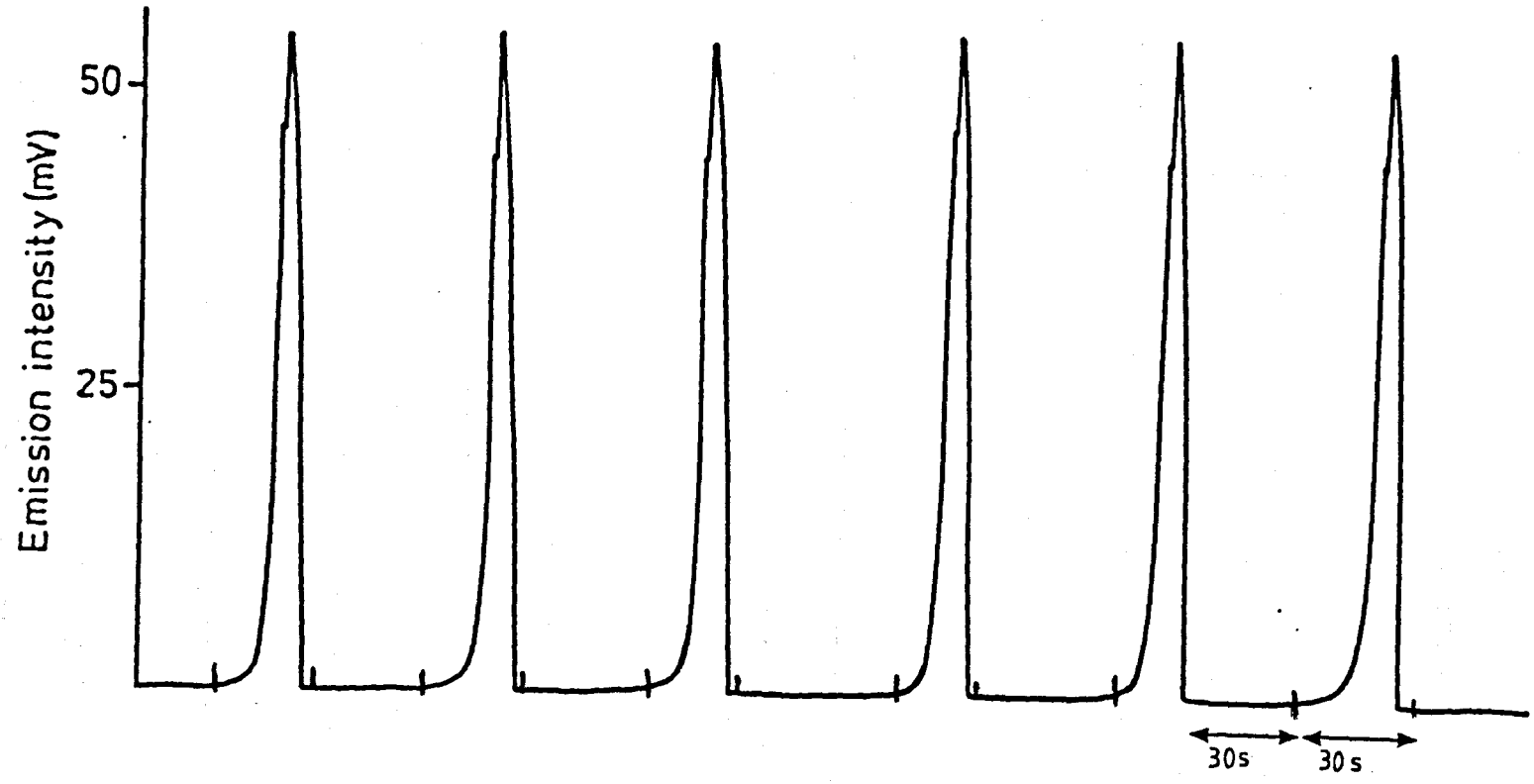

Fig. 4.4 Profiles of europium emission (10ng) by repeated insertions at 30 s pre-heating and 30 s cooling times.

are optimally incorporated into the cation vacancies in the lattice of the matrix, created by the heat, on the first introduction into the flame.

Table 4.2 shows the optimum pre-heating and cooling times for europium-activated rare earths coated on CaO matrices.

Matrix	Pre-heating time (s)	Cooling time (s.)
Y_2C_3	30	30
La_2C_3	20	40
Gd_2C_3	20	30
Lu_2C_3	30	40

Table 4.2 The optimum pre-heating and cooling times for europium in different coated matrices.

4.3.6 Flame Condition and Matrix Position

The flame used and the manner of investigation of optimum flame composition and the optimum matrix positions in the flame are as described in the previous chapter. The results are shown in Figs. 4.5 and 4.6; 2.0, 2.0 and 7.0 l min^{-1} for hydrogen, air and nitrogen, respectively and 2.5cm above the burner head at the edge of the flame were found to be the optimum flame conditions and the Y_2O_3 coated matrix optimum positions in the flame, respectively.

Table 4.3 summarizes the optimum flame conditions and

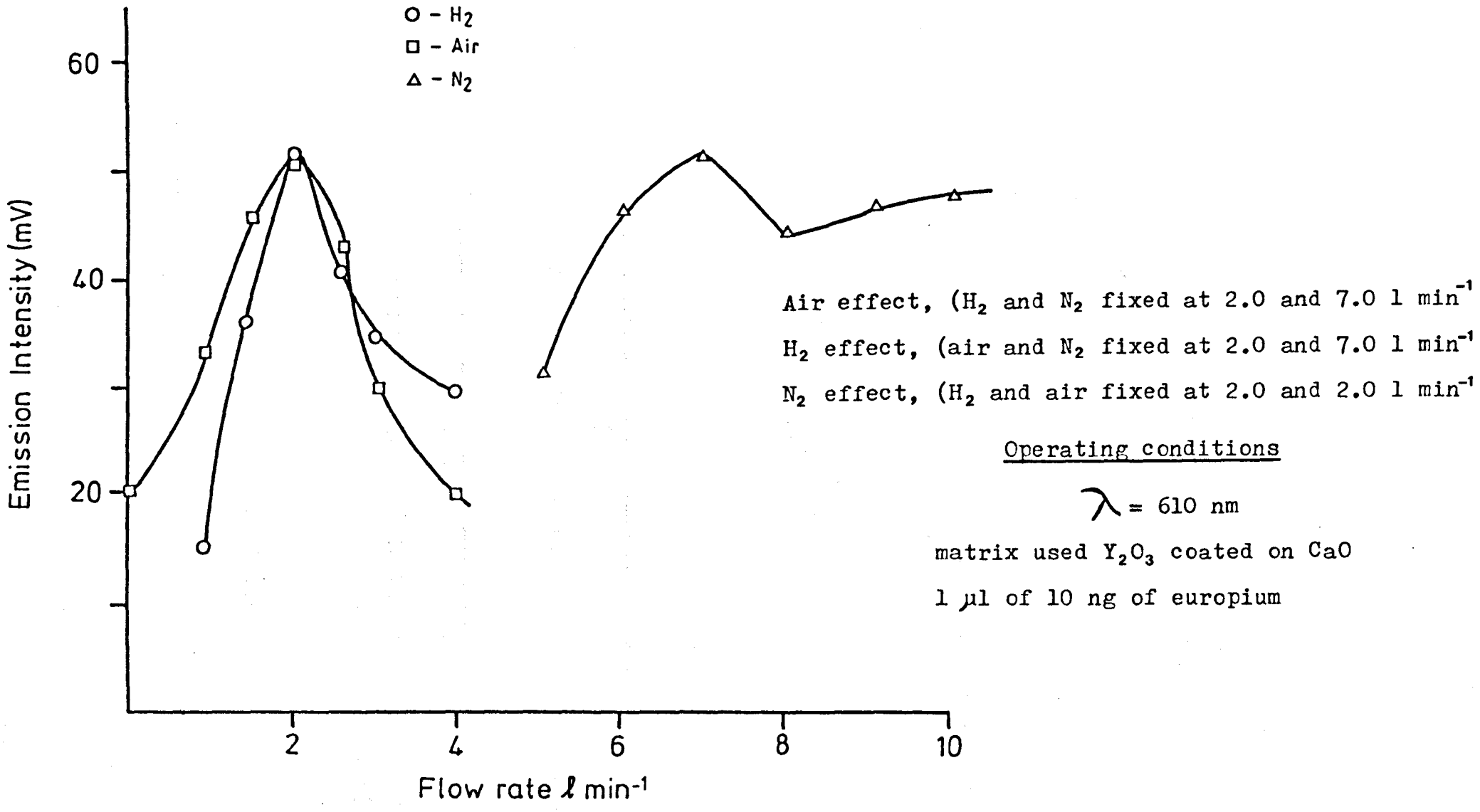

Fig. 4.5 Effect of flame composition on europium emission (10 ng).

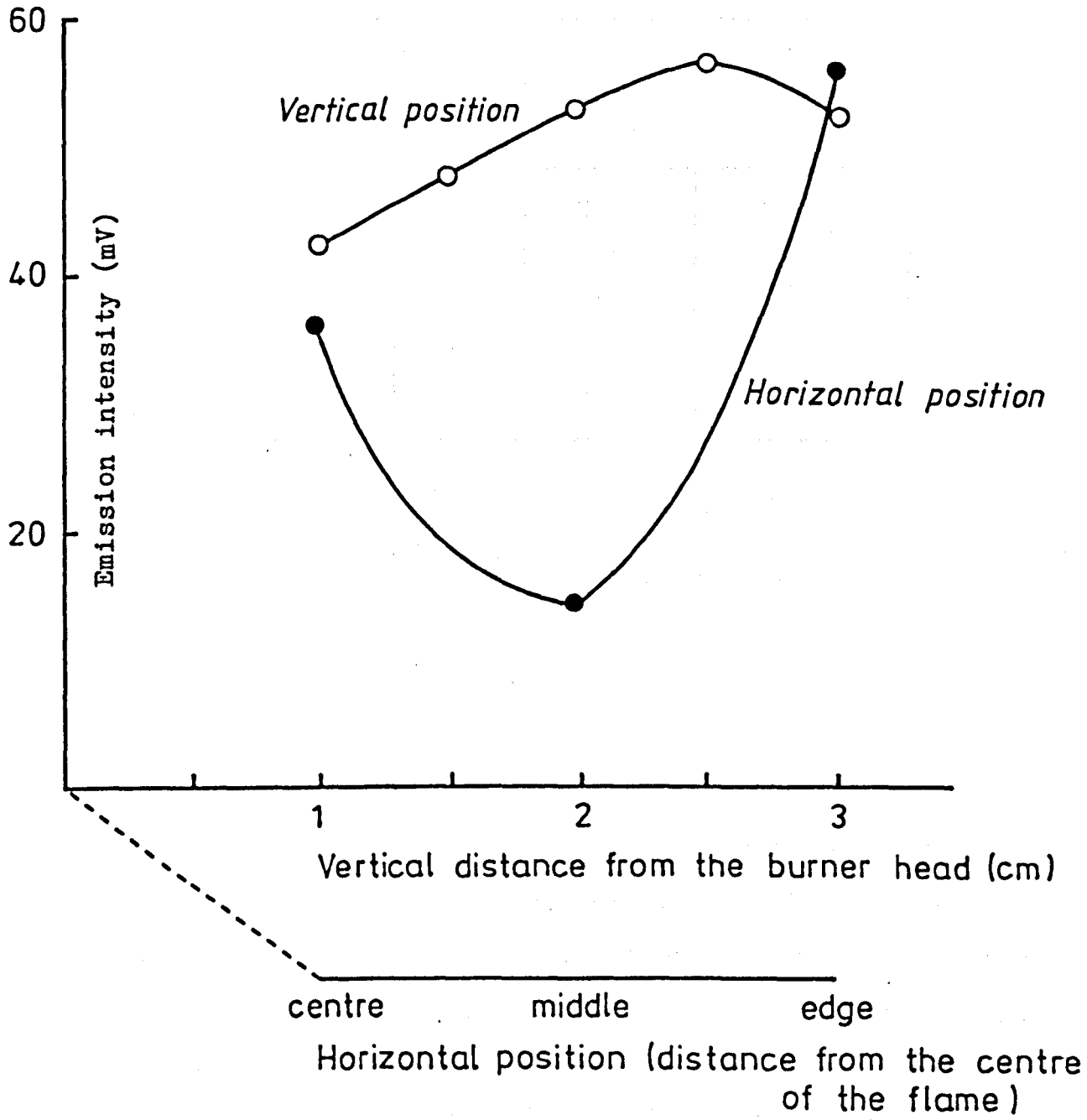

Flame Composition:

H_2 = 2.0 , Air = 2.0 and N_2 = 7.0 l min^{-1}

Operating Conditions:

λ = 610 , matrix = Y_2O_3 coated CaO

Fig. 4.6 Effect of the matrix position in the flame on europium emission (10ng).

matrix positions in the flame. There is little difference in the conditions for each matrix.

Matrix	Flow rate (l min^{-1})			Matrix Position	
	H_2	Air	N_2	Vertical (cm)	Horizontal
Y_2O_3	2.0	2.0	7	2.5	edge of flame
La_2C_3	2.0	2.0	7	2.0	"
Gd_2O_3	2.0	2.0	7.5	2.0	"
Lu_2C_3	2.0	1.5	7	2.0	"

Table 4.3 The optimum flame conditions and matrix positions for europium in different coated matrices.

4.4 Quantitative Measurements

4.4.1 Calibration

Candoluminescence was measured by injection of 1 µl of europium solution onto a smooth, uniform and flat matrix surface. The change in candoluminescence intensity with time after insertion of the matrix into the flame was measured and the maximum intensity noted. The measurements were made under the optimum conditions noted above. The amount of europium was plotted vs. peak emission intensity for the different matrices as shown in Fig. 4.7.

Table 4.4 summarizes the analytical characteristics for europium in all the matrices investigated, under these conditions.

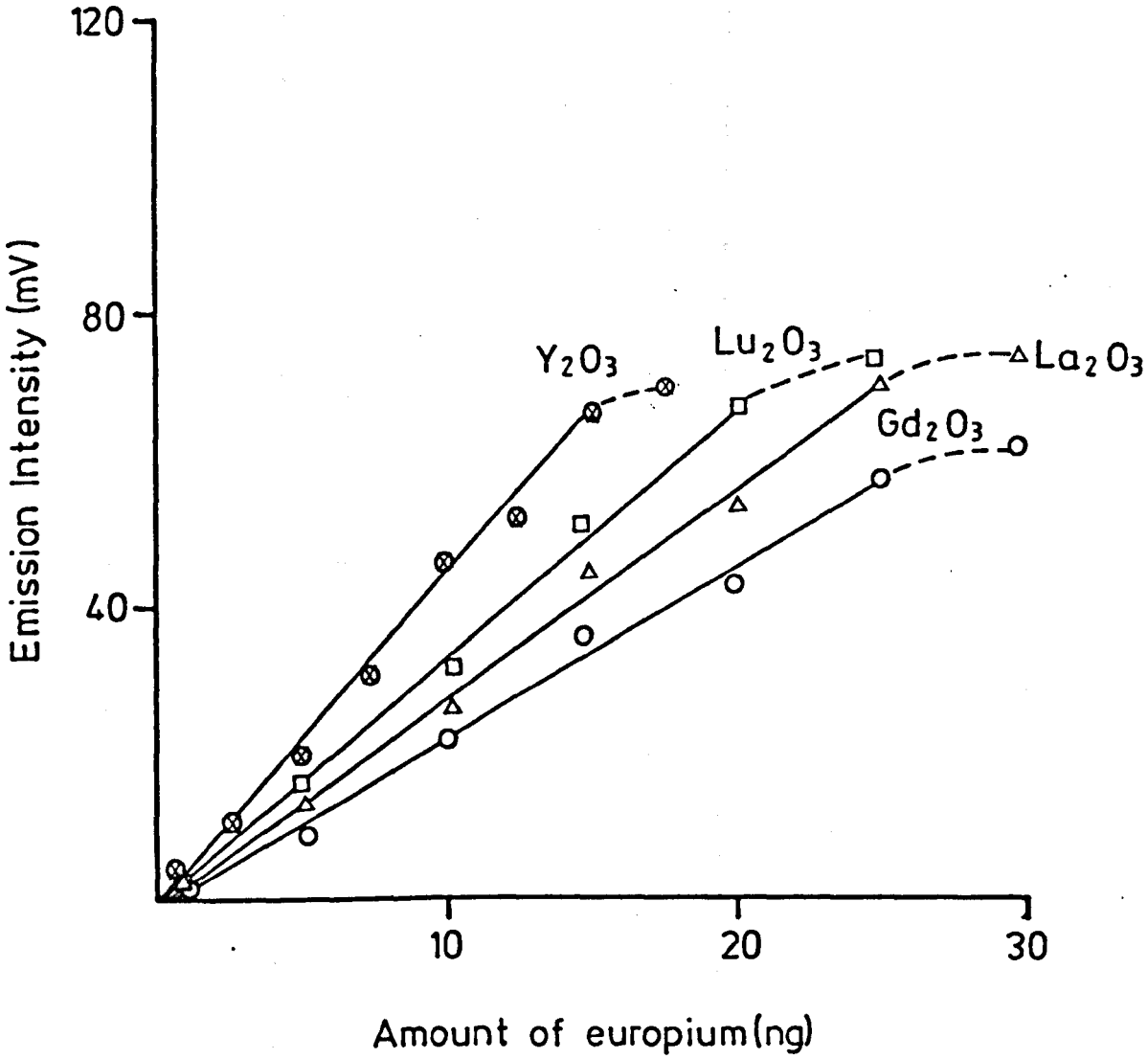

Fig. 4.7 Calibration graph of europium in different coated matrices.

Matrix	Linear range (ng)	Detection limit (ng)	Sensitivity (mV/ng)	R. S. D. % (n = 10)
Y_2O_3	0.1 - 15	0.05	4.5	2.6
La_2O_3	1 - 25	0.1	2.6	3.0
Gd_2O_3	1 - 20	0.1	2.1	2.9
Lu_2O_3	1 - 25	0.1	3.2	2.8

Table 4.4 Analytical characteristics for europium in different rare earth oxides coated on CaO matrices.

4.4.2 Detectability and Reproducibility

Solutions containing various low concentration of europium were injected onto the surface of the coated matrices and the stimulated emission was compared to that obtained from the blank solution (containing no europium) in order to determine the detection limit, where the background emissions in the different matrices were in ranges of 1-8mV. The detection limits (2 x noise) for europium in the different coated matrices are shown in Table 4.4.

The reproducibility was calculated for 10 ng of europium for 10 determinations each in a new matrix. The relative standard deviation was found to be 2.6-3.0% as shown in Table 4.4. The results show that the reproducibility achieved by the automated device is better than the 8.0-13.0% r.s.d. obtained manually[45,47,48].

4.4.3 Interference Study

A study of interferences from other lanthanides was carried out on the response from 10 ng of europium in a Y_2O_3 coated matrix. A series of solutions containing a constant concentration of europium with a different concentration of interfering ions up to 10 times by weight of the europium concentration was prepared. A 1 µl portion of the mixture was injected onto the surface of the coated matrix in each instance and compared with the average emission of five determinations of 10 ng of europium alone. The Y_2O_3 coated

on CaO matrix was chosen because it gives most sensitivity for europium.

Figs. 4.8 and 4.9 show that cerium and Tb interfered seriously by depressing the candoluminescence of europium. All other lanthanide ions enhanced the emission at $5 \geqslant 1$ metal : europium ratios except for Dy which depressed the emission.

4.5 Conclusions

The candoluminescence of europium was investigated in detail in the rare earth oxides coated on CaO matrices (Y_2O_3 , La_2C_3 , Gd_2C_3 and Lu_2C_3) for the first time. Better sensitivity was achieved by using Y_2O_3 coated matrix with 1-25 ng linear range than with the other coated matrices (La_2C_3 , Gd_2C_3 , Lu C_3). The reproducibility achieved by the automated device is better than the 8.0-13% relative standard deviation obtained manually[45,47,48]. The use of a SIT vidicon camera and the automated matrix introducing device provides a very sensitive and versatile detector for rapid measurement of candoluminescence emissions and spectra.

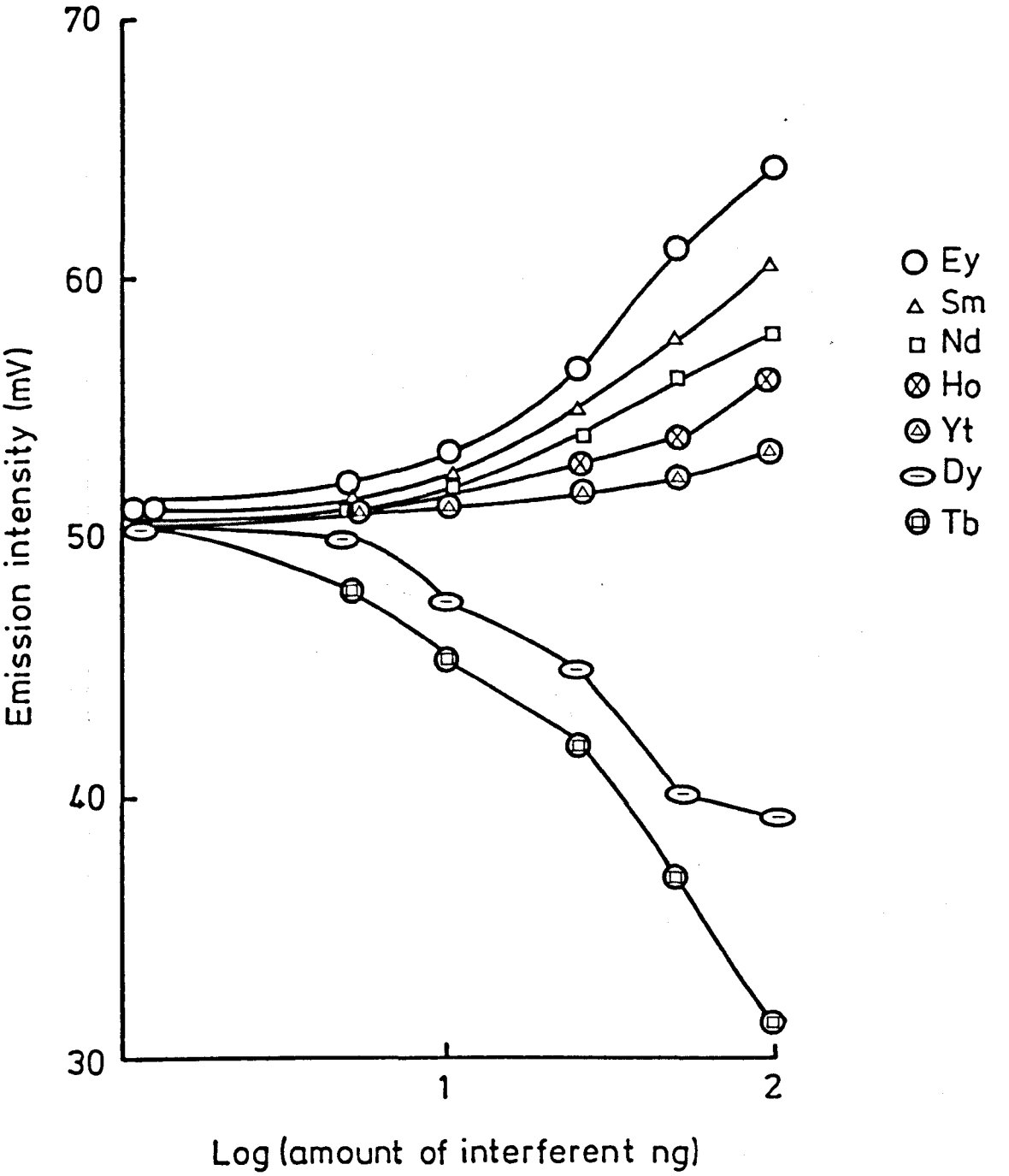

Fig. 4.8 Effect of other lanthanides on europium emission (10 ng).

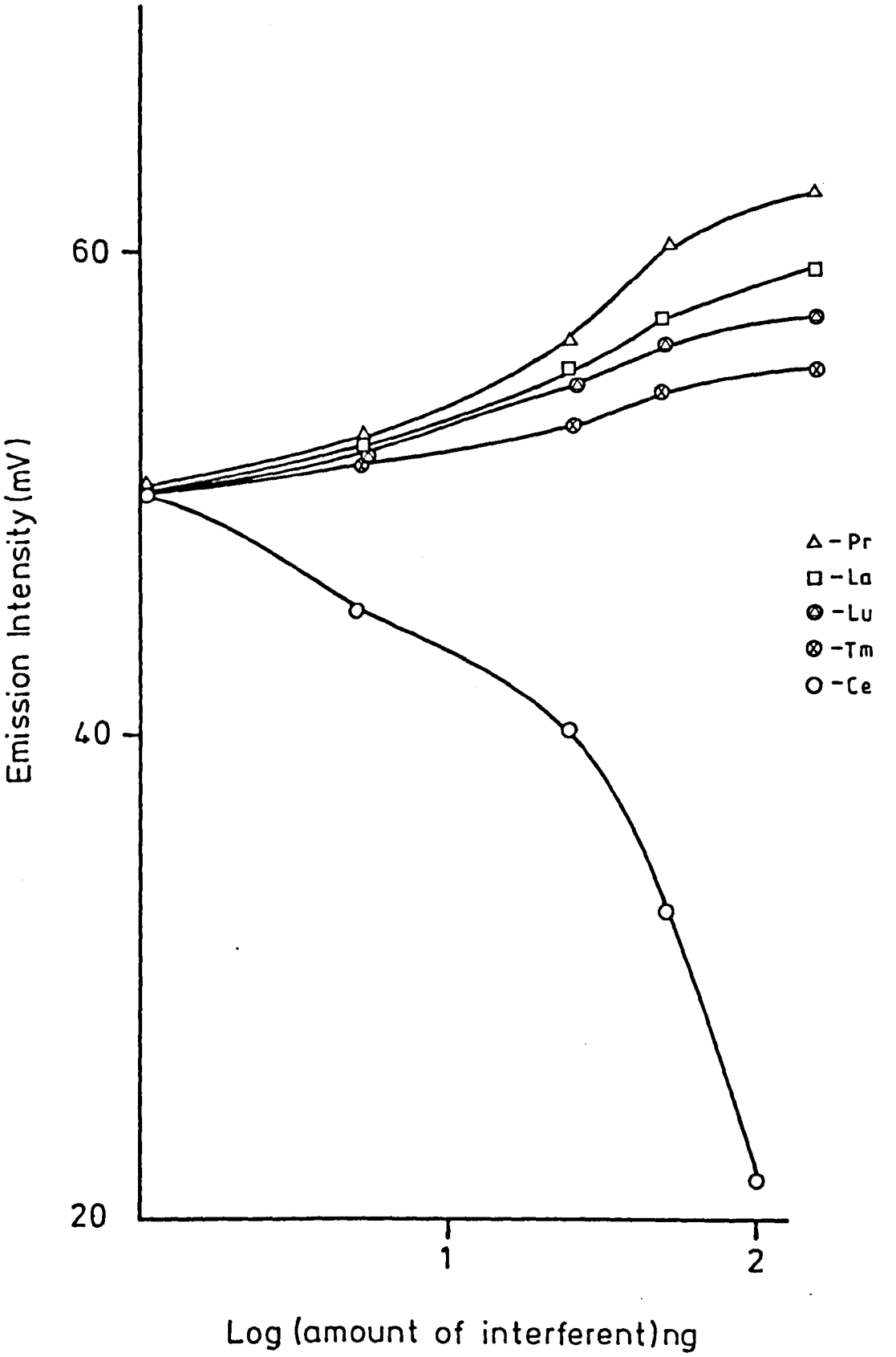

Fig. 4.9 Effect of other lanthanides on europium emission (10 ng).

PART II

FLOW INJECTION SPECTROFLUORIMETRIC DETERMINATION OF LANTHANIDES

CHAPTER FIVE

INTRODUCTION

5.1 Fluorescence Analysis

5.1.1 Introduction

Luminescence is the emission of radiation from an electronically excited substance. That excited substance may be atomic or molecular, solid, liquid or gaseous. The energy to excite the sample can come from many sources and serves to classify different types of luminescence as mentioned previously (see Table 1.3).

The following discussion will deal with the fluorescence (a process of photoluminescence) of solute molecules in solution. Fluorescence spetroscopy has received considerable attention and is now at the stage of active instrumental development[89], further investigation of fluorescence prcesses and extension of its applications as an analytical technique. The reason behind fluorimetry's importance and popularity is its great sensitivity and selectivity. This detection limit is often less than 1 ppb. It is also possible to select particular wavelengths with which to excite and monitor the fluorescence of a specific compound in the presence of many others.

Fluorescence analysis is extremely dependent upon environmental conditions, however. In some cases photodecomposition takes place, and self-absorption may occur, especially at high concentration. Temperature and

solvent viscosity affect the flucrescence intensity because of collisional relaxation from the excited state. Solution conditions such as pH, solvent and ionic strength influence the structural form of a compound and thus its potential to fluorescence. Quenching by simple impurities is also a frequent problem. An understanding of the fluorescence process has served to reduce many of the negative effects of these factors, making fluorescence analysis a very valuable technique.

5.1.2 Principles and Theory

The interaction of electromagnetic radiation with matter occurs by the quantized absorption and emission of energy by matter. Fig. 5.1 illustrates various energy transfer processes. Absorption or excitation often occurs by the absorption of ultra-violet or visible light (10^{-15} sec), raising the energy of the molecule from its ground state, S_o, to an excited vibrational level of an excited singlet state, S (Arrow A). The molecule may lose this acquired energy through one of several alternate pathways. Initially, scattering (Rayleigh and Raman) takes place (within 10^{-15} sec). The intensity, being proportional to the fourth power of the wavelength, is usually low in comparison to the fluorescence. Next, it is far more likely that the molecule will lose its vibrational excitation energy through collisions and fall to the lowest vibrational level of the S state. This process is called vibrational relaxation (10^{-14} - 10^{-12} sec) (Arrow R). In general, there will be excited vibrational levels of the

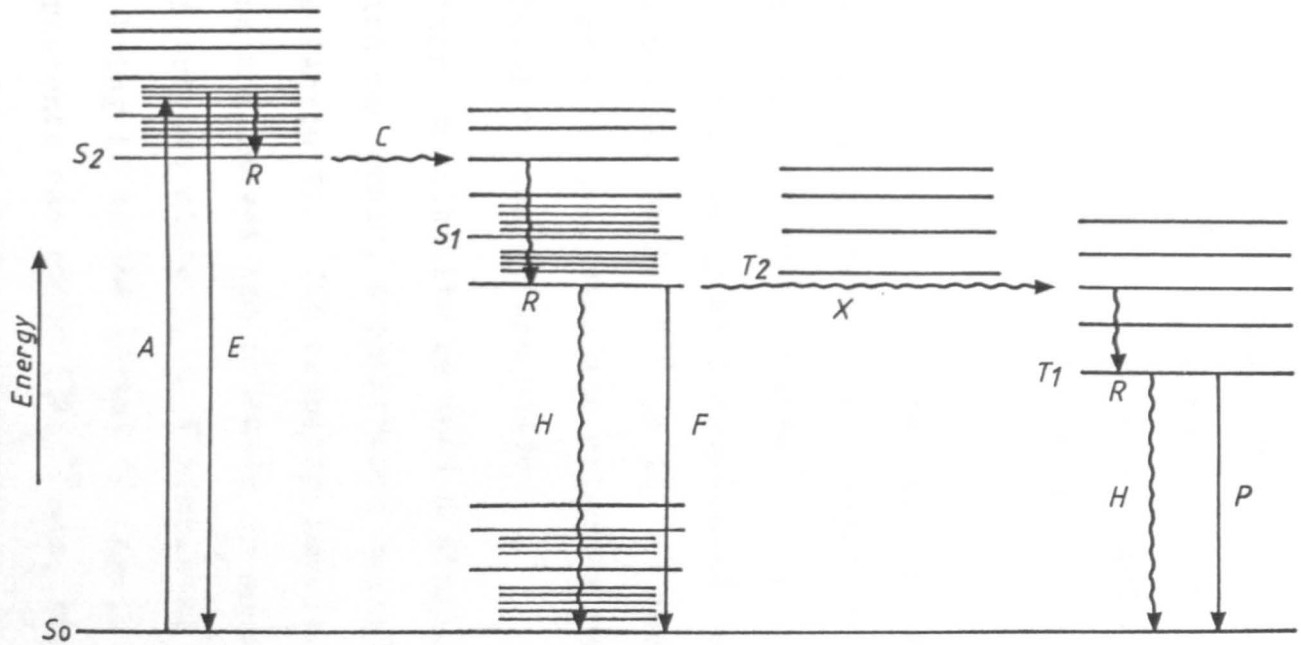

Fig. 5.1 Schematic energy level diagram of singlet and triplet states of a molecule showing luminescence phenomena.

next lowest singlet state (S_1 in this case) that have energies comparable to lowest S_2 state. A transition from lower vibrational levels of S_2 to near-by upper vibrational levels of S_1 may take place. This is called internal conversion (IC, 10^{-12} sec, Arrow C). The molecule then rapidly loses energy through additional collisions until it reaches the lowest level of the lowest excited singlet state, S_1 .

At this point, one of several things may happen. The molecule may simply return to the ground state by further collisions with other molecules in solution (quenching), dissipating the energy as non-radiated heat (Arrow H). Fluorescence (Arrow F, 10^{-9} to 10^{-7}s) can occur, with the release of a photon, when the molecule returns directly from the S_1 level to the ground state.

A third possibility is that a singlet-triplet (S_1 - T_1) transition can occur, a phenomenen called intersystem crossing (Arrow X). The crossing involves unpairing of two electrons and leaves the molecule in an excited vibrational level of triplet state T_1 . Vibrational relaxation will quickly bring it to the lowest T_1 level. From here phosphorescence can occur ($>10^{-5}$ sec, Arrow P) but only a few compounds exhibit phosphorescence, collisional deactivation (Arrow H) being more probable because of the long timescale involved.

5.1.3 Excitation and Emission Spectra

In practice, the fluorescence of a molecule is very dependent on molecular structure, solution conditions and instrument design. Characteristically, two spectra qualitatively and quantitatively describe any fluorescent molecule. The excitation spectrum (relative efficiency of various wavelengths to excite the sample) should ideally be identical to the absorption spectrum but instrumental differences introduce differences. The emission spectrum (relative fluorescence intensity at various wavelengths) appears at longer wavelengths (Stoke's shift) because of the non-radiative losses in the excited electronic state. Often a mirror-image relationship is seen between the excitation and emission spectra reflecting the similarity in vibrational structure of the two singlet states.

5.1.4 Quantitative Aspects

Quantitatively, fluorescence intensity is expressed by:

$$I_f = I_o K \Phi_f (1-e^{-abc}) \qquad 5.1$$

where:-

I_f and I_o are the fluorescence and source intensities, respectively,

K is a proportionality constant which incorporates the optical system and detector efficiencies:-

K = (photons measured) / (photons emitted),

Φ_f is the quantum efficiency, defined as:-

Φ_f = (photons emitted) / (photons absorbed).

a is the molar absorptivity, which is a constant depending mainly on the wavelength, the substance and the solvent,

b is the absorption path length and

c is the molar concentration.

Equation (5.1) can be simplified to:

$$I_f = I_o K \Phi_f (2.3\ abc)$$

In dilute solutions, when concentration is low ($< 10^{-5}$ M), the fluorescence intensity I_f is a linear function of concentration.

5.1.5 Instrumentation

The instrumentation to measure fluorescence, a fluorimeter, is generally very straightforward involving the following basic components: an intense excitation source, a holder of the sample cell, fluorescence detector, wavelength selection optics and the output system.
Fig. 5.2 shows line block diagram of a generalized fluorimeter.

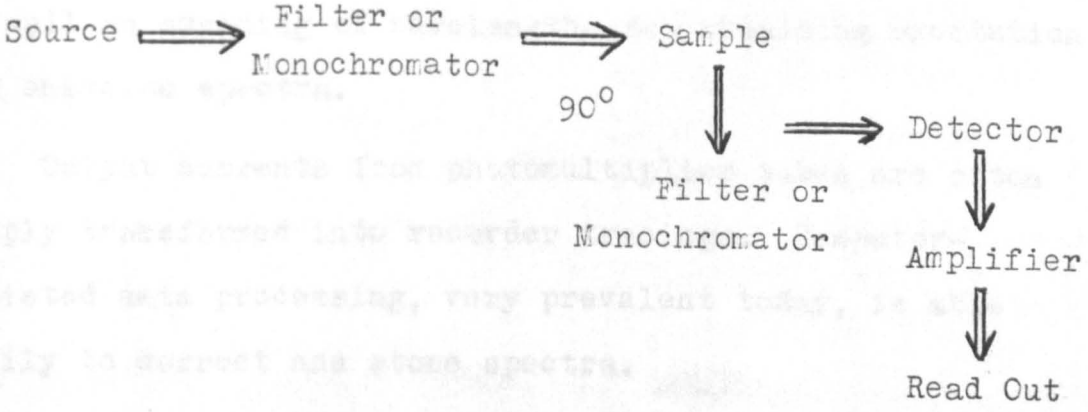

Fig. 5.2 Line block diagram of a generalized fluorimeter.

Radiation from the source is directed on the cell and the fluorescence emission usually detected at 90°. Sources range from continuous, moderately intense incandenscent bulbs to more intense gas-discharge lamp of greater power. But recently the coherent intense monochromatic laser radiation is being utilized to great advantage. Different types of quartz sample cells are used such as rectangular and circular, mirrored and blackened, static and flowing, large and micro-sized.

Photomultiplier tubes are the detectors most often used. Less efficient phototubes occur in less expensive systems while imaging detectors, having special multichannel time advantages, are being used in new specialized applications. For greater sensitivity it is necessary to select a particular wavelength for excitation and for detection. Either filters or monochromators can be used. Filters are a convenient, relatively inexpensive means of accomplishing this. Combinations of interference, band-pass, and cut-off filters generally serve the purpose. Grating monochromators provide enhanced selectivity of wavelengths, as well as scanning of wavelengths for obtaining excitation and emission spectra.

Output currents from photomultiplier tubes are often simply transformed into recorder tracings. Computer-assisted data processing, very prevalent today, is able easily to correct and store spectra.

5.1.6 Applications

Table 5.1 summarizes a wide range of general fluorescence applications. Beside these, there are many recent developments. Derivatization of compounds to fluorescent forms is of growing importance[90]. Labelling key compounds with fluorescent molecules allows the investigation of many additional reactions[91] and compounds[92] The use of matrix isolation methods[93], the interesting possibilities of fluorimetry in micellar solution[94,95] are also interesting. It is apparent that, with the increasing demand for highly sensitive and selective analysis in many areas of inorganic, organic and biological chemistry, the fluorescence technique will continue to be an important and fascinating field of research.

	Area	Analysis	Compounds
1.	Organic	Direct	Aromatics, Heterocyclics, Nitrogen Compounds, Halogen Compounds and Oxygen Compounds
	Biochemical	Clinical	Cells, Steroids, Lipids, Proteins, Amino Acids, Enzymes Drugs, Metabolites, Antibodies Antigens and Vitamins.
2.	Inorganic	Direct	Lanthanides, Uranium and Thorium.
		Chelates	Groups 1A, 11A, 11B, 111A, and 111B, Zr^{+4} , CN^- , F^- , I^- , $SO_4^=$ and Silicates.
		Forensic	Glasses

Table 5.1 Fluorescence Applications[85,96-98]

5.2 Flow Injection Analysis (F.I.A.)

5.2.1 Introduction

Continuous-flow analysis (CFA) techniques refer to methods where samples and reagents are introduced into a flowing stream (in tubing) for transport to a detector. Systems based on this design have been used to automate a wide variety of wet-chemistry assays[99].

Skeggs in 1975[100] revolutionized CFA with introduction of air segmentation to prevent sample dispersion and sample overlap. Air segmentation of samples was used almost exclusively for continuous-flow system throughout the 1960s, due in part to the introduction of the Technicon Auto Analyzer which gained wide acceptance as the standard system for automated analyzer, which was capable of 40 simultaneous assays at 200 samples per hour[99,101]. These types of analyzers have the disadvantages of high reagent consumption, noise and drift problems associated with the introduction and often necessary removal of air bubbles and limits on flow rates[102,103].

By the mid 1970s interest in non-segmented flow systems began to grow due to the efforts of two research groups, Ruzika and Hansen in Denmark (who coined the term "flow injection analysis" (FIA))[104] and Stewart et al. in the USA[105].

FIA is the rapid, reproducible injection of a liquid sample plug into a continuously laminar flowing reagent stream (without air segmentation) where mixing occurs by

diffusion. Response peaks appear proportional to analyte concentration in a more rapid, reproducible and controlled manner than with previous flow techniques[102,103].

The recent upsurge of interest in FIA can be seen in the number of articles published in the last ten years dealing with developments and application of FIA[106].

5.2.2 Theory and Principles of FIA

FIA is based on three main principles:-

(a) introduction of sample plug into an unsegmented continuously flowing reagent (or carrier) stream;

(b) constant residence time of the sample in the manifold (reproducible timing);

(c) controlled dispersion of the sample zone.

A typical diagram of a simple FIA system is shown in Fig. 5.3. It consists of carrier and reagents streams propelled by a peristalic pump and an injection valve, connected to a flow cell via a mixing coil. The product of the chemical reaction between the injected sample and the reagent stream is recorded as a peak as it passes through the detector cell.

The reproducibility of FIA is an essential quality dependent upon the consistency of injecting a precise sample volume and the flow rate.

The theory behind FIA dynamics with its practical results rests on the concept of dispersion. The ability to

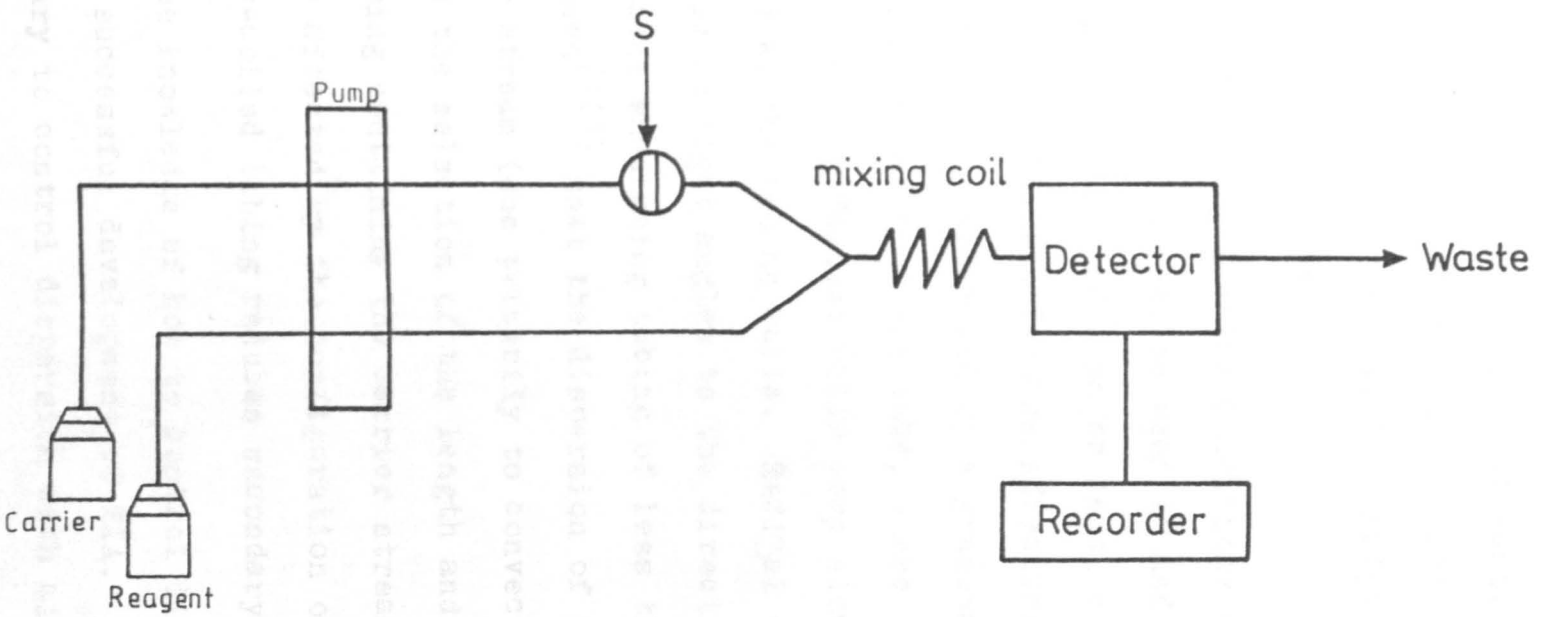

Fig. 5.3 Schematic diagram of a simple FIA system, S, sample injection.

control sample dispersion is a significant advantage of FIA. Dispersion can be thought of as the process of mixing between the sample and reagent streams. The dispersion coefficient, D, is defined conveniently as the ratio of the steady state signal (as with CFA analyzers) to the analytical peak height.

Under the experimental conditions normally used for flow analysis (flow rate between 10 and 0.5 ml/min) tubing diameters (internal) of 1 mm or less, convection and radial diffusion are the main factors affecting dispersion[107,108]. Convection is characterized by a gradient of flow rates across the diameter of the tube, where the centre of the sample is moving fastest while very slow or no flow is observed at the tubing walls. Radial diffusion, diffusion of molecules at right angles to the direction of flow, becomes significant when using tubing of less than 1 mm i.d. It has been shown[107] that the dispersion of plugs injected in a carrier stream (due primarily to convection) can be controlled through the selection of the length and internal diameter of the tubing containing the carrier stream. Dispersion can also be affected by the configuration of the tubing[108] as tightly-coiled tubing reduces secondary radical flow.

The knowledge of how to control dispersion was the key to the successful development of FIA. No longer was it necessary to control dispersion with air segmentation which eliminated high dispersion of injected plugs[109]. The elimination of air segmentation allowed improved precision in sample introduction via direct injection of fixed volumes

rather than timed aspiration techniques used in air segmented systems[110]. Residence times of the injected plugs were also more reproducible since surging of the carrier stream was eliminated when no bubbles were present, thus flow rates could be controlled more precisely[111].

5.2.3 Degrees of Dispersion

Dispersion is most commonly described in terms of three categories of limited (D = 1-3), medium (D = 3-10) and large (D>10) dispersion, each of which is used for different purposes.

For limited dispersion, where the original composition is to be measured as with electrochemical and atomic absorption methods, short, narrow tubes are used with slow flow rates. Rapid sample rates are possible with limited dispersion[103].

Medium dispersion is most advantageous when chemical reactions are utilized as is the case with most systems. Here dispersion increases with increasing flow rate (up to the point of turbulence) increasing tube length, increasing sample volume and increasing tube radius[112]. Colorimetric, and fluorimetric reactions are the major examples for medium dispersion. Such dispersion makes it possible to incorporate various analytical techniques to modify the FIA manifold such as liquid-liquid extraction, ion-exchange, dialysis and a reactor column in order to achieve sample treatment.

Large dispersion can provide some features that allow the application of FIA to several unusual analytical systems with a substantial degree of mixing. An elongated and well-defined peak profile is established containing a concentration gradient useful for special measurements. This is most easily achieved with a mixing chamber prior to the detector, as for example in continuous flow titrations[113]. This technique was subsequently automated, in which a fixed volume of sample is injected and then roughly mixed with titrant in a mechanically stirred chamber to form an exponential concent gradient[114].

5.2.4 Instrumentation

Most FIA apparatus is simple. Fig. 5.3 illustrated the fundamental set up for FIA systems which are as follows:

(a) Pumps

As mentioned previously, stable reagent flow is crucial to the feasibility of FIA. Therefore pumps play an important role. It is found that many simpler pumps supply satisfactory performance. Pumps such as syringe, progressive cavity, piston pressure head, peristalic, reciprocating and proportional pumps work well[111].

Peristalic pumps serve the largest portion of FIA systems. Examples of the most popular peristalic pumps used are the Ismatec[115] and Gilson Minipuls[116].

(b) Injection Port

Injectors need to be rapid, smooth and reproducible.

Increasing in sophistication and quality, injectors range from syringe septum and flap injectors to manual, simple rotary valves and loops, to automatic rotary, solenoid and slider valves and single and double proportional injectors[111,117-120].

(c) Detectors

Detectors are numerous. Any measurement system that can be equipped with a flow-through cell is applicable for FIA purposes. They can be placed sequentially on-line where non-destructive analyses are performed. Each has particular features of design to reduce detrimental effects on the flow dynamics.

They include a wide range of detection principles in combination with FIA, among which are spectrophotometry, fluorimetry, ion-selective electrodes, chemiluminescence, atomic absorption spectrometry, flame photometry, inductively coupled plasma, nephelometry, refractometry, voltammetry and polarography[106,121,122].

(d) Manifold Components in FIA

The manifold is the central component altered to suit specific chemical systems. It can be as simple as a single straight tube to as complex a system as a multichannel manifold with many interconnections and reactor functions.

The manifold is usually made of teflon, polyethylene or polypropylene, with an internal diameter (i.d.) of 0.3-1 mm depending on the dispersion pattern requisites. In practice teflon tubing of 0.5 or 0.8 mm i.d. is used in

most FIA.

Coils and packed reactor columns have significant importance in recent FIA development, either for monitoring a particular chemical phenomenon or for optimizing the dispersion conditions in the manifold[123,124]. Different kinds of chemical phenomenen have been monitored by using a small column in the FIA manifold filled with particles of reactive compound.

Examples of such reactors are ion-exchange resins[125-127], oxidizing agents[128], immobilized enzymes[129-132] and reducing materials[127,133,134]. A recent development is the introduction of a strongly reducing column in the manifold design[135] in order to produce unstable lower oxidation states of metal ions, which are rather difficult to produce and handle by conventional analytical techniques.

(e) Readout Devices

The reading of the output in FIA can be obtained by using a recorder or a microcomputer. Different FIA automation schemes have been employed including control of the various components of the system such as injection port and samplers which can be programmed with microprocessor interfacing. The evaluation of the results via peak height, kinetic data, linear regression, background correction and function monitoring are straightforward using a microprocessor[105].

A sensitive recorder can be used to register the readout and the shape of the peak as well as enabling the analyst to keep a record of the results.

5.2.5 Applications

As mentioned previously, FIA has seen extensive application to a variety of analytical methods, and has nearly unlimited potential. These applications have been reviewed recently by Ruzicka and Hansen[106]. A general list of the measurement systems used is as follows:

(a) Spectrometric Methods (spectrophotometry, atomic absorption spectrometry, fluorimetry, plasma emission spectrometry, chemi- or bio-luminescence, turbidimetry and nephelometry).

(b) Electrochemical Methods (amperometry, conductometry, potentiometry, including ion-selective electrodes, voltammetry).

(c) Enzymatic Methods and immunossay.

(d) Kinetic Methods (nonenzymatic).

(e) Gradient Techniques (gradient calibration dilution or scanning).

(f) Separation Methods (liquid chromatography, extraction, ion-exchange and filtration).

(g) Other Techniques (hydrodynamic injection, viscometry, incorporated column reactors, etc.).

This broad acceptance of FIA is undoubtedly due to its versatility, which allows the method to be used in conjunction with a wide variety of detectors and analytical techniques. It is also fast, reproducible and simple to separate.

5.2.6 F.I.A. for Lanthanides

Up to date, there are only two reports of the use of FIA systems to determine terbium and europium[136,137].

Burguera et al.[136] reported that terbium (1×10^{-2} to 100 $\mu g\ ml^{-1}$) may be determined by measuring the fluorescence of the terbium ternary complex (Tb (111) - EDTA - sulphosalicylic acid) at 545 nm and an excitation wavelength of about 320 nm. The FIA technique is used for monitoring the fluorescent reaction. A sample throughout of 90 analysis per hour is possible, and the relative standard deviation (r.s.d.) is less than 4.0% for ca. 80 pg In 8 μl samples with a detection limit of 1 pg.

Aihara et al.[137] developed a flow injection spectrofluorimetric method for determination of europium(111) as its ternary complex with thenoyltrifluoroactone and triocytlphosphine oxide in a micellar solution of nonaoxyethelenedodecyl ether. This procedure is satisfactory for europium determination in the range 1.5-150 ng ml^{-1} at a sampling rate of 55 per hour. The r.s.d. was less than 1.2% with no interference from 20-fold excesses of other rare earth ion.

The main aim of the second part of this work is to apply the combination of FIA with spectrofluorimetry in order to provide rapid, reproducible, sensitive and selective analytical methods for various lanthanides.

CHAPTER SIX

FLOW INJECTION FLUORIMETRIC DETERMINATION OF CERIUM(III), CERIUM(IV) AND SIMULTANEOUS DETERMINATION OF CERIUM(III), CERIUM(IV)

6.1 Introduction

6.1.1 Principles of Metallic Reductors

A number of pure metals can be used as reducing agents in different physical forms, such as wire coil, shot and powder. Several metals, in particular zinc, silver, cadmium, aluminium, nickel, copper and mercury have been widely used in analytical procedures[138,139]. The value of these reductants is attributed to the selectivity of their reducing action, which is a function of the electrode potential of the metal-metal ion couple and to the ease of removing excess of the reducing agents by filtration, washing or dissolution in acid[140].

Very active metals, such as zinc, cadmium and aluminium not only reduce the analyte but also dissolve in acidic solutions with the evolution of hydrogen. This side reaction is not desirable, since it can consume large amounts of the metal and introduce a considerable quantity of metal ion into the sample solution. The reaction can be largely prevented by amalgamating the metal with mercury.

Amalgamated zinc is commonly known as the Jones reductor, and is generally prepared by treating granulated zinc with a dilute solution of mercury(II) chloride; mercury is produced as a coating of amalgam. The addition of mercury does not affect the standard potential of the Zn(II)/Zn couple (0.76V) as long as solid zinc is present (141). The rate of reduction, however, depends on the concentration of zinc at the surface of the amalgam[142]. With relatively strong

oxidants, such as Fe(lll) and Ce(lV), which are reduced by mercury, a mercury content of 1 or even 5% may be used at high acid concentration to control the rate of hydrogen evolution. With weaker oxidants the mercury content should be minimized so that the reduction reaction is not retarded.

Table 6.1 lists several commonly used metallic reductors and some elements they will reduce[85]. The Jones reductor is relatively non-selective as a reducing agent because of its strongly negative potential. It can reduce many species to lower oxidation states including the metal, as shown in Table 6.1.

The silver reductor, originally developed by Walden et al.[143], has found wider applications due to its milder reducing character and hence more selective reducing properties. The other reductors have been used for specific applications, as illustrated in Table 6.1. However, the Jones and silver reductions are the most widely used in analytical procedures.

6.1.2 Fluorescence of Lanthanides in Solution

Many inorganic substances are capable of fluorescence in the solid state; the only salts which fluoresce in solution are those of some lanthanide elements (Ce, Pr, Sm, Eu, Tb and Dy) uranium and thorium.

It is only this small group of compounds that can be detected in aqueous solution by the luminescence of their simple ions.

Reductor	Element Reduced
Zn(Hg) (Jones reductor)	$Fe(III) \longrightarrow Fe(II)$, $Cr(VI) \longrightarrow Cr(II)$, $Cr(III) \longrightarrow Cr(II)$, $Ti(IV) \longrightarrow Ti(III)$, $V(V) \longrightarrow V(III)$, $Mo(VI) \longrightarrow Mo(III)$, $Ce(IV) \longrightarrow Ce(III)$, $Cu(II) \longrightarrow Cu$.
Ag(1M HCl) (Walden reductor)	$Fe(III) \longrightarrow Fe(II)$, $U(VI) \longrightarrow U(IV)$ $Mo(VI) \longrightarrow Mo(V)$ (2M HCl), $Mo(VI) \longrightarrow Mo(III)$ (4M HCl), $V(V) \longrightarrow V(IV)$, $Cu(II) \longrightarrow Cu(I)$.
Al	$Ti(IV) \longrightarrow Ti(III)$
Pb	$Sn(IV) \longrightarrow Sn(II)$ $U(VI) \longrightarrow U(IV)$
Cd	$ClO^{-1} \longrightarrow Cl^{-1}$

Table 6.1 Metallic reductors[85]

The fluorescence spectra emitted by aqueous solutions of those lanthanide ions when they are irradiated by UV light have been known since the 1930s[144-147].

The analytical aspects of the fluorescence of lanthanides in solution were exploited by a number of groups to detect Ce, Sm, Tb and Dy as impurities in solutions of other lanthanides[148-151]. Zaidel et al.[149-151] made a detailed study of the fluorescence of lanthanides in solution. They reported that Tb, Gd and Ce display the strongest fluorescence.

They regarded fluorescence as the most sensitive method for the detection of these ions. The method is less sensitive for Eu and is not sensitive enough to be applied to Dy and Sm. They also reported that 10^{-8}, 10^{-6} and 10^{-4} g/ml as detectable concentration for Ce, Tb and Eu, respectively. The fluorescence spectra of some lanthanide elements in aqueous solution such as Ce[152,153], Tb[154-156], Sm[154,155], Eu, Gd, Pr and Dy[157,158] have been published.

Cazotti and Abrao[159] studied the direct spectrofluorimetric determination of Ce, Tb, Eu, Gd and Dy in inorganic acid (HCl, $HClO_4$ and H_2SO_4) and thorium solutions. The detection limits and the experimental conditions for those lanthanide elements are shown in Table 6.2.

Of the lanthanide ions, Cerium(III) is one that presents the strongest fluorescence in aqueous inorganic solutions. Armstrong et al.[160] observed the fluorescence of Ce(III) in inorganic acid solutions such as HCl, $HClO_4$

Element	Excitation (nm)	Fluorescence (nm)	Detection limit in	
			HCl ($\mu g\ ml^{-1}$)	$ThCl_4$ ($\mu g/g Th$)
Ce	257	350	0.001	0.01
Tb	226,352*(372)	545	0.5	50
Eu	394	595	10	80
Gd	275	312	10	200
Dy	352	480	100	does not fluorescence

* Excitation peak completely absorbed by Th.

Table 6.2 Experimental conditions and detection limits for direct spectrofluorimetric determination of lanthanides in inorganic acids and thorium solutions[159].

and H_2SO_4 . They suggested the possibility of determination of Ce(111) by fluorimetry, and later Ce(111) fluorescence was studied in inorganic acid solutions[152,159,161]. Ce(111) has a characteristic fluorescence which has its excitation maximum at 260 nm and emission maximum at 350 nm. The detection limit in some cases has been reported as less than 4 ng ml^{-1} , with no interference from other lanthanides[159].

Burns and Qureshi[162] developed a simple procedure to determine Ce(111), in carbon and low alloy steels, based on the native fluorescence of Ce(111) ion. A 0.002% w/w concentration was reported as the detection limit with 4-6% r.s.d. The interference of iron(111) and chromium(V1) was removed by reduction with hydroxylamine or a Jones reductor before fluorimetric determination of Ce(111) at 260 nm and 350 nm as excitation and emission wavelengths, respectively.

Analytically, cerium is usually differentiated from other lanthanide family members on the basis of the strong oxidizing power of Ce(1V) in acidic solution. Ce(1V) is not fluorescent, but can easily be reduced to Ce(111) which offers a method for the indirect spectrofluorimetric determination of Ce(1V) and several other species which cannot be determined directly by spectrofluorimetry, but which can reduce Ce(1V) to Ce(111).

Cukor and Welberling[152] reported that a rapid and direct method for determination of cerium in yttrium oxide can be achieved by reduction of Ce(1V) with titanium(111) and measured the fluorescence of Ce(111) at 260 nm/355 nm.

0.1 μgCe / g yttrium oxide was reported as the detection limit, with 6% r.s.d. Kirkbright et al.[153] reported an indirect spectrofluorimetric method for As(III), Fe(II), oxalate, Cs(VIII) and iodide by measurement of the Ce(III) fluorescence produced by their reduction of Ce(IV) or catalysed redox reaction of As(III) with Ce(IV) (e.g. osmium).

Nitrate, thiosulphate and iodide can similarly be determined after chromatographic separation by their reaction with Ce(IV) in a postcolumn packed reactor[163]. Application of a solid reductant in the form of minireductor columns have been found to be particularly effective in FIA. A recent development is the introduction of a strongly reducing minicolumn in the manifold design[136,164] in order to produce unstable lower oxidation states of metal ions which are rather difficult to produce and handle by conventional analytical techniques. As a reducing agent a Jones reductor appeared to be very effective. Recently, Faizullah and Townshend[133] described an FIA procedure for the simultaneous spectrophotometric determination of iron(II) and iron(III). The injected sample was split into two, part reacted directly with 1,10-phenanthroline to give a response for iron(II), the remainder was directed through a zinc reductor minicolumn before rejoining the original stream for reaction with 1,10-phenanthroline, so as to give a second peak corresponding to total iron.

This work describes a direct spectrofluorimetric determination of Ce(III) by FIA, based on the fluorescence of Ce(III) ion and describes the determination of Ce(IV)

after reduction to the fluorescence species Ce(lll). It also describes the simultaneous spectrofluorimetric determination of Ce(lll) and Ce(lV) based on the same principle to that described above for iorn, in which part of the sample is directed through a zinc reductor minicolumn to reduce Ce(lV) to Ce(lll).

6.2 Experimental

6.2.1 Reagents and Chemicals

All chemicals were of analytical grade except for cerium(lll) nitrate ($Ce(NC_3)_3 \cdot 6H_2O$) which was 99.9% pure (Koch-Light Laboratories) ammonium cerium(lV) nitrate ($(NH_4)_2Ce(NO_3)_6$) which was 99.9% pure (Sigma). The other lanthanide interfering ions were as described in Chapter 3.

6.2.1.1 Cerium(lll) and Cerium(lV) Solutions

A 100 $\mu g\ ml^{-1}$ Ce(lll) solution was prepared by dissolving 0.2810g of $Ce(NC_3)_3.6H_2O$ in distilled water and diluting to 1 l with deionized water, which was used throughout.

A 100 $\mu g\ ml^{-1}$ Ce(lV) solution was prepared by dissolving 0.3912g of $\left((NH_4)_2Ce(NO_3)_6\right)$ in 600ml of deionized water containing 10ml of concentrated sulphuric acid, 2g of sodium peroxodisulphate and 2ml of 0.1 M silver nitrate. The solution was boiled for 10 min and diluted to 1 l with water[165,166]. Calibration solutions were prepared by serial dilution of the stock solution with water.

6.3 Apparatus

The detector used for all measurements was a Perkin-Elmer model 3000 fluorescence spectrometer with a flow cell comprising a silica tube, i.d. 2.5mm, 40mm long, held vertically in the sample compartment in a rigid mount[167].

6.3.1 Preparation of the Reductor

The Jones reductor was prepared as follows[127,168]. Zinc shot (BDH, 20-30 mesh) was sieved through a 22-mesh sieve, 4g was covered with 1 M hydrochloric acid and stirred for 1 min. The liquid was decanted and 30ml of 0.25 M mercury(11) nitrate (or chloride) solution added. The mixture was stirred thoroughly for 3 min. The liquid was again decanted and the amalgam was washed three times with water. The amalgam was added slowly to a 25mm long glass tube (2mm i.d.) until the required packing was achieved. A thin layer of glass wool was put at both ends of the column to prevent movement of the amalgam by the carrier stream. A small piece of silicon rubber tubing (0.8mm i.d.) was pushed into each end of the column so as to achieve a very tight connection. An electronic vibrator (Pifco, 50HZ) was used to settle the particles uniformly in the column. Water was passed through the column and the reductor was stored in this condition until required for use.

6.3.2 Flow Manifold

The manifold used for the determination of Ce(111) is shown in Fig. 6.1. A peristaltic pump (Ismatec SA 8031,

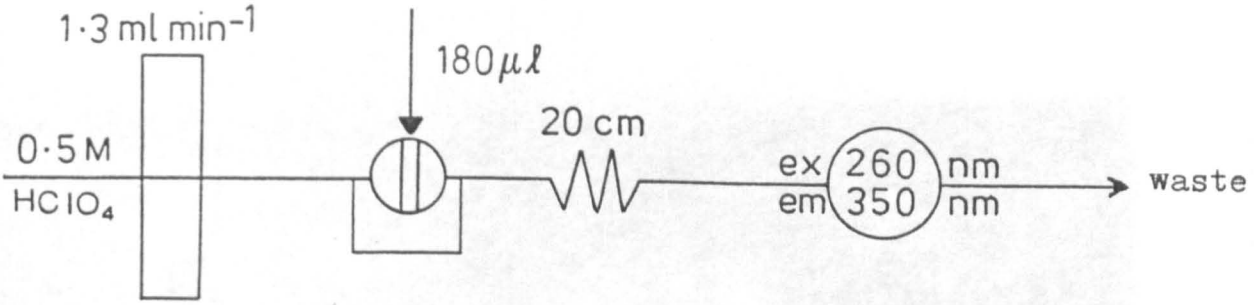

Fig. 6.1 Manifold for the determination of Ce(III).

Zurich) was used with 1 ml min^{-1} pump tubing, and the sample was introduced via a Rheodyne RH5020 injection valve (Anachem) with a sample loop of 180 µl. Teflon tubing (0.5mm i.d.) was used for the rest of the manifold.

The fluorescence was measured at 260 nm (excitation) and 350 nm (emission) and the spectrofluorimeter was set with excitation and emission slits at 10. The spectrofluorimeter was connected to a Teckman Labwriter TE200 recorder. The complete FIA system is shown in Fig. 6.2.

Ce(IV) can be determined by incorporating a zinc reductor minicolumn into the system between the pump and the 20cm delay coil in Fig. 6.1. Simultaneous determination of Ce(III) and Ce(IV) was achieved by modifying the manifold shown in Fig. 6.1 by splitting the sample injected into two streams and incorporating a zinc reductor minicolumn into the system. The complete assembly is shown in Fig. 6.3.

6.4 Results and Discussion

6.4.1 Optimization of Variables


B
A
D
C
E
Waste

A. Perkin-Elmer Model 3000 fluorescence spectrometer

B. Peristaltic pump

C. Rheodyne RH5020 injection valve

D. Home-made flow cell

E. Zn amalgam mini-reductor column

Fig. 6.2 The complete FIA system used for the spectrofluorimetric determination of cerium(III) and total cerium.

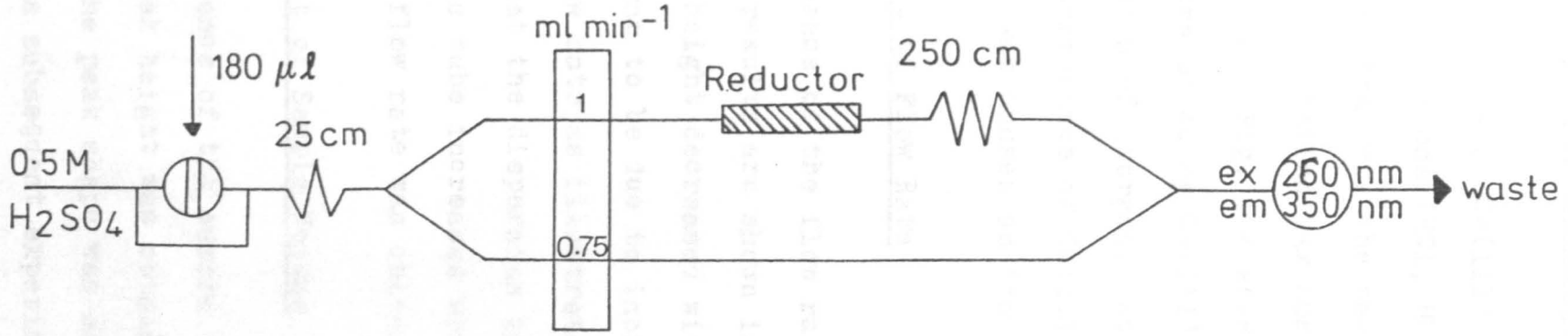

Fig. 6.3 Manifold for the determination of Ce(IV) and total cerium.

6.4.1.1 Excitation and Emission Spectra of Cerium in Inorganic Acids (HCl, $HClO_4$ and H_2SO_4)

The fluorescence of Ce(III) was studied in various inorganic acid solutions (HCl, $HClO_4$ and H_2SO_4). The fluorescence spectra were the same in the three acids. Ce(III) has an excitation maximum at 260 nm and emission maximum at 350 nm. Fig. 6.4 shows the excitation and emission spectra of 40 ng Ce(III) ml^{-1} in perchloric acid. The concentration of inorganic acids was found not to affect the fluorescence of Ce(III) in the range 0.01 - 1 M, so 0.5 M $HClO_4$ was chosen as the carrier stream.

6.4.1.2 Effect of Flow Rate

The influence of the flow rate on the peak height was studied. The results are shown in Fig. 6.5, which indicated that the peak height decreased with increasing flow rate. This was thought to be due to increasing dispersion with increasing flow rate as illustrated in Table 6.3. This table shows that the dispersion and the length of the solution in the tube increases with increasing flow rate. A 1.3 ml min^{-1} flow rate was chosen for subsequent work.

6.4.1.3 Effect of Sample Volume

The influence of the sample volume is shown in Fig. 6.6. The maximum peak height was obtained when 205 µl was injected but the peak shape was somewhat distorted, so 180 µl was injected in subsequent experiments.

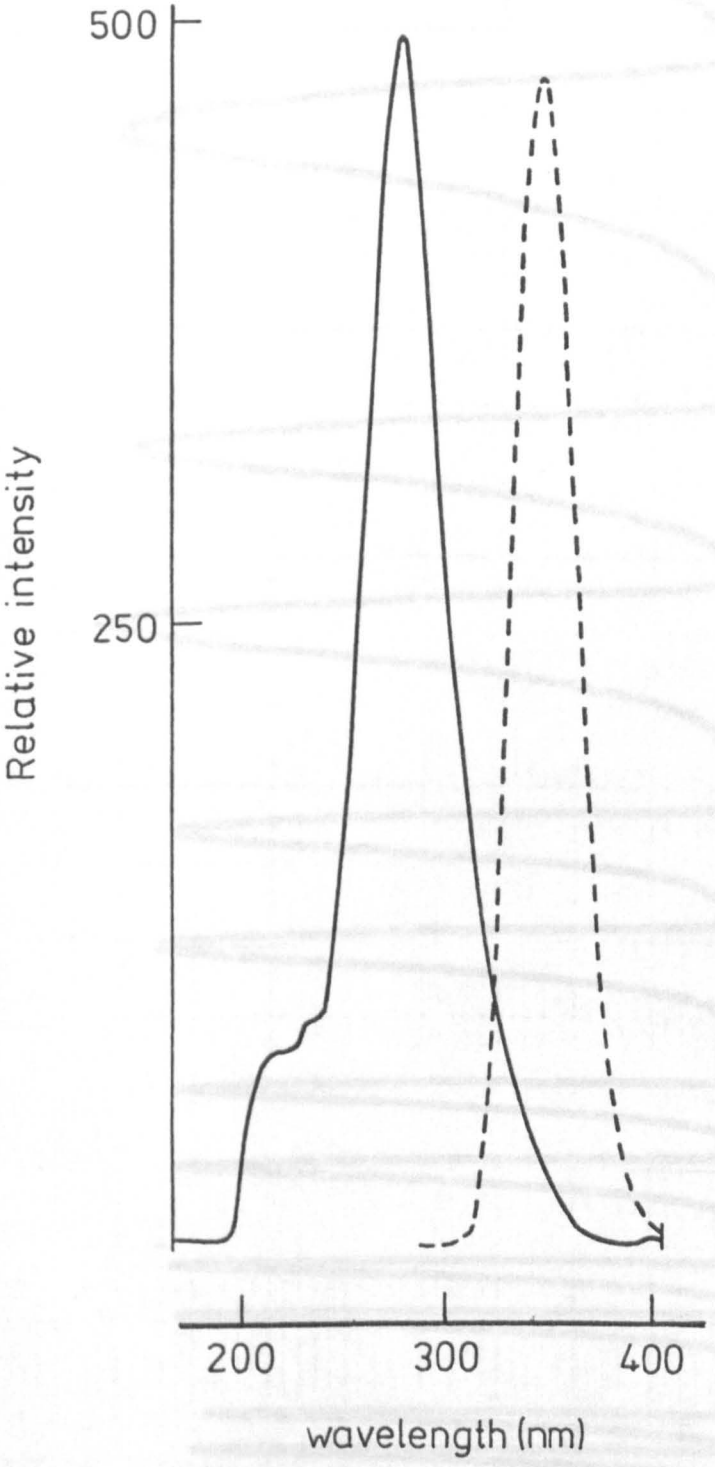

Fig. 6.4 Fluorescence spectra of cerium(III) in 0.5 M $HClO_4$:

(—) excitation spectrum, emission measured at 350 nm ;

(---) emission spectrum, excitation at 260 nm.

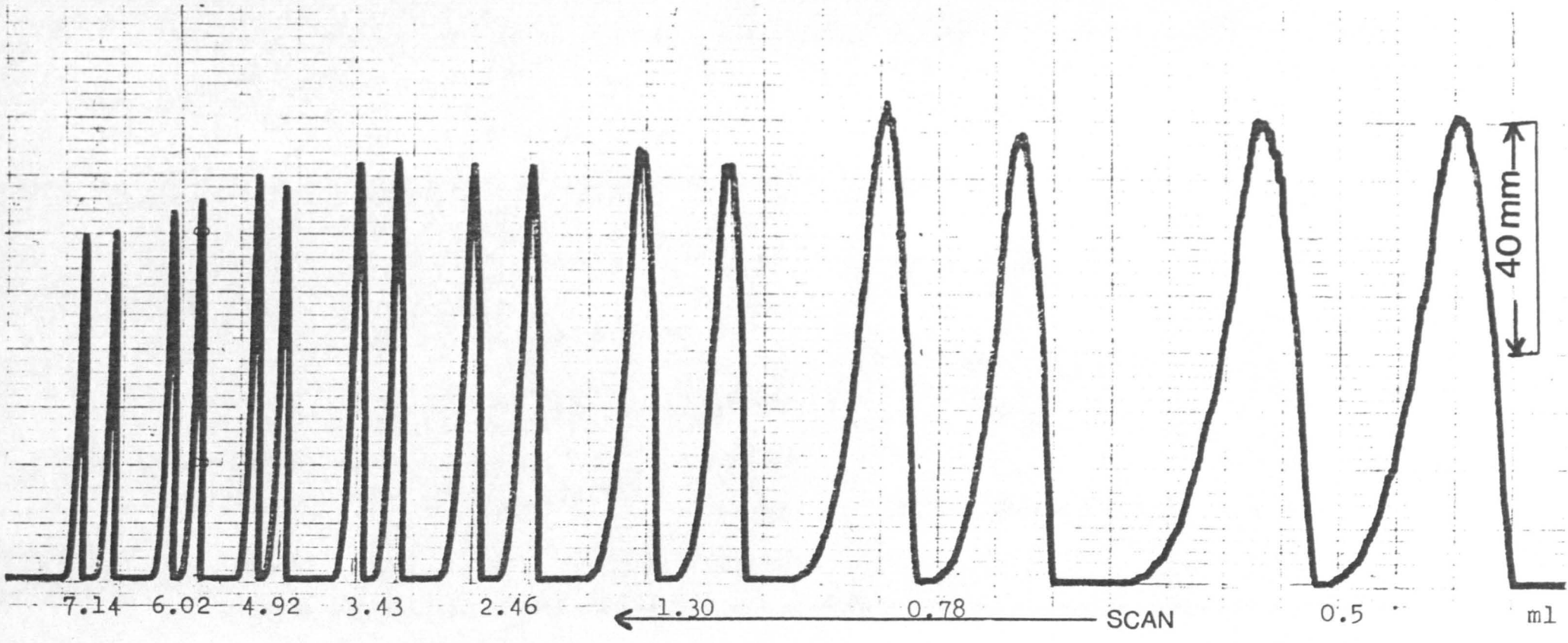

Fig. 6.5 The effect of the flow rates on the peak height and shape of 40 ng Ce(lll) ml .

Flow rate (ml min^{-1})	Peak height (mm)	½ Peak width (min)	Length of solution in detector (cm)	Dispersion (D)
0.51	81.5	0.080	20.2	2.72
0.78	80	0.050	19.9	2.77
1.30	74	0.040	23.9	3.00
2.46	71.5	0.023	29.2	3.10
3.43	70	0.020	33.9	3.17
4.92	69	0.015	37.6	3.21
6.02	64.5	0.012	38.3	3.44
7.14	60	0.011	40.3	3.70

Table 6.3 The effect of the flow rates on the peak height, peak width, length of solution in detector and dispersion.

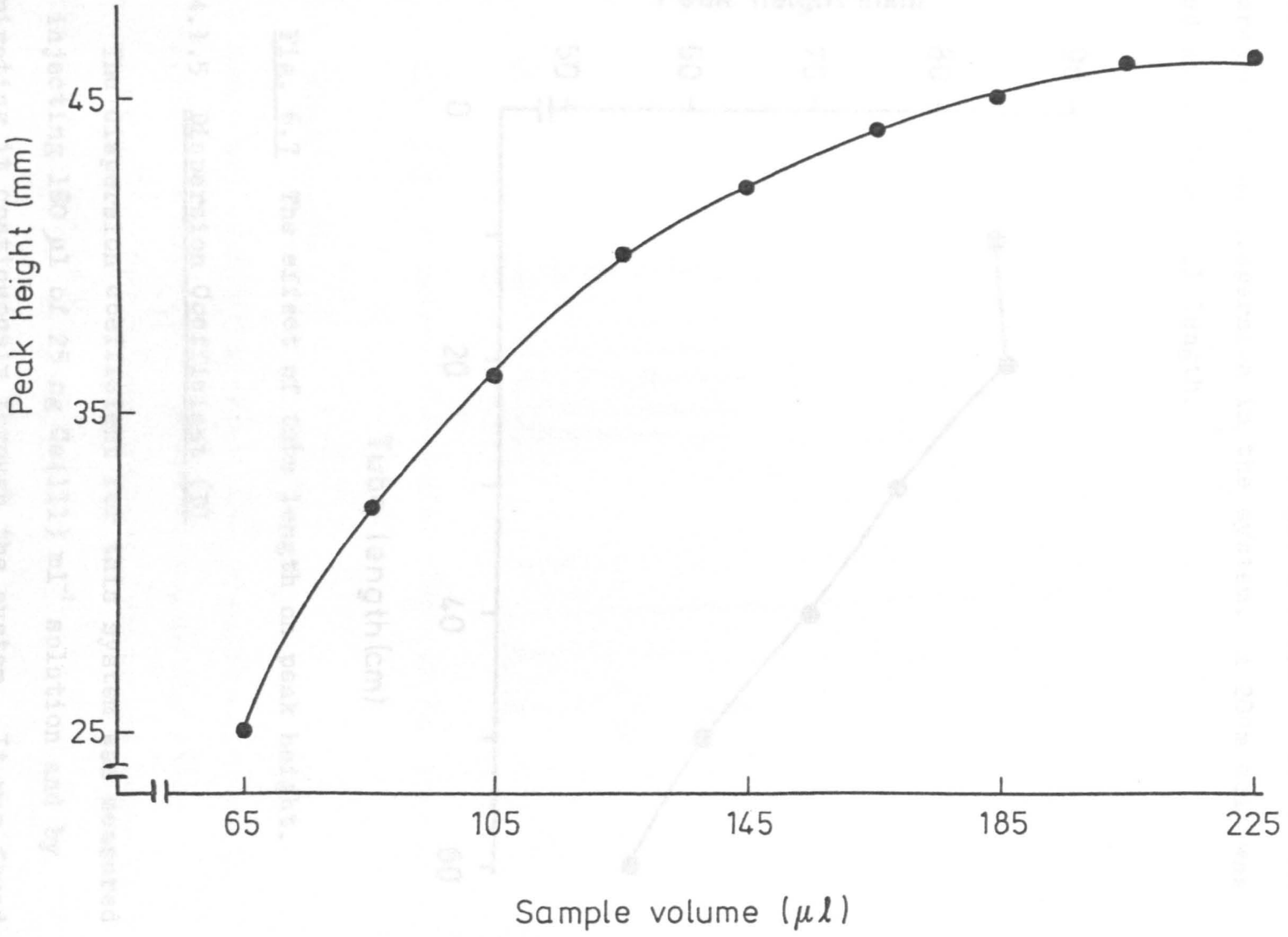

Fig. 6.6 The effect of the sample volume on the peak height of 40 ng Ce(III) ml^{-1} .

6.4.1.4 The Effect of the Tube Length

Figure 6.7 shows the effect of tube length on the 40 ng ml^{-1} Ce(111) peak height. It is clear that as the tube length increases the peak height decreases due to the increase of the dispersion in the system. A 20cm coil was used as optimum coil length.

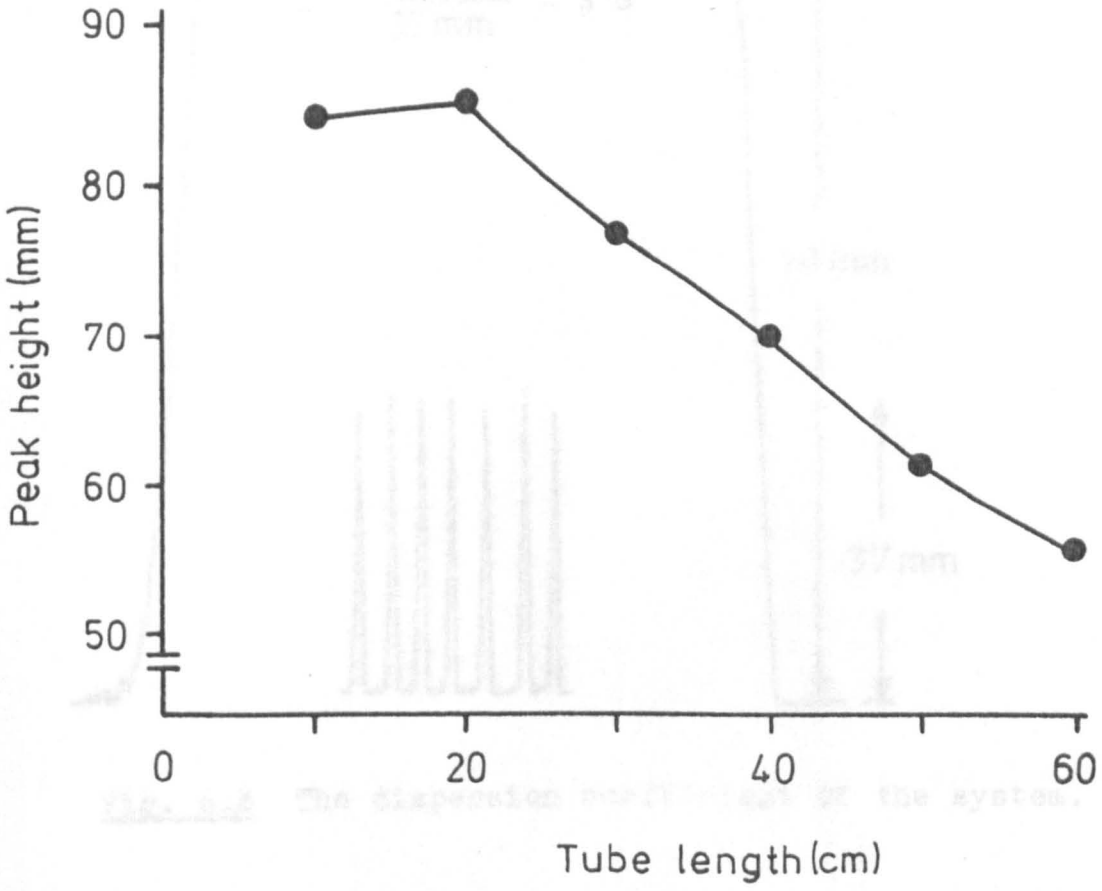

Fig. 6.7 The effect of tube length on peak height.

6.4.1.5 Dispersion Coefficient (D)

The dispersion coefficient for this system was measured by injecting 180 µl of 25 ng Ce(111) ml^{-1} solution and by aspirating it continuously through the system. It was found

to be 3.0 as shown in Fig. 6.8.

The residence time was 23 s and the sample throughput could be 150 h^{-1} .

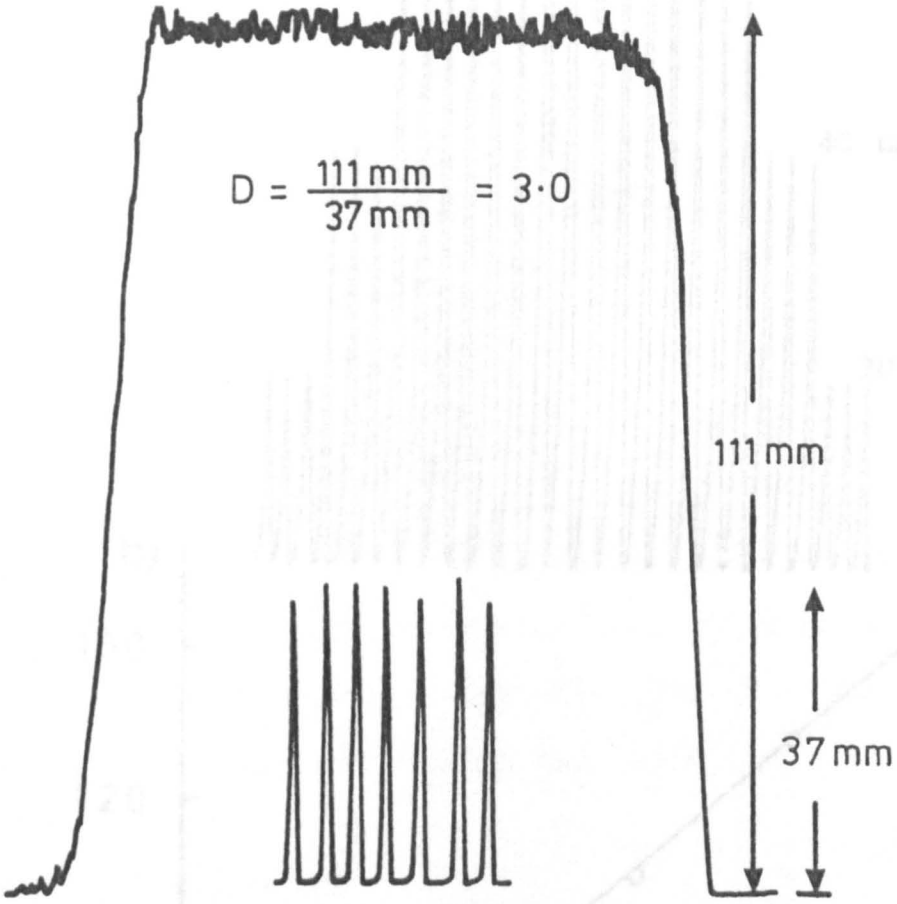

Fig. 6.8 The dispersion coefficient of the system.

6.4.2 Calibration

Under the conditions established a calibration graph for Ce(lll) was obtained. It was linear in the range 0 - 100 ng ml^{-1} . Typical calibration results are shown in Table 6.4 and Fig. 6.9.

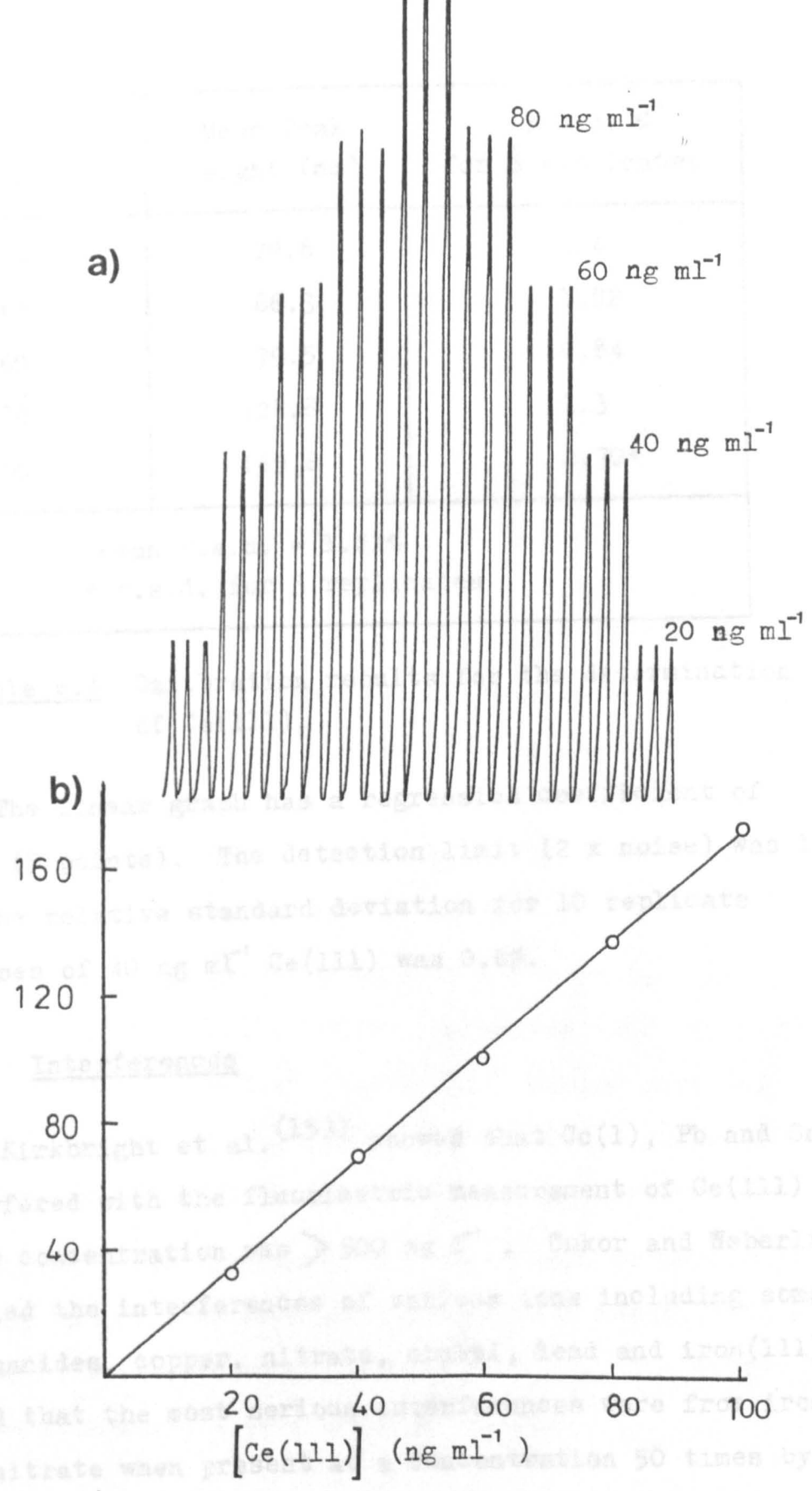

Fig. 6.9 (a) Peaks obtained by injecting Ce(III) standards in the concentration range shown; (b) the corresponding calibration graph.

Ce(III) Conc. ng ml^{-1}	Mean Peak height (mm)	r.s.d. % for 6 replicates
20	29.8	1.4
40	66.3	1.82
60	99.5	0.84
80	128.8	1.3
100	165.6	0.70*
Mean r.s.d. = 1.21% * r.s.d. for 3 replicates		

Table 6.4 Calibration results for the determination of Ce(III).

The linear graph has a regression coefficient of 0.999 (5 points). The detection limit (2 x noise) was 1 ng and the relative standard deviation for 10 replicate analyses of 40 ng ml^{-1} Ce(III) was 0.6%.

6.4.3 Interferences

Kirkbright et al.[153] showed that Co(II), Pb and Sn(II) interfered with the fluorimetric measurement of Ce(III) when their concentration was $>$ 500 mg l^{-1}. Cukor and Weberling[152] studied the interferences of various ions including some lanthanides, copper, nitrate, nickel, lead and iron(III) and found that the most serious interferences were from iron(III) and nitrate when present at a concentration 50 times by weight that of Ce(III). Other workers also showed that iron(III) and nitrate caused great quenching of Ce(III)

fluorescence[159,162] due to their strong absorbance in the ultraviolet region. Nitrate can be eliminated by several evaporations with HCl or $HClO_4$. The interference of Fe(111) is easily minimized by its reduction to Fe(11) with hydroxylamine or a Jones reductor[159,162], because Fe(11) does not interfere.

Gazotti and Abrão[159] studied the quenching effect of thorium on Ce(111) fluorescence. A concentration of 200g Th l^{-1} decreased the intensity to 20% of its value, but even so it was possible to determine 4 ng Ce ml^{-1} in a solution of 200g Th l^{-1} . It is reported[159,162] that Ce(1V) interferes by decreasing the fluorescence of Ce(111) because Ce(1V) absorbs radiation near to 260 nm and also absorbs radiation from fluorescence of Ce(111) at 350 nm. For the determination of total cerium, Ce(1V) can be reduced with hydroxylamine or a Jones Reductor.

In this work, only the effects of other lanthanide ions were studied (Fig. 6.10). Most lanthanide ions (La, Nd, Pr, Gd, Er, Ho and Lu) had no effect, and terbium gave only a slight depression of the fluorescence. Ce(1V) also did not interfere at $\leq$ 100 times the Ce(111) concentration.

Sodium peroxodisulphate was added when preparing Ce(1V) solution in order to oxidize any Ce(111) present, with silver nitrate to catalyse the oxidation[166,167]. The excess of peroxodisulphate was destroyed by boiling.

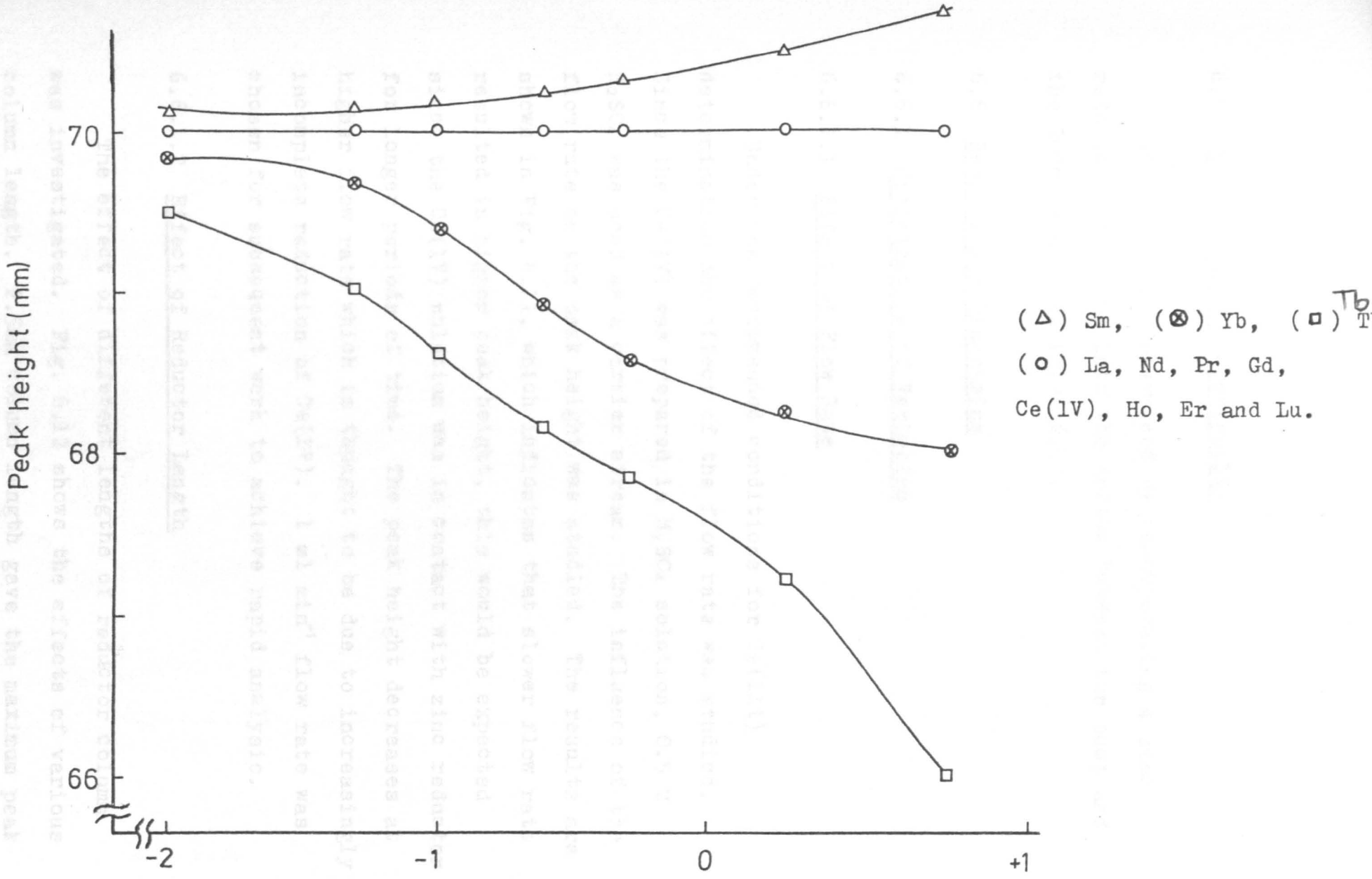

Fig. 6.10 Effect of other lanthanides on the determination of Ce(lll) 40 ng ml^{-1} in 0.5 M $HClO_4$.

6.5 Determination of Cerium(1V)

Ce(1V) can be determined by incorporating a zinc reductor minicolumn into the system between the pump and the 20cm delay coil (Fig. 6.1).

6.6 Results and Discussion

6.6.1 Optimization of Variables

6.6.1.1 Effect of Flow Rate

Under the recommended conditions for Ce(111) determination the effect of the flow rate was studied. Since the Ce(1V) was prepared in H_2SO_4 solution, 0.5 M H_2SO_4 was used as a carrier stream. The influence of the flow rate on the peak height was studied. The results are shown in Fig. 6.11, which indicates that slower flow rate resulted in higher peak height, this would be expected since the Ce(1V) solution was in contact with zinc reductor for longer periods of time. The peak height decreases at higher flow rate which is thought to be due to increasingly incomplete reduction of Ce(1V). 1 ml min^{-1} flow rate was chosen for subsequent work to achieve rapid analysis.

6.6.1.2 Effect of Reductor Length

The effect of different lengths of reductor column was investigated. Fig. 6.12 shows the effects of various column length. 2.5mm column length gave the maximum peak height. The internal diameter was kept constant at 2mm

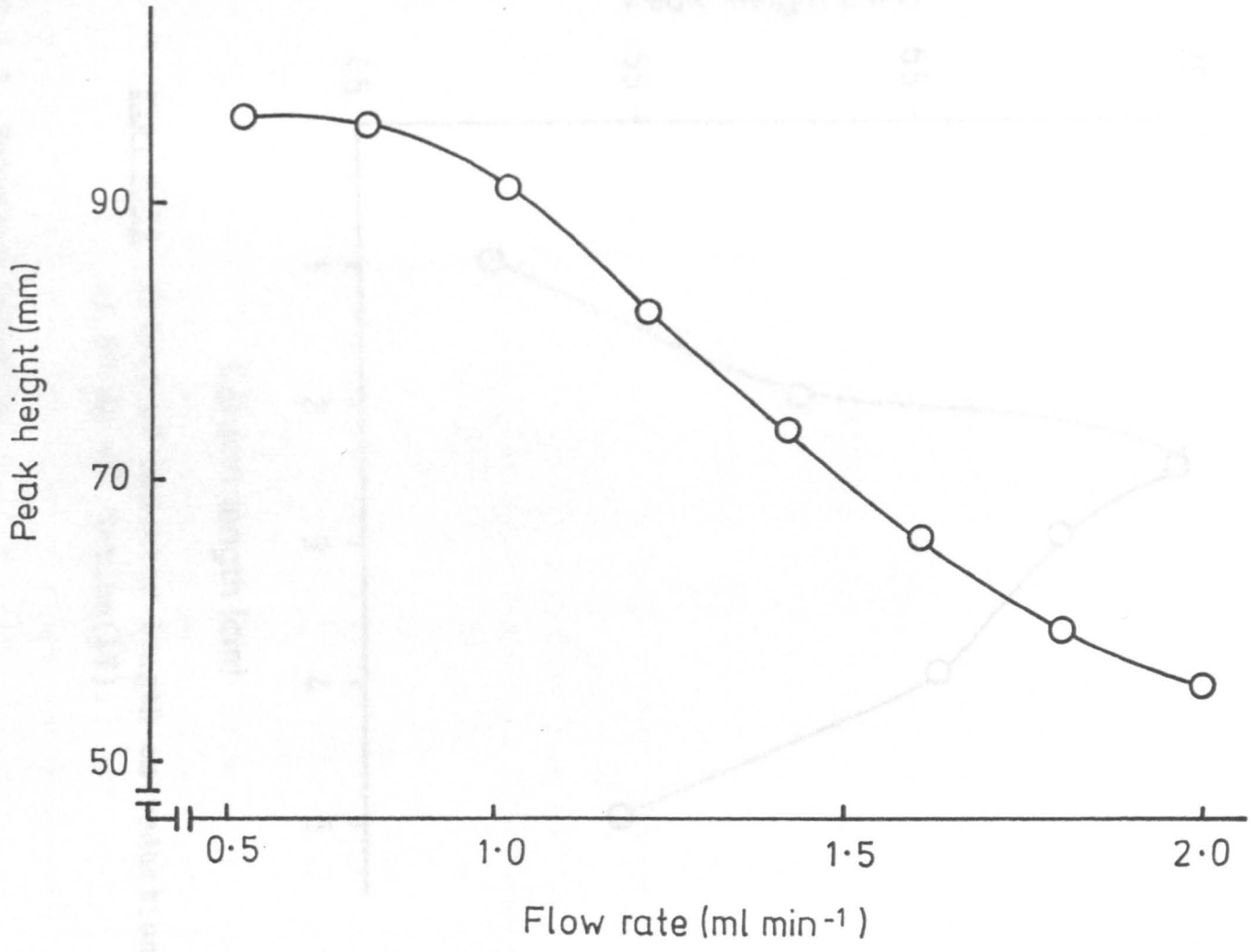

Fig. 6.11 The effect of the flow rate on the peak height of 100 ng ml^{-1} cerium(IV).

during this study, which is the minimum diameter that can suitably be packed with the amalgam particles, and therefore no attempt was made to use a wider column, to avoid a further increase in dispersion. Hence a 2.5mm column length and 2mm i.d. is recommended.

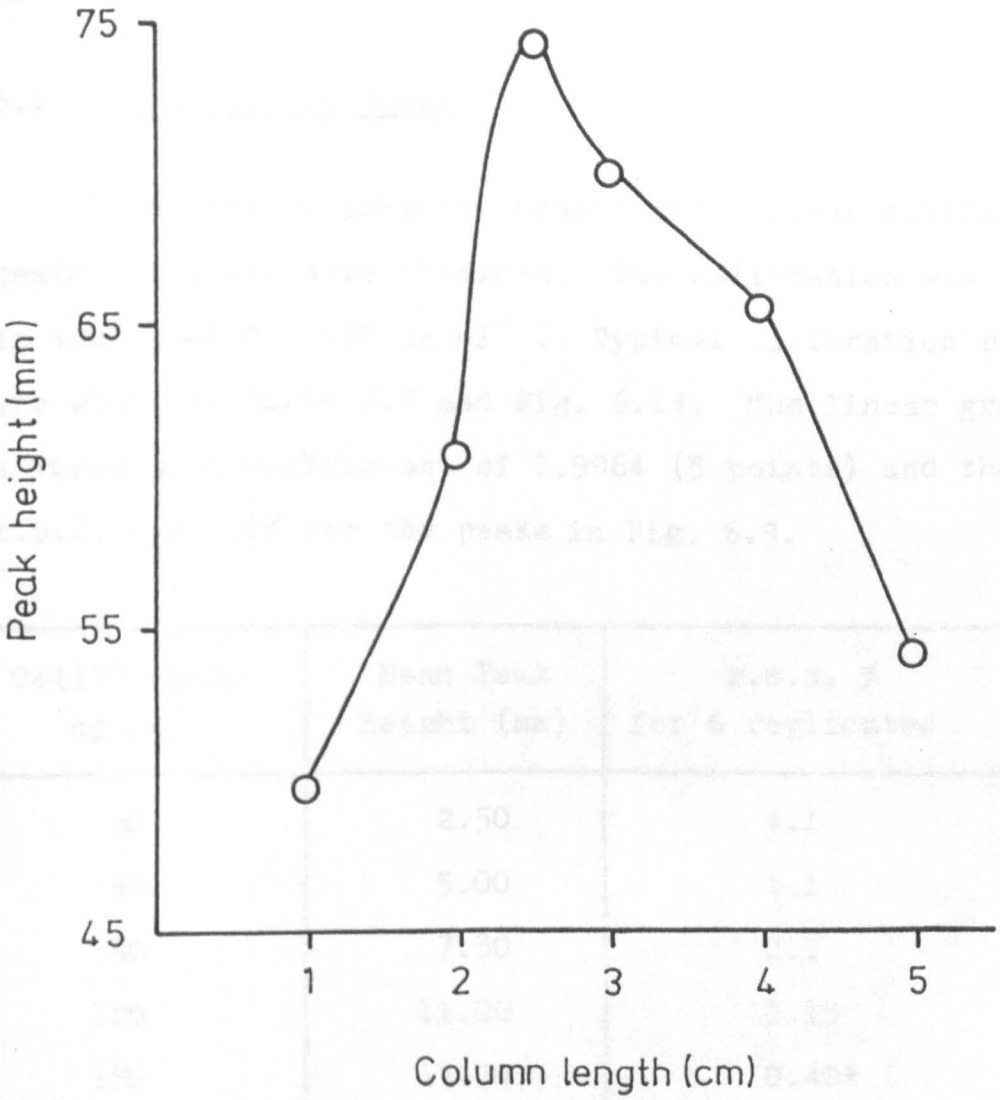

Fig. 6.12 Effect of reductor length on reduction of 50 ng ml^{-1} Cerium(IV).

6.6.1.3 Reductor Capacity

Such a mini-reductor column exhibits a high reduction

capacity, as concluded by repetitive 180 µl injections of 100 ng of Ce(IV) ml^{-1} , as shown in Fig. 6.13. Reproducible measurements are obtained for up to 66 injections (1.18 µg). After 66 injections the response has lost about 5% of its peak height, up to 132 injections (2.38 µg) and replacement or regeneration with 0.25% nitric acid may be necessary after ca 130 injections.

6.6.2 Calibration Graph

Under the recommended conditions typical calibration peaks and graph were obtained. The calibration was linear in the range 0 - 150 ng ml^{-1} . Typical calibration results are shown in Table 6.5 and Fig. 6.14. The linear graph has a regression coefficient of 0.9964 (5 points) and the mean r.s.d. was 1.8% for the peaks in Fig. 6.9.

Ce(IV) Conc. ng ml^{-1}	Mean Peak height (mm)	r.s.d. % for 6 replicates
30	2.50	4.1
60	5.00	1.1
90	7.80	2.1
120	11.00	1.15
150	14.20	0.40*
Mean r.s.d. = 1.8% *r.s.d. for 3 replicates		

Table 6.5 Calibration results for the determination of Ce(IV).

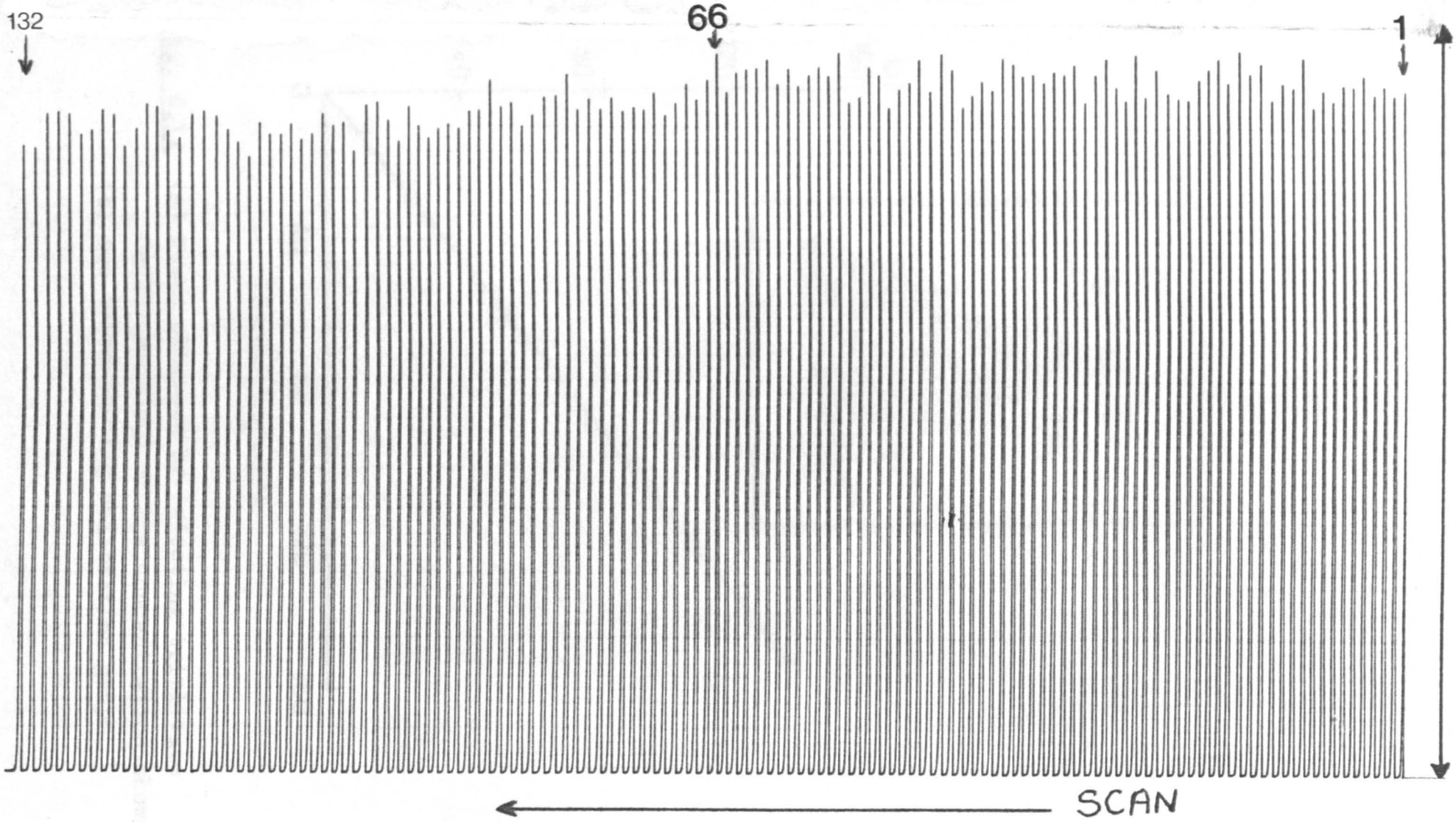

Fig. 6.13 Capacity of the reductor column. The cerium IV concentration was used 100 ng ml^{-1} (180 µl).

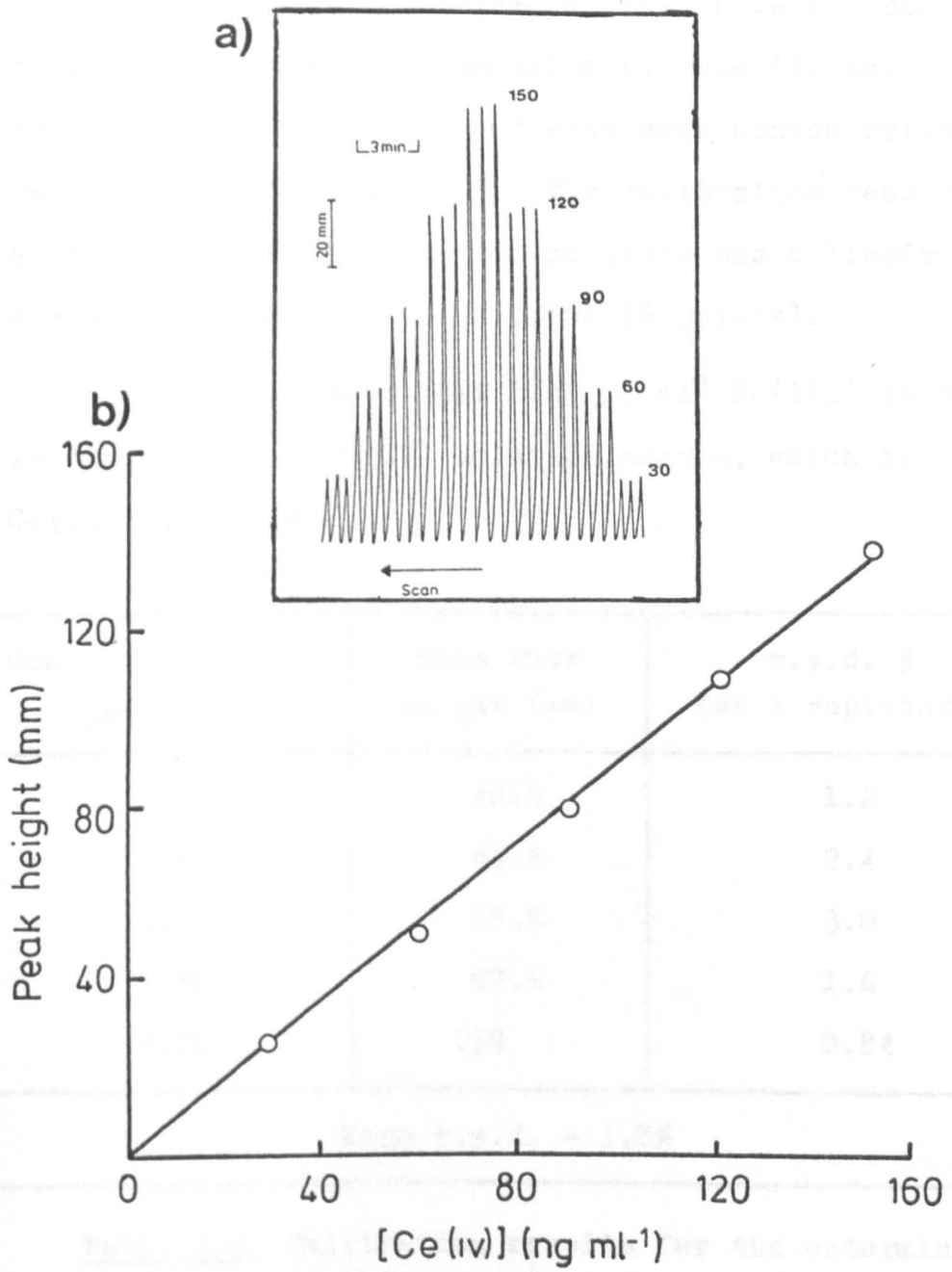

Fig. 6.14 (a) Peaks obtained by injecting triplicate Ce(IV) standard of the concentration shown; (b) the corresponding calibration graph.

6.7 Determination of Ce(III) in Ce(IV) Solution

Under the recommended conditions, the standard addition method was used to determine Ce(III) in Ce(IV) solution prepared from 98% ceric ammonium nitrate (Fluka). A 40 $\mu g\ ml^{-1}$ Ce(IV) was present with each concentration of Ce(III) shown in Table 6.6. The calibration results are shown in Fig. 6.15. The linear graph has a linear correlation coefficient of 0.998 (5 points).

The figure shows that 0.47 $\mu g\ ml^{-1}$ Ce(III) is present in the 40 $\mu g\ ml^{-1}$ Ce(IV) solution sample, which is 1.2% Ce(III) in Ce(IV).

Conc. of Ce(III) $\mu g\ ml^{-1}$	Mean Peak height (mm)	r.s.d. % for 3 replicates
0.4	40.8	1.2
0.8	63.6	2.4
1.20	77.6	3.0
1.60	97.6	1.6
2.00	119	0.84
Mean r.s.d. = 1.8%		

Table 6.6 Calibration results for the determination of Ce(III) in Ce(IV) solution.

6.8 Simultaneous Determination of Ce(III) and Ce(IV)

Simultaneous determination of Ce(III) and Ce(IV) can be achieved by incorporating a zinc reductor minicolumn into

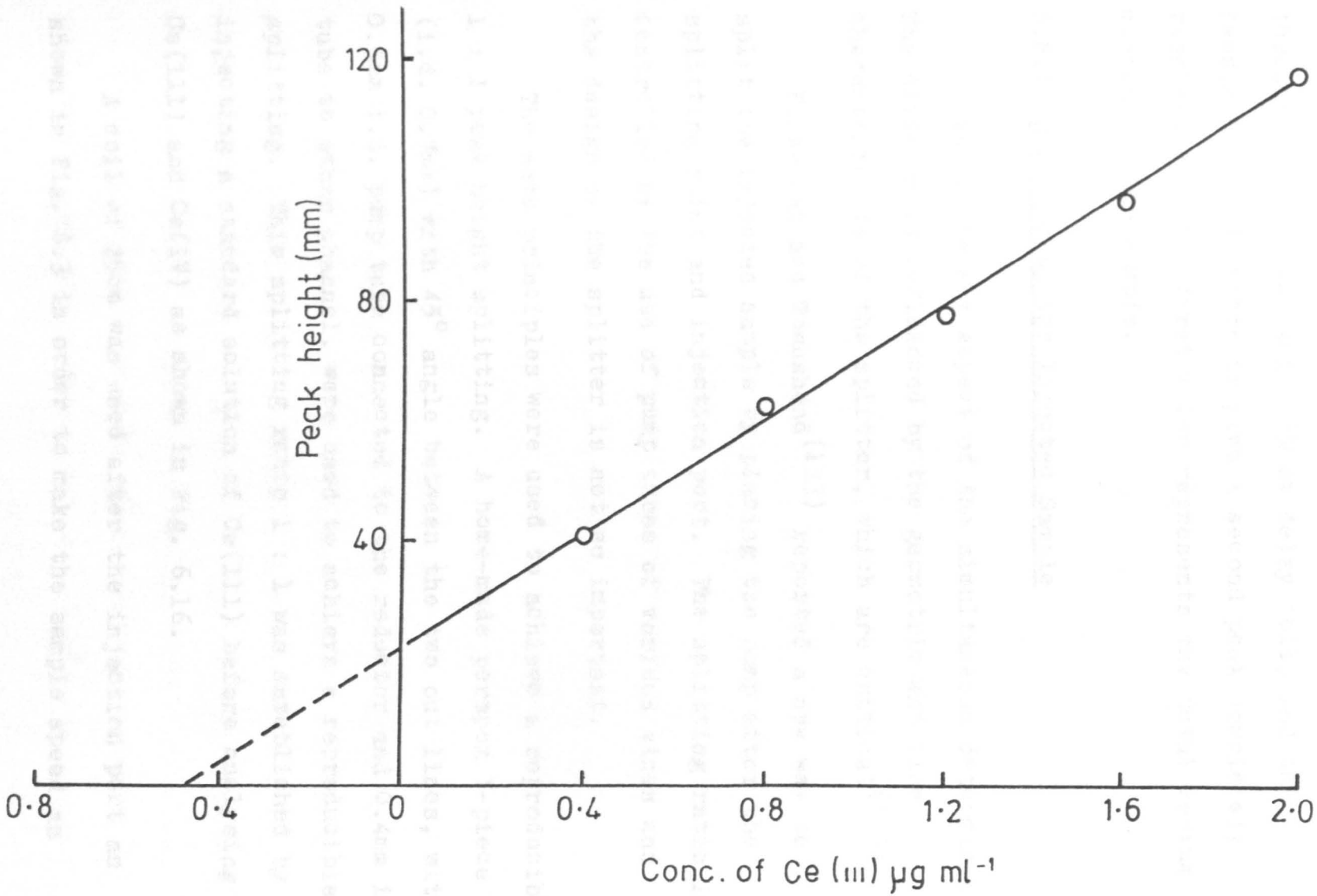

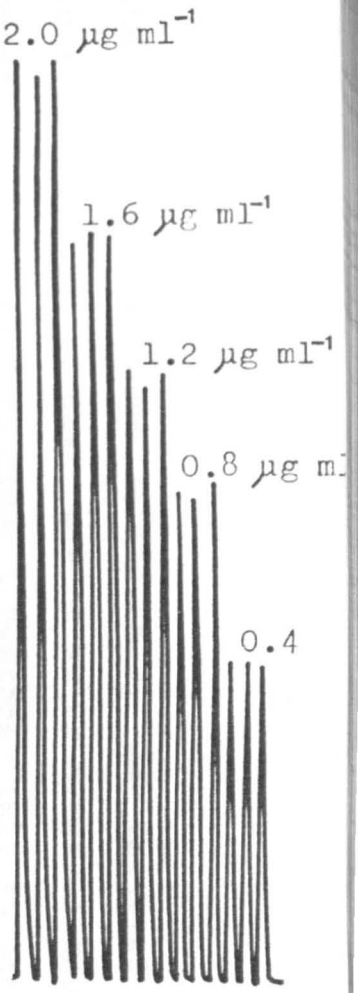

Fig. 6.15 Peaks obtained by injecting Ce(III) standards in the concentration range shown and the corresponding calibration graph.

the system[133] as shown in Fig. 6.2. The injected sample is split into two streams, one of which bypasses the reductor, and therefore gives a response only to the original Ce(lll) in the sample. The remainder passes through the detector and a 250cm delay coil, and then passes to the detector to give a second peak completely resolved from the first which represents the total cerium content of the sample.

6.8.1 Division of the Injected Sample

This is the key aspect of the simultaneous determination. The division is influenced by the geometric and flow characteristics of the splitter, which are critical[169].

Faizullah and Townshend[133] reported a new way to split the injected sample by placing the pump after the splitting point and injection port. The splitting ratio is controlled by the use of pump tubes of various sizes and the design of the splitter is not so important.

The same principles were used to achieve a reproducible 1 : 1 peak height splitting. A home-made perspex Y-piece (i.d. 0.7mm) with 45° angle between the two out lines, with 0.5mm i.d. pump tube connected to the reductor and 0.4mm i.d. tube to other channel, were used to achieve a reproducible splitting. This splitting ratio 1 : 1 was established by injecting a standard solution of Ce(lll) before analysing Ce(lll) and Ce(lV) as shown in Fig. 6.16.

A coil of 25cm was used after the injection port as shown in Fig. 6.3 in order to make the sample speed as

constant as possible before splitting[127,170]. The flow rate should be less than 1 ml min^{-1} in order to reduce all Ce(IV) to Ce(III) in the reductor column.

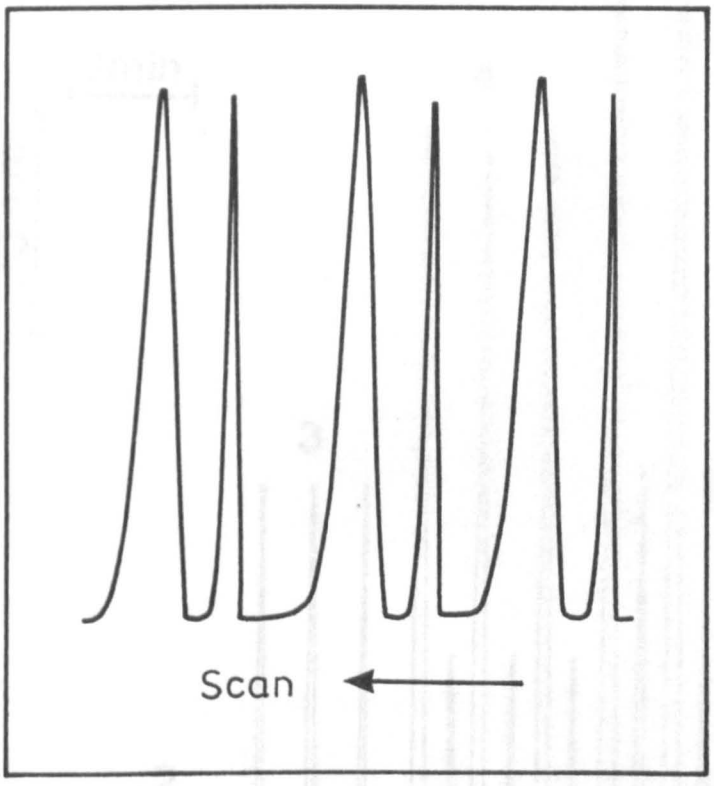

Fig. 6.16 Splitting of 300 ng ml^{-1} of Ce(III) solution.

6.8.2 Calibration Graph

Using the optimal conditions for the reduction of Ce(IV) and splitting of the injected sample (to give a 1 : 1 peak height ratio), calibration for Ce(III) - Ce(IV) mixtures was successfully achieved. Typical calibration results for 180 µl injections of Ce(III)/Ce(IV) solutions are shown in Fig. 6.17 for the concentrations shown in Table 6.7. The sample throughput was 55 h^{-1} with a mean

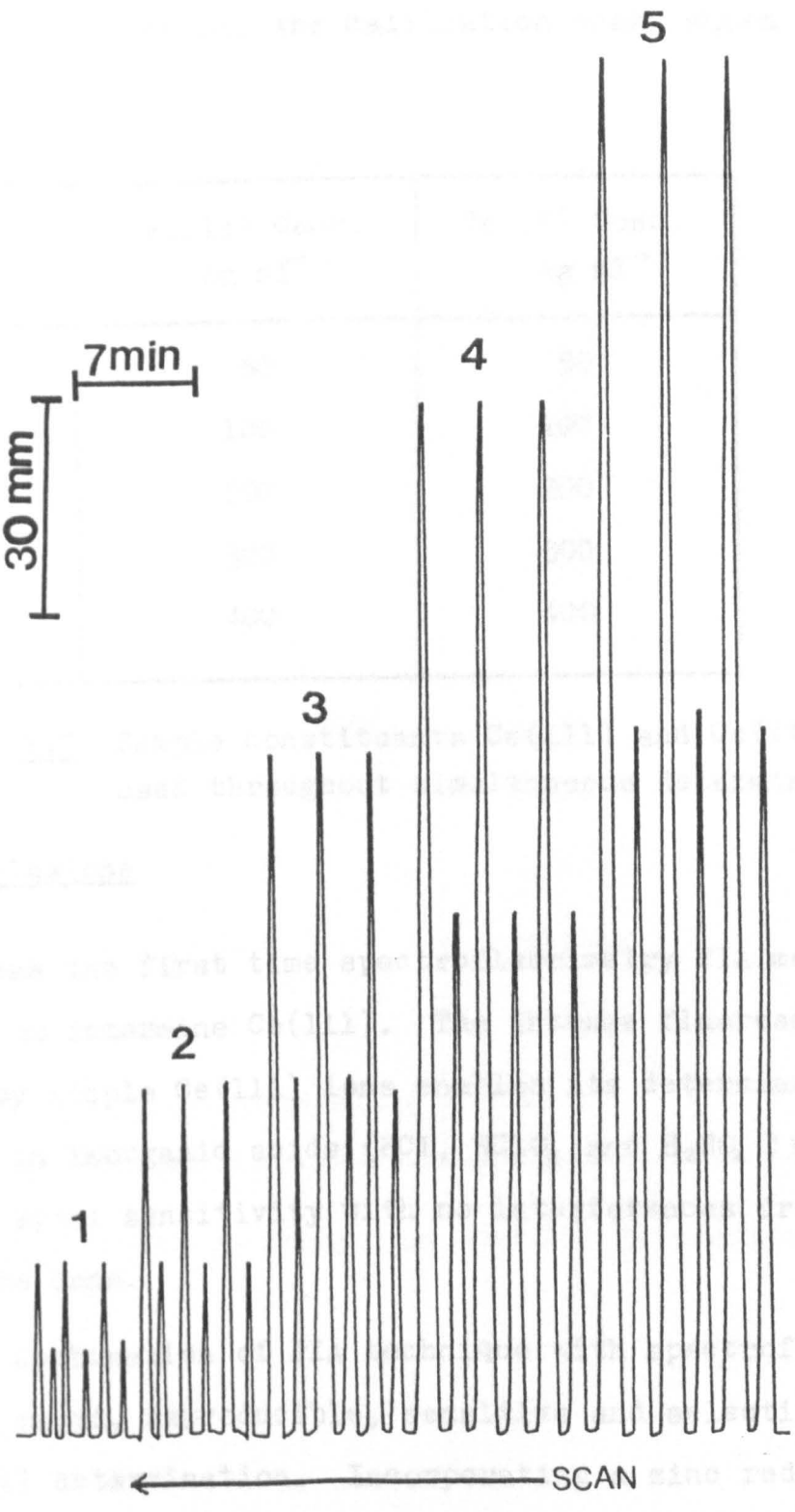

Fig. 6.17 Typical calibration for simultaneous determination of Ce(lll) and Ce(lV) for the concentration shown in Table 6.7.

r.s.d. of 2.5% over all the calibration peaks shown in Fig. 6.16.

Sample no.	Ce(III) Conc. ng ml^{-1}	Ce(IV) Conc. ng ml^{-1}
1	50	50
2	100	100
3	200	200
4	300	300
5	400	400

Table 6.7 Sample constituents Ce(III) and Ce(IV) used throughout simultaneous determination.

6.9 Conclusions

It was the first time spectrofluorimetry FIA method was used to determine Ce(III). The intense fluorescence emitted by simple Ce(III) ions enables its determination directly in inorganic acids (HCl, $HClO_4$ and H_2SO_4) with high and equal sensitivity with no interferences from other lanthanide ions.

The combination of FIA technique with spectrofluorimetry proved a rapid, reproducible, sensitive and selective means of Ce(III) determination. Incorporating a zinc reductor minicolumn into the FIA system provided a simple means of indirect fluorimetric determination of Ce(IV). Table 6.8 summarizes the optimum conditions for spectrofluorimetric determination of Ce(III).

The method of splitting of the injected sample made possible the simultaneous determination of Ce(III) and Ce(IV) with a simple FIA manifold.

Parameter	Value
Carrier stream	0.5 M $HClO_4$
Flow rate	1.3 ml min^{-1}
Sample volume	180 µl
Linear calibration range	0 - 100 ng ml^{-1}
Detection limit (2 x noise)	1 ng
r.s.d.	0.6%
Sample rate	150 h^{-1}
Excitation wavelength	260 nm
Emission wavelength	350 nm
Excitation and emission slits	10

Table 6.8 Optimum conditions for the determination of Ce(III).

CHAPTER SEVEN

FLOW INJECTION DETERMINATION OF EUROPIUM AFTER ON-LINE REDUCTION

7.1 Introduction

Three lanthanide elements that are known to form aqueous dipositive ions are Sm, Eu and Yb. Table 7.1 shows the colour and electronic configuration along with the value of E^{o} (Lu(lll)/Lu(ll)) for these dipositive ions.

Ion	Colour	Configuration	E^{o}(V)
Sm(ll)	red	(Xe)$4f^{6}$	1.50
Eu(ll)	colourless	(Xe)$4f^{7}$	0.35
Yb(ll)	green	(Xe)$4f^{14}$	1.10

Table 7.1 Colour, electronic configuration and E^{o} value for known dipositive aqueous lanthanide ions

Eu(lll) ions are more easily reduced than Sm(lll) and Yb(lll) ions. Reduction may be carried out by several methods[171], of which the more commonly used ones are electrolytic reduction[172-174], treatment with amalgamated zinc (Jones reductor)[175-177], and reduction with sodium amalgam[178,179].

The method of reducing Eu(lll) to Eu(ll) quantitatively with a Jones reductor offers a very selective method for determination of Eu(lll) in the presence of all other lanthanides because the only two other lanthanides (Yb and Sm) which exist in the bivalent state, are not reduced by a

zinc reductor (E^{o} = o.76V). Eu(lll) may be determined titrimetrically after reduction in a Jones reductor by an iodimetric method[175,176,180], or by collecting the solution from the Jones reductor in an excess of iron(lll) chloride solution and titrating the iron reduced by the Eu(ll) ions with standard solution of potassium permanganate[181], or potassium dichromate[177]. Eu(ll) is a very strong reducing agent and its solution obtained from the Jones reductor is usually collected under an atmosphere of carbon dioxide to prevent oxidation of Eu(ll) ions by the oxygen in air.

In the FIA technique detection occurs in a flow-through cell. The great advantage of this method is that the unstable oxidation state of the metal ion, produced after on-line reduction or oxidation, only needs to be sufficiently stable during its residence time in the flow system, which may be less than 1 min[164]. Since FIA is done in a closed system, there is no need to prevent oxidation of the unstable oxidation state produced on-line by use of inert gases.

In this work, a zinc reductor mini-column is used in a flow injection system for reduction of Eu(lll) to Eu(ll), which is indirectly detected either spectrofluorimetrically by reaction with Ce(lV), and measurement of the Ce(lll) produced by the method established in chapter 6, or spectrophototometrically by reaction of the Eu(ll) with Fe(lll), and determination, with 1,lO-phenanthroline, of the Fe(ll) formed[127].

7.2 Experimental

7.2.1 Reagents and Chemicals

All chemicals were of analytical grade except for europium(III) nitrate ($Eu(NO_3)_3 \cdot 5H_2O$) which was 99.9% pure (Koch-Light Laboratories).

Europium Solution

A 1000 $\mu g\ ml^{-1}$ europium solution was prepared as described in chapter 4.

Cerium(IV) Solution

A 100 $\mu g\ ml^{-1}$ Ce(IV) solution was prepared as described in chapter 6.

Iron(III) Solution

A 0.5M Fe(III) solution was prepared by dissolving 13.515g of $FeCl_3$ (BDH) in 0.1M HCl. Other solutions were prepared by appropriate dilution with the 0.1M HCl.

1,10-Phenanthroline Solution

A 1.5% (w/v) solution was prepared by dissolving 1.5g of 1,10-phenanthroline hydrochloride (BDH) in 100 ml of 0.05M HCl. This solution was prepared every 4 days.

Buffer Solution

Citrate buffers of different pH values were prepared by mixing appropriate volumes of 0.1M citric acid and 0.1M sodium citrate to give the desired pH values between 3.0 and 6.2[182].

7.2.2 Apparatus

For the indirect spectrofluorimetric determination, the instrumentation described in chapter 6 was used, except the home-made cell was changed for one that had a smaller volume where the silica tube was, i.d. 0.8mm, 40mm long.

The absorbance was measured at 512 nm using a Cecil CE 373 linear readout spectrophotometer.

The Jones reductor was prepared as described in chapter 6[127,168].

7.2.3 Flow Manifold

The manifold used for the indirect fluorimetric determination of Eu(lll) is shown in Fig. 7.1. A peristaltic pump (Ismatec 8031, Zurich) was used, and Eu(lll) solutions were introduced via a Rheodyne RH 5020 injection valve (Anachem) with a sample loop of 80 µl. The Jones reductor was inserted in the system as shown in Fig. 7.1. Teflon tubing (0.5mm i.d.) was used for the rest of the manifold.

The indirect spectrophotometric determination of Eu(lll) was achieved by the manifold shown in Fig. 7.2. The same pump and injection valve described above were used.

7.3 Indirect Spectrofluorimetric Determination of Eu(lll)

7.3.1 Results and Discussions

7.3.1.1 Optimization of Variables

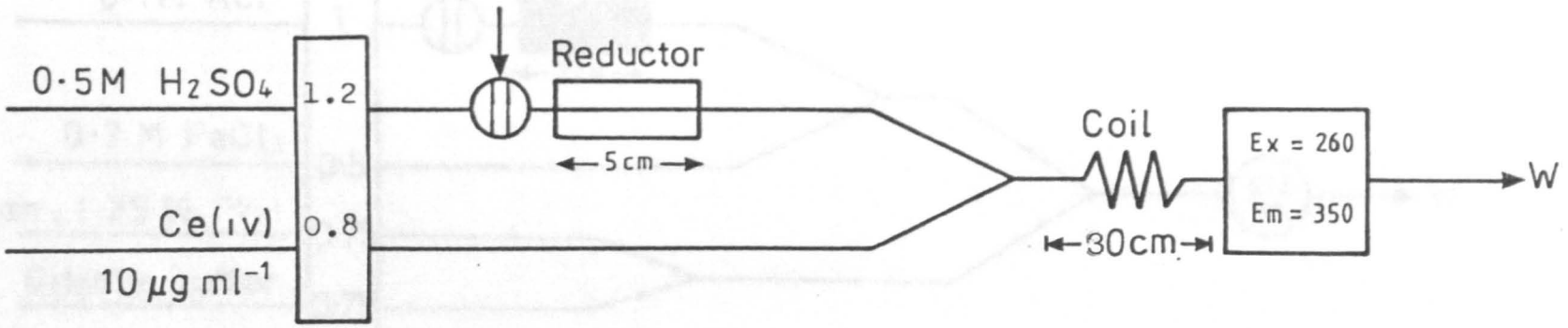

Fig. 7.1 Manifold for indirect spectrofluorimetric determination of Eu(III).

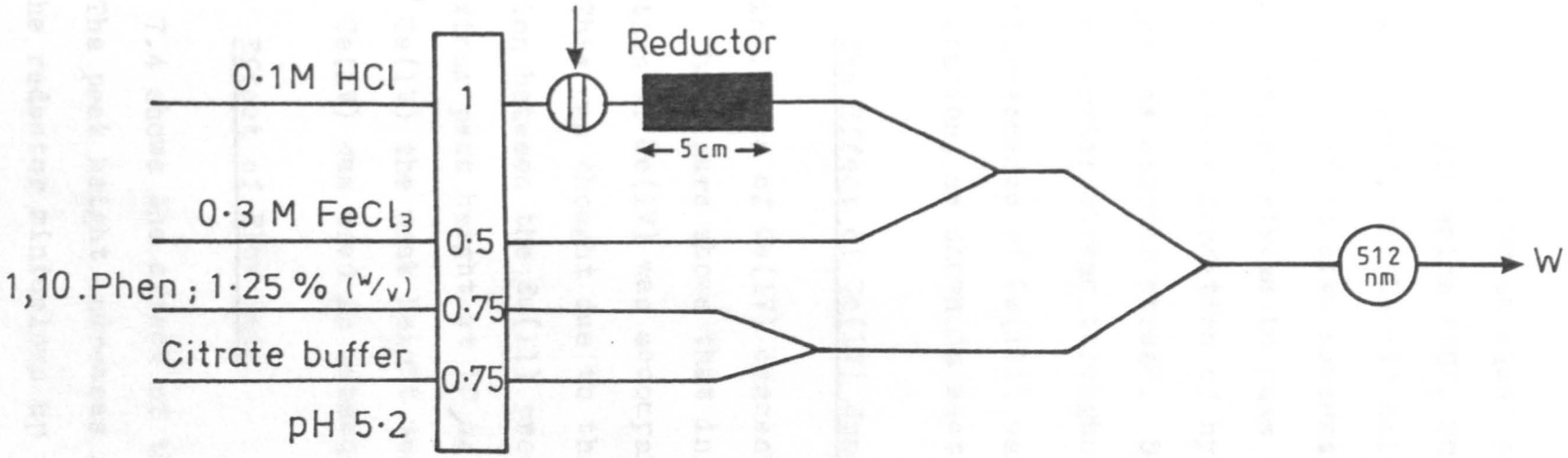

Fig. 7.2 Manifold for indirect spectrophotometric determination of Eu(lll).

7.3.1.1.1 Carrier Stream

Since Ce(111) shows an equal sensitivity of fluorescence in several inorganic acids (HCl, $HClO_4$ and H_2SO_4) in the range 0.05-1 M acid, the Ce(1V) solution was prepared in sulphuric acid. It is also necessary to use the acidic solution as carrier stream to pass through the zinc reductor in order to prevent formation of hydrogen peroxide when water is used as carrier stream. So 0.5 M sulphuric acid was used as carrier stream throughout this work.

The fluorescence of Ce(111) was measured at 350 nm with 260 nm excitation, as shown in section 6.4.1.1.

7.3.1.1.2 The Effect of Ce(1V) Concentration

The influence of Ce(1V) concentration is shown in Fig. 7.3. The figure shows that initially increasing the concentration of Ce(1V) was accompanied by increasing peak height. This was thought due to the increase of the rate of the reaction between the Eu(11) produced and Ce(1V), which gave a maximum peak height at 10 $\mu g\ ml^{-1}$ Ce(1V). Above 10 $\mu g\ ml^{-1}$ Ce(1V) the peak height was nearly constant. Thus 10 $\mu g\ ml^{-1}$ Ce(1V) was used in subsequent experiments.

7.3.1.1.3 Effect of Flow Rate

Fig. 7.4 shows the effect of the flow rate on the peak height. The peak height increases as the flow rate increases through the reductor minicolumn up to 1.2 ml min^{-1}. This was thought to be attributed to the decrease of the dispersion.

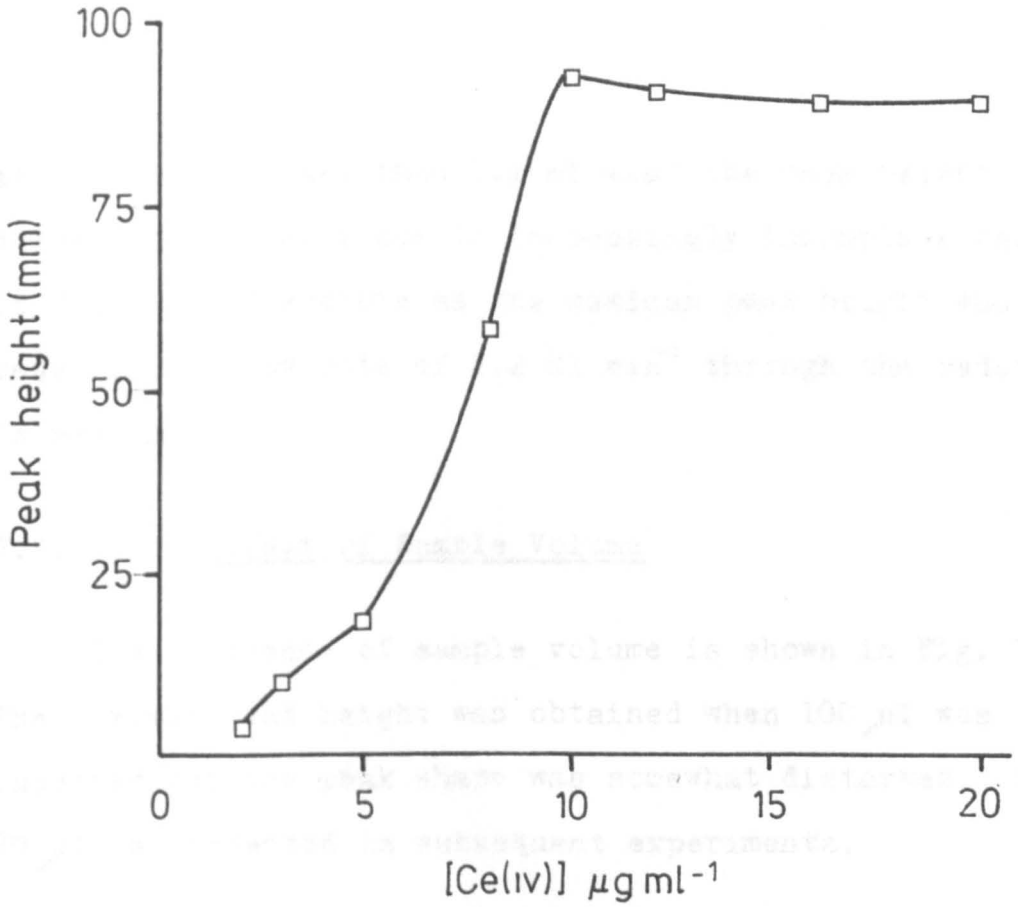

Fig. 7.3 Effect of Ce(1V) concentration on 2 μg ml^{-1} Eu(111).

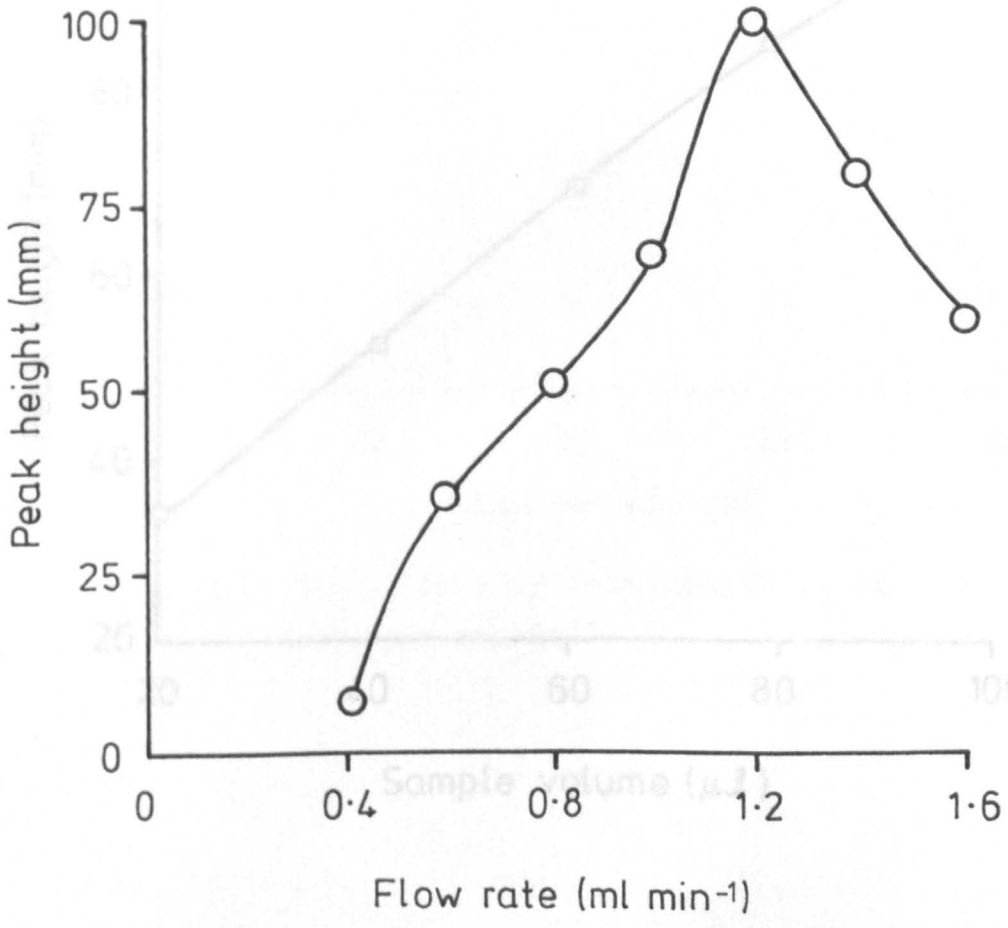

Fig. 7.4 Effect of flow rate on peak height of 2 μg ml^{-1} Eu(111).

At flow rate higher than 1.2 ml min^{-1} the peak height decreased gradually due to increasingly incomplete reductio of Eu(111). Therefore as the maximum peak height was required, a flow rate of 1.2 ml min^{-1} through the reductor is recommended.

7.3.1.1.4 Effect of Sample Volume

The influence of sample volume is shown in Fig. 7.5. The maximum peak height was obtained when 100 µl was injected but the peak shape was somewhat distorted. So, 80 µl was injected in subsequent experiments.

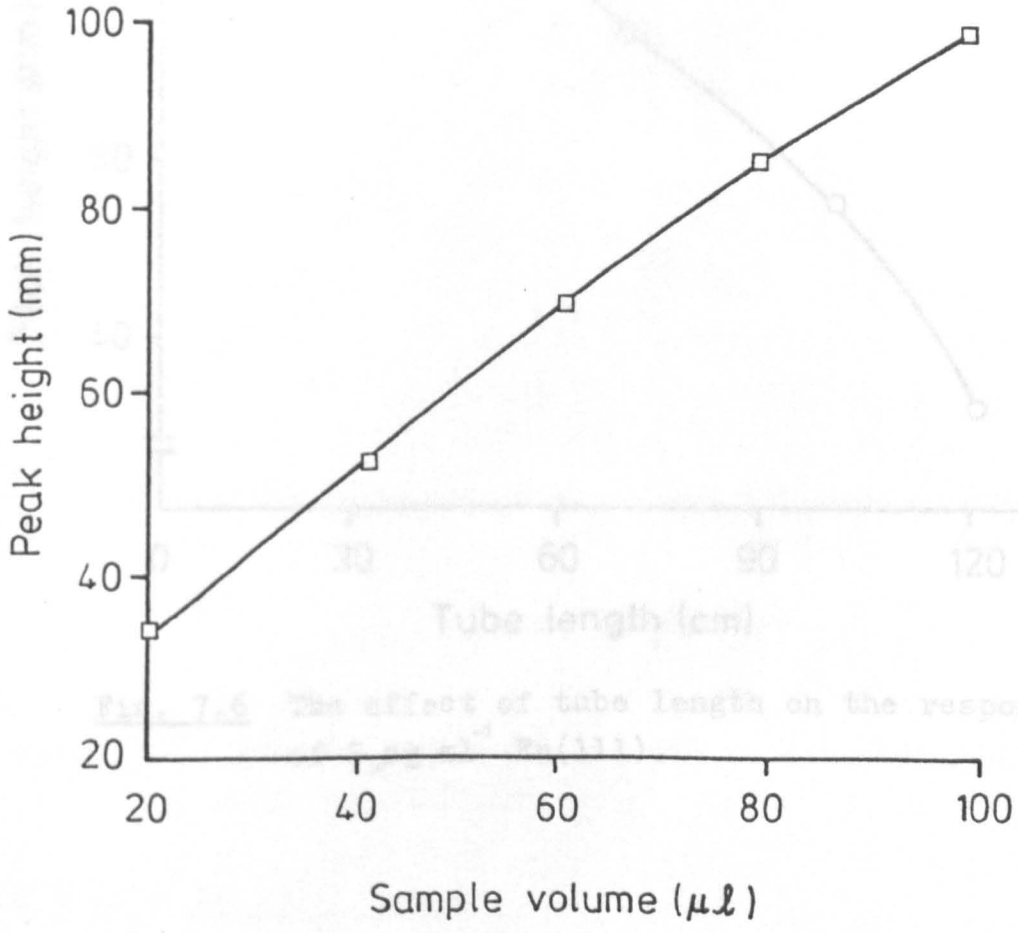

Fig. 7.5 Effect of the sample volume on the peak height of 2 µg ml^{-1} Eu(111).

7.3.1.1.5 Effect of Tube Length

Fig. 7.6 shows the effect of tube length on the 2 μg ml^{-1} Eu(lll) peak height. It is clear that as the tube length increases the peak height decreases due to the increase in the dispersion in the system. A 30cm coil was used as optimum.

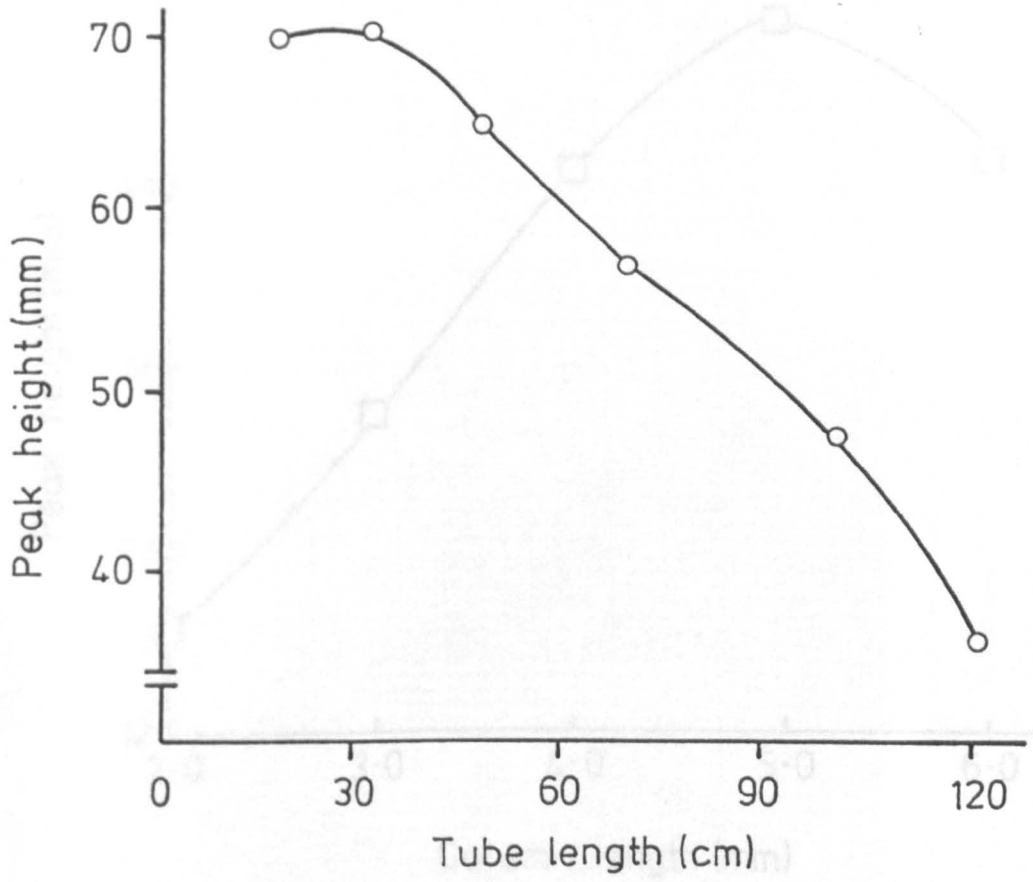

Fig. 7.6 The effect of tube length on the response of 2 μg ml^{-1} Eu(lll).

7.3.1.1.6 Effect of Reductor Length and Internal Diameter

Keeping the internal diameter of the reductor column constant at 2mm, the effect of different lengths of reductor column was investigated. Fig. 7.7 shows the effect of various columns on the peak height. The maximum peak height was obtained at 5cm reductor length. A 2mm i.d. column was the minimum diameter used as explained in section 6.4.1.4.

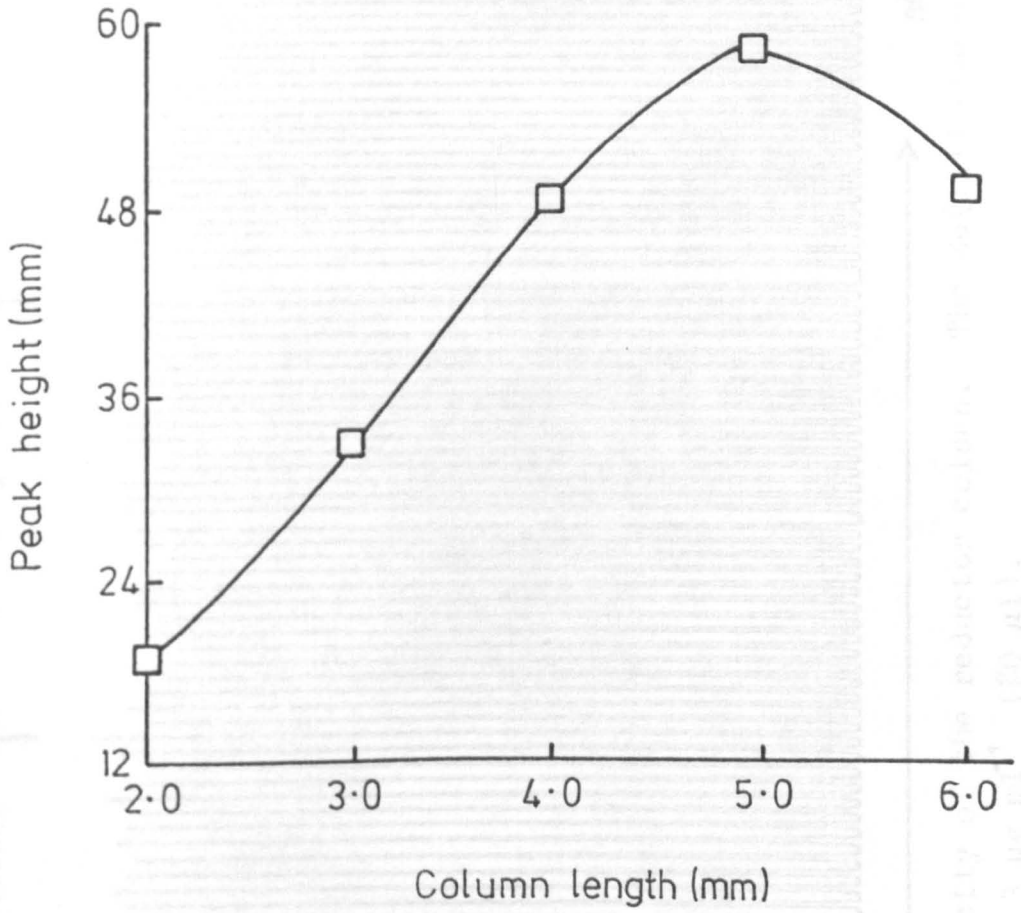

Fig. 7.7 Effect of reductor length on reduction of 2 $\mu g\ ml^{-1}$ Eu(III).

7.3.1.1.7 Reductor Capacity

Fig. 7.8 shows the results of 120 repetitive injections

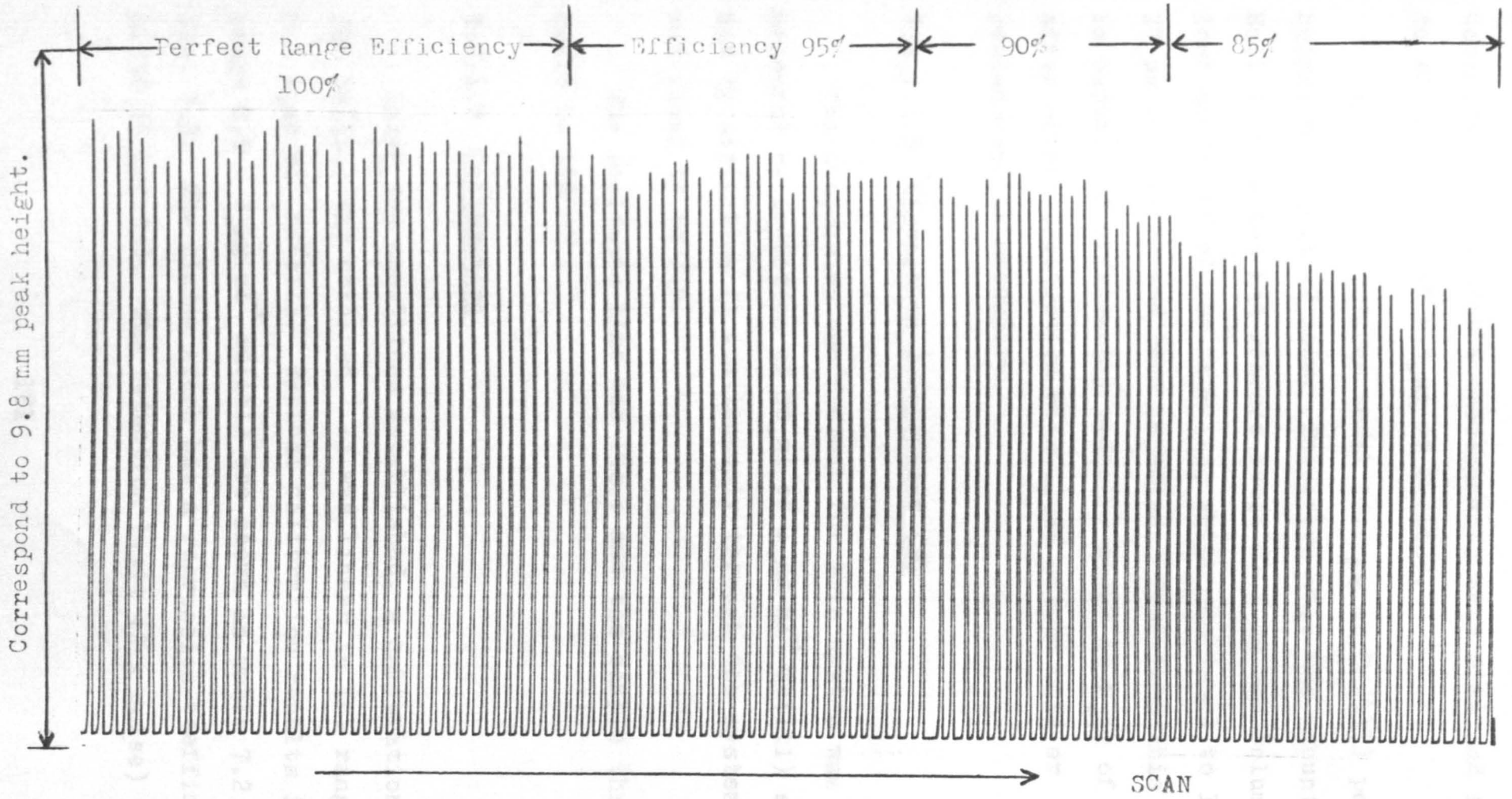

Fig. 7.8 Capacity of the reductor column. The Eu(lll) concentration was used 3 $\mu g\ ml^{-1}$ (80 μl).

of 3 μg ml^{-1} Eu(III) (80 μl) through the 5cm long mini-reductor column. Such column exhibits a high reduction capacity. Reproducible measurements were obtained for up to 40 injections of 6.9 μg of Eu(III).

After 70 injections total 16.6 μg of Eu(III) peak height was about 5% less. Therefore when the amount of Eu(III) injected had reached about 21.6 μg the column had lost about 10% of its capacity, which increased to 15% when 27 μg of Eu(III) had been injected. Therefore this column is capable of efficiently reducing about 16.6 μg of Eu(III), after which regeneration with 0.25% nitric acid or replacement is necessary.

7.3.1.1.8 Dispersion Coefficient (D)

The dispersion coefficient for this system was measured by injection of 80 μl of 1 μg ml^{-1} Ce(III) solution, and by aspirating it continuously through the system. It was found to be 7.5.

The residence time was 15 s ; and the sample throughput could be 110 h^{-1} .

7.3.1.2 Calibration

Under the conditions established, a calibration graph for Eu(III) was obtained. It was linear in the range 0 - 4 μg ml^{-1} Eu(III). Typical calibration results in the range 0.5 - 4 μg ml^{-1} Eu(III) are shown in Table 7.2 and Fig. 7.9. The linear graph has a regression coefficient of 0.999 (5 points). The detection limit (2 x noise) was

0.2 $\mu g\ ml^{-1}$ and the r.s.d. for 11 replicate analyses of 3 $\mu g\ ml^{-1}$ Eu(111) was 1.1%.

Eu(111) Conc. $\mu g\ ml^{-1}$	Mean Peak height (mm)	r.s.d. % for 10 replicates
0.5	17	4.3
1.0	36	3.1
2.0	63	1.2
3.0	100	1.8
4.0	138	0.72
Mean r.s.d. = 2.58%		

Table 7.2 Calibration results for the determination of Eu(111).

7.3.1.3 Interferences

The effects of Sm^{3+} and Yb^{3+}, which are the only lanthanide ions that can exist in solution as dipositive ions, were measured by adding different amounts of each ion in the range of 25 - 200 $\mu g\ ml^{-1}$ to 2 $\mu g\ ml^{-1}$ Eu(111) solution. The peak height obtained was compared with that with no interferent ion present. Sm gave a slight enhancement in the peak height, where Yb gave a slight depression of the peak height, as shown in Fig. 7.10.

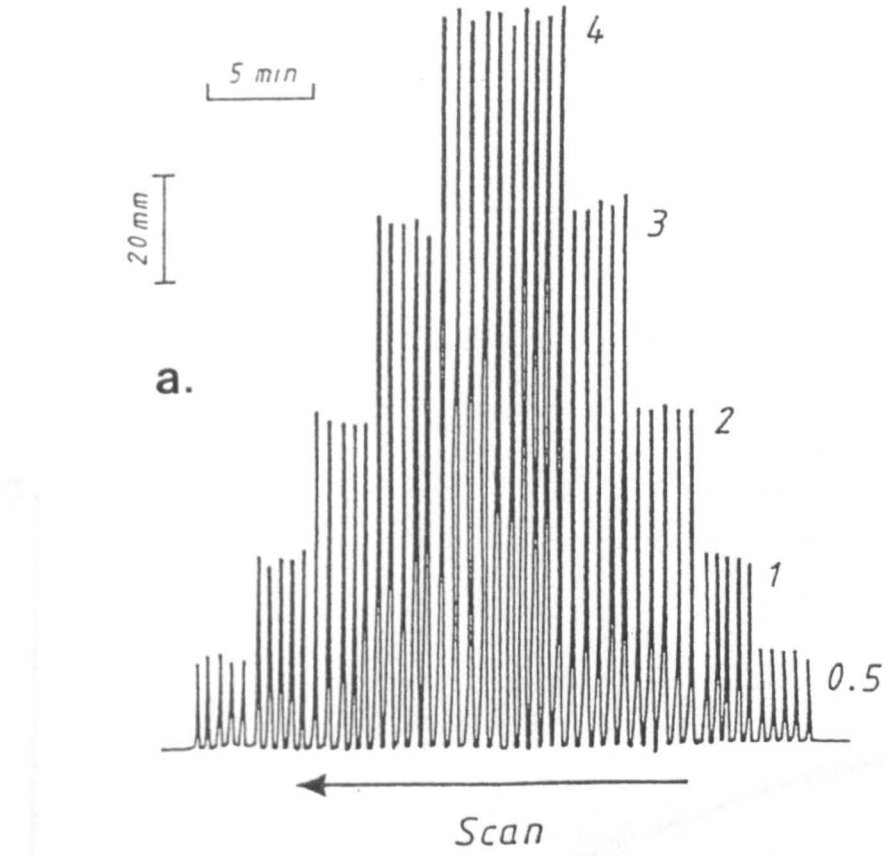

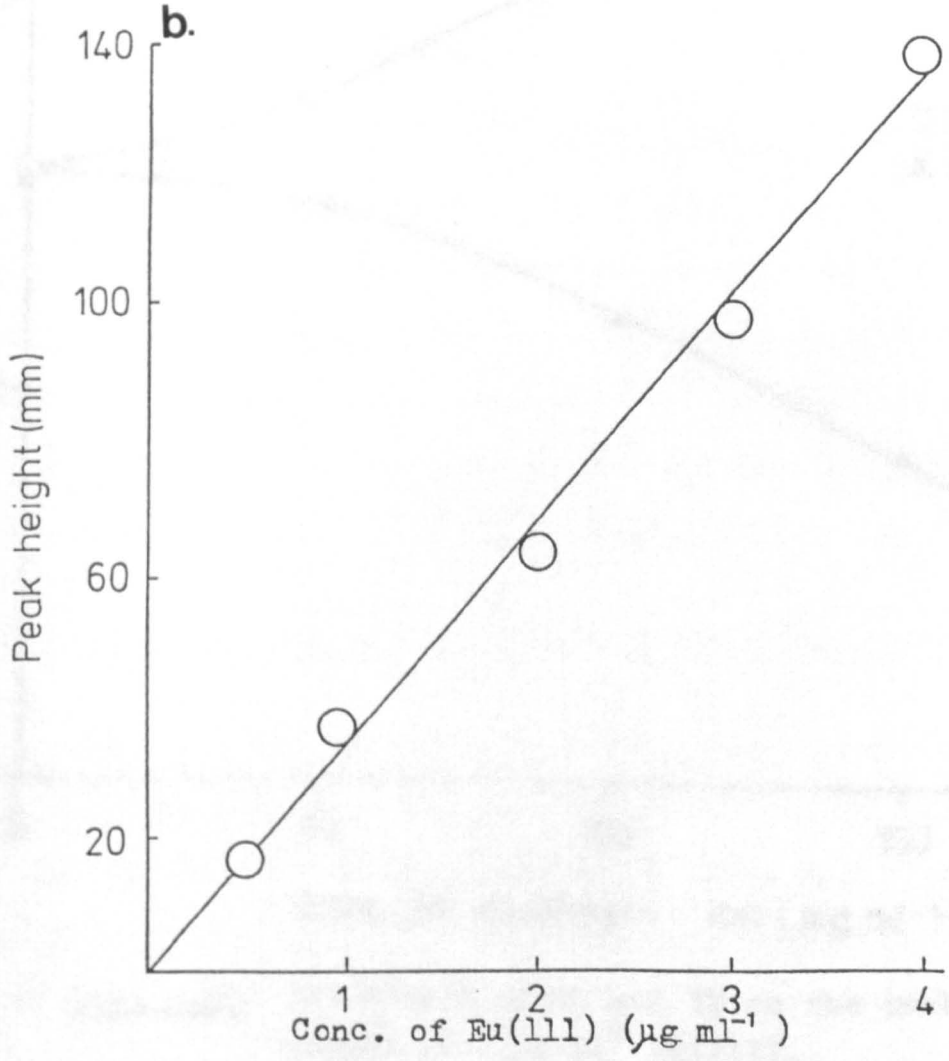

Fig. 7.9 (a) Peaks obtained by injecting Eu(III) standards in the concentration range shown;
(b) the corresponding least squares calibration graph.

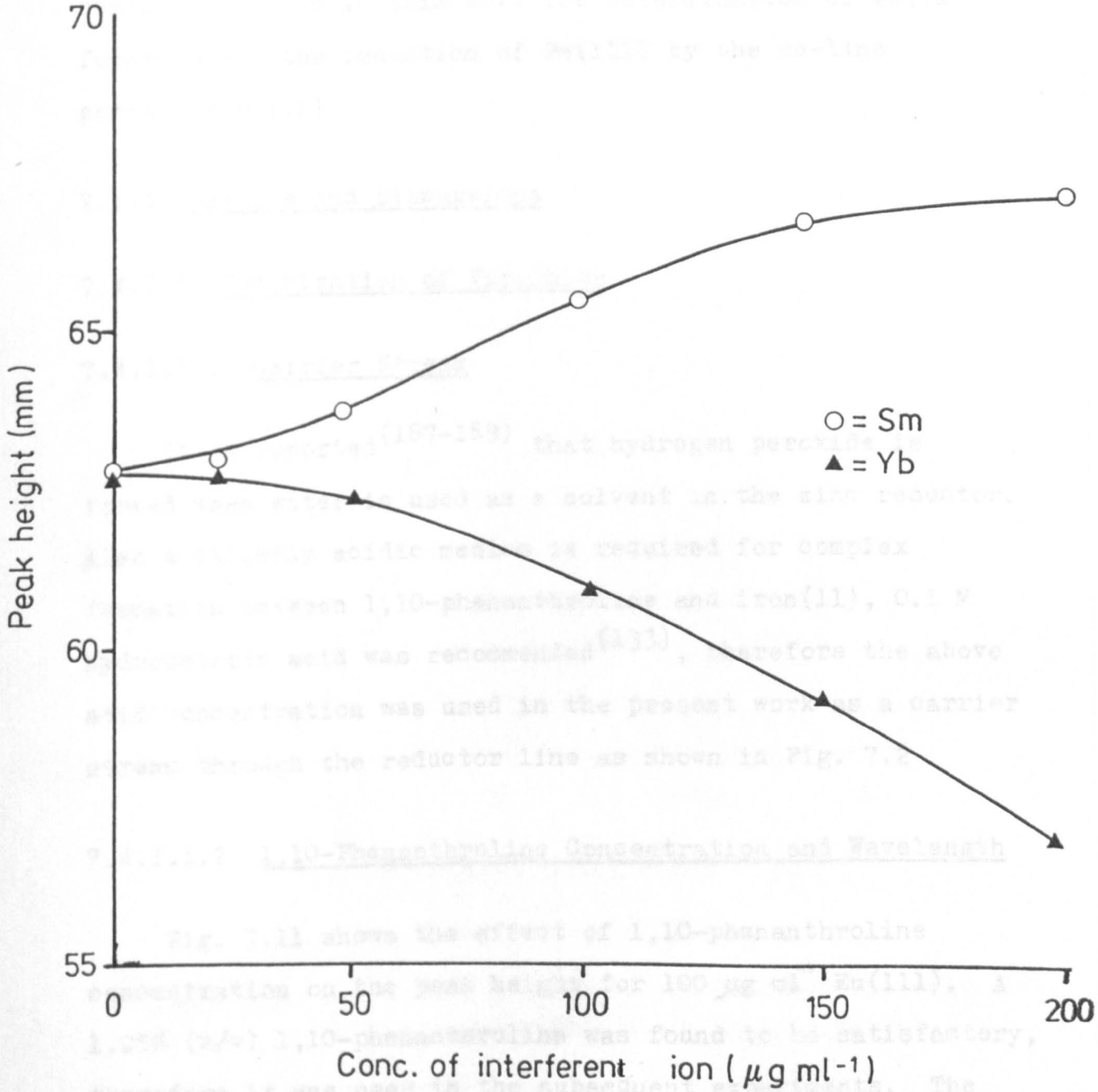

Fig. 7.10 The effect of Sm and Yb on the peak height of 2 μg ml^{-1} Eu(III).

7.4 Indirect Spectrophotometric Determination of Eu(lll)

Various selective organic reagents are widely used for spectrophotometric determination of iron by FIA. One of these reagents is 1,10-phenanthroline[133,183-186]. This reagent was used in this work for determination of Fe(ll) formed after the reduction of Fe(lll) by the on-line generated Eu(ll).

7.4.1 Results and Discussions

7.4.1.1 Optimization of Variables

7.4.1.1.1 Carrier Stream

It is reported[187-189] that hydrogen peroxide is formed when water is used as a solvent in the zinc reductor. Also a slightly acidic medium is required for complex formation between 1,10-phenanthroline and iron(ll), 0.1 M hydrochloric acid was recommended[133], therefore the above acid concentration was used in the present work as a carrier stream through the reductor line as shown in Fig. 7.2

7.4.1.1.2 1,10-Phenanthroline Concentration and Wavelength

Fig. 7.11 shows the effect of 1,10-phenanthroline concentration on the peak height for 100 $\mu g\ ml^{-1}$ Eu(lll). A 1.25% (w/v) 1,10-phenanthroline was found to be satisfactory, therefore it was used in the subsequent experiments. The concentration of 1,10-phenanthroline needs to be sufficient because it also reacted with ions which do not absorb at

512 nm such as Eu(lll). So the interference of Eu(lll) on Fe(ll) determination can be eliminated by using excess of 1,10-phenanthroline.

Fig. 7.12 shows the absorption spectrum of Fe(ll)-1,10-phenanthroline complex. Maximum absorbance was at 512 nm and this wavelength is recommended for use.

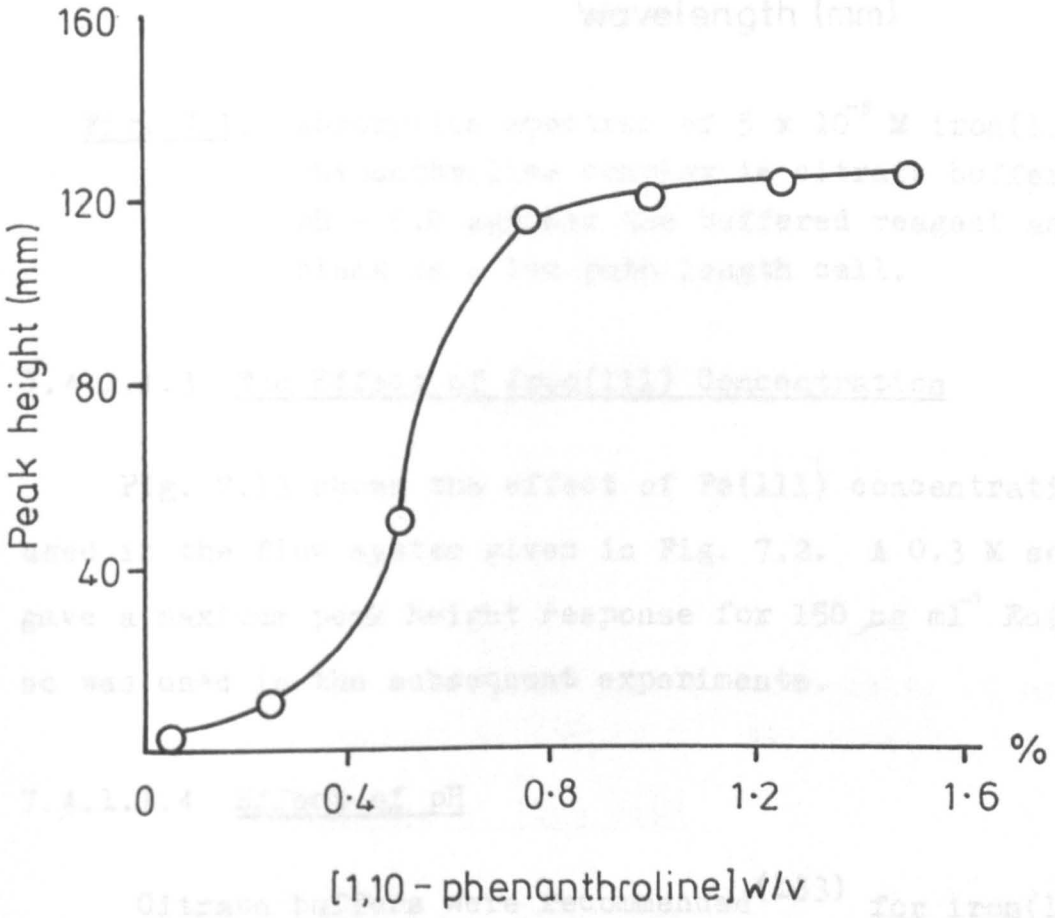

Fig. 7.11 The effect of 1,10-phenanthroline concentration on the peak height of 100 μg ml^{-1} Eu(lll).

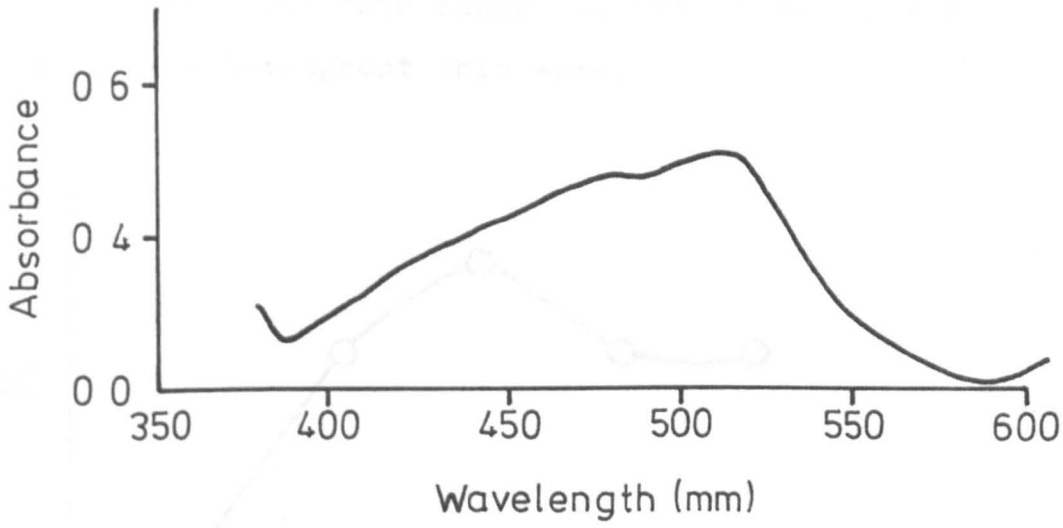

Fig. 7.12 Absorption spectrum of 5 x 10^{-5} M iron(11)-phenanthroline complex in citrate buffer pH = 5.0 against the buffered reagent as a blank in a 1cm path length cell.

7.4.1.1.3 The Effect of Iron(111) Concentration

Fig. 7.13 shows the effect of Fe(111) concentration used in the flow system given in Fig. 7.2. A 0.3 M solution gave a maximum peak height response for 150 μg ml^{-1} Eu(111), so was used in the subsequent experiments.

7.4.1.1.4 Effect of pH

Citrate buffers were recommended[133] for iron(11) determination because they do not produce any coloured complex with iron(111), while acetate buffer which produces a greenish yellow colour (λ_{max} = 382 nm), and also citrate buffer can mask certain potential interferences[139,190]. The effect of citrate buffers in the pH range 3.0 - 6.2[182] was studied. The responses of 100 μg ml^{-1} Eu(111) was found to

be the same throughout this range, therefore pH 5.2 was selected for use throughout this work.

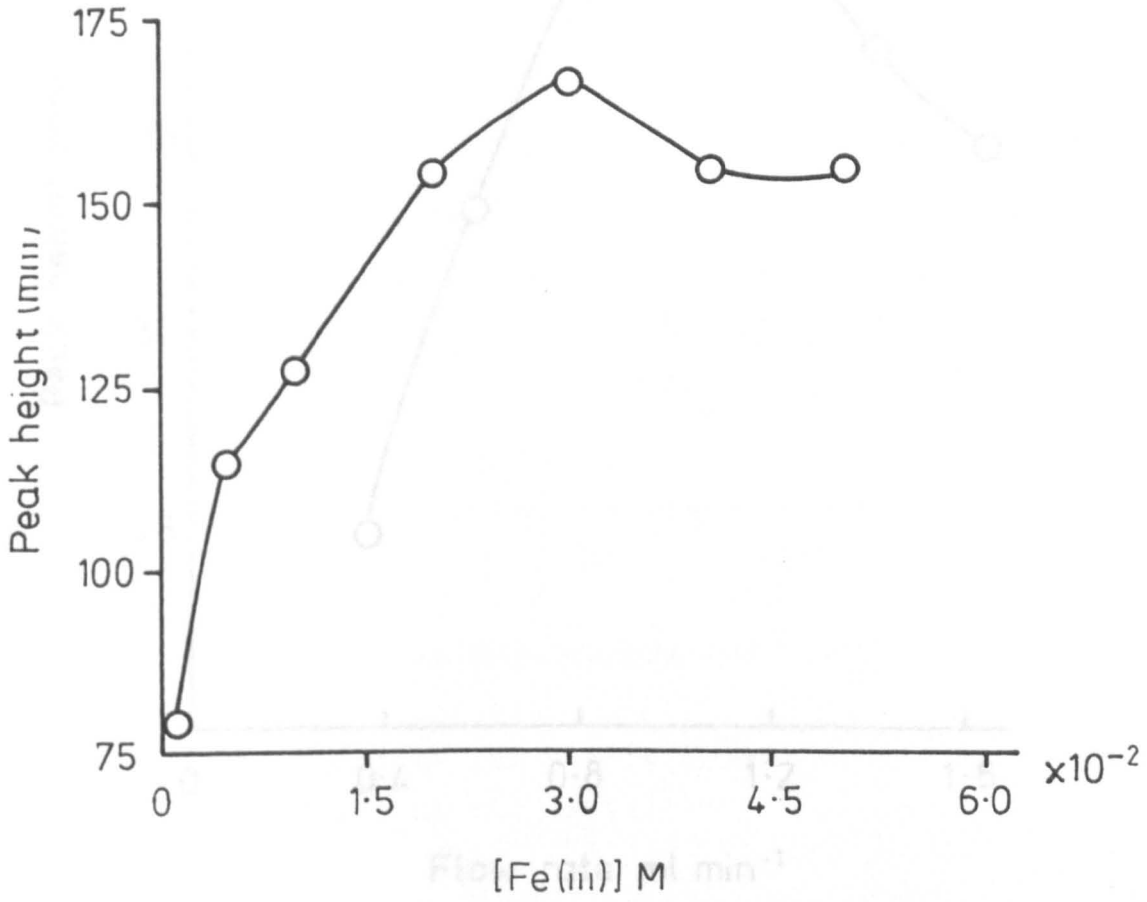

Fig. 7.13 Effect of Fe(III) concentration of peak height of 150 µg ml^{-1} Eu(III).

7.4.1.1.5 The Effect of Flow Rate

Fig. 7.14 shows the effect of the flow rate in the sample line. At the beginning increasing the flow rate through the reductor column up to 1 ml min^{-1} was accompanied by an increase in peak height. This was thought to be due to a decrease in the dispersion. Above 1 ml min^{-1} the peak height decreased. This must be due to increasingly incomplete reduction of Eu(III). A 1 ml min^{-1} flow rate through the reductor was recommended.

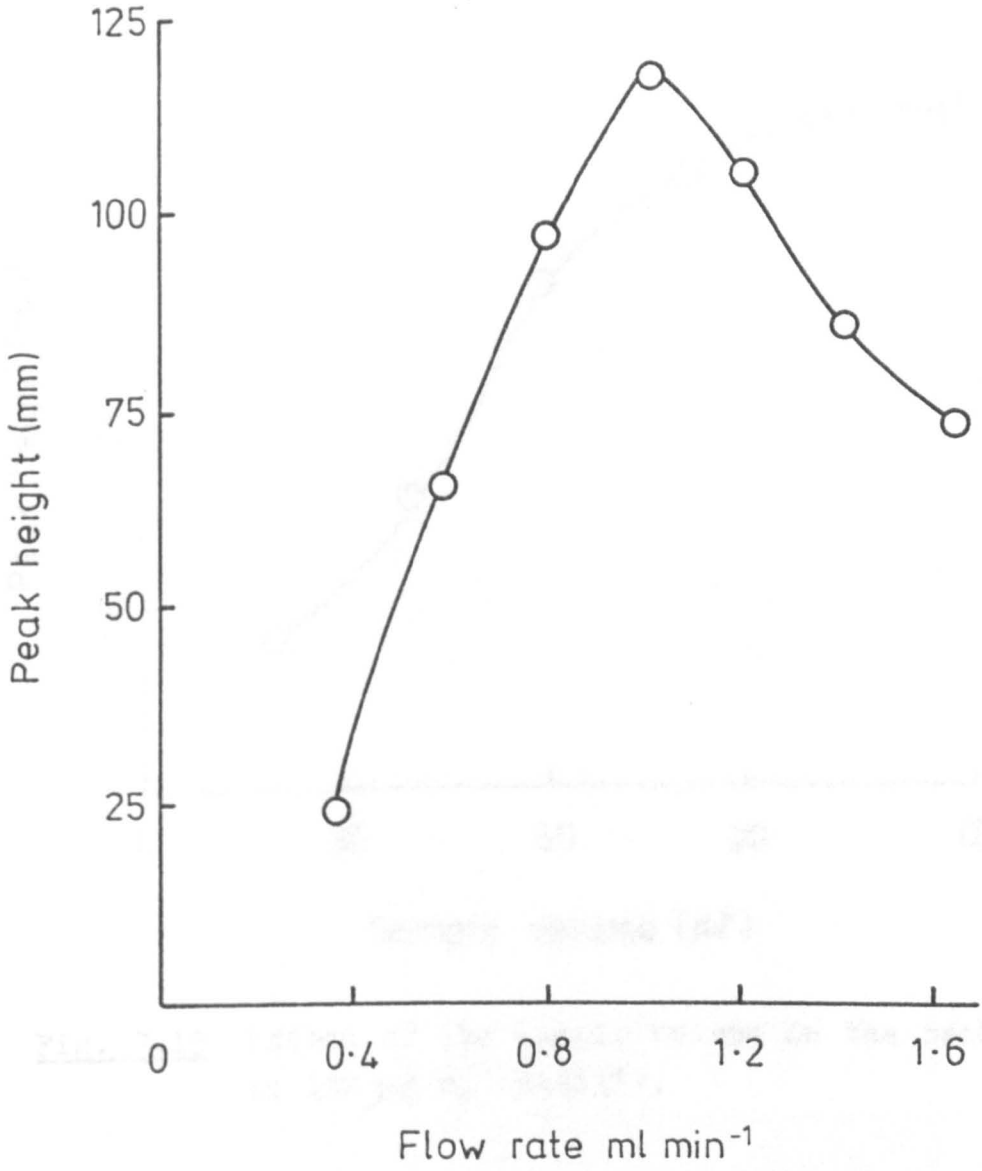

Fig. 7.14 Effect of flow rate on peak height of 100 µg ml^{-1} Eu(III).

7.4.1.1.6 Effect of Sample Volume

The effect of the sample volume was studied at the manifold shown in Fig. 7.2. The results are shown in Fig. 7.15. The maximum peak height was obtained at 120 µl, but the peak shape was somewhat distorted, so 100 µl was injected in subsequent experiments.

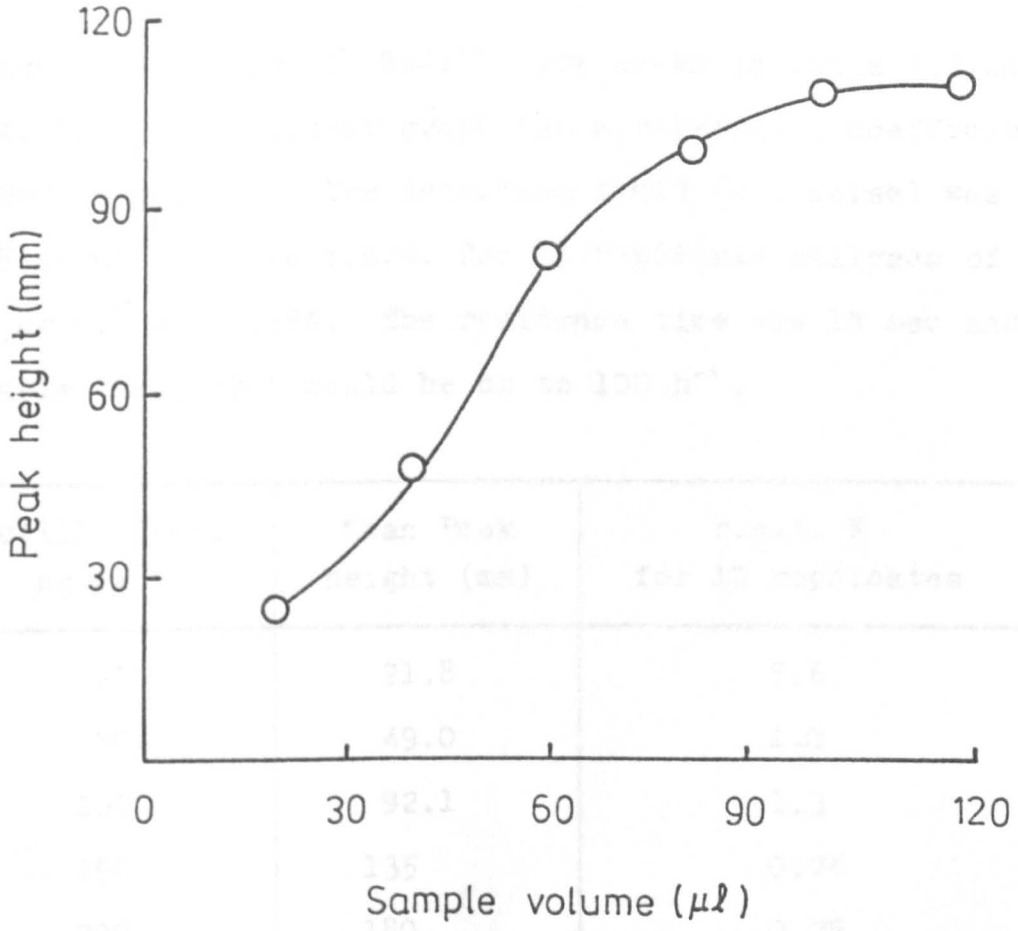

Fig. 7.15 Effect of the sample volume on the peak height of 100 μg ml^{-1} Eu(111).

7.4.1.1.7 Dispersion Coefficient (D)

The dispersion coefficient for this system was measured by injection of 100 μl of a 0.015% solution of methylene blue, and also by aspirating it continuously through the system. It was found to be 8.0. A 5cm long zinc reductor minicolumn was used with 2mm i.d.

7.4.1.2 Calibration Graph

Under the conditions established, a calibration graph for Eu(111) was obtained. It was linear in the range 0 - 200 μg ml^{-1} Eu(111). Typical calibration results in the

range 25 - 200 $\mu g\ ml^{-1}$ Eu(111) are shown in Table 7.3 and Fig. 7.16. The linear graph has a regression coefficient of 0.999 (5 points). The detection limit (2 x noise) was 2.5 $\mu g\ ml^{-1}$ and the r.s.d. for 11 replicate analyses of 50 $\mu g\ ml^{-1}$ was 1.56%. The residence time was 15 sec and the sample throughput could be up to 100 h^{-1}.

Eu(111) Conc. $\mu g\ ml^{-1}$	Mean Peak height (mm)	r.s.d. % for 10 replicates
25	21.8	5.6
50	49.0	1.0
100	92.1	1.3
150	135	0.76
200	180	0.75
Mean r.s.d. = 1.88%		

Table 7.3 Calibration results for the determination of Eu(111).

7.4.1.3 Interferences

There are many metals which have already been reported to affect the Fe(11) absorbance such as Cu(11), Co(11) and Ni[186,191].

Faizullah and Townshend[133] reported that the interference of such metals can be eliminated by using citrate buffer to mask them. Also, they reported that molybdate and vanadium interfered seriously. Molybdate interfered by forming a black precipitate on the reductor

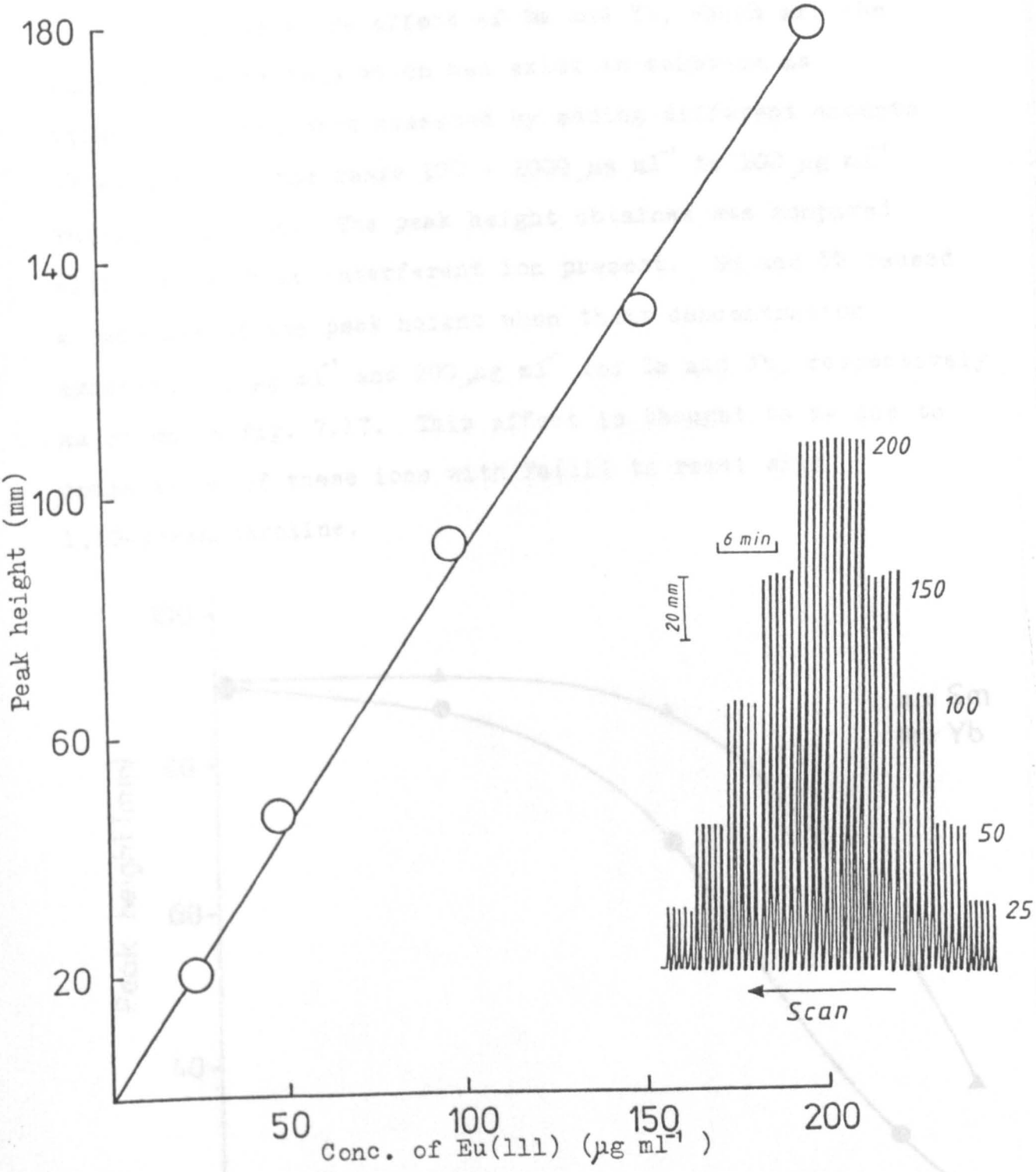

Fig. 7.16 Peaks obtained by injecting Eu(111) standards in the concentration range shown and the corresponding calibration graph.

and vanadium interfered by competition between vanadium and iron(11) to react with 1,10-phenanthroline.

In this work the effect of Sm and Yb, which are the only lanthanide ions which can exist in solution as dipositive ions, were measured by adding different amounts of each ion in the range 100 - 1000 $\mu g\ ml^{-1}$ to 100 $\mu g\ ml^{-1}$ Eu(111) solution. The peak height obtained was compared with that with no interferent ion present. Sm and Yb caused a decrease of the peak height when their concentration exceeded 400 $\mu g\ ml^{-1}$ and 200 $\mu g\ ml^{-1}$ for Sm and Yb, respectively as shown in Fig. 7.17. This effect is thought to be due to competition of these ions with Fe(11) to react with 1,10-phenanthroline.

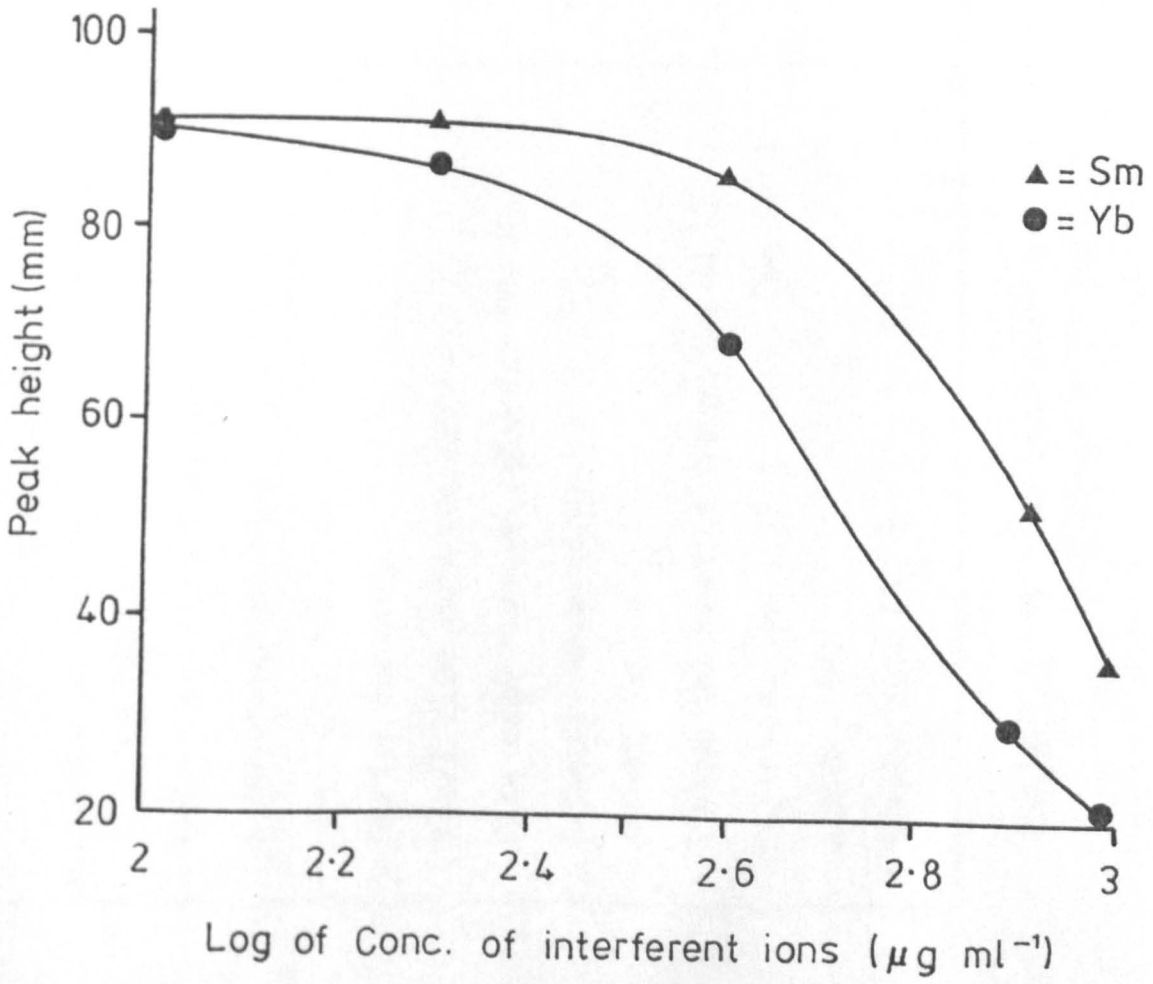

Fig. 7.17 The effect of Sm and Yb on the peak height of 100 $\mu g\ ml^{-1}$ Eu(111).

7.5 Conclusions

The incorporation of a mini-reductor column into the FIA system provides a simple and selective indirect spectrofluorimetrical and spectrophotometrical determination of Eu(III).

Optimum conditions for the above methods are summarized in Table 7.4. It is clear from Table 7.4 that spectrofluorimetric detection is more sensitive than spectrophotometric detection. It is clear by comparing Fig. 7.1 and 7.2, which show the flow manifolds, that the determination of Eu(III) by spectrofluorimetry can be achieved by a simpler manifold than the one used for spectrophotometry.

Parameter	Spectrofluorimetric	Spectrophotometric
Carrier Stream	0.5 M H_2SO_4	0.1 M HCl
Ce(1V) concentration ($\mu g\ ml^{-1}$)	10	-
1,10-Phenanthroline	-	1.25% (w/v)
Iron(111) solution	-	0.3 M
Buffer solution	-	Citrate, pH 5.2
Total flow rate ($ml\ min^{-1}$)	2.0	3
Flow rate through reductor ($ml\ min^{-1}$)	1.2	1
Reductor dimensions	5cm long, 2mm i.d.	5cm long, 2mm i.d.
Sample volume (μl)	80	100
Linear calibration range ($\mu g\ ml^{-1}$)	0.0 - 7.0	0.0 - 200
Detection limit (2 x noise) ($\mu g\ ml^{-1}$)	0.2	25
r.s.d. (%)	1.07	1.56
Sample rate (h^{-1})	110	100

Table 7.4 Optimum condition for the indirect spectrofluorimetric and spectrophotometric determination of Eu(111).

FLOW INJECTION FLUORIMETRIC DETERMINATION OF SAMARIUM, TERBIUM AND EURCPIUM

8.1 Introduction

Most luminescence in inorganic analysis is achieved by complexing the metal ion with a fluorescent organic ligand, to form a fluorescent complex. For instance, this forms the basis of highly sensitive and selective method of lanthanide determinations. Of these organic ligands β-diketones[192] have been widely used as chelating agents for the spectrofluorimetric determination of traces of some lanthanide ions[193,194]. Among the β-diketones used as fluorimetric reagents the fluorinated β-diketones were reported to produce a greater fluorescence intensity than non-fluorinated β-diketones[192]. Table 8.1 lists some of the applications of thenoyltrifluoroacetone and hexafluoroacetylacetone as fluorimetric reagents for Sm, Eu and Tb.

Characteristic intra-4f shell line fluorescence of triple charged lanthanide ions is excited in certain organic complexes by irradiation with light absorbed only by the organic part of the compounds. The ionic fluorescence is the result of an intramolecular energy transfer (IMET) from the organic ligand to the chelated metal ion[200-203]. The fluorescence occurs at similar wavelengths to the free lanthanide ion but with a much higher intensity.

8.2 Mechanism of the IMET Process in Chelates

Since the work of Weissman in 1942[203], the mechanism involved in the IMET processes is reasonably well understood.

Figure 8.1 is an illustration of the IMET processes

B-Diketone	Metal	Condition	Metal λex(nm)	Chelate λem(nm)	Limit of detection (ng ml^{-1})	Remarks	Ref.
2-Thenoyltrifluoroacetone	Eu	pH 8.2～8.3, EDTA	-	613	0.05	Other lanthanides do not interfere, Al, Be, Gd, Sn Te and Th do	195
	Eu	pH 3.6, TOPO* Triton X-100	352	613	1.5	Sc and Th (50-fold) do not interfere	196
	Sm	pH 3.6, TOPO Triton X-100	372	561	1.5	Sc and Th (50-fold) do not interfere	196
Hexafluoroacetylacetone	Eu	95% ethanol	312	614	4	Pr and Sm interfere	197
	Eu	pH 3, TOPO, extraction with Methylcyclohexane	360	615	0.2		199
	Sm	In ethanol	312	563	30	Eu and Tb (30-fold) do not interfere	198
	Sm	pH 3, TOPO, extraction with Methylcyclohexane	350	565	1.5		199

/Continued

B-Diketone	Metal	Condition	Metal λ_{ex}(nm)	Chelate λ_{em}(nm)	Limit of detection (ng ml^{-1})	Remarks	Ref.
Hexafluoro-acetylacetone	Tb	95% ethanol	312	544	4	Dy, Er and Yb interfere	199
	Tb	pH 3, TOPO, extraction with Methylcyclohexane	350	550	0.05	Other lanthanides do not interfere	195

Table 8.1 Applications of β-Diketone as fluorimetric reagents.

*TOPO = Tri-n-octylphosphine

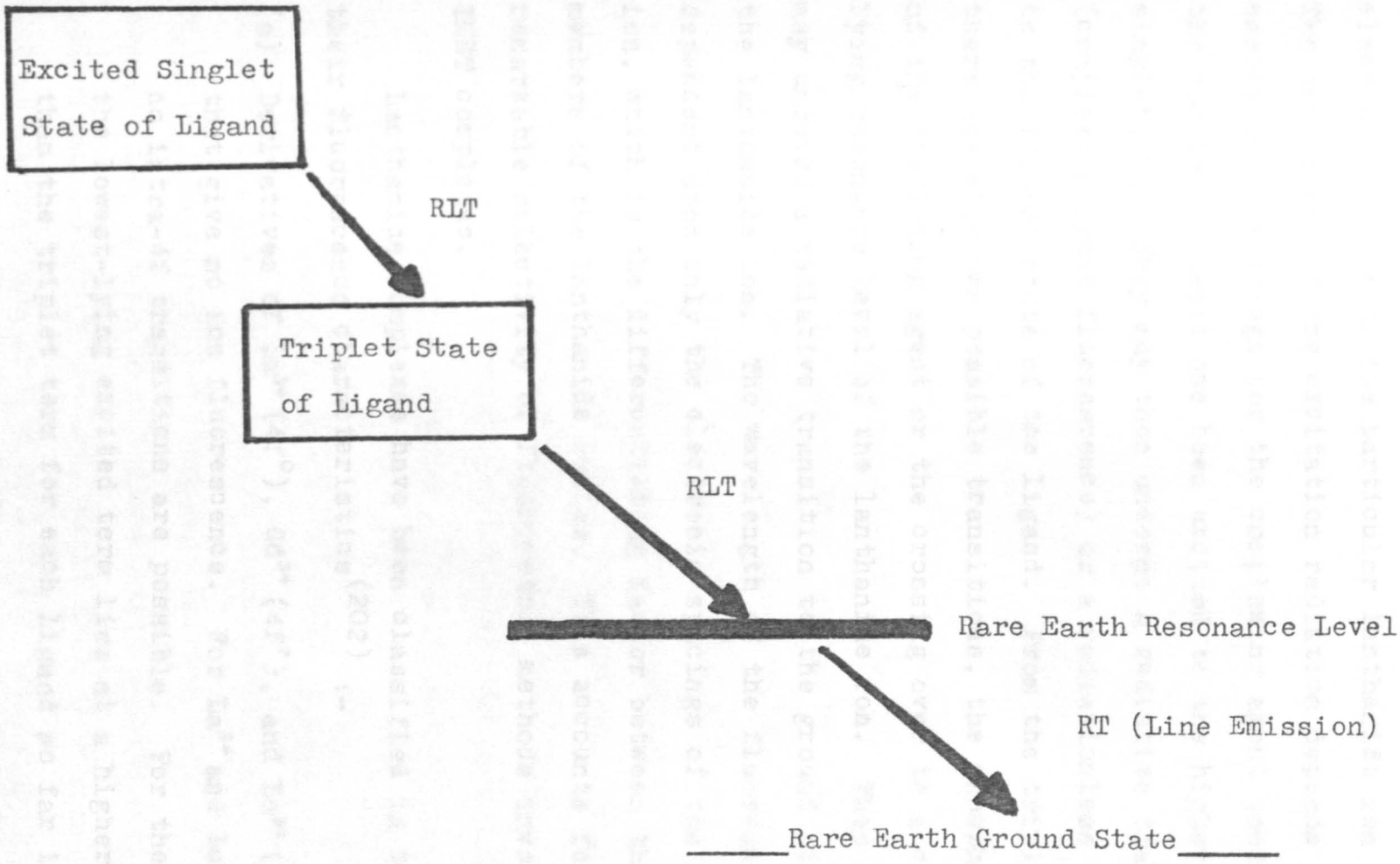

Fig. 8.1 An oversimple diagram to represent the IMET process in chelates[200]

RLT = radiationless transition, RT = radiative transition

which are involved in the excitation of the complex and the consequent emission of radiation characteristic of the electronic levels of the particular lanthanide ion involved. The wavelength of the excitation radiation depends upon the energy level spacings for the complexing agent used. Once the complexing agent has been excited to the higher level singlet, the energy may then undergo a radiative transition (complexing agent fluorescence) or a radiationless transition to the triplet state of the ligand. From the triplet state there are also two possible transitions, the phosphorescence of the complexing agent or the crossing over to a close-lying resonance level of the lanthanide ion. Then the system may undergo a radiative transition to the ground state of the lanthanide ion. The wavelength of the fluorescence is dependent upon only the electronic spacings of the lanthanide ion, which is the differentiating factor between the members of the lanthanide series. This accounts for the remarkable selectivity of fluorimetric methods involving IMET complexes.

Lanthanide complexes have been classified in terms of their fluorescence characteristics[202] :-

(a) Derivatives of La^{3+} ($4f^{0}$), Gd^{3+} ($4f^{7}$), and Lu^{3+} ($4f^{14}$) that give no ion fluorescence. For La^{3+} and Lu^{3+} ions no intra-4f transitions are possible. For the Gd^{3+} ion, the lowest-lying excited term lies at a higher level than the triplet term for each ligand so far investigated, thus forbidding any metal ion energy transfer.

(b) Complexes of Sm^{3+}, Eu^{3+}, Tb^{3+} and Dy^{3+} which exhibit

strong ion fluorescence. For each of these ions, there exists an excited term lying close of the ligand triplet level.

(c) Complex derivatives of Pr^{3+}, Nd^{3+}, Ho^{3+}, Er^{3+}, Tm^{3+} and Yb^{3+} which show weak ion fluorescence. For each of these ions there are only small energy differences between terms, increasing the probability of non-radiative energy transfer with the dissipation of smaller quantities of energy.

The intensity of the lanthanide fluorescence depends upon the quantity of energy available in the triplet state, the efficiency of the transfer of energy to the metal ion, and the probability that ion emission, rather than non-radiative deactivation, will occur. The efficiency of transfer is related both to the energy difference between the triplet state and the resonance level of the cation and to the nature of the bond between cation and ligand. The intensity of the fluorescence also depends upon type of the ligand, substituents attached to the ligand rings, temperature and solvent.

As mentioned earlier[192,197,198] fluorinated B-diketones produced a greater fluorescence intensity than the non-fluorinated β-diketones. In this work, it was thought that a more highly fluorinated β-diketone, specifically hexafluoracetylacetone, would lead to a more sensitive and selective fluorimetric method for the determination of Sm^{3+}, Eu^{3+} and Tb^{3+}, with combination of FIA as a simple, rapid and reproducible technique.

8.3 Reagents and Chemicals

All chemicals were of analytical grade except for $Eu(NO_3)_3 .5H_2O$, Tb_2O_3 and the other lanthanide interfering ions, which were as described in chapters 3 and 4. Also $Sm_2O_3 .5H_2O$ (Koch-Light Laboratories), which was 99.9% and hexafluoracetylacetone (HFAA), (Fluka), which was ca. 80 - 90% were used.

Europium and Samarium Solutions

1000 $\mu g\ ml^{-1}$ solutions of Eu and Sm were prepared by dissolving 0.3095 g and 0.2836 g of $Eu(NO_3)_3 .5H_2O$ and $Sm(NO_3)_3 .5H_2O$, respectively, in a 100 ml volumetric flask and diluting to volume with tetrahydrofuran (THF).

Terbium Solution

A 1000 $\mu g\ ml^{-1}$ Tb solution was prepared by dissolving 0.1176 g of Tb_2O_3 (Koch-Light Laboratories) in a few drops of AnalaR concentrated hydrochloric acid by gentle warming and diluting to exactly 100 ml with THF.

1% HFAA Solution

The stock complexing agent solution was prepared by diluting 1.0 ml of HFAA (Fluka) to 100 ml with THF.

8.4 Determination of Samarium

8.4.1 Flow Manifold

The manifold used for the determination of Sm^{3+} is shown in Fig. 8.2. A 4-channel peristaltic pump (Gilson

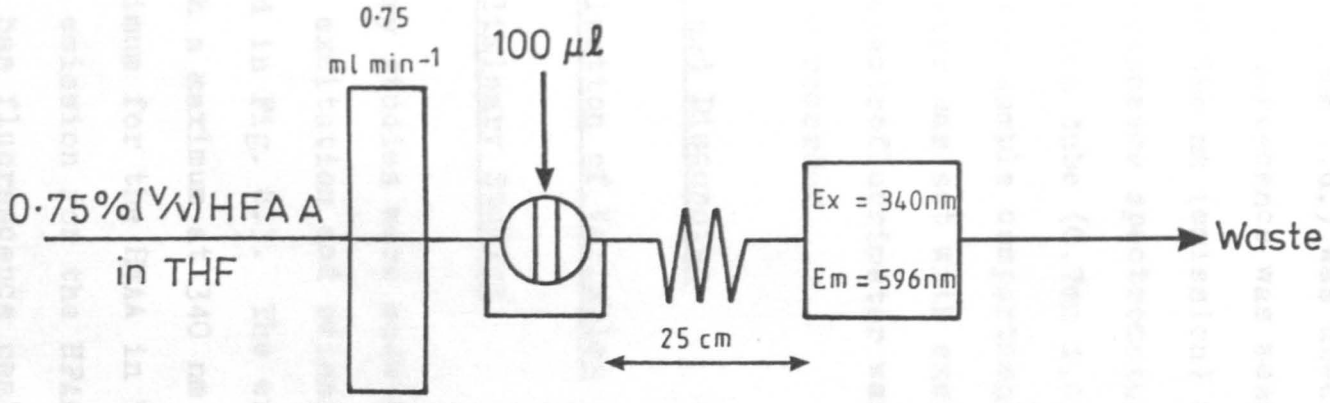

Fig. 8.2 Manifold for the determination of Sm(lll)

Minipuls 2) was used with 1 ml min^{-1} pump tubing (Watson-Marlow) and the sample was introduced via a Rheodyne 5020 injection valve (Anachem) with a sample loop of 100 µl. Teflon tubing (0.5mm i.d.) was used for the rest of the manifold. The fluorescence was measured at 340 nm (excitation) and 596 nm (emission) with a Perkin-Elmer model 3000 fluorescence spectrometer with a flow cell comprising a silica tube (0.7mm i.d. and 3.5mm long) held vertically in the sample compartment in a rigid mount. The spectrofluorimeter was set with excitation and emission slits at 10 and the spectrofluorimeter was connected to a Tekman Labwriter TE-200 recorder.

8.4.2 Results and Discussion

8.4.2.1 Optimization of Variables

8.4.2.1.1 Preliminary Studies

Preliminary studies were made with the Sm-HFAA complex to measure the excitation and emission spectra. These spectra are illustrated in Fig. 8.3. The excitation spectrum shows a broad peak with a maximum at 340 nm, which corresponds to the excitation maximum for the HFAA in THF. The spectra of excitation and emission for the HFAA are given in Fig. 8.4. The Sm complex has fluorescence peak at 565, 596 and 645 nm, with the 596 nm peak apparently the most intense, and which was used for the analytical purposes in subsequent experiments.

Figure 8.5 shows the emission spectrum of Sm in THF only, which give the same fluorescence spectrum as the complex of

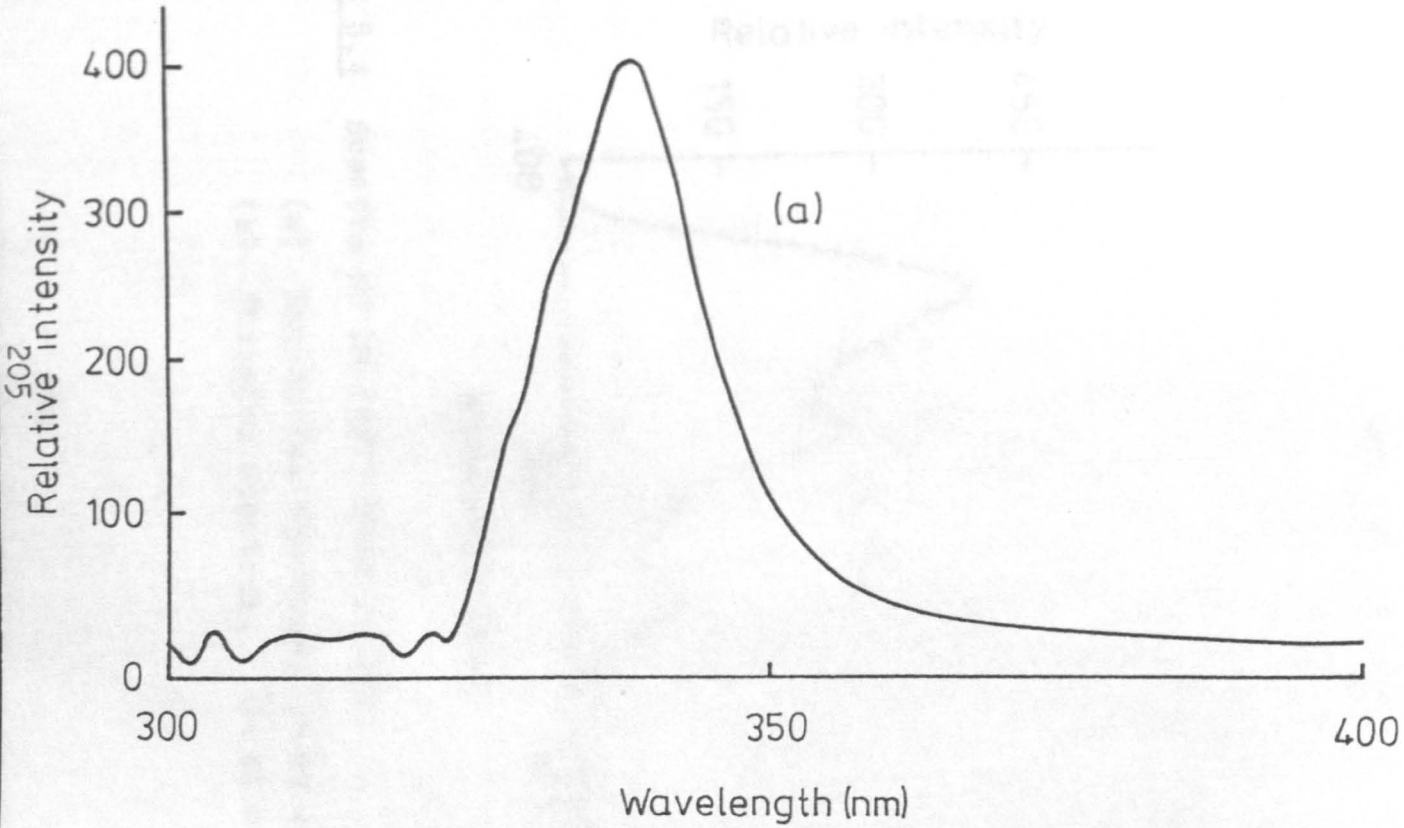

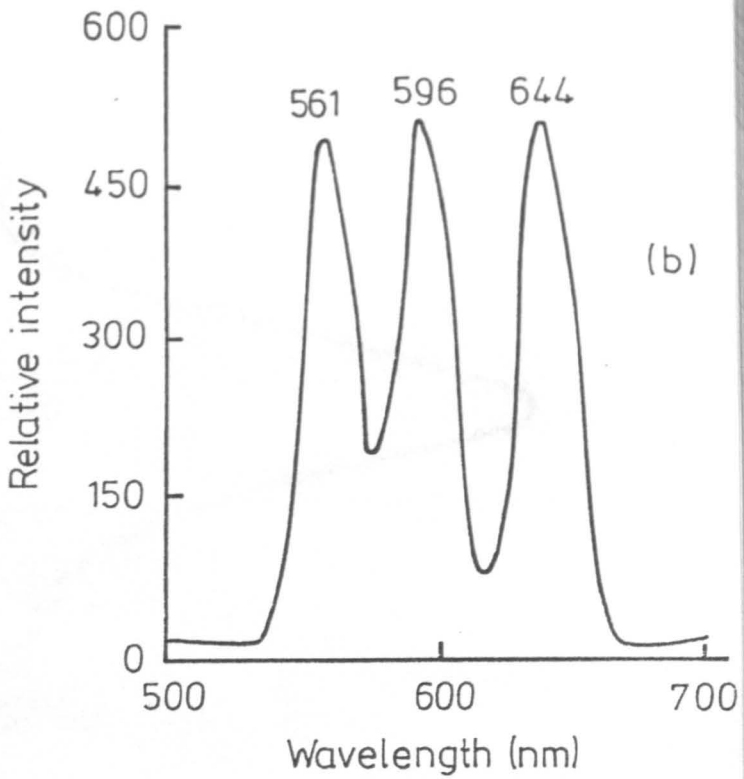

Fig. 8.3 Samarium (5 $\mu g\ ml^{-1}$) HFAA 1% v/v in THF complex spectra

(a) Excitation spectrum, λ em = 596 nm.

(b) Emission spectrum, λ ex = 340 nm.

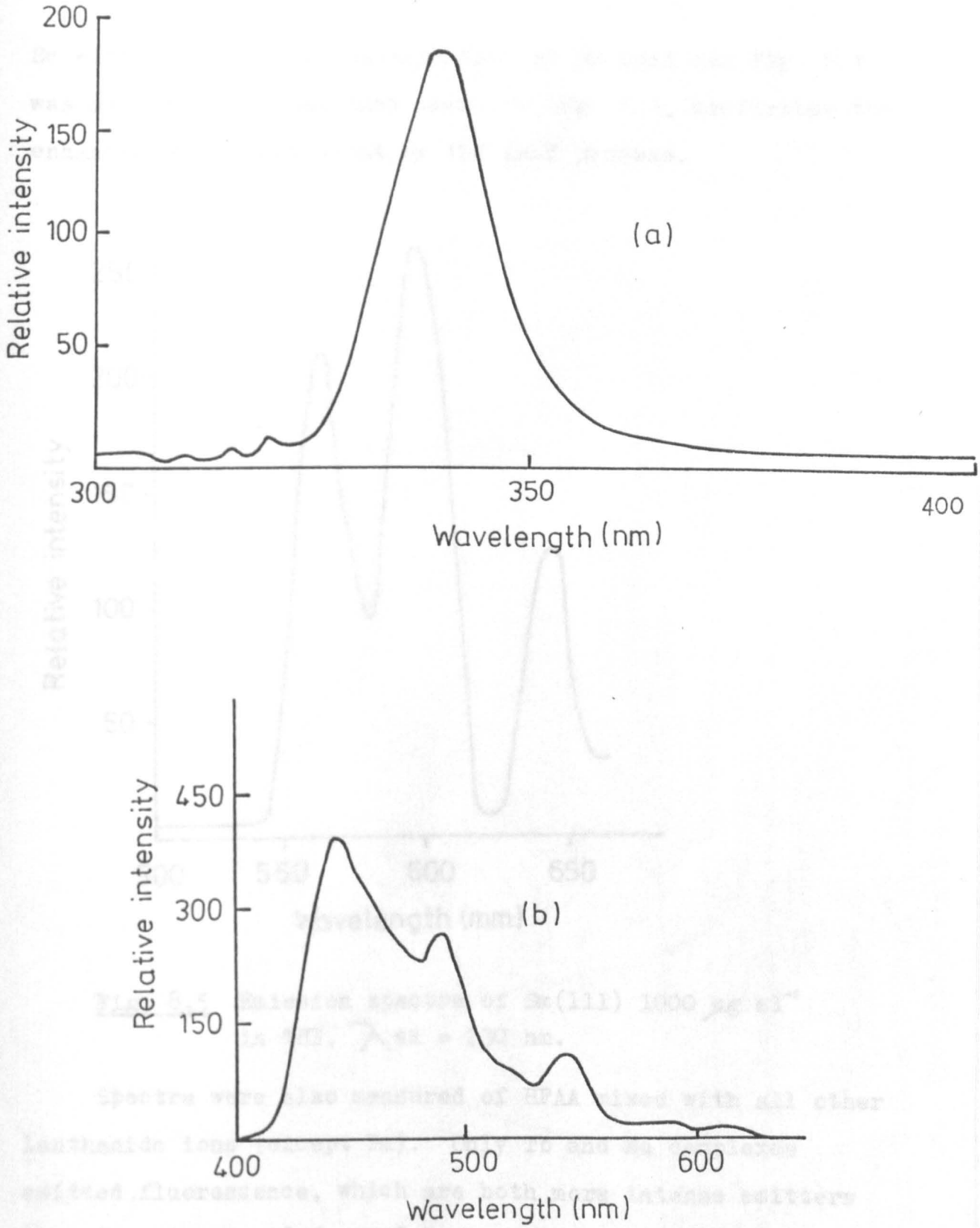

Fig. 8.4 Spectra of 1% (v/v) HFAA in THF.

(a) Excitation spectrum, λ em = 542 nm.
(b) Emission spectrum, λ ex = 340 nm.

Sm with HFAA but the concentration of Sm used for Fig. 8.4 was much greater than that used for Fig. 8.3, confirming the enhancement brought about by the IMET process.

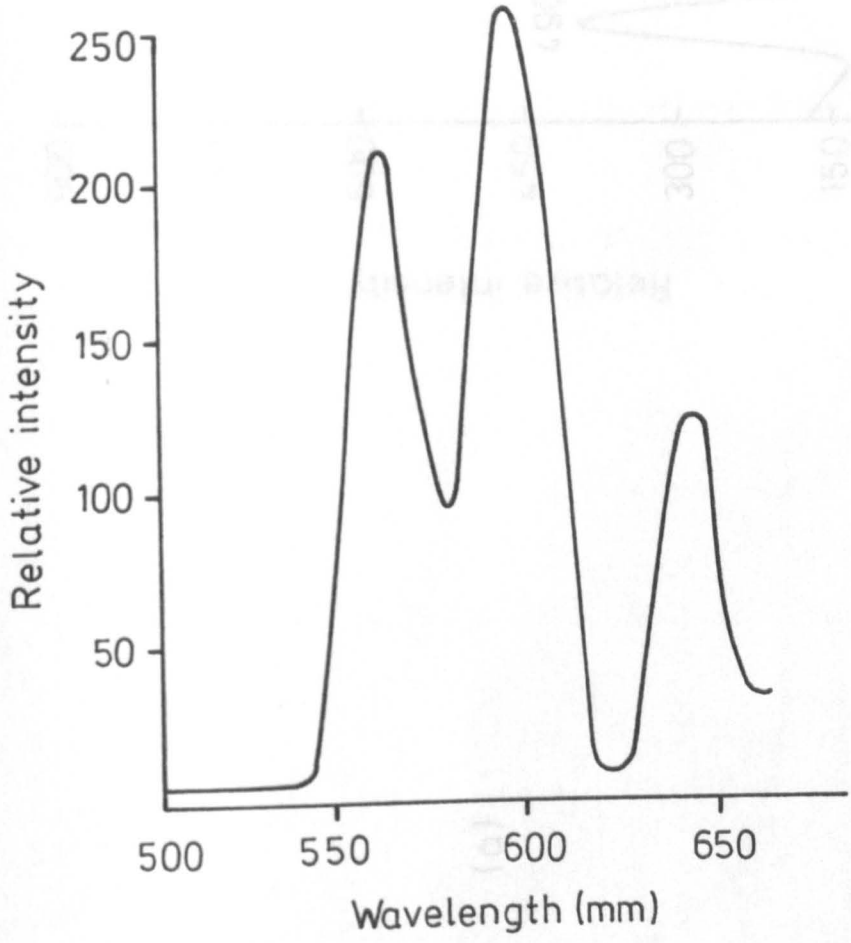

Fig. 8.5 Emission spectra of Sm(111) 1000 μg ml^{-1} in THF, λex = 230 nm.

Spectra were also measured of HFAA mixed with all other lanthanide ions (except Pm). Only Tb and Eu complexes emitted fluorescence, which are both more intense emitters than Sm. Figures 8.6 and 8.7 show the excitation and fluorescence spectra of Tb and Eu, respectively, the peaks being at 490 and 545 nm for Tb, and 593 and 614 nm, for Eu.

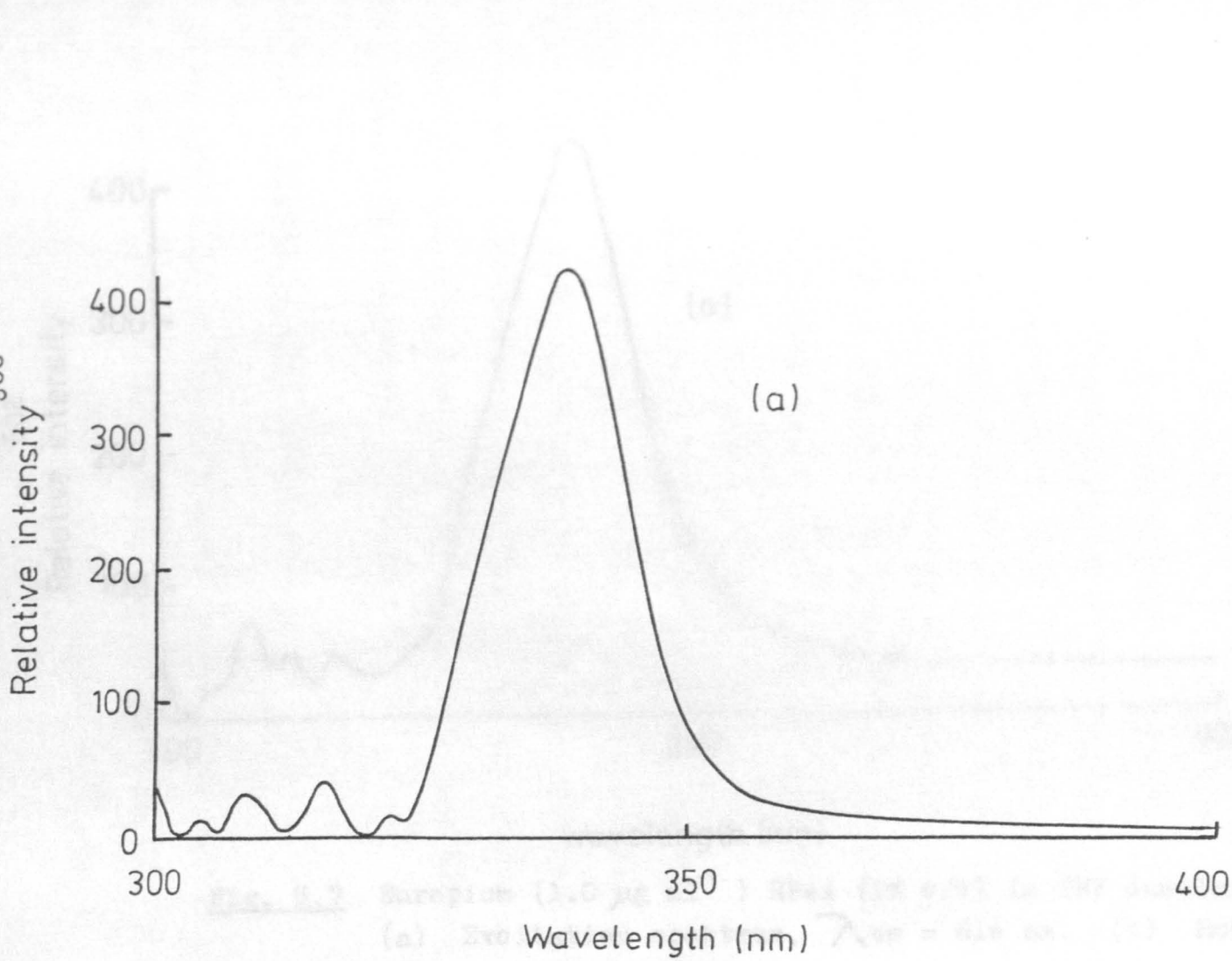

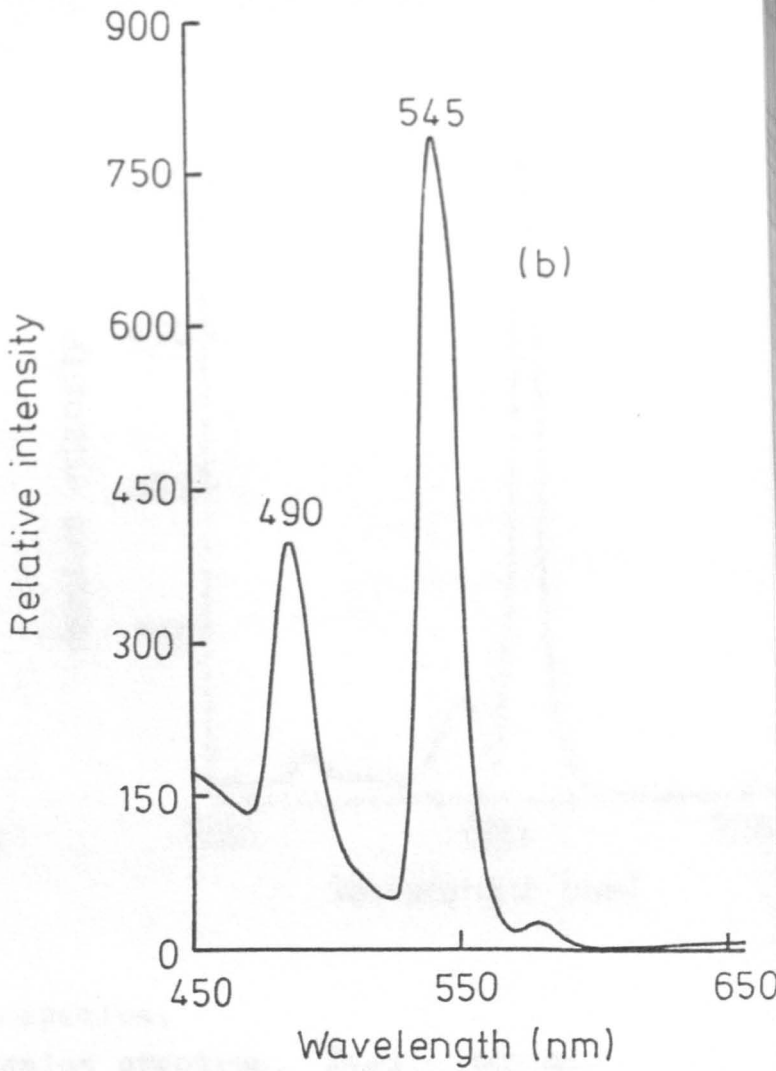

Fig. 8.6 Terbium (1 μg ml^{-1}) HFAA (1% v/v) in THF complex spectra.
(a) Excitation spectrum, λem = 545 nm. (b) Emission spectrum, λex = 340 nm.

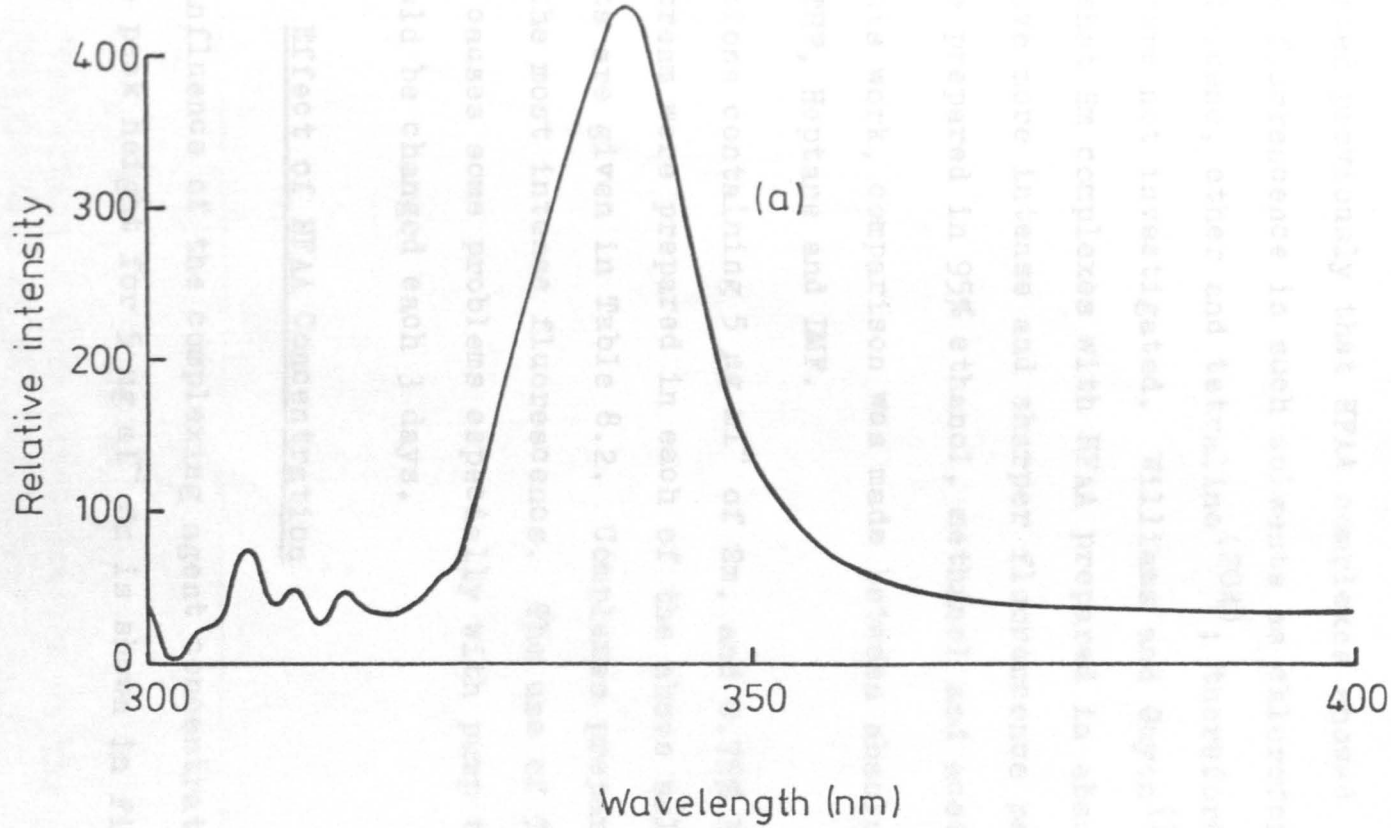

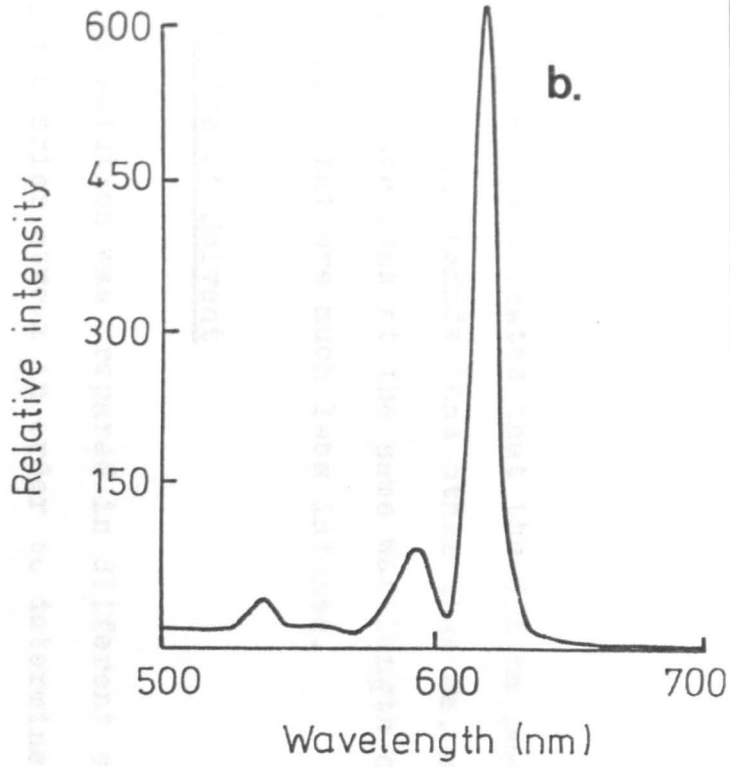

Fig. 8.7 Europium (1.0 $\mu g\ ml^{-1}$) HFAA (1% v/v) in THF complex spectra.
(a) Excitation spectrum, λem = 616 nm. (b) Emission spectrum, λex = 340 nm.

These figures illustrated that the 596 nm peak is not characteristic of lanthanide ions other than Sm, and HFAA shows a fluorescence peak at the same wavelength on the complex (596 nm), but are much less intense.

8.4.2.1.2 Choice of Solvent

The HFAA solution was prepared in different solvents and used as a carrier stream in order to determine in which the most intense fluorescence could be obtained. It has been reported previously that HFAA complexes showed negligible fluorescence in such solvents as chloroform, pyridine toluene, ether and tetraline[204]; therefore, these solvents were not investigated. Williams and Guyon[197] reported that Sm complexes with HFAA prepared in absolute ethanol gave more intense and sharper fluorescence peaks than those prepared in 95% ethanol, methanol and acetone.

In this work, comparison was made between absolute ethanol, THF, Heptane and DMF.

Solutions containing 5 μg ml^{-1} of Sm, and 0.75% HFAA as a carrier stream were prepared in each of the above solvents. The results are given in Table 8.2. Complexes prepared in THF gave the most intense fluorescence. The use of THF as a solvent causes some problems especially with pump tubing which should be changed each 3 days.

8.4.2.1.3 Effect of HFAA Concentration

The influence of the complexing agent concentration in THF on the peak height for 5 μg ml^{-1} Sm is shown in Fig. 8.8.

Solvent	Mean Peak For height (mm) 5 $\mu g\ ml^{-1}$ Sm(111)	r.s.d. % for 3 replicates
THF	90.2	0.6
Ethanol	71.3	3.6
DMF	40.7	2.2
Heptane	5.0	8.0

Table 8.2 Effect of solvents on the peak height for 5 $\mu g\ ml^{-1}$ Sm(111). (λ_{ex} = 340 and λ_{em} = 569)

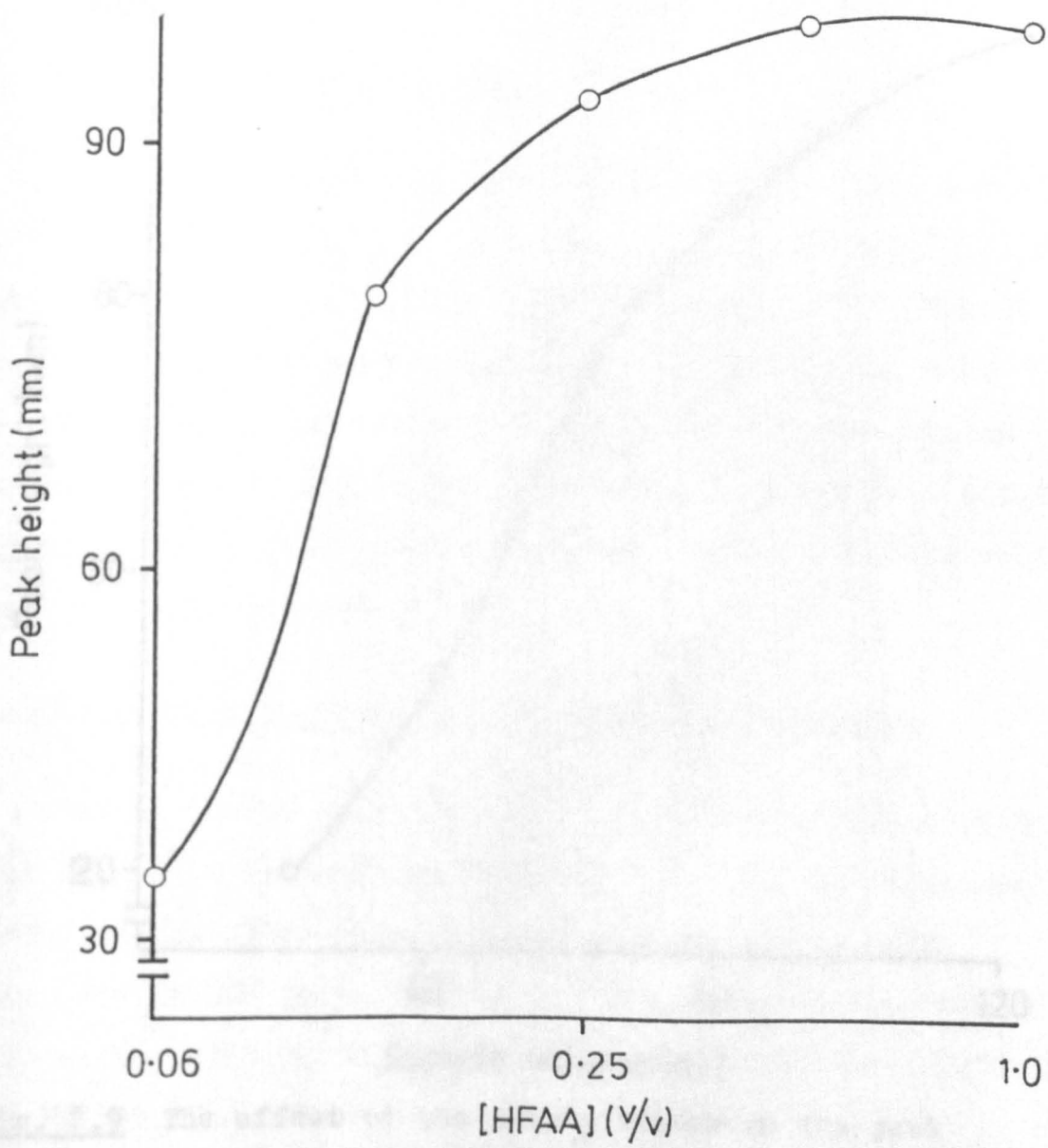

Fig. 8.8 The effect of HFAA concentration on the peak height of 5 $\mu g\ ml^{-1}$ Sm(111).

The peak height increases with increasing concentration of HFAA which thought to be due to more complex formation. Above 0.75% (v/v) the peak heights was nearly constant. Thus 0.75% (v/v) was used in subsequent experiments.

8.4.2.1.4 Effect of Sample Volume

The effect of sample volume is shown in Fig. 8.9. The maximum peak height was obtained when 120 µl was injected but the peak shape was somewhat distorted. So, 100 µl was injected in subsequent experiments.

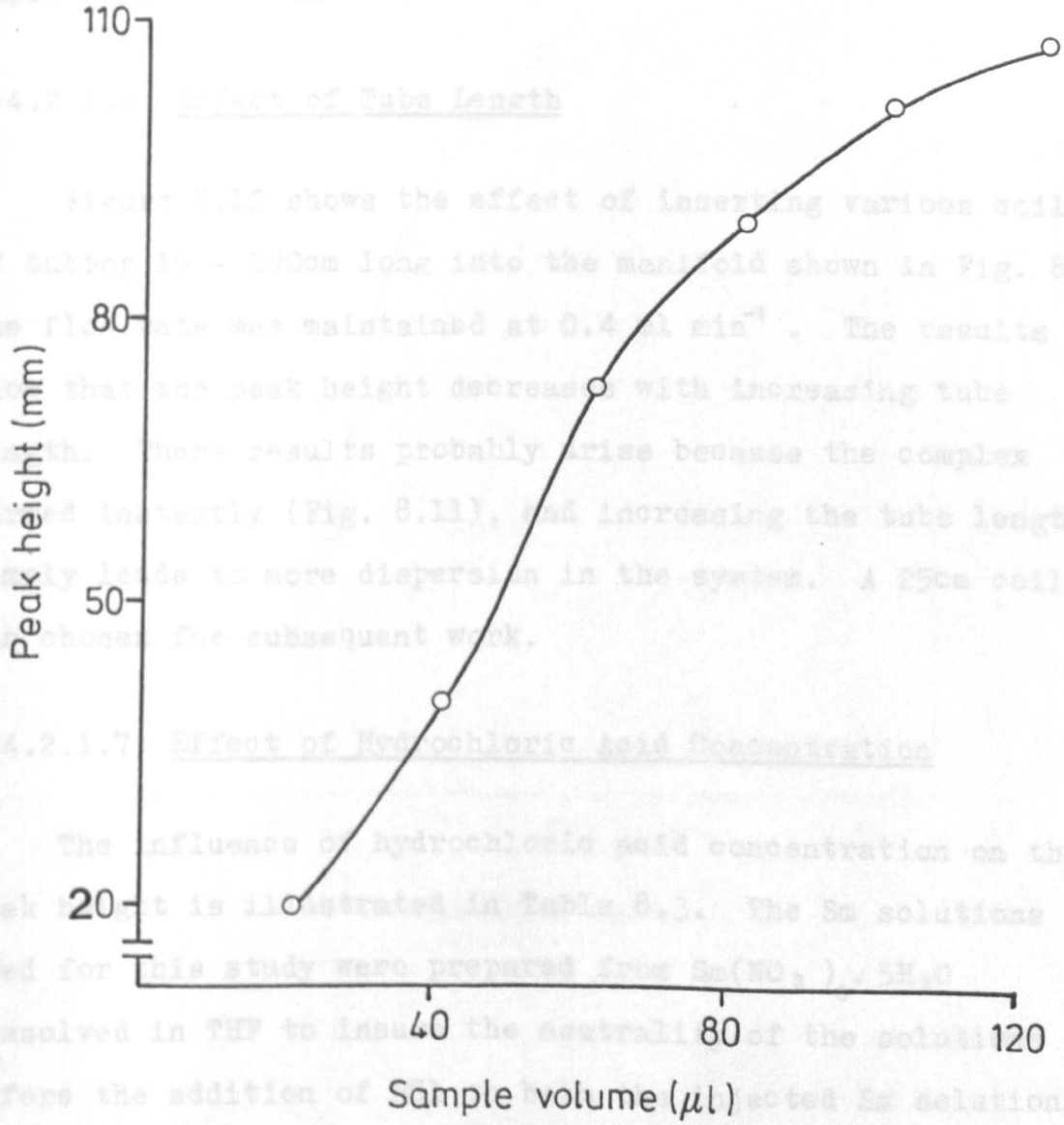

Fig. 8.9 The effect of the sample volume on the peak height of 5 µg ml^{-1} Sm(III)
(HFAA concentration = 0.75% (v/v) in THF).

8.4.2.1.5 Effect of Flow Rate

Figure 8.10 shows the effect of the flow rate of the reagent stream on the peak height. The reaction between Sm and HFAA was found to be instant as shown when the stopped-flow method was used (Fig. 8.11). Fig. 8.10 shows that the peak height decreases with increasing flow rate, which is thought to be due to the increase of the dispersion with increasing flow rate. A 0.75 ml min^{-1} flow rate was chosen for subsequent work because of the good reproducibility and rapid analysis achieved.

8.4.2.1.6 Effect of Tube Length

Figure 8.12 shows the effect of inserting various coils of tubing 15 - 100cm long into the manifold shown in Fig. 8.2. The flow rate was maintained at 0.4 ml min^{-1} . The results show that the peak height decreases with increasing tube length. These results probably arise because the complex formed instantly (Fig. 8.11), and increasing the tube length simply leads to more dispersion in the system. A 25cm coil was chosen for subsequent work.

8.4.2.1.7 Effect of Hydrochloric Acid Concentration

The influence of hydrochloric acid concentration on the peak height is illustrated in Table 8.3. The Sm solutions used for this study were prepared from $Sm(NO_3)_3 . 5H_2O$ dissolved in THF to insure the neutrality of the solutions before the addition of HCl to both the injected Sm solutions and to the HFAA stream.

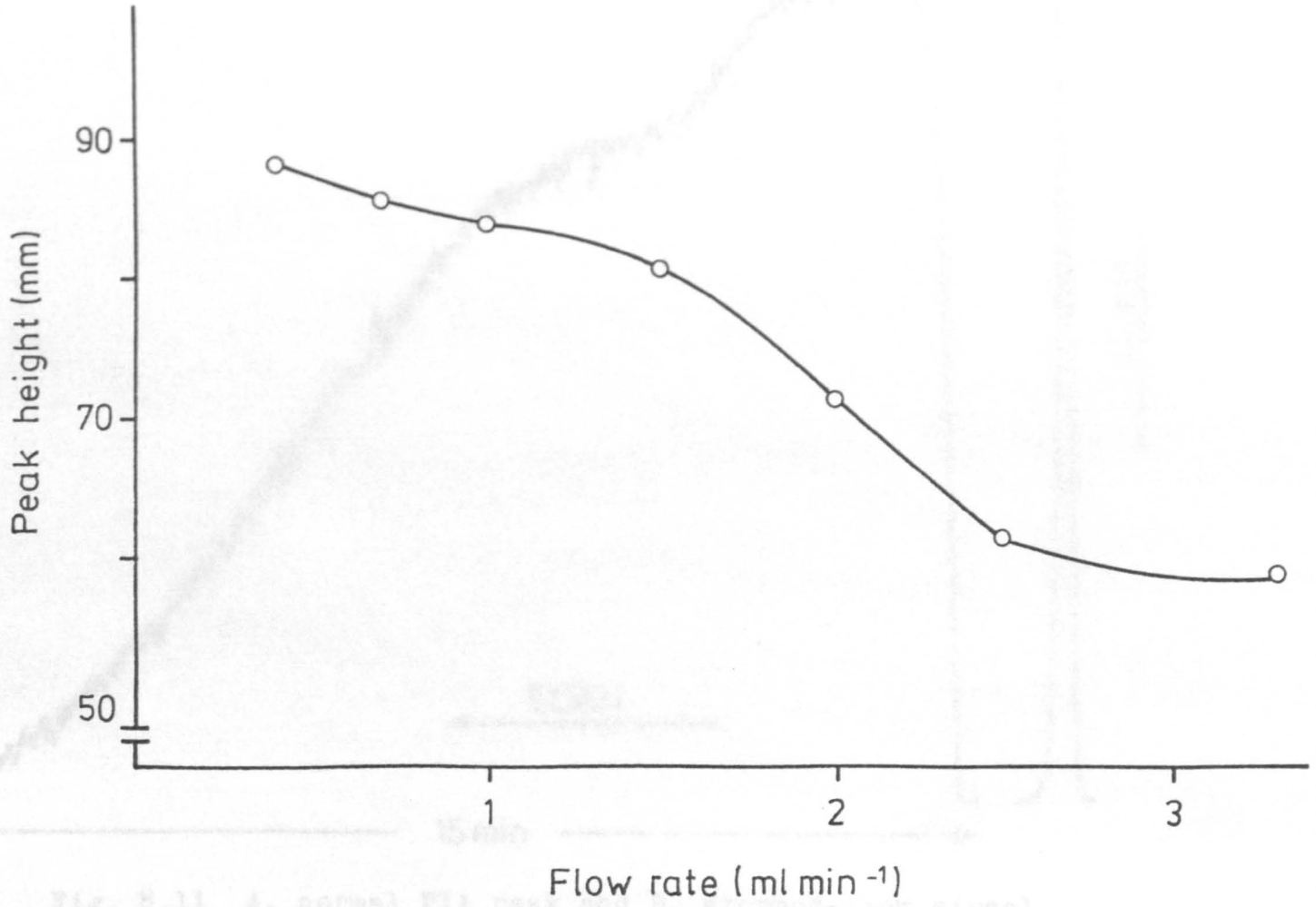

Fig. 8.10 The effect of flow rate on the peak height for 5 μg ml^{-1} Sm(lll).

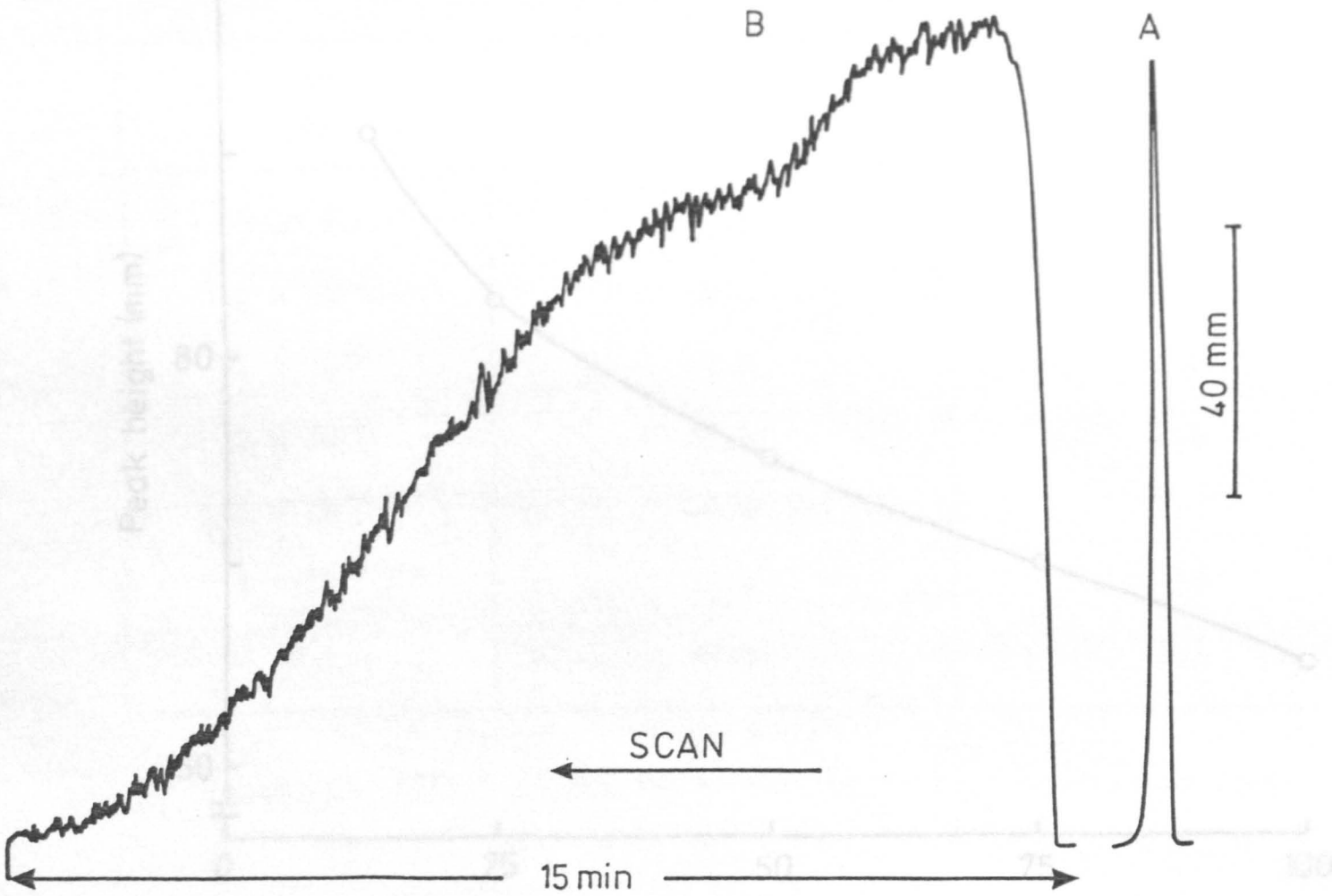

Fig. 8.11 A. normal FIA peak and B. stopped-flow signal obtained with flow system. Manifold as in Fig. 8.2, Sm(III) concentration (5 $\mu g\ ml^{-1}$).

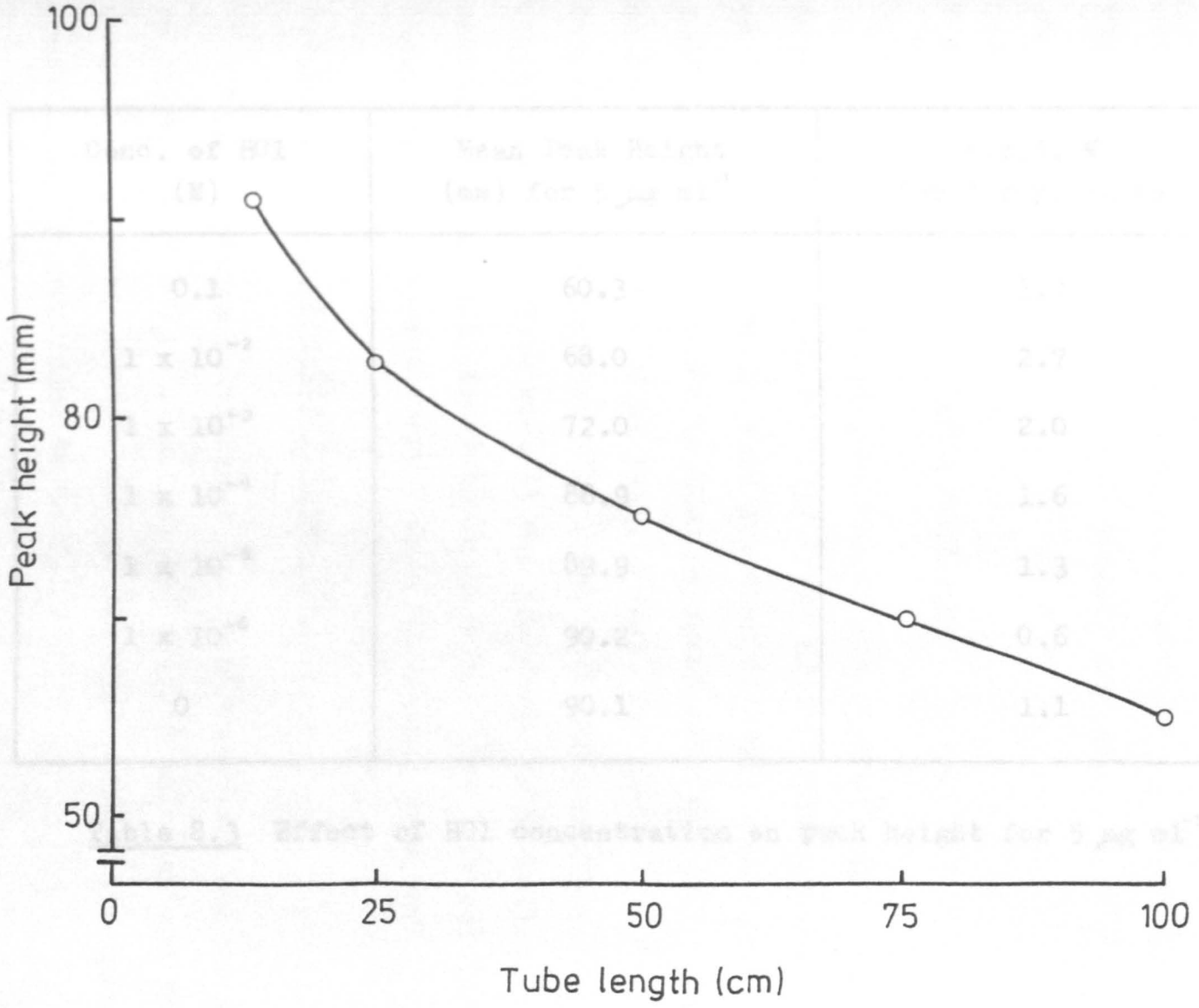

Fig. 8.12 Effect of tube length on the peak height of 5 $\mu g\ ml^{-1}$ Sm(lll).

Conc. of HCl (M)	Mean Peak Height (mm) for 5 $\mu g\ ml^{-1}$	r.s.d. % for 3 replicates
0.1	60.3	3.0
1×10^{-2}	68.0	2.7
1×10^{-3}	72.0	2.0
1×10^{-4}	88.9	1.6
1×10^{-5}	89.9	1.3
1×10^{-6}	90.2	0.6
0	90.1	1.1

Table 8.3 Effect of HCl concentration on peak height for 5 $\mu g\ ml^{-1}$ Sm(III).

The results showed that the peak height stayed nearly constant, with a slight increase between 10^{-4} - 10^{-6} M HCl. Also the peak height of the Sm solution without any acid gave the same value as in the range of HCl concentration above. So, Sm solutions prepared from $Sm(NO_3)_3 . 5H_2O$ and HFAA prepared in THF were used without any addition of HCl in the subsequent work.

8.4.2.1.8 Stability of HFAA Solutions

Table 8.4 lists the peak height for 5 µg ml^{-1} Sm solution injected into a stream of 0.75% (v/v) HFAA in THF, obtained on various days from the same solution of HFAA. The data indicated that the stock complexing agent solution (HFAA) is stable over a period of at least a week, but shows deterioration thereafter. The stock solution was also visibly different from when it was prepared, being yellow, whereas it originally had been colourless. The HFAA solution therefore was prepared every 7 days throughout this work.

8.4.2.1.9 Dispersion Coefficient (D)

The dispersion coefficient for this system was measured by injection of 100 µl of 0.5 µg ml^{-1} Ce(lll) solution and by aspirating it continuously through the system under the same conditions. D was found to be 4.

8.4.2.2 Calibration Graph

Under the conditions established, a calibration graph for Sm(lll) was obtained. It was linear in the range

0 - 10 $\mu g\ ml^{-1}$ Sm(111). Typical calibration results in the range 1.25 - 10 $\mu g\ ml^{-1}$ are shown in Table 8.5 and Fig. 8.13. The linear graph has a regression coefficient of 0.999 (6 points). The detection limit (2 x noise) was 0.2 $\mu g\ ml^{-1}$ and the r.s.d. for 11 replicate analyses of 5 $\mu g\ ml^{-1}$ was 1.5%. The sample throughput could be up to 80 h^{-1}.

Conc. of Sm(111) ($\mu g\ ml^{-1}$)	Mean Peak Height (mm)	r.s.d. % for 5 replicates
0.0	3.3	8.0
1.25	22.6	7.0
2.5	46.0	1.5
5.0	92.6	0.5
7.5	130	0.8
10.0	170	1.3

Table 8.5 Calibration results for determination of Sm(111).

8.4.2.3 Interferences

A study of interferences from other lanthanide ions was carried out on the determination of 2.5 $\mu g\ ml^{-1}$ Sm(111). The results are given in Table 8.6. It was found that a 20-fold excess of the ions listed in Table 8.6 had no significant effect on the peak height.

8.5 Determination of Terbium

Under the conditions shown in Fig. 8.14 a FIA fluorimetric method based on formation of fluorescent complex between Tb and HFAA was used to determine Tb(111). The calibration

Date	Mean Peak Height (mm) of 5 $\mu g\ ml^{-1}$	r.s.d. % for 3 replicates
2 - 12 - 85	90.6	1.3
4 - 12 - 85	91.0	0.5
6 - 12 - 85	89.0	1.1
10 - 12 - 85	87.3	4.0
12 - 12 - 85	85.7	3.0
16 - 12 - 85	78.0	3.2
18 - 12 - 85	71.0	5.0
20 - 12 - 85	68.0	3.2

Table 8.4 Stability of HFAA solution (75% v/v), Sm concentration 5 $\mu g\ ml^{-1}$.

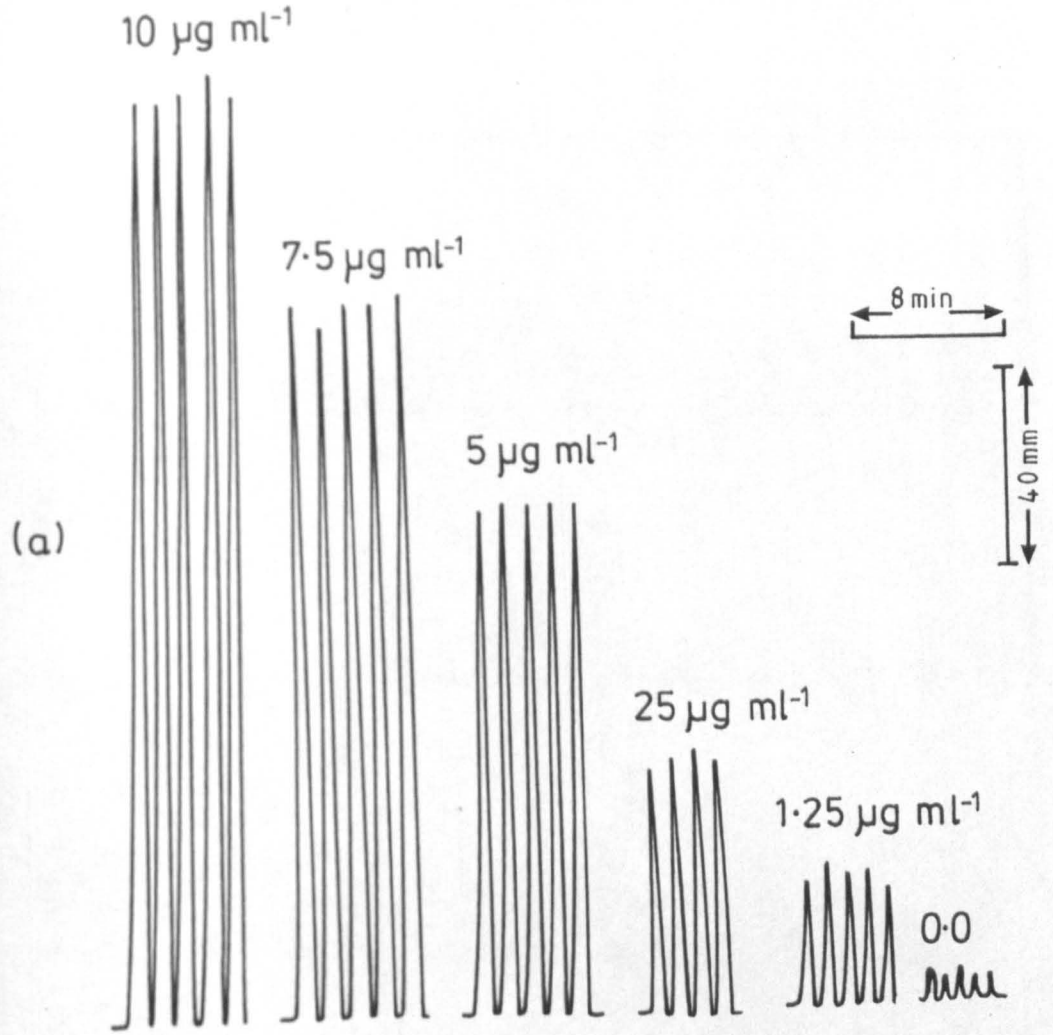

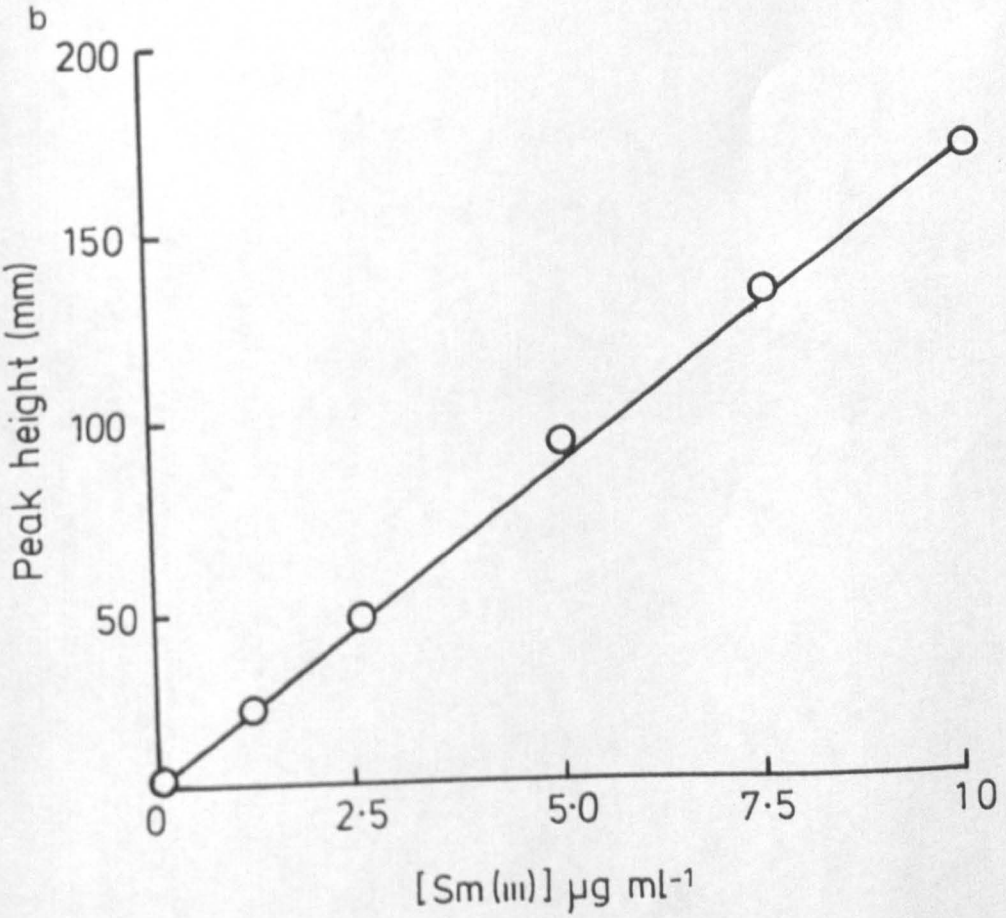

Fig. 8.13 (a) Peaks obtained by injecting Sm(III) standards in the concentration range shown, (b) the corresponding calibration graph.

Ion Added	Peak Height (mm) of Sm(III) in presence of 50 $\mu g\ ml^{-1}$ of interfering ions	Peak Height (mm) of Eu(III) in presence of 30 $\mu g\ ml^{-1}$ of interfering ions	Peak Height (mm) of Tb(III) in presence of 40 $\mu g\ ml^{-1}$ of interfering ions
-	46.0	73.0	50.6
La	39.0	72.2	49.2
Ce	44.3	70.5	45.0
Pr	46.0	71.3	46.1
Nd	45.5	69.0	48.0
Sm	-	80.1	56.0
Eu	48.6	-	62.0
Gd	46.0	69.0	45.0
Tb	47.5	87.0	-
Dy	46.0	68.3	47.3
Tm	45.2	70.6	45.1
Yb	47.0	80.2	54.2
Er	46.0	73.0	49.0
Lu	45.0	73.0	46.3
Y	47.0	65.0	47.8

Table 8.6 Effect of other ions on determination of 2.5 $\mu g\ ml^{-1}$ Sm(III), 1.5 $\mu g\ ml^{-1}$ Eu(III) and 2.0 $\mu g\ ml^{-1}$ Tb(III).

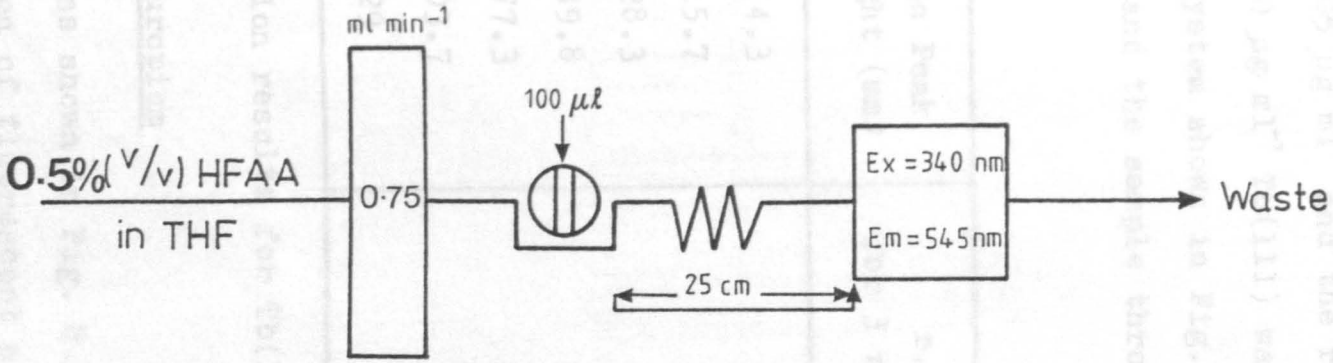

Fig. 8.14 Manifold for the determination of Tb(lll).

graph obtained was linear in the range 0 - 5 $\mu g\ ml^{-1}$ Tb(111) as shown in Table 8.7 and Fig. 8.15. The linear graph had a regression coefficient of 0.9999 (7 points). The detection limit (2 x noise) was 0.05 $\mu g\ ml^{-1}$ and the r.s.d. for 11 replicate analyses of 2.0 $\mu g\ ml^{-1}$ Tb(111) was 1.2%. The dispersion in the flow system shown in Fig. 8.11 under the conditions used was 4.5 and the sample throughput could be up to 80 h^{-1}.

Conc. of Tb(111) ($\mu g\ ml^{-1}$)	Mean Peak Height (mm)	r.s.d. % for 3 replicates
0.0	4.3	7.0
0.5	15.7	3.0
1.0	28.3	1.7
2.0	49.8	1.0
3.0	77.3	1.2
4.0	103.7	0.9
5.0	129	0.4

Table 8.7 Calibration results for Tb(111).

8.6 Determination of Europium

Under the conditions shown in Fig. 8.16, a fluorimetric method based on formation of fluorescent complex between Eu and HFAA are used to determine Eu(111). The calibration graph was linear in the range 0 - 3.0 $\mu g\ ml^{-1}$ Eu(111) as shown in Table 8.8 and Fig. 8.17. The linear graph has a regression coefficient of 0.998 (6 points). The detection limit (2 x noise) was 0.01 $\mu g\ ml^{-1}$ and the r.s.d. for 11

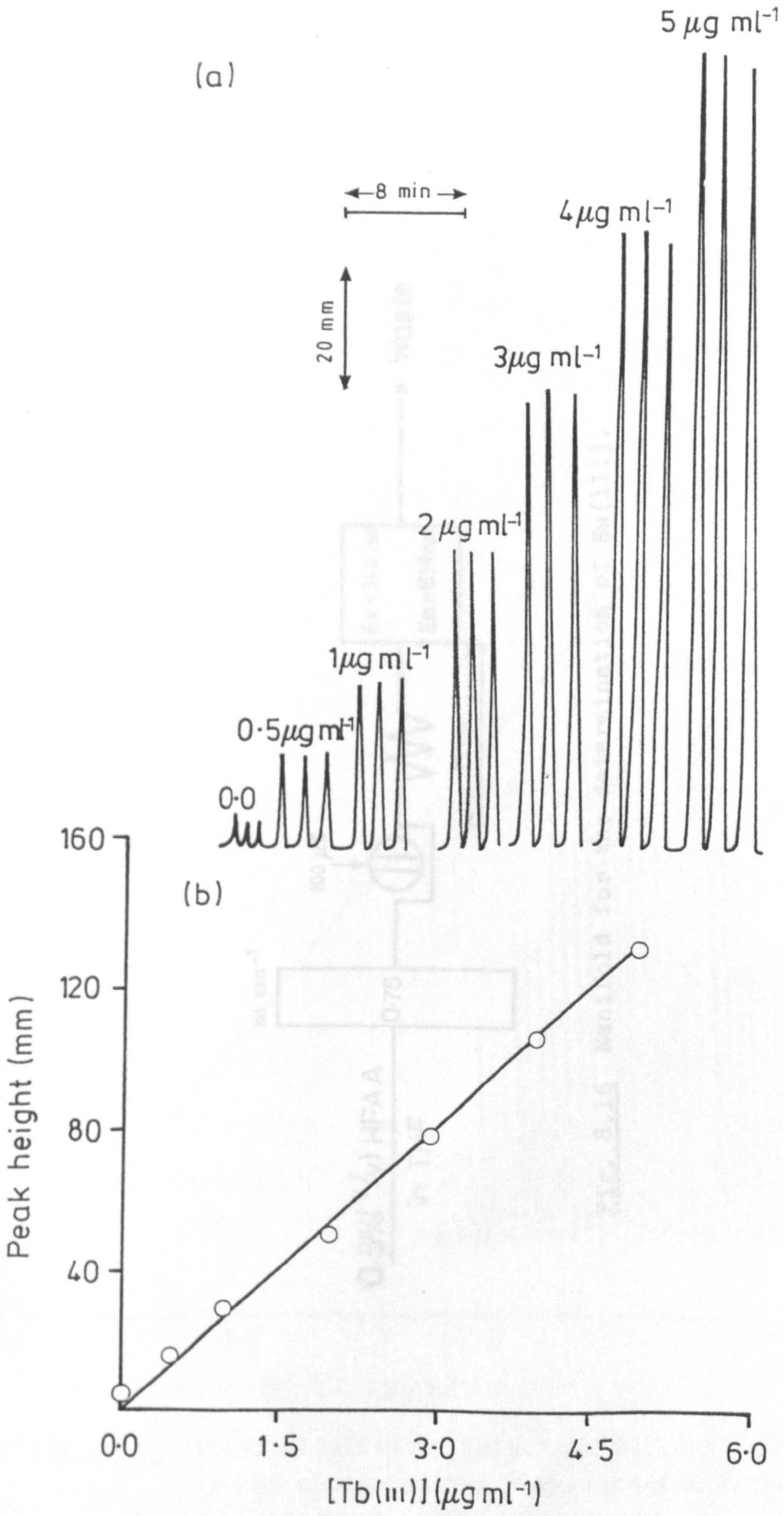

Fig. 8.15 (a) Peaks obtained by injecting triplicate Tb(111) standards in the concentration range shown, (b) the corresponding calibration graph.

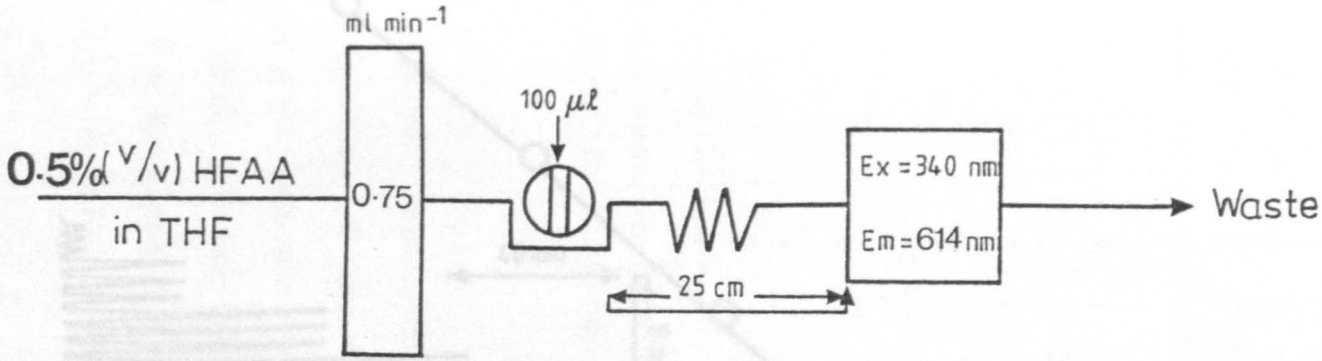

Fig. 8.16 Manifold for the determination of Eu(III).

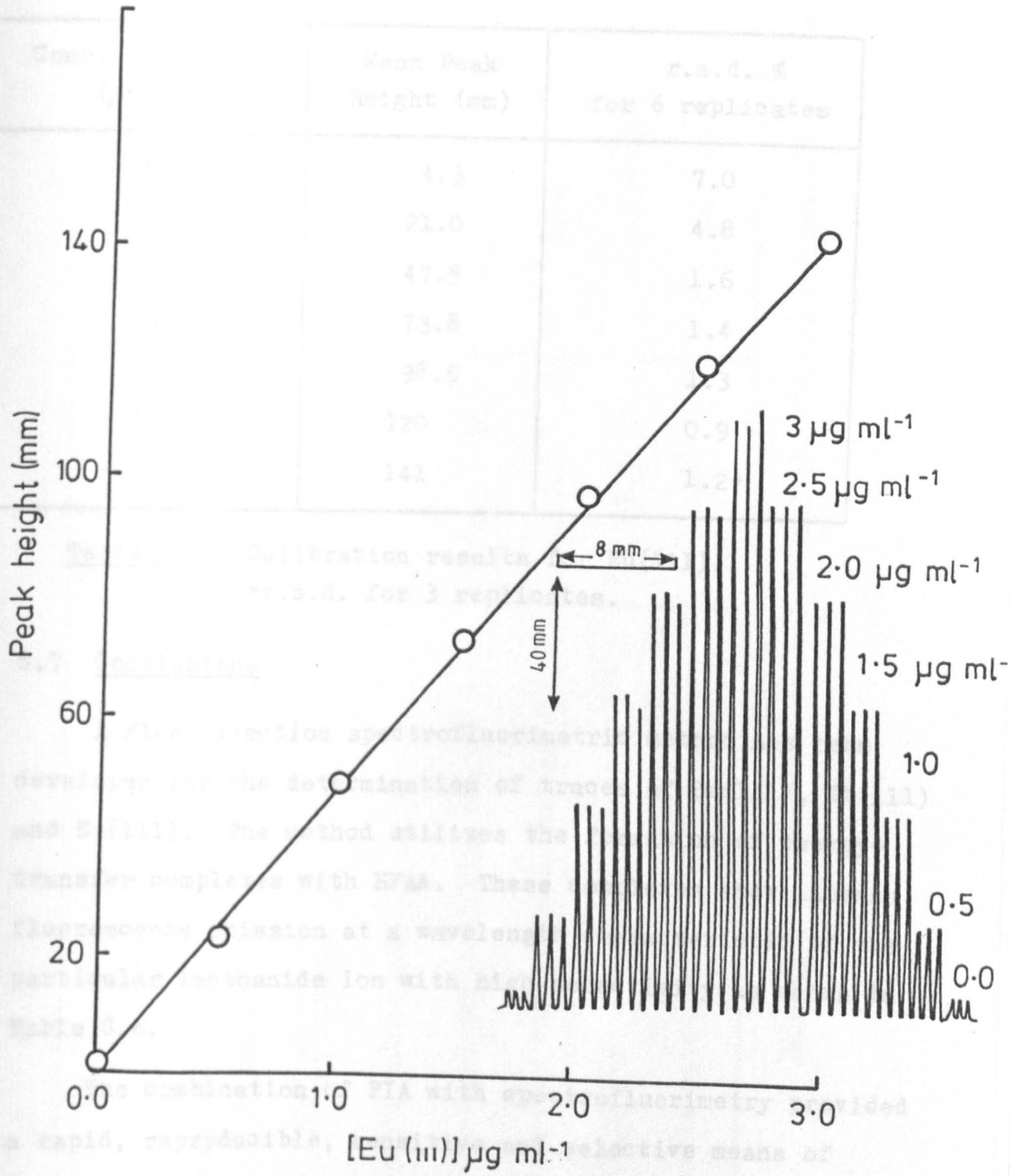

Fig. 8.17 Peaks obtained by injecting Eu(III) standards in the concentration range shown and the corresponding calibration graph.

replicate analyses of 1.0 $\mu g\ ml^{-1}$ Eu(III) was 1.6%. The dispersion in the flow system shown in Fig. 8.12 was 4 and the sample throughput could be up to 80 h^{-1} .

Conc. of Eu(III) ($\mu g\ ml^{-1}$)	Mean Peak Height (mm)	r.s.d. % for 6 replicates
0.0	4.3	7.0
0.5	21.0	4.8
1.0	47.5	1.6
1.5	73.8	1.4
2.0	98.5	1.3
2.5	120	0.9
3.0	141	1.2*

Table 8.8 Calibration results for Eu(III).
*r.s.d. for 3 replicates.

8.7 Conclusions

A flow injection spectrofluorimetric method has been developed for the determination of traces of Sm(III), Tb(III) and Eu(III). The method utilizes the formation of energy-transfer complexes with HFAA. These complexes show intense fluorescence emission at a wavelength characteristic of the particular lanthanide ion with high selectivity as shown in Table 8.6.

The combination of FIA with spectrofluorimetry provided a rapid, reproducible, sensitive and selective means of determination of lanthanide ions. Table 8.9 summarizes the optimum conditions for the Sm(III), Tb(III) and Eu(III) determination.

Parameter	Flow injection Spectrofluorimetric method of determination		
	Sm(III)	Tb(III)	Eu(III)
HFAA concentration (v/v) in THF	0.75	0.5	0.5
Flow rate (ml min^{-1})	0.75	0.75	0.75
Sample volume (µl)	100	100	100
Linear calibration range (µg ml^{-1})	0.0 - 10	0.0 - 5.0	0.0 - 3.0
Detection limit (2 x noise) µg ml^{-1}	0.2	0.05	0.01
r.s.d. (%)	1.5	1.2	1.6
Sample rate (h^{-1})	80	80	80

Table 8.9 Optimum conditions of Sm(III), Tb(III) and Eu(III) determination.

CHAPTER NINE

GENERAL CONCLUSIONS AND SUGGESTIONS

FOR

FUTURE WORK

9.1 General Conclusions and Suggestions for Future Work

The work presented in this thesis is the most recent development in candoluminescence and flow injection spectrofluorimetric methods for lanthanide determination. The following conclusions and suggestions for future work depend upon the new developments established in this work.

9.1.1 Candoluminescence

Candoluminescence has been proved to be potentially useful for lanthanide determination. In the present investigation, for the first time the candoluminescence emission of Tb and Eu in MgO and rare earth oxides coated on CaO (Y_2O_3, La_2O_3, Gd_2O_3 and Lu_2O_3) matrices, respectively, have been used for analytical purposes. The use of rare earth-coated matrices for stimulated candoluminescence emission provides a very sensitive means for Tb and Eu determination, with a detection limit in some cases as low as 0.01 ng. The use of these matrices can be suggested for determination of other ions such as Bi, Pb and Te.

The improvement of the reproducibility achieved in this work is attributed to the development of the matrix making and the automated matrix introducing devices. Further work can be suggested for more development in candoluminescence instrumentation especially for automated sample injection, in order to avoid any human error by injecting a small amount of the activator, usually 1 µl, by syringe. Also the possibility of using candoluminescence for multielement

determination can be suggested. In conclusion, it can be said that the greatest advantage of candoluminescence is its sensitivity and simplicity when used as analytical method for lanthanide determination.

9.1.2 Flow Injection Spectrofluorimetric Lanthanide Determination

The work presented in this part of the research is to develop methods for lanthanide determination by a combination of flow injection analysis and spectrofluorimetry.

For the first time, a simple, rapid, sensitive and reproducible flow injection spectrofluorimetric method has been used for Ce(lll) determination. The method is based on monitoring its native fluorescence. A same method can be suggested for future work for determination of uranium and thorium. A method is also established for indirect spectrofluorimetric of Ce(lV) by incorporation of a Jones reductor minicolumn in a simple manifold to reduce Ce(lV) to fluorescent Ce(lll). Many future projects can be suggested for flow injection indirect spectrofluorimetric for determination for many inorganic species (reductants - As(lll), Fe(ll) nitrate and thiosulphate) and organic compounds (oxalic acid, ascorbic acids and phenols) which can reduce Ce(lV) to the fluorescent Ce(lll).

Another method developed in this work, utilizes the formation of energy-transfer complexes between the lanthanide ions and HFAA. This work can be developed further by combination of flow injection spectrofluorimetry with

micelles and microemulsions. The technique of FIA, which involves controlled mixing of sample and reagent within an enclosed system, is a very suitable tool for studying the analytical potential of microemulsions. A procedure based on this combination will provide a simple, sensitive, rapid method and have environmental advantage that separates organic solvents which are unnecessary.

In conclusion it can be said that the attractive features of the combination of FIA with spectrofluorimetry: sensitivity, reproducibility, rapidity and selectivity can be extended for determination of many inorganic and organic compounds.

REFERENCES

REFERENCES

1. S. P. Sinha, Systematics and the Properties of Lanthanides, Reidel, Dordrecht, Holland (1982).

2. C. F. Liptrot, Modern Inorganic Chemistry, Fourth Edition, Bell and Hyman, London (1983).

3. M. A. McMahon, Proc. 13th Rare Earth Res. Conf., Wheeling, West Virginia, 1, 593 (1977).

4. M. J. Weber, Handbook of the Physics and Chemistry of Rare Earths, North-Holland, Amsterdam, 4, 275 (1979).

5. A. Bril and C. D. J. C. de Laat, Electrochem. Techn. 4, 21 (1966).

6. E. A. Nesbitt and J. H. Wernick, Rare Earth Permanent Magnets, Academic Press, New York (1973).

7. E. Wiedmann, Wiedmann's Ann., 37, 177 (1889).

8. C. A. Parker, Photoluminescence of Solutions, Elsevier, Amsterdam (1968).

9. P. Goldberg, Luminescence of Inorganic Solids, Academic Press, New York (1966).

10. G. F. Garlick, Solid Luminescence Materials, Wiley, New York (1948).

11. E. N. Harvey, A History of Luminescence, The American Philosophical Society, Philadelphia (1957).

12. H. W. Leverenz, An Introduction to Luminescence of Solids, Wiley, New York (1950).

13. E. L. Nichols, H. L. Howes and D. T. Wilber, Cathodoluminescence and the Luminescence of Incandescent Solids, Carnegie Institution of Washington, Publ. No. 384 (1928).

14. W. H. Balmain, Phil. Mag., (Ser. 3) 21, 270 (1842).

15. T. Scheerer, Ann. Phys., 51, 465 (1840).

16. H. Rose, Ann. Phys., 103, 311 (1858).

17. R. W. von Bunsen, Liebig's Ann. Chem. Pharm., 131, 255 (1864).

18. J. Bahr, Liebig's Ann. Chem. Pharm., 135, 1375 (1865).

19. V. Gutmann, J. Chem. Ed., 47, 209 (1970).

20. J. Donau, Graz. Monatsh., 34, 949 (1913), in Chem. Abs., 7, 3445 (1913).

21. J. Donau, Graz. Monatsh., 34, 335 (1915), in Chem. Abs., 10, 3025 (1916).

22. E. L. Nichols, H. L. Howes and D. T. Wilber, Phys. Rev., 21, 35 (1918).

23. E. L. Nichols and F. G. Wick, J. Opt. Soc. Amer., 2, 357 (1932).

24. E. L. Nichols and H. L. Howes, ibid., 22, 170 (1932).

25. E. L. Nichols and M. A. Ewer, ibid., 22, 456 (1932).

26. E. L. Nichols and C. L. Stanford, ibid., 26, 91 (1936).

27. F. G. Wick and C. G. Throop, ibid., 25, 57 (1935).

28. E. C. W. Smith, Inst. Gas Eng., 237, 519 (1940).

29. O. Neunhoeffer, Z. Phys. Chem., 132, 91 (1951), in Chem. Abs., 45, 3289e (1951).

30. V. A. Sokolov, I. S. Grozina and A. N. Gorban, Opt. i Spectroscopia, 3, 92 (1957), in Chem. Abs., 52, 2556f (1958).

31. Idem., ibid., 4, 409 (1958), in Chem. Abs., 52, 16893a (1958).

32. D. M. Mason, Am. Chem. Soc., Div. Fuel. Chem. Prepints, 11(2), 540 (1967).

33. J. R. Sweet, W. B. White, H. K. Hensch and R. Roy. Phys. Lett., 33(A), 95 (1970).

34. J. R. Sweet and W. B. White, Proc. 9th Rare Earth Res. Conf., Blacksburg, West Virginia, 2, 450 (1971).

35. A. Corredor, I. S. T. Tsong and W. B. White, Proc. 13th Rare Earth Res. Conf., Wheeling, West Virginia, 1, 573 (1977).

36. C. K. Jorgensen, Chem. Physics. Lett., 34, 14 (1975).

37. C. K. Jorgensen, H. Bill and R. Reisfield, J. Luminescence, 24, 91 (1981).

38. C. K. Jorgensen, Structure and Bonding, 25, 1 (1975).

39. R. Belcher, S. Bogdanski and A. Townshend, Talanta, 19, 1049 (1972).

40. R. Belcher, K. P. Ranjitkar and A. Townshend, Analyst, 100, 415 (1975).

41. Idem., ibid., 101, 666 (1976).

42. R. Belcher, T. A. K. Nasser, L. Polo. Diez and A. Townshend, Analyst, 102, 391 (1977).

43. R. Belcher, T. A. K. Nasser, M. Shahidullah and A. Townshend, Amer. Lab., 9, 61 (1977).

44. K. P. Ranjitkar, Ph.D. thesis, Birmingham University. (1975).

45. S. Karpel, Ph.D. thesis, Birmingham University, (1971).

46. M. Shahidullah, Ph.D. thesis, Birmingham University, (1976).

47. T. A. K. Nasser, Ph.D. thesis, Birmingham University, (1977).

48. M. Matsuoka, Ph.D. thesis, Birmingham University, (1979).

49. S. M. Dhaher and Z. M. Kassir, Anal. Chem., 52, 459 (1980).

50. Z. M. Kassir, A. Al-Muaibed and A. H. A. Kareem, Anal. Chim. Acta., 160, 235 (1984).

51. A. Al-Muaibed, M.Sc. thesis, Basrah University, (1980).

52. F. Paneth and E. Winternitz, Phys. Ber., (Ser. 2) 51, 1728 (1918), in Chem. Abs., 13, 1431 (1919).

53. E. Tiede and F. Buescher, ibid., (Ser. 2) 53, 2206 (1920), in Chem. Abs., 15, 1459 (1921).

54. E. L. Nichols, J. Opt. Soc. Amer., 20, 106 (1930).

55. L. T. Minchin, Trans. Far. Soc., 35, 103 (1939).

56. K. F. Bonhoeffer, Z. Phys. Chem., 113, 199 (1924), in Chem. Abs., 19, 915 (1925).

57. D. T. A. Townend, Fuel, 29, 64 (1950), Chem. and Ind., 23, 346 (1945).

58. J. R. Arthur, Nature, 165, 557 (1950).

59. K. M. Sancier, W. J. Frederick and H. Wise, J. Chem. Phys., 37, 854 (1962).

60. A. N. Gorban and V. A. Sokolov, Opt. i Speck., 12, 116 (1962), in Chem. Abs., 57, 4153h (1962).

61. V. V. Styrov and V. A. Sokolov, Izv. Tomsk. Politekh. Inst., 184, 3 (1970), in Chem. Abs., 75, 69201g (1971).

62. Idem. ibid., 184, 7 (1970), in Chem. Abs., 75, 145695p (1971).

63. Th. Volkenstein, V. A. Sokolov, A. N. Gorban and V. G. Kornich, Proc. Intl. Conf. Luminescence, Budapest, 2, 1432 (1966).

64. A. I. Bazhin, V. V. Styrov and V. A. Sokolov, Izv. Vyssh-Ucheb Zaved, Fiz., 11, 140 (1968), in Chem. Abs., 69, 91597p (1968).

65. E. L. De Kalb and V. A. Fassel, Handbook of the Physics and Chemistry of Rare Earth, North-Hall, Amsterdam, 4, 405 (1979).

66. V. A. Fassel, R. H. Curry and R. N. Kniseley, Spectro. chim. Acta. 18, 1127 (1970).

67. G. C. Grosby, Mol. Cryst., 1, 37 (1966).

68. G. Blasse, Handbook of the Physics and Chemistry of Rare Earth, North-Holland, Amsterdam, 4, 237 (1979).

69. A. P. Golovina, V. K. Runov and N. B. Zorov, Structure and Bonding, 47, 53 (1981).

70. R. P. Fischer and J. D. Winefordner, Anal. Chem., 43, 454 (1971).

71. D. E. Ryan, H. Rollier and J. Holzbecker, Com. J. Chem., 52, 1942 (1974).

72. J. C. Wright, Anal. Chem., 49, 1690 (1977).

73. K. M. Busch and B. Malloy, in "Multichannel Image Detectors", Y. Talmi, Ed, ACS Symp., Ser. No. 102, 27 (1979).

74. P. Gloersen, J. Opt. Soc. Amer., 48, 712 (1958).

75. M. Margoshes, Spectrochim. Acta, B25, 113 (1970).

76. Y. Talmi, in "Multichannel Image Detectors", Y. Talmi, Ed, ACS Symp., Ser. No., 102, 3 (1979).

77. M. H. Crowell, T. M. Buck, E. E. Labunda, J. V. Dalto and E. J. Walsh, Bell Sys. Tech. J., (2)46, 491 (1967).

78. Y. Talmi, Anal. Chem., 47, 658A (1975).

79. K. W. Jackson, K. M. Aldous and D. G. Mitchell, Spectrosc. Lett., 6, 1315 (1973).

80. K. W. Busch, N. G. Howell and G. H. Morrison, Anal. Chem., 46, 575 (1974).

81. D. O. Knapp, N. Omenetto, L. P. Hart, F. W. Plankey and J. O. Winefordner, Anal. Chem. Acta, 69, 455 (1974).

82. J. R. Jadamec, W. A. Sancer and R. W. Sager, in "Multichannel Image Detectors", Y. Talmi, Ed, ACS Symp., Ser. No. 102, 115 (1979).

83. A. E. McDowell and H. L. Pardue, Anal. Chem., 49, 1171 (1977).

84. I. M. Warner, J. B. Callis, E. R. Davidson and G. D. Christian, Clin. Chem., 22, 1483 (1976).

85. D. W. Johnson, J. B. Callis and G. D. Christian, Anal. Chem., 49, 747A (1977).

86. S. L. Bogdanski, Ph.D. thesis, Birmingham University, (1973).

87. I. H. El-Hage, Ph.D. thesis, Birmingham University, (1982).

88. W. R. Brode, Chemical Spectroscopy, John Wiley London (1945).

89. I. M. Warner and L. B. McGown, Critical Reviews in Analytical Chemistry, 14, 155 (1982).

90. J. N. Miller, T. A. Ahmad and A. F. Fell, Anal. Proc., 19, 37 (1982).

91. U. E. Handschin and W. J. Ritschard, Anal. Bioch., 71, 143 (1976).

92. B. Joseffson, P. Lindroth and G. Ostling, Anal. Chim. Acta., 89, 21 (1977).

93. R. C. Stroupe, P. Tokousbalides, R. B. Dickinson, E. L. Wehry and G. Mamantov, Anal. Chem., 49, 701 (1977).

94. W. L. Hinze, H. N. Singh, Y. Baba and N. G. Harvey, Trends in Analytical Chemistry, 36, 193 (1984).

95. T. Taketatsu, Anal. Chim. Acta., 174, 323 (1985).

96. G. G. Guilbault, Practical Fluorescence, Dekker, New York (1973).

97. G. M. O'Donnell and I. M. Solie, Anal. Chem., 50, 189R (1978).

98. E. L. Wehry, Anal. Chem., 52, 75R (1980).

99. W. B. Furman, Continuous-Flow Analysis, Theory and Practice, Dekker, New York (1976).

100. L. T. Skeggs, Am. J. of Clin. Path., 28, 311 (1957).

101. M. K. Schwartz, Anal. Chem., 45, 739A (1973).

102. L. R. Snyder, J. Levine, R. Story and R. A. Conetta, Anal. Chem., 48, 942A (1976).

103. L. R. Snyder, Anal. Chim. Acta., 114, 3 (1980).

104. J. Ruzicka and E. H. Hansen, Anal. Chim. Acta., 78, 145 (1975).

105. K. K. Stewart, G. R. Beecher and P. E. Hare, Anal. Biochem., 70, 167 (1976).

106. J. Ruzicka and E. H. Hansen, Anal. Chim. Acta., 179, 1 (1986).

107. J. T. Vanderslice, K. K. Stewart, A. G. Rosenfeld and D. J. Higgs, Talanta, 28, 11 (1981).

108. J. F. Tyson, Lecture presented at Flow Injection Analysis Short Course, Loughborough University of Technal., Sept., (1983).

109. J. Ruzicka and E. H. Hansen, Anal. Chim. Acta., 114, 19 (1980).

110. B. Rocks and C. Riley, Clin. Chem., 28, 409 (1982).

111. C. B. Ranger, Anal. Chem., 53, 21A (1981).

112. J. Ruzicka and E. H. Hansen, Anal. Chim. Acta., 99, 37 (1978).

113. J. Ruzicka, E. H. Hansen and H. Moseback, Anal. Chim. Acta., 92, 235 (1977).

114. K. K. Stewart and A. G. Rosenfeld, J. Autom. Chem., 3, 30 (1981).

115. Technical Data, Ismatec 5, Ismatec SA, Limmatstrasse 109, 8031 Zurich, Switzerland.

116. Anachem Ltd., Catalogue (1982/1983) 15 Power Court, Luton, Bedfordshire, U.K.

117. D. Betteridge, Anal. Chem., 50, 832A (1978).

118. H. Bergamin, E. A. G. Zagatto, F. J. Krug and B. R. Reis, Anal. Chim. Acta., 101, 17 (1978).

119. L. Nord and B. O. Karlberg, Anal. Chim. Acta., 118, 285 (1980).

120. D. J. Hooley and R. E. Dessy, Anal. Chem., 55, 313 (1983).

121. J. Ruzicka and E. H. Hansen, Flow Injection Analysis, Wiley, New York (1981).

122. Flow Injection Analysis - Bibliography Tecator, Tecator House, Cooper Road, Thornbury, Bristol BS12 2UP, (1985).

123. J. H. M. Van de Berg, R. S. Deelder and H. G. M. Egberlink, Anal. Chim. Acta., 114, 91 (1980).

124. J. M. Reijn, W. E. Van der Linden and H. Poppe, Anal. Chim. Acta., 126, 1 (1980).

125. J. L. Burguera, M. Burguera and A. Townshend; Anal. Chim. Acta., 127, 199 (1981).

126. A. T. Faizullah and A. Townshend, Anal. Chim. Acta., 179, 232 (1986).

127. A. T. Faizullah, Ph.D. thesis, University of Hull (1985).

128. R. C. Schothorst, O. O. Schmitz and G. den Boef, Anal. Chim. Acta., 179, 229 (1986).

129. M. Massom and A. Townshend, Anal. Proc., 22, 6 (1985).

130. P. J. Worsfold and A. Nabi, Anal. Chim. Acta., 179, 307 (1986).

131. H. A. Mottola, Anal. Chim. Acta., 145, 27 (1983).

132. B. Olsson and L. Ogren, Anal. Chim. Acta., 145, 87 (1983).

133. A. T. Faizullah and A. Townshend, Anal. Chim. Acta., 167, 225 (1985).

134. Idem., ibid., 172, 291 (1985).

135. R. C. Schothorst, J. M. Reijn, H. Poppe and G. den Boef, Anal. Chim. Acta., (a) 145, 197 (1983). (b) 153, 133 (1983), (c) 161, 1 (1984), (d) 162, 27 (1984).

136. J. L. Burguera, M. Burguera and M. Gallignani, Acta. Cient. Venez., 33, 99 (1982).

137. M. Aihara, M. Arai and T. Taketatsu, Analyst, 111, 641 (1986).

138. I. M. Kolthoff and R. Belcher, Volumetric Analysis, Vo. 3, Interscience Publishers, New York (1957).

139. C. L. Wilson and D. W. Wilson, Comprehensive Analytical Chemistry, Vol. 1C, Elsevier Publishing Company, New York (1962).

140. H. A. Laitinen and W. E. Harris, Chemical Analysis, McGraw-Hill Kogakusha, Ltd., Tokyo (1975).

141. W. J. Clayton and W. C. Vosburgh, J. Amer. Chem. Soc., 58, 2093 (1936).

142. H. W. Stone and D. N. Hume, Ind. Eng. Chem., Anal. Ed., 11, 598 (1939).

143. G. H. Walden, L. P. Hammit and S. M. Edmonds, J. Amer. Chem. Soc., 56, 350 (1934).

144. O. Deutschbein, Z. Physik, 102, 772 (1936), in Chem. Abs., 31, 4201 (1937).

145. O. Deutschbein and R. Tomaschek, Nature, 131, 473 (1933).

146. A. Zaidel, Nature, 139, 248 (1937).

147. P. C. Mukherji, Indian J. Phys., 13, 185 (1939).

148. H. Gobrecht and R. Tomaschek, Ann. Physik, 29, 324 (1937), in Chem. Abs., 31, 6999 (1937).

149. A. N. Zaidel, Ya. I. Larionov and A. N. Filippov, J. Gen. Chem. (USSR), 8, 943 (1938), in Chem. Abs., 33, 500 (1939).

150. A. N. Zaidel and Ya. I. Larionov, Uspekki Fiz. Nauk, 21, 211 (1939), in Chem. Abs., 33, 6151 (1939).

151. Idem., Trudy Vssesoynz. Konferentssi Anal. Khim, 2, 615 (1943), in Chem. Abs., 39, 3755 (1945).

152. P. Cukor and R. P. Weberling, Anal. Chim. Acta, 41, 404 (1968).

153. G. F. Kirkbright, T. S. West and C. Woodward, Talanta, 12, 517 (1965).

154. G. Alberti and M. A. Massucci, Anal. Chem, 38, 214 (1966).

155. Idem., Anal. Chim. Acta, 35, 303 (1966).

156. V. A. Fassel and R. H. Heidel, Anal. Chem., 26, 1134 (1954).

157. R. Belcher, R. Perry and W. I. Stephen, Analyst, 94, 26 (1969).

158. T. Taketatsu, M. A. Carey and C. V. Banks, Talanta, 13, 1081 (1966).

159. P. I. Gazotti and A. Abrao, Publicaco TEA No. 294 (1973). Instituto De Engergia Atomica, Brasil.

160. W. A. Armstrong, D. W. Grant and W. G. Humphreys, Anal. Chem., 35, 1300 (1963).

161. G. Albert and M. Massucci, Gazz. Quim. Ital., 95, 997 (1965), in Chem. Abs., 64, 4464f (1966).

162. D. T. Burns and M. Y. Qureshi, Proc. Royal. Irish Acad. Sect B, 77, 353 (1977).

163. S. H. Lee and L. R. Field, Anal. Chem., 56, 2647 (1984).

164. R. Applequist, C. Den Boff and C. Schothorst, Anal. Chim. Acta., 180, 1 (1986).

165. C. W. C. Milner and G. W. Sneddon, Atomic Energy Research Establishment C/R 1470 (1955) England.

166. J. S. Fritz et al., Treastise on Analytical Chemistry, Part 11, Volume 8, Wiley, New York (1963).

167. M. Morelos, M.Sc. thesis, University of Hull (1983).

168. D. A. Skoog and D. M. West; Fundamentals of Analytical Chemistry, Reinhart and Winston, New York, 3rd Ed. (1976).

169. A. Fernandez, M. A. Gomez-Nieto, D. D. Luque de Castro and M. Valcarcel, Anal. Chim. Acta., 165, 217 (1984).

170. J. Ruzicka, J. W. B. Stewart and E. A. Zagatto, Anal. Chim. Acta., 81, 387 (1976).

171. W. C. Fernelius, Inorganic Syntheses, Mc.Mcraw-Hill Book Co., Inc., New York (1946).

172. L. F. Yntema, J. Amer. Chem. Soc., 52, 2782 (1930).

173. A. Bruki, Angew. Chem, 49, 159 (1936).

174. H. C. McCoy, J. Amer. Chem. Soc., 63, 3432 (1941).

175. Idem., ibid., 57, 1756 (1935).

176. Idem., ibid., 59, 1131 (1937).

177. D. C. Foster and H. E. Kermers, Anal. Chem., 25, 1921 (1953).

178. J. K. Marsh, J. Chem. Soc., 398 (1942).

179. Idem., ibid., 531 (1943).

180. H. N. McCoy, J. Amer. Chem. Soc., 58, 1577 (1936).

181. Idem., ibid., 61, 2455 (1939).

182. D. D. Perrin and B. Dempsey; Buffers for pH and Metal Ion Control, Chapman and Hall, London (1974).

183. J. L. Burguera and M. Burguera, Anal. Chim. Acta., 161, 375 (1984).

184. T. P. Lynch, N. J. Kernoghan and J. N. Wilson, Analyst 109, 839 (1984).

185. Ibid, idem., 109, 843 (1984).

186. B. P. Bubnis, M. R. Straka and G. E. Pacey, Talanta, 30, 841 (1983).

187. W. L. Burdick, J. Am. Chem. Soc., 48, 1179 (1926).

188. G. E. F. Lundell and H. B. Knowles; Ind. Eng. Chem., 16, 723 (1924).

189. M. A. Salam Khan and W. I. Stephen, Anal. Chim. Acta., 41, 43 (1968).

190. H. W. Stone and D. N. Hume, Ind. Eng. Chem. Anal. Ed., 11, 598 (1939).

191. P. W. Alexander, R. J. Finlayson, L. E. Smythe and A. Thalib; Analyst 107, 1335 (1982).

192. K. L. Cheng, U. Keihei and I. Toshiaki, Handbook of Organic Analytical Reagents, CRC Press, Inc., Florida, (1982).

193. R. Belcher, R. Perry and W. I. Stephen, Analyst, 94, 26 (1969).

194. T. Shigematsui, M. Mastsui and R. Wake, Anal. Chim. Acta., 46, 101 (1969).

195. M. A. Tischchenko, I. I. Zheltvai, I. V. Bakshun and N. S. Poluektov; Zh. Anal. Khim, 28, 1954 (1973), in Anal. Abs., 28, 6B97 (1975).

196. T. Taketatsu and A. Sato, Anal. Chim. Acta., 108, 429 (1979).

197. D. E. Williams and J. C. Guyon, Anal. Chem., 43, 139 (1971).

198. Idem., Mickrochim. Acta., 6, 194 (1972).

199. R. P. Fisher and J. D. Winefordner, Anal. Chem., 43, 454 (1971).

200. S. P. Sinha, Complexes of the Rare Earths, Pergamon Press Ltd., London (1966).

201. G. A. Grosby, Molecular Crystal, 1, 37 (1966).

202. R. E. Whan and G. A. Grosby, J. Mol. Spectrosc., 8, 315 (1962).

203. S. I. Weissman, J. Chem. Phys., 10, 214 (1942).

204. J. N. Filipescu and N. McAvoy, J. Inorg. Nucl. Chem., 28, 253 (1966).

APPENDIX 1

Appendix 1

POSTERS AND PUBLICATIONS

The work described in this thesis has been presented as follows:-

(a) As Posters

1. "Simultaneous Determination of Ce(lll) and Ce(lV) by flow injection analysis"
   K. H. Al-Sowdani and Alan Townshend.

   "Flow Analysis III", Birmingham, September 6/9 (1985)

2. "Candoluminescence Spectrometry with a Vidicon Detector"
   K. H. Al-Sowdani.

   "Research and Development Topics in Analytical Chemistry
   Analytical Division, Royal Society of Chemistry,
   London, April 16 (1986)

3. "Flow Injection Determination of Europium after on-line Reduction"
   K. H. Al-Sowdani and Alan Townshend.

   "SAC 86 Int. Conf. on Anal. Chem., Bristol, July (1986)

(b) Publications

1. Simultaneous Determination of cerium(lll) and cerium (lV) by flow injection analysis.
   K. H. Al-Sowdani and Alan Townshend.
   Anal. Chim. Acta., 179, 469 (1986)

2. Candoluminescence Spectrometry with a Vidicon Detector.
   K. H. Al-Sowdani.
   Anal. Proc., 23, 432 (1986)